# *Soil Liquefaction Response in Mid-America Evaluated by Seismic Piezocone Tests*

**Mid-America Earthquake Center**
**Report MAE-GT-3A**

**prepared by**

**James A. Schneider**

**and**

**Paul W. Mayne**

***Geosystems Program***
***Civil & Environmental Engineering***
***Georgia Institute of Technology***
***Atlanta, GA 30332***

**October 1999**

## TABLE OF CONTENTS

## ACKNOWLEDGEMENTS

The number of people who have aided directly as well as indirectly to this research effort are gratefully thanked. Much appreciation is expressed to my research advisor Dr. Paul W. Mayne. His knowledge, interest, enthusiasm, and guidance have been valuable for this project as well as the many others we have worked on together over the past 4 years. Appreciation is expressed to my additional committee members, Dr. J. David Frost and Dr. Glenn J. Rix, for the support they have provided on this project as well as the wealth of knowledge they have passed on through discussions and class lectures. Dr. J. Carlos Santamarina and his entire research group are thanked for the insight and help they have provided throughout my time at Georgia Tech. Discussions as well as class lectures have shaped many of the thoughts incorporated into this thesis, and expanded my understanding of soil behaviour and the finer aspects of *yerba mate* preparation. Alec McGillivray is thanked for initially reviewing much of this thesis and helping to get it turned in. Discussions with him on a range of subjects including, geotechnical engineering in general, CPT electronics and data acquisition systems, CPT calibration, the use of Spanglish to convey directions to Puerto Rican drillers, and computer network support have been helpful and are appreciated. The attitude, knowledge, and good nature of all the students and faculty in the Geosystems group at Georgia Tech have made my graduate, as well as undergraduate, education enjoyable and rewarding.

The Mid-America Earthquake (MAE) center through the National Science Foundation (NSF) is acknowledged for support on this project. The number of academic institutions and fields of expertise involved with the center provided a multidisciplinary atmosphere that enhanced the issues considered. Seminars and meetings allowed for an exchange of ideas that helped the progress and focus of this project.

The amount of fieldwork associated with this research effort could not have been accomplished without the help of many people. Thanks is expressed to Ken Thomas (e.g., Geosystems lab manager, CEE building manager, Head of GT cone truck operations, etc...) for his help on a most of the field trips to the New Madrid seismic zone, as well as testing on Campus and in Alabama. His attention to detail, patience, knowledge, and ability to fix all types of broken equipment made this research possible. The amount of personal time on weekends and long days in the field that he gave up is acknowledged and appreciated. Craig Wise is thanked for running the show in Charleston, initial training on the use of SCPTu equipment, providing additional CPT and SPT data in the New Madrid area, as well as getting me a prime window office in Hightower. *If I can make it there, I'll make it anywhere*. Tom Casey, Tracy Hendren, Ethan Cargill, and Scott Olson are also thanked for the help they provided in the field as well. Brad Pemberton and others at Gregg In-Situ are thanked for donating a rig and personnel necessary to perform the fieldwork in Charleston, SC.

Selection of the field test sites associated with this project has been a group effort. Appreciation is expressed to Dr. Buddy Schweig (USGS), Professor Martitia Tuttle (University of Maryland), Professor Roy VanArsdale (University of Memphis), Joan

Gomberg (USGS), Marion Haynes (Blytheville, AR), Dr. Loraine Wolf (Auburn), Kevin McLain (MODOT), as well as many others at the Center for Earthquake Research and Information (CERI) in Memphis. Dr. Howard Hwang is thanked for access to his database of boring logs and soil index properties from Memphis & Shelby County.

Laboratory resonant column tests performed by Brendan Sheppard and data provided by Laureano Hoyos Jr. was helpful for this research effort.

Correspondence though e-mail and/or data sets provided by Professor Les Youd (BYU), Dr. Ron Andrus (NIST), Dr. Ed Kavazanjian (GeoSyntec - Huntington Beach), Professor Ross Boulanger (U.C.-Davis), Professor I.M. Idriss (U.C.-Davis), and others at the United States Geologic Survey (USGS), have been helpful to provide additional perspective to the issues associated with this study. Dr. Bob Herrmann (St. Louis University) is thanked for help with his synthetic ground motion program, as well as discussions of ground motion parameters in Mid-America.

Finally, I would like to thank my parents, sister, and relatives for the support they have provided throughout my education, and understanding of my busy schedule. I would also like to thank my father for his insightful comments concerning drafts of this thesis.

## LIST OF TABLES

## LIST OF FIGURES

## SUMMARY

The Mid-America earthquake region is now recognized as containing significant seismic hazards from historically-large events that were centered near New Madrid, MO in 1811 and 1812 and Charleston, SC in 1886. Large events prior to these times are also acknowledged. Methods for evaluating ground hazards as a result of soil liquefaction and site amplification are needed in order to properly assess risks and consequences of the next seismic event in these areas. In-situ tests provide quick, economical, and practical means for these purposes. The seismic piezocone penetration test (SCPTu) is a hybrid in-situ test method, which provides downhole measurements of shear wave velocity in addition to penetration test parameters within a single vertical sounding. The SCPTu provides four independent readings that can be used for soil classification, site amplification analysis, direct liquefaction analysis, as well estimation of soil properties for a rational engineering assessment of soil liquefaction.

For this research effort, in-situ penetration tests have been performed at a number of test sites in the heart of the Mid-America earthquake regions. Testing areas include Charleston SC, Memphis TN, West Memphis AR, Blytheville AR, Steele MO, and Caruthersville, MO. Many of these sites have already been associated with liquefaction features such as sand dikes, sand boils, or subsidence, observed during geologic and paleoseismic studies. Seismic piezocone penetration tests have been performed in these localities. Data collected at these sites have been analyzed under current methodologies

to assess the validity of empirical relations developed for Chinese, Japanese, and Californian interplate earthquakes when applied to historical Mid-American earthquakes. Simplified cyclic strain theory will be combined with empirical estimation of soil properties to evaluate pore pressure generation and liquefaction potential.

Evaluation of liquefaction response of soils is complicated in Mid-America due to the deep soil columns of the Mississippi River Valley and Atlantic Coastal plain, infrequency of large events needed for calibration of models and analysis techniques, and uncertainty associated with the mechanisms and subsequent motions resulting from intraplate earthquakes. These aspects of Mid-America earthquakes have been considered in analyses conducted for this study.

Six earthquake events in Mid-America have been evaluated using four separate types of analyses on 22 critical layers from 12 sites. The results of these analyses indicate that:

- current methods generally agree in the prediction of liquefaction at a site;
- modulus reduction schemes used in cyclic strain based procedures tend to bridge the gap between the small strain measurement of shear wave velocity and large strain phenomena of liquefaction; and
- liquefaction may have occurred throughout the thickness of the soil deposits analyzed.

The use of attenuation relationships which do not account for the non-linear nature of soil deposits adds uncertainty to these results and remains the subject of additional research.

# CHAPTER 1

# INTRODUCTION

## 1.1 Motivation

It is now recognized that several of the largest historical earthquake events in the United States occurred in the New Madrid, MO area during 1811 and 1812, and in Charleston, SC in 1886. The New Madrid series of 1811-1812 consisted of over 200 separate seismic events, which would have created an equivalent single event with a moment magnitude ($M_w$; Appendix II) of about 8.3 (Johnston & Schweig, 1996). The three largest individual events of the series were estimated to have moment magnitudes of about 7.9, 7.6, and 8.0 on December 16, 1811, January 23, 1812, and February 7, 1812 respectively (Johnston & Schweig, 1996). The Charleston, SC earthquake consisted of a single event on September 1, 1886, with a $M_w$ estimated at 7.0 (Stover & Coffman, 1993).

Ongoing research on the magnitude, attenuation, and recurrence of earthquake events in Mid-America has led to the increased awareness of the potential for serious ground failures in the New Madrid, MO seismic zone and Charleston, SC earthquake region. Strong ground motions can lead to injury and death from damaged structures, primarily from the collapse of buildings and bridges. Site amplification and liquefaction-induced ground failures may increase the severity of earthquake effects. Large lateral

and vertical movements will rupture pipelines and utilities, crippling lifeline facilities needed to provide aid and relief to the injured.

It will be desirable to evaluate the response of soils to earthquake shaking and potential for liquefaction in an expedient and cost effective manner in the Central and Eastern United States (CEUS). However, the evaluation of liquefaction response of soils is complicated in Mid-America due to the:

- deep vertical soil columns (600 m to 1400 m) of the Mississippi River Valley and Atlantic Coastal plain;
- infrequency of large events needed for calibration of models and analysis techniques (most recent severs events, $M_w > 6.5$, more than 100 years ago);
- uncertainty associated with the mechanisms and subsequent motions resulting from intraplate earthquakes (e.g., California earthquakes are interplate events).

## 1.2 Background on Soil Liquefaction

Liquefaction is the result of excess porewater pressure generated in saturated granular soils from rapid loading, and is often associated with earthquake shaking. Since soil strength is proportional to the effective vertical stress ($\sigma_{vo}'$; Appendix I), the reduction of effective stress from increased pore pressures (u) will lead to strength loss in a soil deposit. The porewater pressure in the soil will be a combination of initial in-situ porewater stress ($u_o$) and the shear induced porewater pressure ($\Delta u$). When the pore water pressure ($u = \Delta u + u_o$) equals the total overburden stress ($\sigma_{vo}$), the effective stress ($\sigma_{vo}' = \sigma_{vo} - u$) will go to zero causing initial liquefaction (Seed & Lee, 1966).

The engineering terminology used to describe soil liquefaction is varied, so an overview of definitions as discussed in Kramer (1996) and Robertson and Wride (1997) will be presented here. There are two main terms that can be used to describe soil liquefaction: *flow liquefaction* and *cyclic softening*. These terms are distinguished in Table 1.1. Cyclic softening can be separated into *cyclic liquefaction* as well as *cyclic mobility*. This study focuses specifically on cyclic liquefaction at sites with level ground.

Initial studies of liquefaction involved stress-controlled laboratory tests of reconstituted specimens (Seed & Lee, 1966). Since the effects of structure, aging, cementation, and strain history cannot be replicated in these specimens, the use of in-situ testing results and field performance data has become a popular means of assessing liquefaction susceptibility. Penetration resistance at sites where surface manifestations of liquefaction were or were not evident have been compared to evaluate cyclic soil resistance. Databases consisting predominantly of sites from China, Japan, and California are available for the Standard Penetration Test (SPT; e.g., Seed et al., 1983), cone penetration test (CPT; e.g., Olson & Stark, 1998), flat dilatometer test (DMT; e.g., Reyna & Chameau, 1991), and shear wave velocity ($V_s$; Andrus et al., 1999). Analyses by these methods are considered as direct methods for liquefaction assessment of soils.

Estimation of soil properties using in-situ tests (e.g., Kulhawy & Mayne, 1990) and incorporating these results into a theoretical framework for analysis can be considered an indirect, yet rational, method for soil liquefaction assessment. Some theoretical frameworks for liquefaction assessment that currently are in use include the cyclic-strain based method (Dobry et al., 1982), nonlinear effective stress-based analyses (e.g., Finn et

al., 1977), and the critical-state approach for sands (e.g., Jefferies, 1999). Computer models have been developed which incorporate these theories, and it should be noted that the accuracy of the model prediction will only be as reliable and meaningful as the values of input parameters.

**Table 1.1. Comparison of Flow Liquefaction and Cyclic Mobility**

| | Flow Liquefaction | Cyclic Softening | |
|---|---|---|---|
| | | Cyclic Liquefaction | Cyclic Mobility |
| **Loading Conditions** | Static or Cyclic | Cyclic with stress reversal[1] | Cyclic without stress reversal[1] |
| **Drainage** | Undrained | Undrained | Undrained |
| **Soil Response to Shear (Appendix I)** | Strain Softening | Strain Softening and Strain Hardening | Strain Softening and Strain Hardening |
| **Controlling Stresses** | Static Shear Stress | Static and Cyclic Shear Stresses | Static and Cyclic Shear Stresses |
| **Induced Stress State** | In-situ shear stresses greater than minimum undrained shear strength | Effective stress state reaches essentially zero | Zero effective stress does not develop |
| **Failure or Deformation Potential** | Sufficient volume of soil must strain soften. Failure can result in slide or flow depending upon internal geometry and stress state. | Strain softened shear modulus can lead to large deformations during cyclic loading. Soils will tend to stabilize upon termination of cyclic loading. | Limited deformations, unless very loose soil results in flow liquefaction. |
| **Soil Types** | Any metastable saturated soil; very loose granular deposits, very sensitive clays, and loess deposits | Almost all saturated sands, with limited deformations in clayey soils. | Almost all saturated sands, with limited deformations in clayey soils. |

[1] Stress reversal - during cyclic loading, the shear stresses alternate from positive to negative.

The significance of local site conditions and amplification of ground motions have received increased recognition since the 1985 Mexico City and 1989 Loma Prieta earthquakes (Kramer, 1996). Therefore, the use of computer codes for site-specific cyclic stress-, cyclic strain-, or effective stress-based analysis may be necessary. Commercially available software packages fall into the categories of equivalent linear 1-D programs (e.g., SHAKE; Schnabel et al., 1972), true non-linear programs (e.g., DESRA; Lee & Finn, 1978), or equivalent linear 2-D programs (e.g., QUAD4; Idriss et al., 1973). Analyses of sites at low peak ground accelerations (PGA < 0.4 g; Appendix II) can commonly be achieved using equivalent linear 1-D codes. Large strains generated by high peak ground accelerations (PGA > 0.4) from an extreme event may require analysis by a 1-D true nonlinear program or a 2-D equivalent linear program to account for additional complexities at individual sites.

To obtain parameters for engineering analysis and model studies, field test data are necessary. The seismic piezocone penetrometer is an electronic probe that rapidly provides four independent parameters to assess the subsurface profile with depth at an individual site. Figure 1.1 depicts a seismic piezocone sounding, and displays the location of tip resistance ($q_c$), sleeve friction ($f_s$), porewater pressure measurement ($u_m$), and horizontal geophone for determining shear wave velocity ($V_s$). The tip resistance can be used for a direct empirical analysis of soil liquefaction potential. Tip resistance can also be used to evaluate effective stress friction angle ($\phi'$), overconsolidation ratio (OCR), in-situ coefficient of horizontal stress ($K_o$), or relative density ($D_R$) for an indirect, yet rational analysis of soil behavior during seismic loading. Sleeve friction measurements

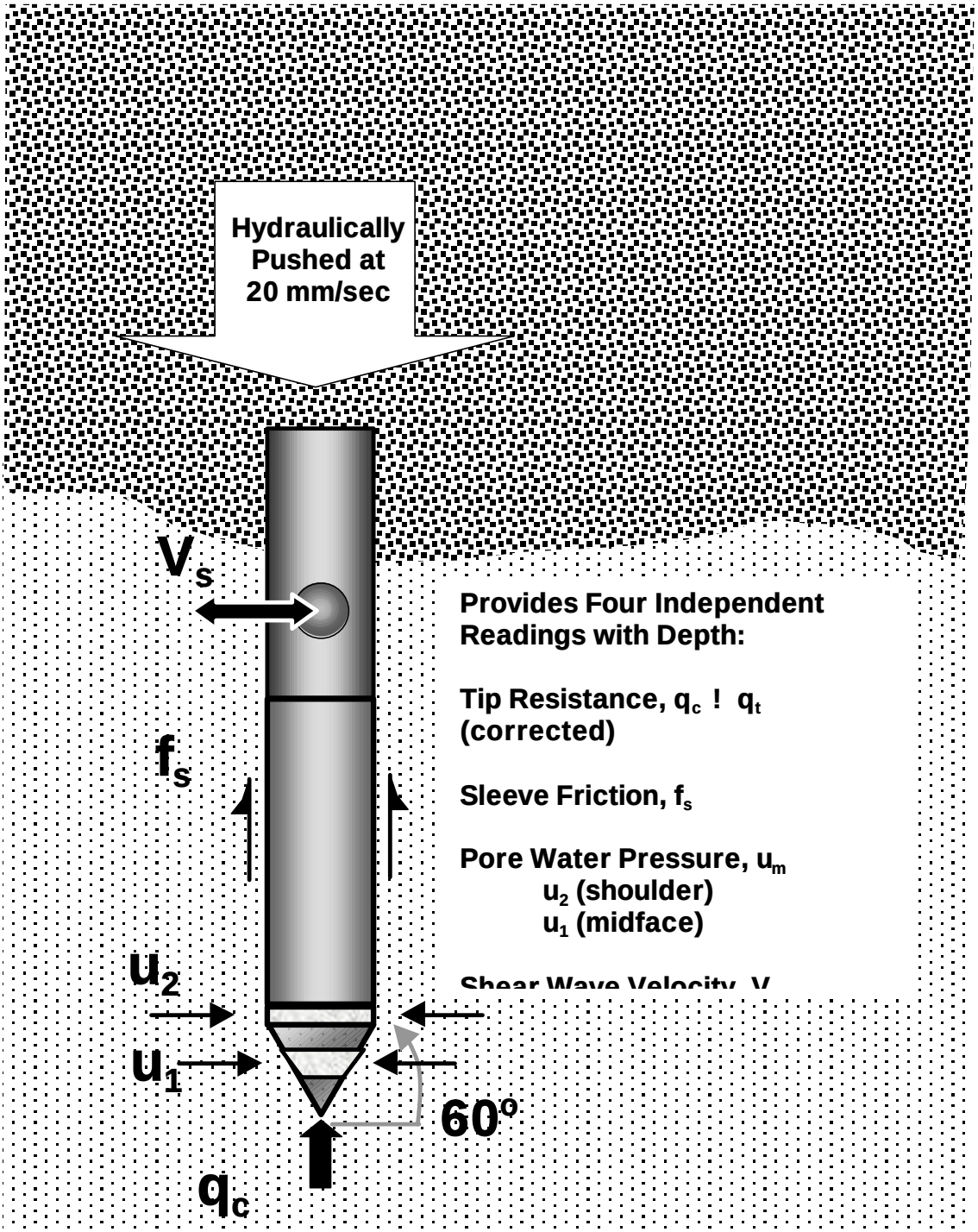


**Figure 1.1. Seismic Dual-Element Piezocone Penetrometer Indicating the Position and Direction of the Measurements**

can be used for stratigrafic profiling and as an estimate of fines content necessary for both direct and indirect methods. Porewater pressure, $u_m$, can be used for stratigraphic profiling, as well as for the determination of groundwater table in sands and the stress history of clays. Penetration porewater pressure dissipation tests can provide information of the flow characteristics of the localized strata, including the coefficient of consolidation ($c_v$) and permeability (k). The shear wave velocity ($V_s$) is measured with a horizontal geophone located about 25 cm behind the cone tip. Measurements are taken at 1-m depth intervals, so the downhole $V_s$ is an averaged property over discrete depths. Shear wave velocity can be used for direct liquefaction analysis through simplified charts. Rational indirect analyses can be enhanced from the measurement of soil stiffness, or evaluations of void ratio (e), and total mass density ($\rho_{tot}$).

Before an earthquake analysis can be performed, critical ground motion parameters must be selected. An assessment of ground motion hazards is difficult in the Mid-America earthquake region due to the lack of strong earthquakes in recent historical times ($t \approx 100+$ years), and lack of recorded data from the limited events that have occurre. For seismic hazard analysis, probabilistic hazard information is available through the USGS web site at (http://www.geohazards.cr.usgs.gov/eq). A stochastic ground motion model has been under development for the Central and Eastern United States (CEUS), and attenuation relationships have been determined utilizing this model (e.g., Toro et al., 1997). Synthetic ground motions based on a representative stiffness profile of the Mississippi River Valley deep soil column are still under development for the Mid-America region (Herrmann & Akinci, 1999) at the time of this writing.

## 1.3 Scope

The purpose of this project is to assess the liquefaction response of Mid-American soils. The use of in-situ testing methods and their application to geotechnical earthquake engineering will be reviewed. Current and evolving methods for liquefaction assessment will be discussed, with an emphasis on their use in Mid-America. There is a great deal of uncertainty in assessing appropriate earthquake parameters for the Central and Eastern United States (CEUS) due to the deep soil column over bedrock (600 m < z < 1400 m), and infrequency of large events (f ≈ 250 years). Attenuation models for rock sites are reviewed and compared to a recent deep soil model developed specifically for Mid-America.

Seismic piezocone testing and limited surface sampling have been performed at a number of sites across the New Madrid Seismic zone and Charleston, SC earthquake region. The majority of these sites are historic liquefaction sites, having shown indisputable evidence of sand boils, sand dikes, subsidence, and other geologic liquefaction features. Data from index, laboratory, and field testing will be presented. To assess soil liquefaction potential in Mid-America, the collected data will be incorporated into a number of frameworks including:

- direct cyclic stress methods for cone tip resistance and shear wave velocity;
- direct Arias intensity method for cone tip resistance;
- evaluation of soil properties and input into cyclic strain-based theory.

Conclusions emanating from these studies will be derived and recommendations for future work will be proposed to improve research and practice in Mid-America.

# CHAPTER 2

# IN-SITU GEOTECHNICAL TESTING

## 2.1 Introduction

Traditional means of geotechnical exploration of soil deposits consists of rotary drilling techniques to generate soil borings. From these procedures, auger cuttings, drive samples, and pushed tubes may be recovered. During the process of drive sampling, the number of blows of a drop weight advancing a hollow pipe a given distance provides a crude index of soil consistency. This procedure can be called an in-situ test. Modern electronics have permitted advances in cone penetration test technology, allowing for increased resolution with depth and more repeatable results. Enhanced in-situ tests have incorporated additional sensors such as piezometers, geophones, as well as measurements of electromagnetic properties such as resistivity and dielectric permittivity. This chapter will provide background on in-situ testing, including the Standard Penetration Test (SPT), the cone penetration test (CPT), with special emphasis on the seismic piezocone test (SCPTu) and its application to geotechnical site characterization will be discussed.

## 2.2 Standard Penetration Test (SPT)

The standard penetration test (SPT) has been the most commonly-used in-situ test in geotechnical subsurface investigations (Decourt et al., 1988). The test obtains both a

numerical resistance (N-value) for the soil, as well as a disturbed drive sample for classification and index testing. "Undisturbed" sampling of sands would require expensive and advanced techniques such as ground freezing (Sego et al., 1999). Because frozen samples are very difficult to obtain, and only then in limited quantity, alternative methods based on in-situ methods are preferred.

For the Standard Penetration Test (SPT), procedures consist of repeatedly dropping a 63.5-kg mass from a height of 760 mm to drive a split-spoon sampler into the ground (ASTM D-1586). Figure 2.1 displays some representative SPT equipment and procedures. A theoretical free-fall energy of 474.5 J would be delivered under ideal conditions, but frictional losses and operator variability results in a delivered energy which is much lower (Skempton, 1986). The number of blows are recorded for three increments of 152 mm each. The initial 152-mm is a "seating," and is neglected. The blows from the second and third intervals are totaled as the N-value over 304-mm of penetration. Figure 2.2 shows a representative boring log with SPT N-values from the Mid-America region.

Numerous correction factors to the measured N-value are necessary because of energy inefficiencies and procedural variation in practice. When all factors are applied to the field recorded N-value ($N_{meas}$), the corrected and normalized $(N_1)_{60}$ value can be determined by:

$$(N_1)_{60} = N_{meas} C_N C_E C_B C_S C_R \qquad (2.1)$$

where correction factors are presented in Table 2.1 and include the effects of stress level ($C_N$), energy ($C_E$), borehole diameter ($C_B$), sampling method ($C_S$), and rod length ($C_R$). In practice, the N-value is typically only corrected for overburden stress ($C_N$), and the energy efficiency is assumed to be 60 percent in the United States. Seed et al. (1985) reviewed typical hammer energy efficiency around the world, and Farrar (1998) performed a review of SPT energy measurements for a number of different SPT systems in North America. For liquefaction studies it is recommended that energy efficiency measurements be performed (ASTM D6066) to apply the correction factor ($C_E$). The additional correction factors for particle size ($C_P$), aging ($C_A$), and overconsolidation ($C_{OCR}$), are presented, but these particular corrections are usually used only in research studies and improved interpretations.

The overall effect of having so many corrections, each with its own great uncertainty, is that little confidence can be assigned to the SPT as a reliable means for assessing the liquefaction potential of soils. Due to these compounding errors, much interest has been directed to the use of alternative in-situ test methods for evaluating seismic ground response. The electronic cone penetrometer offers some clear advantages in this regard.

## 2.3 Cone Penetration Test (CPT)

Originally, a cone penetrometer was a mechanical device that produced tip stress measurements with depth, with later adaptations for a sleeve resistance (Broms & Flodin, 1988). The probe is hydraulically pushed into the ground without the need for a soil boring. The test equipment has evolved to its current state of electric and electronic cone

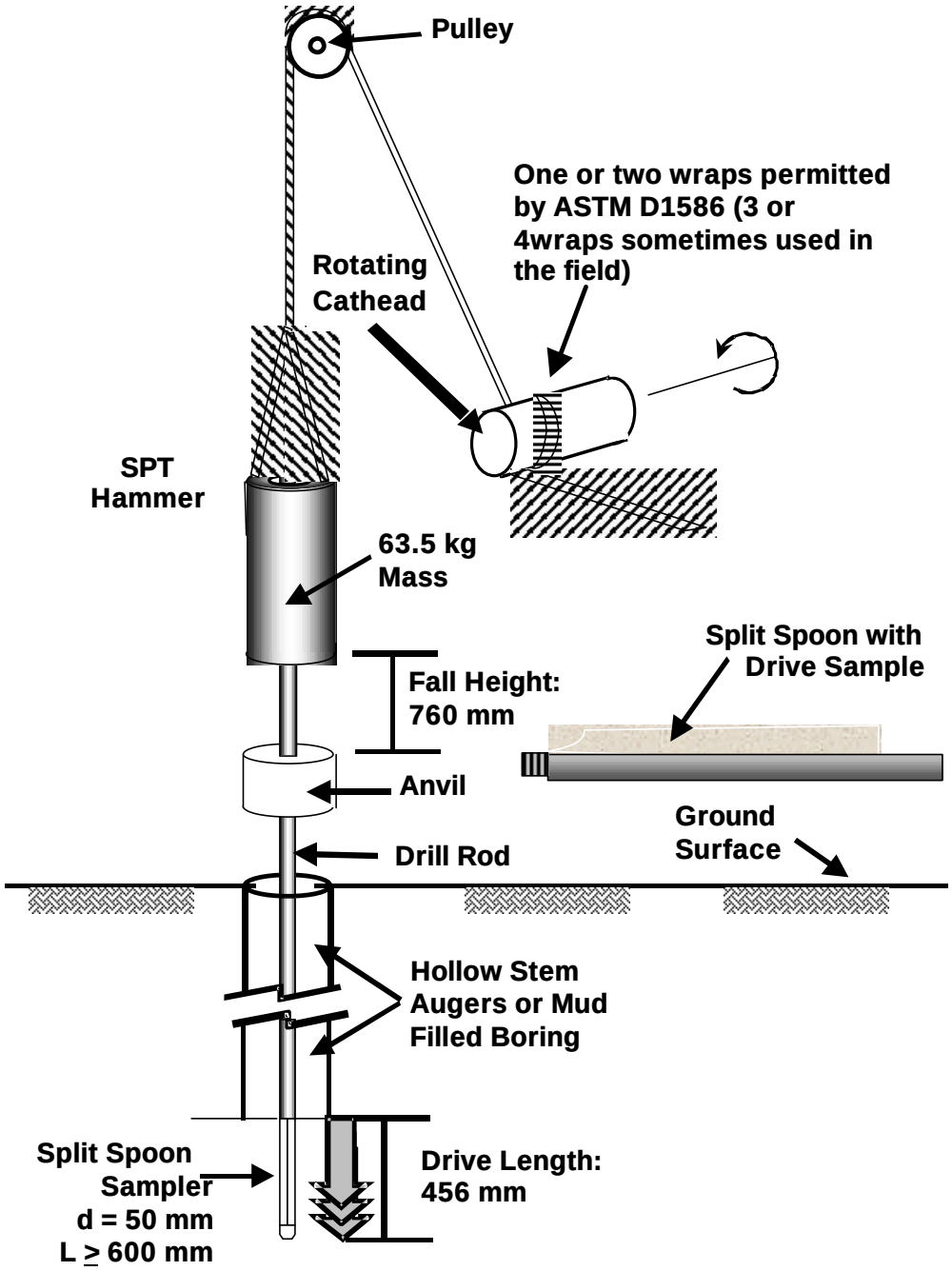


**Figure 2.1. Setup and Equipment for the Standard Penetration Test (SPT) (adapted from Kovacs et al., 1981)**

**Table 2.1. Correction Factors for Standard Penetration Test (based on Skempton, 1986; Kulhawy & Mayne, 1990; Robertson & Wride, 1997)**

| Effect | Variable | Term | Value |
|---|---|---|---|
| Overburden Stress | $\sigma_{vo}'$ | $C_N$ | $(P_a/\sigma_{vo}')^{0.5}$ but $\leq 2$ |
| Energy Ratio[1] | • Safety Hammer<br>• Donut Hammer<br>• Automatic Hammer | $C_E$ | 0.6 to 0.85<br>0.3 to 0.6<br>0.85 to 1.0 |
| Borehole Diameter | • 65 to 115 mm<br>• 150 mm<br>• 200 mm | $C_B$ | 1.00<br>1.05<br>1.15 |
| Sampling Method | • Standard sampler<br>• Sampler without liner | $C_S$ | 1.0<br>1.1 to 1.3 |
| Rod Length | • 10 m to 30 m<br>• 6 to 10 m<br>• 4 to 6 m<br>• 3 to 4 m | $C_R$ | 1.0<br>0.95<br>0.85<br>0.75 |
| Particle Size | Median Grain Size ($D_{50}$) of Sand in mm | $C_P$ | $60 + 25 \log D_{50}$ |
| Aging | Time (t) in years since deposition | $C_A$ | $1.2 + 0.05 \log (t/100)$ |
| Overconsolidation | OCR | $C_{OCR}$ | $OCR^{0.2}$ |

[1] Obtain by energy measurement per ASTM D4633

**Figure 2.2. Typical Boring Log from Shelby Forest, TN (Liu et al., 1997)**

penetrometers with standard readings of tip resistance ($q_c$) and sleeve friction ($f_s$), as shown in Figure 2.3.a. The readings are collected by computerized data acquisition systems converting analog signals from strain gauges to digital data. New sensors have been added to cone penetrometers including pore pressure transducers with porous filters located at the shoulder (Fig. 2.3.b.) or midface (Fig 2.3.c.) in order to measure penetration porewater pressures ($u_2$ or $u_1$ respectively). Moreover, by incorporating velocity geophones and a surface source, the shear wave arrival time ($t_s$) can be recorded with depth. Testing with this probe is known as the seismic piezocone penetration test (SCPTu) as detailed by Campanella (1994). Figure 2.5 presents raw data from a SCPTu sounding in Memphis, TN showing the four independent measured readings with depth; $q_c$, $f_s$, $u_2$, and $t_s$. The four characteristic shear wave arrival times (first arrival, first trough, crossover, and first peak) are described in Appendix III. This site is near areas of historic liquefaction features with prior geologic evidence of sand dikes projecting through overlying clayey silt stratum along the banks of the Wolf River near Mud Island (personal communication, R. VanArsdale, 1998). Additionally, an inclinometer may be installed in the cone to assess the verticality of the sounding to warn against excessive drift andpossible rod buckling. Figure 2.4 shows a photograph of the three seismic piezocones used during this study, including 5-tonne, 10-tonne, and 15-tonne probes.

Standard cone penetrometers have a $60^o$ apex at the tip, 10-$cm^2$ projected tip area, 35.7 mm diameter, and 150-$cm^2$ sleeve surface area. Cone penetrometers may also have a $60^o$ apex at the tip, 15-$cm^2$ projected tip area, 44 mm diameter, and either 200- or 225-$cm^2$ sleeve surface area. The maximum capacity of the load cells may vary, with lower

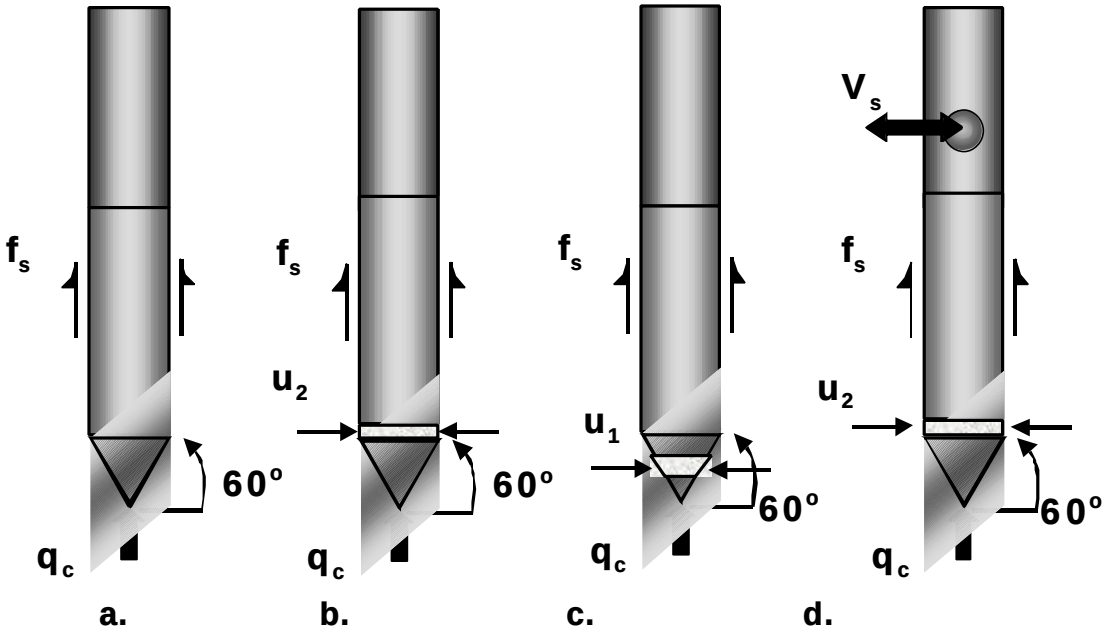


**Figure 2.3. Types of Cone Penetrometers and Measurement Locations: a. Electric Cone Penetrometer, CPT; b. Piezocone Penetrometer (filter behind tip), $CPTu_2$; c. Piezocone Penetrometer (mid-face filter) $CPTu_1$; d. Seismic Piezocone, $SCPTu_2$;**

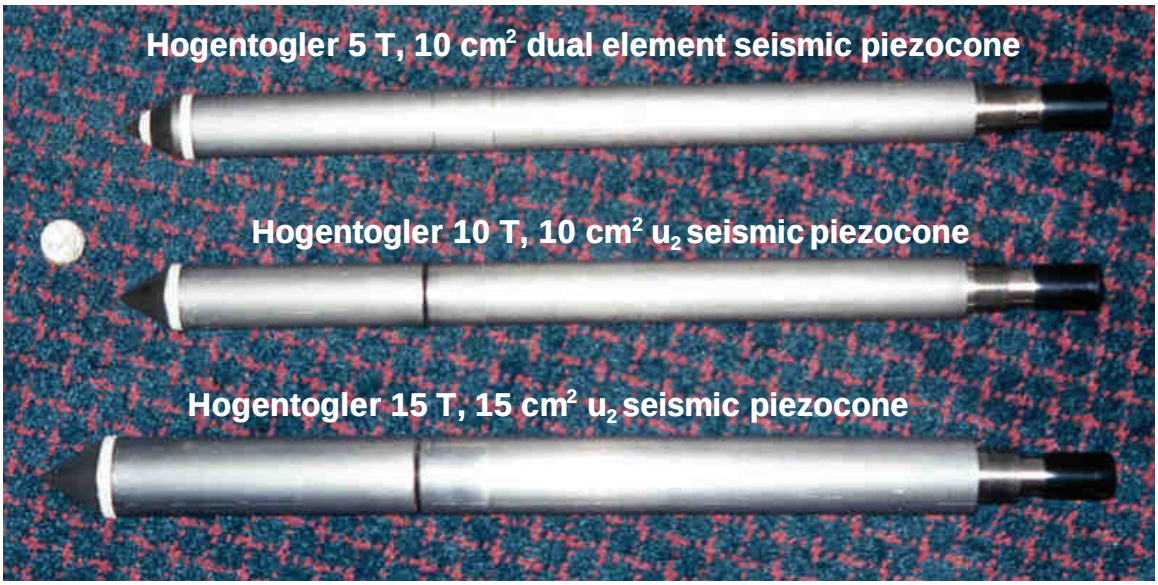


**Figure 2.4. Seismic Piezocone Probes used in this Study (quarter for scale)**

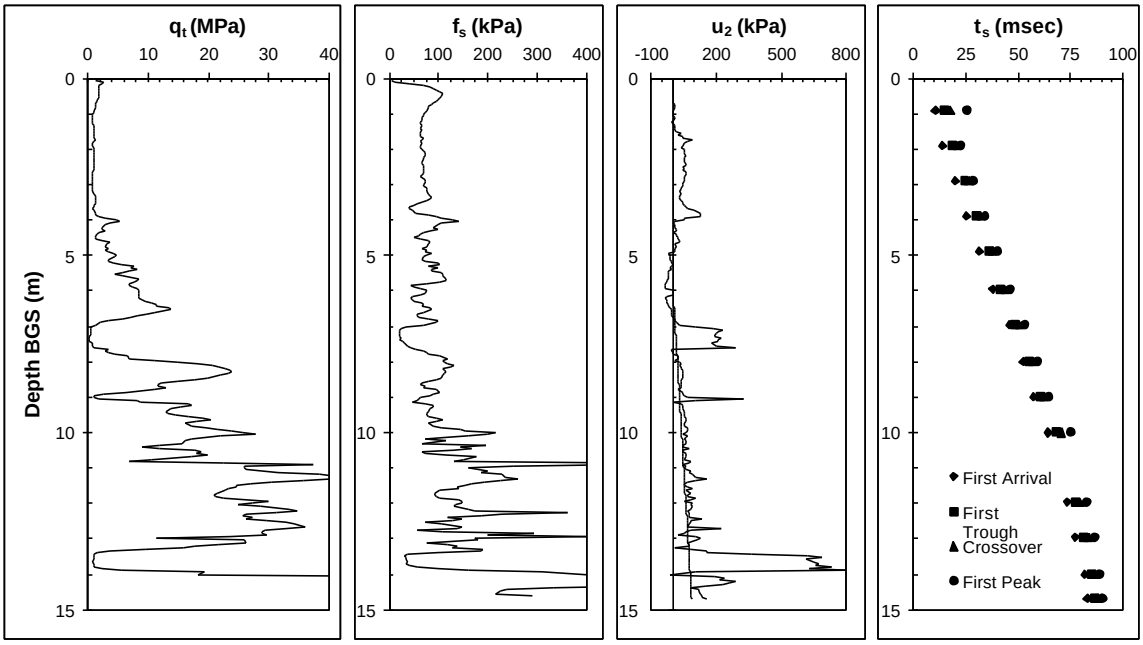


**Figure 2.5. Raw SCPTu data from Bell Properties, Memphis, TN**

capacity load cells providing higher resolution necessary for investigations in low resistance soils, such as soft clays. The location of piezocone filters for pore pressure measurement may be at mid-face ($u_1$) and/or behind the shoulder ($u_2$), as seen in Figure 2.3. Differences in penetrometer size, capacity, and pore pressure filter location will be discussed further in Section 2.4.2 on the comparison of penetrometers.

Test procedures consist of hydraulically pushing the cone at a rate of 2 cm/s (ASTM D5778) using either a standard drill rig or specialized cone truck. The advance of the probe requires the successive addition of rods (either AW or EW drill rods or specialized cone rods) at approximately 1 m or 1-5 m intervals. Readings of tip resistance ($q_c$), sleeve friction ($f_s$), inclination (*i*), and pore pressure ($u_m$) are taken every 5-cm (2.5-sec). Depending upon limitations of the data acquisition system, the readings may be recorded

at higher sampling rates to distinguish variations in soil strata, fabric, and layering. Shear wave arrival times ($t_s$) are typically recorded at rod breaks corresponding to 1-m intervals. More information on cone penetration test procedures and equipment can be found in Appendix III.

The cone tip resistance ($q_c$) is the measured axial force over the projected tip area. It is a point stress related to the bearing capacity of the soil. In sands, the tip resistance is primarily controlled by the effective stress friction angle ($\phi'$), relative density ($D_r$), and effective horizontal stress-state ($\sigma_{ho}'$). For intact clays, the tip resistance is primarily controlled by the undrained shear strength ($s_u$). Particularly in clays and silts, the measured $q_c$ must be corrected for porewater pressures acting on the cone tip geometry, thus obtaining the corrected tip stress, $q_t$ (Lunne, et al., 1997):

$$q_t = q_c + (1\text{-}a_n)u_2 \qquad (2.2)$$

where $a_n$ is the net area ratio determined from laboratory calibration (Appendix III) and $u_2$ is the shoulder penetration porewater pressure. A general rule of thumb is that $q_t > 5$ MPa in sands, while $q_t < 5$ MPa in clays and silts.

The sleeve friction ($f_s$) is determined as an axial load acting over the area of a smooth sleeve. This value is typically expressed as the Friction Ratio ($FR = f_s / q_t \times 100$), which is indicative of soil type (Lunne et al., 1997). Often, FR< 1% in clean sands and FR > 4 % in clays and silts.

The penetration porewater pressures are monitored using a transducer and porous filter element. The filter element position can be located mid-face on the cone ($u_1$) or behind the cone tip at the shoulder ($u_2$), with the latter required for the correction of tip resistance. These readings represent the fluid pressures between the soil particles. At the shoulder position, the pressures are near hydrostatic in sands ($u_2 \approx u_o$) whilst considerably higher than hydrostatic ($u_2 > u_o$) in soft to firm to stiff intact clays. The pore pressure parameter, $B_q = (u_2 - u_o) / (q_t - \sigma_{vo})$, has been developed as a means to normalize CPTu data for the purpose of soil classification and undrained shear strength estimation (Senneset et al., 1982; Wroth, 1984). At the mid-face location ($u_1$), penetration porewater pressures are always positive, while at the $u_2$ location measurements are either positive in intact materials or negative in fissured soils (Mayne et al., 1990).

## 2.4 Seismic Piezocone Penetration Test (SCPTu)

Seismic cone penetration systems provide rapid, repeatable, near continuous, measurements of multiple parameters that can be used to assess soil properties. To analyze earthquake hazards, an understanding of each soil behavioral parameter available from various cone penetration tests is necessary. Available measurements from seismic cone penetrometers along with controlling parameters are presented in Table 2.2. With regards to liquefaction evaluation, the individual recordings from seismic piezocone penetration tests (SCPTu) can be valuable in evaluating input parameters as illustrated by Figure 2.6. Specifically, the readings are processed to obtain:

- Direct measure of small strain shear stiffness ($G_{max} = \rho \cdot V_s^2$);

**Table 2.2. Primary Soil Parameters Controlling CPT Measurements**

| CPT Measurement | | Primary Controlling Parameters |
|---|---|---|
| Tip Resistance, $q_t = q_c + u_2(1-a_n)$ | | Sand: • effective stress friction angle ($\phi'$)<br>• relative density ($D_R$)<br>• horizontal effective stress ($\sigma_{ho}'$) |
| | | Clay: • undrained shear strength ($s_u$)<br>• preconsolidation stress ($\sigma'_p$) |
| Penetration Porewater Pressures | behind the tip, $u_2 = u_b$ | Sand: • hydrostatic water pressure ! water table |
| | | Clay: • overconsolidation ratio (OCR) in intact clays |
| | mid-face, $u_1$ | • soil type and stratigraphy<br>• OCR in either intact or fissured clays |
| | dissipation test ($u_1$ or $u_2$) | Silt & Clay: • horizontal flow characteristics ($k_h$)<br>• coefficient of consolidation ($c_v$) |
| Sleeve Friction, $f_s$ (or Friction Ratio, $FR = f_s/q_t \cdot 100$) | | • remolded shear strength of clays<br>• soil type |
| Shear Wave Velocity, $V_s$ | | • small strain stiffness ($G_{max}$)<br>• total mass density ($\rho_{tot}$)<br>• void ratio ($e_o$) |

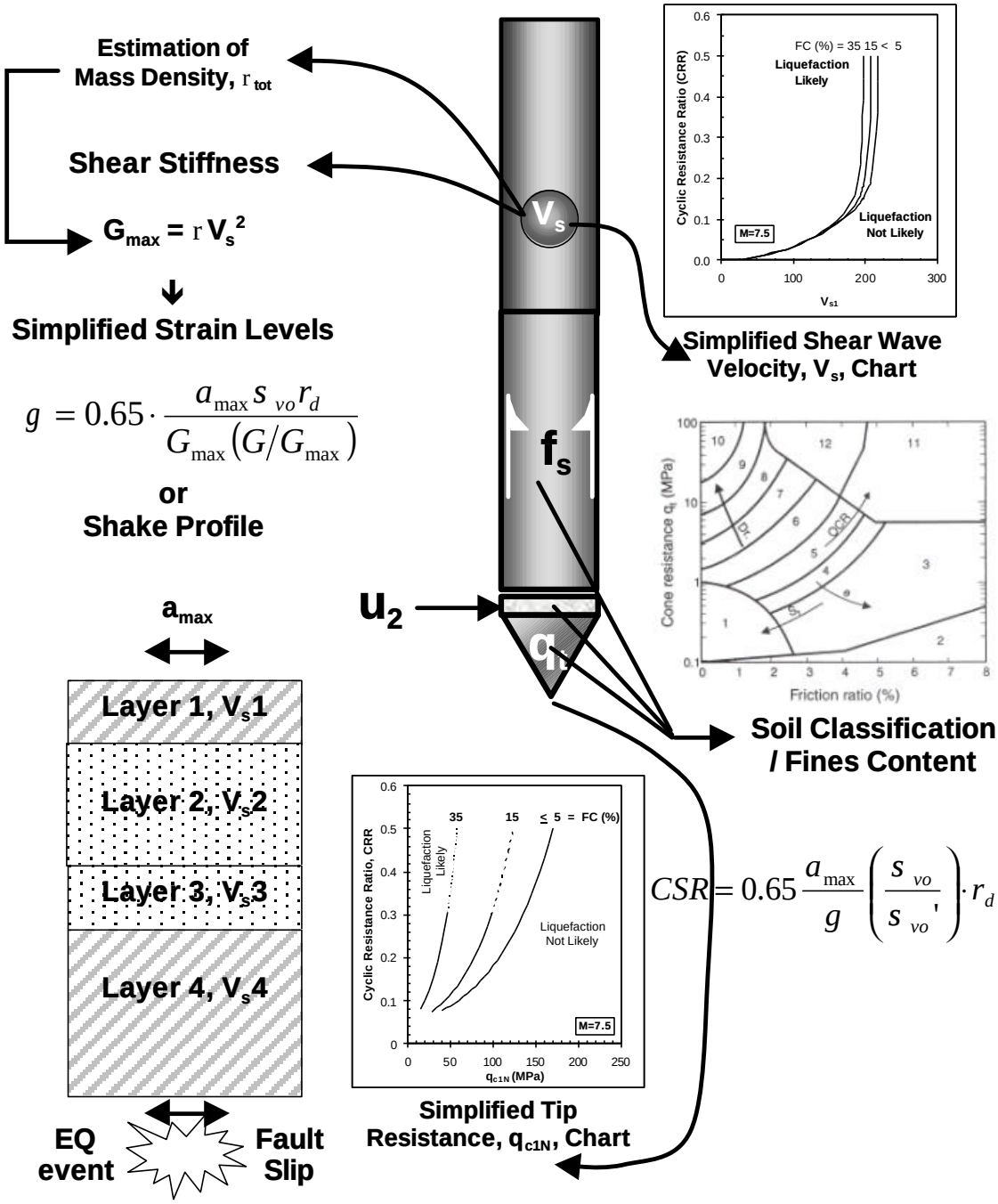


**Figure 2.6. Seismic Piezocone Parameters used for Earthquake Analysis of Soil**

- Soil type and stratigraphy ($q_t$, FR, $u_2$);
- Liquefaction susceptibility from direct analysis ($q_c$ and $V_s$);
- Estimations of properties for rational analysis ($\phi'$, $D_r$, OCR, $K_o$).

Of additional concern in liquefaction studies is the presence of thin clay layers that may prevent dissipation of pore pressures in a sand layer during earthquake shaking. CPT tip resistance is influenced by the properties of soil ahead and behind an advancing cone. This value is an averaged property effected by material up to about 0.6 m ahead of an advancing cone and up to 1.5 m radially, depending upon soil stiffness. The sleeve friction measurement is an averaged property as well, due to the sleeve length (134 mm to 164 mm) and properties of the cylindrical expanding cavity of soil which controls the reading. Penetration pore pressure measurements are a more localized reading which have a quicker response to changes in soil type. A sharp increase in this measurement above hydrostatic pore pressures should provide a more reliable indicator of thin clay seems, as long as the pore pressure elements are properly saturated. The $u_2$ position behind the shoulder is a more reliable reading to locate clay seems, since compression of the $u_1$ mid-face element may lead to high pore pressures in dense sand layers.

2.4.1 Shear Wave Velocity and Stiffness

The shear wave velocity ($V_s$) is a fundamental property that can be used to determine the small strain shear modulus, $G_{max}$, of the soil:

$$G_{max} = r \cdot V_s^2 \qquad (2.3)$$

where $\rho = \gamma_t/g$ = mass density, $\gamma_t$ is the total unit weight, and g is the acceleration due to gravity = 9.8 m/s$^2$. The mass density of saturated geomaterials can be estimated as a function of shear wave velocity and depth (z) for the determination of shear modulus (Mayne et al., 1999):

$$r \approx 1 + \frac{1}{0.614 + 58.7(\log z + 1.095)/V_s} \qquad (2.4)$$

with z in meters and $V_s$ in m/s.

There are a number of different lab and field methods that can be used to determine shear wave velocity (Campanella, 1994). Field measurements of shear wave velocity include the crosshole test (CHT), downhole test (DHT), suspension logging, seismic reflection, seismic refraction, and spectral analysis of surface waves (SASW). In the laboratory, low-strain measurements of shear modulus (where $V_s = \sqrt{G/r}$ ) can be determined from the resonant column (RC), torsional shear (TS), piezoelectric bender elements, as well as triaxial apparatus with internal local strain measurements. Woods (1994) provides a review of laboratory testing methods for determining $V_s$. Figure 2.7 graphically displays various methods used to determine shear wave velocity. Shear waves obtained in this study consisted of pseudo-interval analysis of downhole shear wave velocity arrival times from successive events made at one-meter depth intervals. This method is described in more detail in Campanella et al. (1986) and Appendix III.

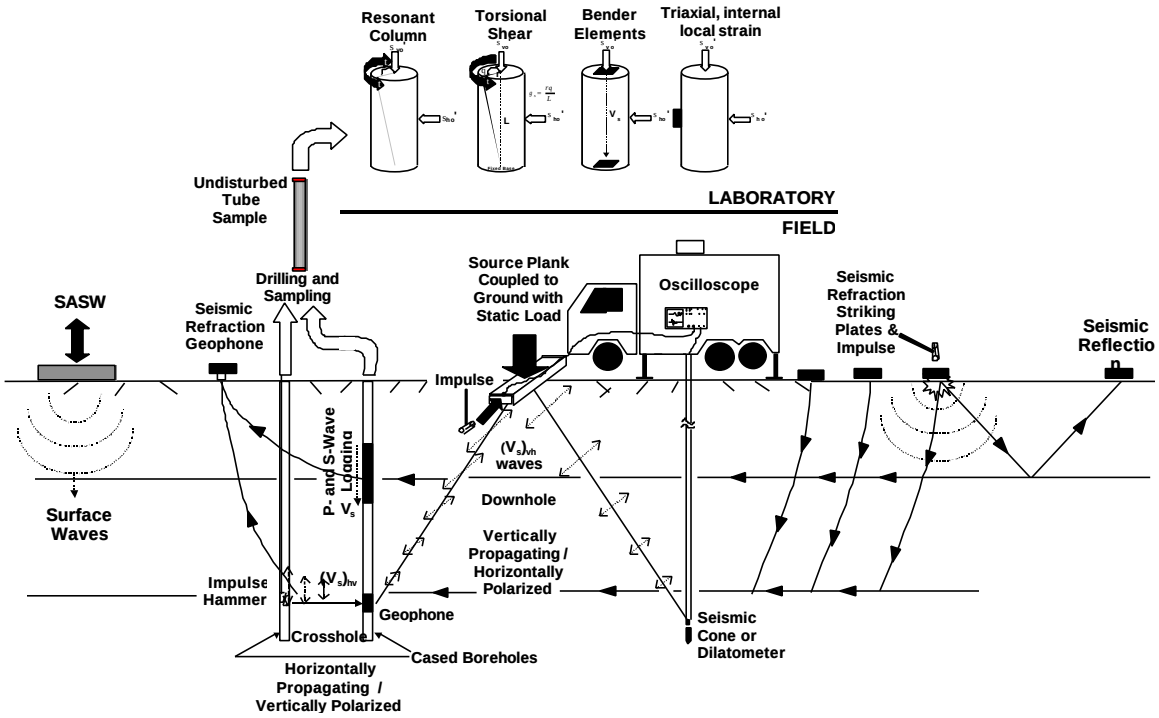


**Figure 2.7. Field and Laboratory Methods to Determine Shear Wave Velocity**

For plane waves, the shear strain ($\gamma_s$) is defined as the ratio of peak particle velocity ($\dot{u}$), to shear wave velocity:

$$g_s = \frac{\dot{u}}{V_S} \qquad (2.5)$$

At very small strains, particle motion resulting from propagation of shear waves is nondestructive. As $\gamma_s$ increases past the elastic threshold shear strain, $\gamma^e_{th}$ (Dobry et al., 1982), the shear modulus will decrease from the maximum small strain value, $G_{max}$. In-

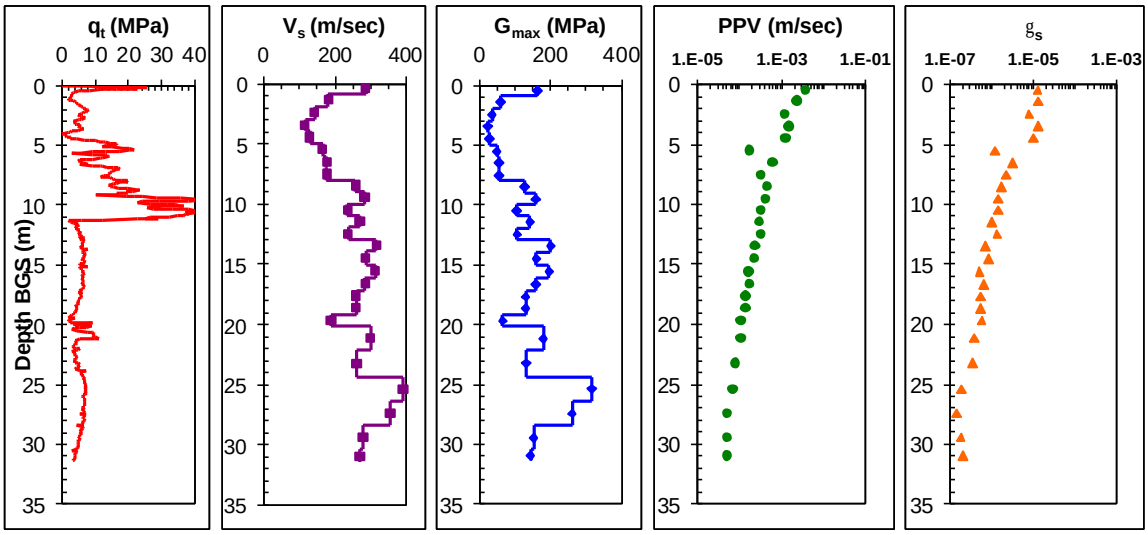


**Figure 2.8. Dynamic Properties Determined from Seismic Piezocone Sounding at Shelby Farms, Shelby County, TN**

situ tests are commonly assumed to be small strain events ($\gamma_s < \gamma^e_{th}$), and the measurement of shear wave velocity will be directly related to the maximum shear modulus.

A set of processed SCPTu results can be obtained to determine dynamic soil properties. Figure 2.8 displays dynamic soil properties determined from a seismic piezocone sounding including: shear wave velocity ($V_s$), small strain shear modulus ($G_{max}$), peak particle velocity (PPV = $\dot{u}$ ), and corresponding shear strain (Eq. 2.5).

As strian levels increase, the shear modulus degrades from its maximum value. This relationship is often expressed as a normalized value ($G/G_{max}$). Intermediate-strain level properties of Memphis area sands were determined from laboratory tests using the resonant column device (Hoyos et al., 1999). The importance of elastic threshold strain and modulus reduction will be presented later in Chapter 4 when discussing the cyclic strain method. There are a number of empirical modulus reduction curves for

representing the dynamic loading of soils (e.g., Vucetic & Dobry, 1991). Ishibashi (1992) presented data to reinforce the dependence of elastic threshold shear strain of granular soils on confining stress. Figure 2.9 displays several relationships including: Vucetic & Dobry curve for nonplastic soils, Ishibashi curves based on confining stress, laboratory resonant column data for Memphis sands, and the modified hyperbolic model used in this study. For the data on Memphis area sands, the resonant column test stage carried out to intermediate strain levels was performed at 200 kPa . These data match well with the Ishibashi curve for a 200 kPa confining stress. The critical layers for liquefaction assessment are anticipated to exist at stress levels between 50 kPa and 200 kPa. A modified Hardin-type hyperbolic equation (Hardin & Drnevich, 1972) was determined for modulus reduction to be used in this study:

$$G/G_{\max} = \frac{1}{1+\left(\frac{g}{g_r}\right)^n} \qquad (2.6)$$

where the reference strain $\gamma_r$ was selected as 0.01 percent and the exponent (n) was selected as 0.8 to best fit the average of the Ishibashi (1992) curves for effective confining stresses of 50 kPa and 200 kPa.

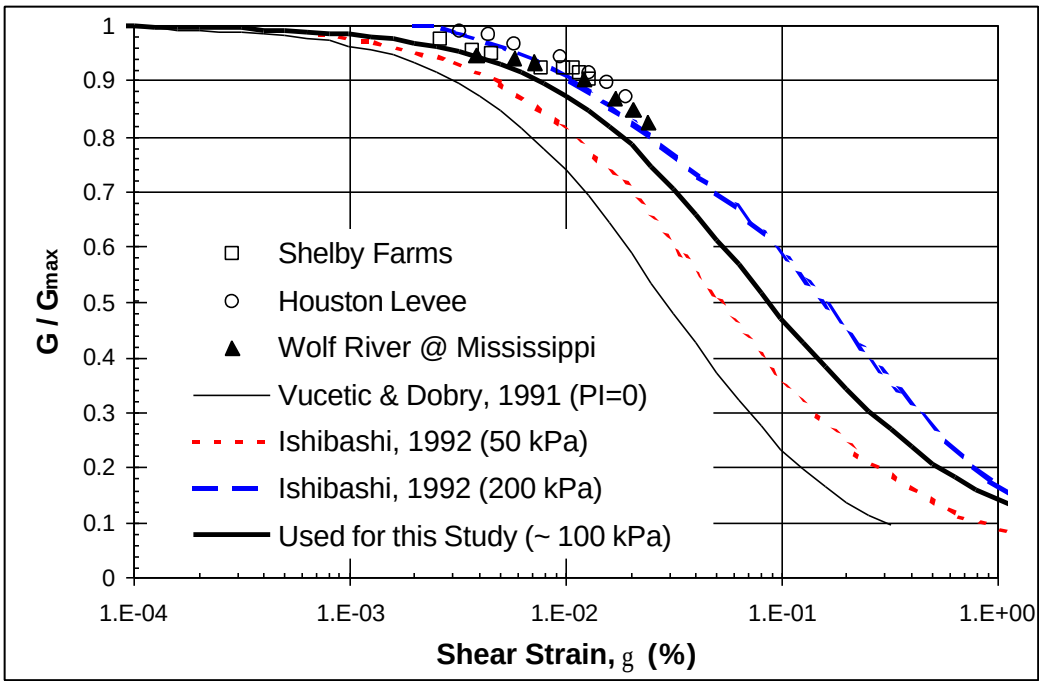


**Figure 2.9. Shear Modulus Reduction Schemes with Increasing Strain**

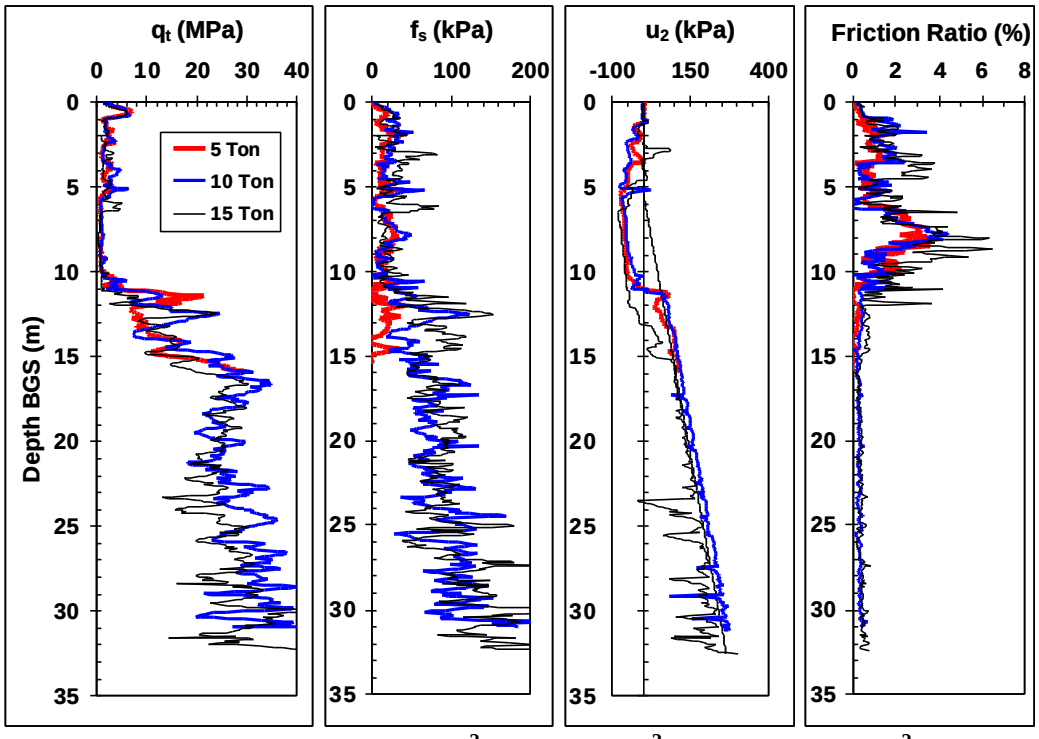


**Figure 2.10. Comparison of 5T (10 cm$^2$), 10T(10 cm$^2$), and 15T (15 cm$^2$) Hogentogler electronic cones at 3MS617 Site (Blytheville, AR)**

2.4.2 Comparison of Penetrometers

Standard cones have a diameter of 35.7-mm (10-$cm^2$ tip surface area; ASTM D5778), but more rugged 43.7-mm diameter cones (15-$cm^2$ tip surface area) have been developed for denser sands. Higher capacity load cells are typically associated with larger diameter cones, thus less precision may be available from larger diameter penetrometers.

Load cell size, pore pressure filter location, as well as equipment diameter may have slight effects on penetrometer readings. Sleeve friction measurements may be obtained from tip load subtracted from a total load (cone & sleeve) measurement, as in a subtraction-type cone, or alternatively $f_s$ can be recorded as an independent measurement. Due to the order of magnitude difference in these measurements, it will be desirable to have independent load cells for tip and sleeve friction measurements. Each of the penetrometers used in this study had a subtraction cone load cell geometry. Load cell resolution is typically expressed as a percentage of full-scale output (ASTM D5778), so increased precision will result from a load cell with a lower maximum capacity.

Figure 2.10 displays three side-by-side soundings performed at a paleoliquefaction site in Blytheville, AR. This figure compares the output of a 5-tonne 10 $cm^2$ cone, to a 10-tonne 10 $cm^2$ cone, to a 15-tonne 15 $cm^2$ cone. The 10-tonne and 15-tonne cone soundings were ended at just over 30 m depth, while the 5-tonne cone sounding was terminated at 15 m to prevent any potential damage to the cone. Data from the three soundings compare very well, considering minor variances due to the local heterogeneity of Mississippi River Valley braided bar deposits. For liquefaction evaluation, we are primarily concerned with finding loose sand deposits below the groundwater table.

Dense sands, gravel, and potentially hard cemented layers evident in the Mississippi Valley and surrounding areas necessitate the use of a robust penetrometer.

As shown in Figure 2.3, the pore pressure filter may be located mid-face, $u_1$, or behind the tip, $u_2$. Pore pressure measurements taken at $u_2$ position are typically high positive values in intact clays and hydrostatic in clean sands. In stiff fissured clays as well as Piedmont residual silts, negative pore pressures up to one atmosphere have been observed below the water table. At the mid-face location, penetration pore pressures are always positive and larger than the $u_2$ readings.

Piezocone soundings with pore pressure measurements taken mid-face (10 $cm^2$ cone) and behind the tip (15 $cm^2$ cone) were performed side-by-side at the I-155 bridge site in

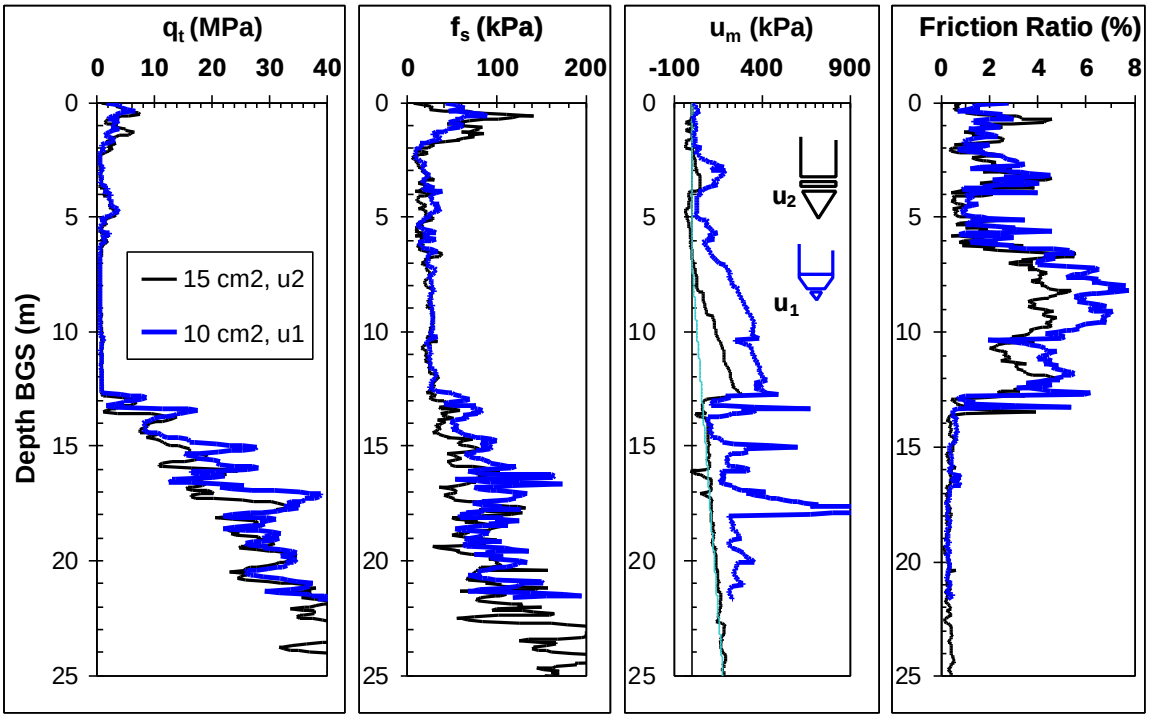


**Figure 2.11. Comparison of $u_1$ and $u_2$ Piezocone Tests at I-155 Bridge (Caruthersville, MO)**

Caruthersville, MO. Figure 2.11 displays the two soundings for comparison. Three lines are shown in the pore pressure chart in Figure 2.11: Hydrostatic ($u_o$, thin line), $u_2$ penetration porewater pressures (thicker line), and $u_1$ penetration porewater pressures (thickest line). The soil profile consists of a loose sandy layer at the surface (0 to 0.5 m), a silty soft clay layer (0.5 to 4 m), a loose sand layer (4 to 5 m), a soft clay layer (5 to 13 m), and a sand layer with a clay seam at 14 .5 m (13 m to 25 m at end of test). The pore pressure response at the $u_2$ position was negative to slightly positive in the clay layers above the water table, and slightly negative in the loose sand within the capillary zone. There was a response above hydrostatic in the soft clay layer, which dropped to hydrostatic in the sand layer. The pore pressure response at the $u_1$ position was always positive and greater than the readings at $u_2$ position. Below 12.8 m (clayey soils), the $u_2$ readings were about 56 percent of the $u_1$ readings.

2.4.3 Stress Normalization

Since strength and stiffness properties of soils are controlled by effective confining stress, stress-normalization factors are needed to relate the parameters over a range in depths. Typical normalization schemes for the SPT N-value and CPT parameters are presented in Table 2.3 and 2.4, respectively. Typical normalization schemes for shear wave velocity data ($V_s$) are presented in Table 2.5. These factors are presented for the SPT, CPT, and shear wave velocity, to show similarities in the development of the methods. The general equation for stress normalized parameters can be expressed as:

$$M_1 = C_M \cdot M \qquad (2.7)$$

where $M_1$ is the in-situ test measurement normalized to an effective vertical confining stress equal to one atmosphere (e.g., $N_1$, $q_{c1}$, $V_{s1}$). It is noted that 1 atm = $p_a$ = $\sigma_a$ = 1 bar ≈ 100 kPa ≈ 1 tsf. The coefficient $C_M$ is the stress correction factor for the normalization scheme (e.g., $C_N$, $C_q$, $C_V$) and M is the corrected measured in-situ property (e.g., $N_{60}$, $q_t$, $V_s$).

Most overburden normalization schemes take on a form similar to:

$$C_M = 1 / (\sigma_{vo}')^n \tag{2.8}$$

where $\sigma_{vo}'$ is the effective overburden stress in atmospheres, and *n* is a stress exponent that may be density dependent (e.g., Seed et al., 1983), soil type dependent (e.g., Olsen, 1988; Robertson & Wride, 1997), or dependent upon soil type and stiffness (Olsen & Mitchell, 1995). These terms go to infinity as effective overburden stress approaches zero. To account for this, some schemes incorporate an arbitrary maximum correction (e.g., $C_N \leq 2$; Robertson & Wride, 1997), while others have adapted the following form (Skempton, 1986; Shibata & Teparaksa, 1988; Kayen et al., 1992):

$$C_M = \frac{a/b + 1}{a/b + s_{vo}'} \tag{2.9}$$

where $\sigma_{vo}$' is the effective overburden stress in atmospheres, and *a/b* is an empirical parameter varying between 0.6 and 2.0 and relating to the consistency (e.g., $D_r$) and stress history (OCR) of the sand. This format matches well for sandy soils (n = 0.5 to 0.7) and does not reach infinite values at zero effective confining stresses.

Figure 2.11 displays a comparison of normalized SCPTu measurements at the I-155 bridge site in Caruthersville, MO. The problem of the stress exponent normalization using a power function reaching extreme values of $q_c$ and $V_s$ at low overburden stresses is observed. Minor differences are also noticed in the friction ratio of soft clays between the depths of 7 and 13 m. This results from the utilization of net cone tip resistance ($q_t$ - $\sigma_{vo}$) in the Wroth (1984) scheme, and measured tip resistance in the Olsen (1988) scheme. Utilization of net tip resistance is fundamentally correct and necessary in clays, but is often insignificant and neglected in sands.

**Table 2.3. Overburden Normalization Schemes for SPT N-value**

| Corrected Measured Parameter | Normalized Parameter, $(N_1)_{60}$ | Soil Type | Reference |
|---|---|---|---|
| $N_{60}$ | $N_{60} / (\sigma_{vo}')^{0.55}$ | Sand $D_R$=40-60% | Seed et al., 1983 |
| | $N_{60} / (\sigma_{vo}')^{0.45}$ | Sand $D_R$=60-80% | Seed et al., 1983 |
| | $N_{60} / (\sigma_{vo}')^{0.56}$ | Sand | Jamiolkowski et al., 1985a |
| | $N_{60} \cdot (1/\sigma_{vo}')^{0.5}$ | Sand | Liao & Whitman, 1986 |
| | $2 \cdot N_{60} / (1 + \sigma_{vo}')$ | Med. Dense Sand | Skempton, 1986 |
| | $3 \cdot N_{60} / (2 + \sigma_{vo}')$ | Dense Sand | Skempton, 1986 |
| | $1.7N_{60}/(0.7 + \sigma_{vo}')$ | OC Fine Sand | Skempton, 1986 |
| | $N_{60} / (\sigma_{vo}')^{n}$ | n=1 clay<br>n=0.7 loose sand<br>n=0.6 sand | Olsen, 1997<br>Olsen, 1994 |

**Table 2.4. Overburden Normalized CPT Parameters**

| Corrected Measured Property | Normalized Parameter | Soil Type | Reference |
|---|---|---|---|
| Tip Stress, $q_t$ | $q_t / (\sigma_{vo}')^n$ | n=1.0 clay<br>n=0.83 silt mixture<br>n=0.66 sand mix<br>n=0.6 clean sand | Olsen, 1988 |
| | $(q_t - \sigma_{vo}) / \sigma_{vo}'$ | Clay | Wroth, 1988 |
| | $1.7q_t/(0.7 + \sigma_{vo}')$ | Sand | Shibata & Teparaksa, 1988 |
| | $q_t / (\sigma_{vo}')^{0.72}$ | Sand | Jamiolkowski et al., 1985a |
| | $q_t \cdot (p_a/\sigma_{vo}')^{0.5}$ | Sand | Mayne & Kulhawy, 1991 |
| | $1.8q_t/(0.8 + \sigma_{vo}')$ | Sand | Kayen et al., 1992 |
| | $(q_t - \sigma_{vo}) / (\sigma_{vo}')^c$ | c=1.0 soft / loose<br>c=0.75 medium<br>c=0.55 dense<br>c = 0.35 dense / OC<br>c=0.15 very dense / heavily OC | Olsen & Mitchell, 1995 |
| | $q_t / (\sigma_{vo}')^n$ | n=0.5 Sand<br>n=0.75 Silty Sand | Robertson & Wride, 1997 |
| | $(q_t - \sigma_{vo}) / \sigma_{vo}'$ | FC > 35 | Robertson & Wride, 1997 |
| Friction Ratio $FR = f_s/q_t \cdot 100$ | $\frac{f_s}{q_t} \frac{1}{(s_{vo}')^{(1-n)}} \cdot 100$ | n is the soil type dependent CPT $q_{c1}$ exponent, see CPT | Olsen, 1988 |
| | $f_s / (q_t - \sigma_{vo})$ | Clay | Wroth, 1988 |
| $u_2$ | $B_q = \frac{(u_2 - u_o)}{(q_t - s_{vo})}$ | All | Senneset et al., 1982 |

$\sigma_{vo}'$ is the effective confining stress in atmospheric units
$q_t$ is the CPT tip stress corrected for unequal end area ratio, in atmospheric units
$f_s$ is the cone sleeve friction, in atmospheric units
$u_2$ is the penetration porewater pressure taken behind the tip, in atmospheric units

**Table 2.5. Field- and Laboratory-Based Overburden $V_s$ Normalization Exponents**

| Soil | Normalization Exponent, n $C_V = (P_a / \sigma_{vo}')^n$ | Shear Wave Test Setup | Reference |
|---|---|---|---|
| Sand | 0.33 | SASW | Tokimatsu et al., 1991 |
| Sand | 0.25 | DHT | Robertson et al., 1992b |
| Alaska Sand | 0.23 | DHT | Fear & Robertson, 1995 |
| Intact and Fissured Clays | 0.56 | CHT, DHT, SASW | Mayne & Rix, 1993 |
| All Soils | $n_{qc}/2$; where n is the soil type specific stress exponent from Olsen, 1988 | Field Data | Olsen, 1994 |
| Loose Dry Sand | 0.36 | BE | Hryciw & Thomann, 1993 |
| Dense Dry Sand | 0.195 | BE | Hryciw & Thomann, 1993 |
| Sensitive Clay | 0.62 | RC | Shibuya et al., 1994 |
| Kaolinite | 0.235 | BE | Fam & Santamarina, 1997 |
| Bentonite | 0.443 | BE | Fam & Santamarina, 1997 |
| Silica Flour | 0.33 | BE | Fam & Santamarina, 1997 |
| Simple cubic packing | 0.167 | Lab | Santamarina & Fam, 1999 |
| Mica | 0.28 to 0.38 | RC | Santamarina & Fam, 1999 |
| Cemented Sand | 0.02 | RC | Santamarina & Fam, 1999 |
| Reconstituted Memphis Sands | 0.25 to 0.275 | RC | This Study |
| Nonplastic undisturbed specimens | 0.27 | RC | Stokoe et al., 1999 |
| Undisturbed NC specimens with plasticity | 0.24 | RC | Stokoe et al., 1999 |
| Shallow undisturbed heavily OC specimens with plasticity | 0.07 | RC | Stokoe et al., 1999 |

SASW - spectral analysis of surface waves
DHT - Downhole test
CHT - Crosshole test
RC - Resonant Column
BE - Bender elements
$\sigma_{vo}'$ is the effective confining stress in atmospheric units

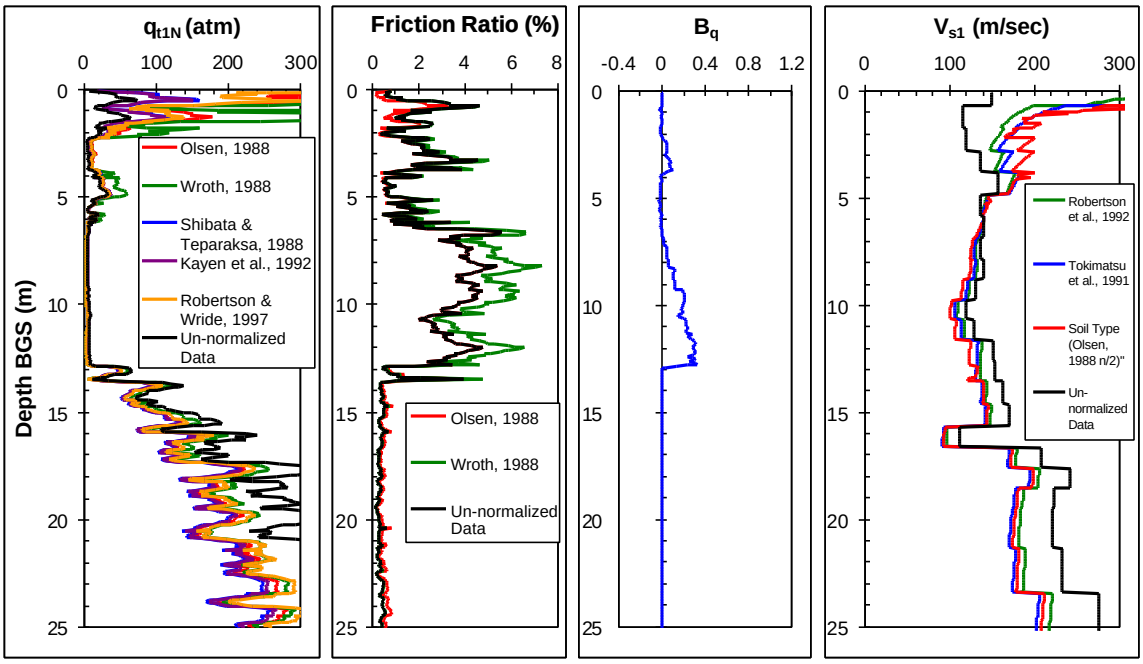


**Figure 2.11. Normalized Parameters from I-155 Bridge Data (Caruthersville, MO)**

2.4.4 Soil Classification

Liquefaction response of soils depends strongly on soil type. Since there are no samples obtained by cone penetration testing, soil type and fines content must be estimated using correlations instead of visual examination and laboratory index testing. Soil behavior charts have evolved over the years and reviews of various classification methods are given in Douglas and Olsen (1981) and Kulhawy and Mayne (1990). Figure 2.12 displays both the Robertson et al. (1986) and overburden stress normalized Robertson (1990) classification charts. Figure 2.13 displays the normalized Olsen & Mitchell (1995) classification charts.

For this study, classification schemes were not used in their typical sense. Discrepancies noticed between classification methods (e.g., $q_t$ vs. FR and $q_t$ vs. $B_q$) led to a lack of confidence in current methods, so a hybrid method involving tip resistance, pore pressure, sleeve friction, as well as shear wave velocity was undertaken.

The hybrid method involved determination of layering by looking for distinct changes in one or more parameters. While shear wave velocity is not indicative of soil type, the soil stiffness will be paramount for liquefaction and site amplification analyses and thus important for layering. Side-by-side plots of tip resistance, friction ratio, pore water pressure, and shear wave velocity will provide insight into soil stratigraphy. Sharp changes in one or more parameters were noted as a change in density, stiffness, and/or soil type, and thus a soil layer. Classification was based primarily upon the Robertson et al. (1986) charts, which use the matched set of $q_t$, FR, and $B_q$ parameters from each depth. It should be noted that the zone of influence for each of the readings is

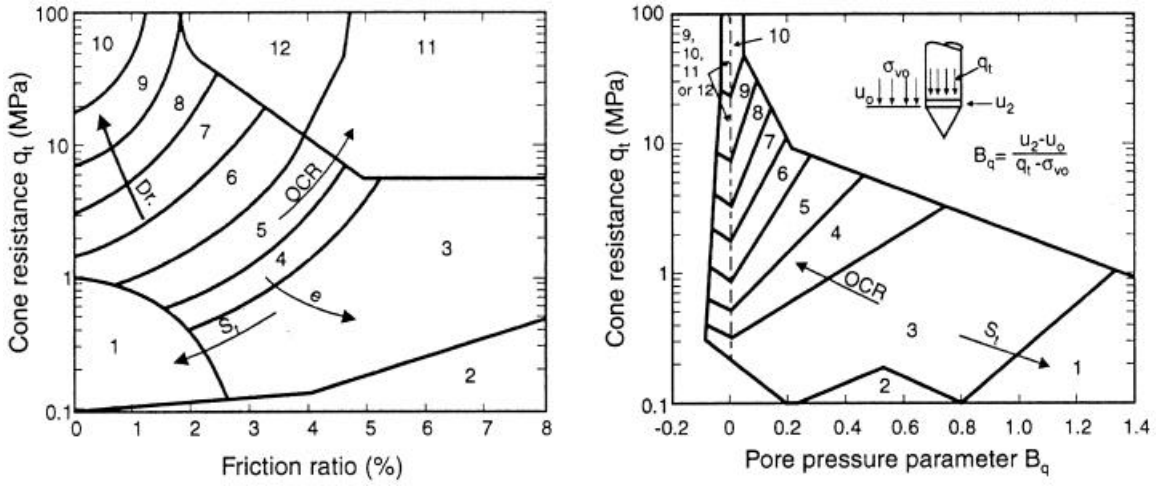


**Soil Behavior Type (Robertson et al.,1986; Robertson & Campanella, 1988)** **a.**

| | | |
|---|---|---|
| 1 – Sensitive fine grained | 5 – Clayey silt to silty clay | 9 – sand |
| 2 – Organic material | 6 – Sandy silt to silty sand | 10 – Gravelly sand to sand |
| 3 – Clay | 7 – Silty sand to sandy silt | 11 – Very stiff fine grained* |
| 4 – Silty clay to clay | 8 – Sand to silty sand | 12 – Sand to clayey sand* |

** Overconsolidated or cemented*

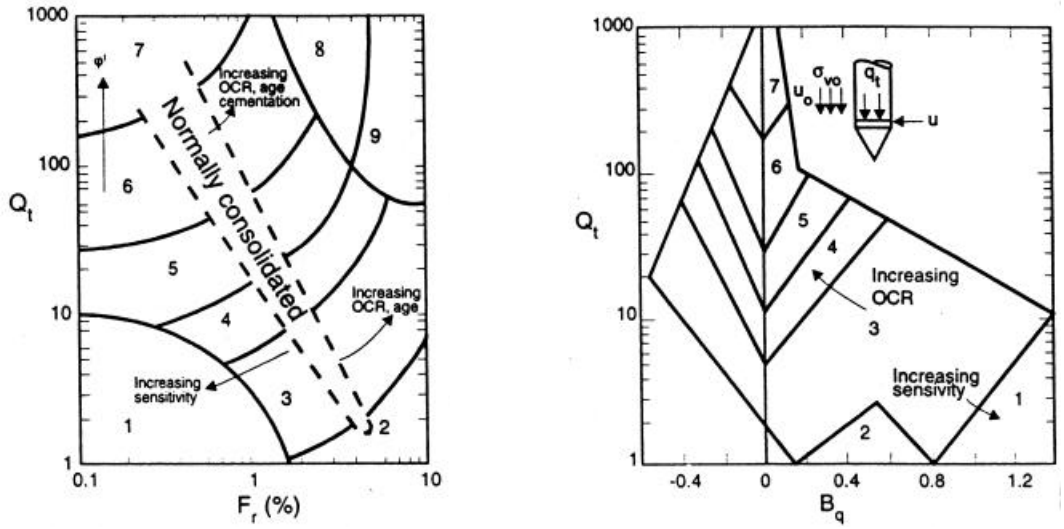


**Soil Behavior Type (Robertson, 1990)** **b.**

| | | |
|---|---|---|
| 1 – Sensitive fine grained | 4 – Clayey silt to silty clay | 7 – Gravelly sand to sand |
| 2 – Organic soils-peats | 5 – Silty sand to sandy silt | 8 – Very stiff sand to clayey sand |
| 3 – Clay-clay to silty clay | 6 – Clean sand to silty sand | 9 – Very stiff fine grained |

**Figure 2.12. CPTu Soil Classification Charts (a) Robertson et al., 1986 (b) Robertson, 1990**

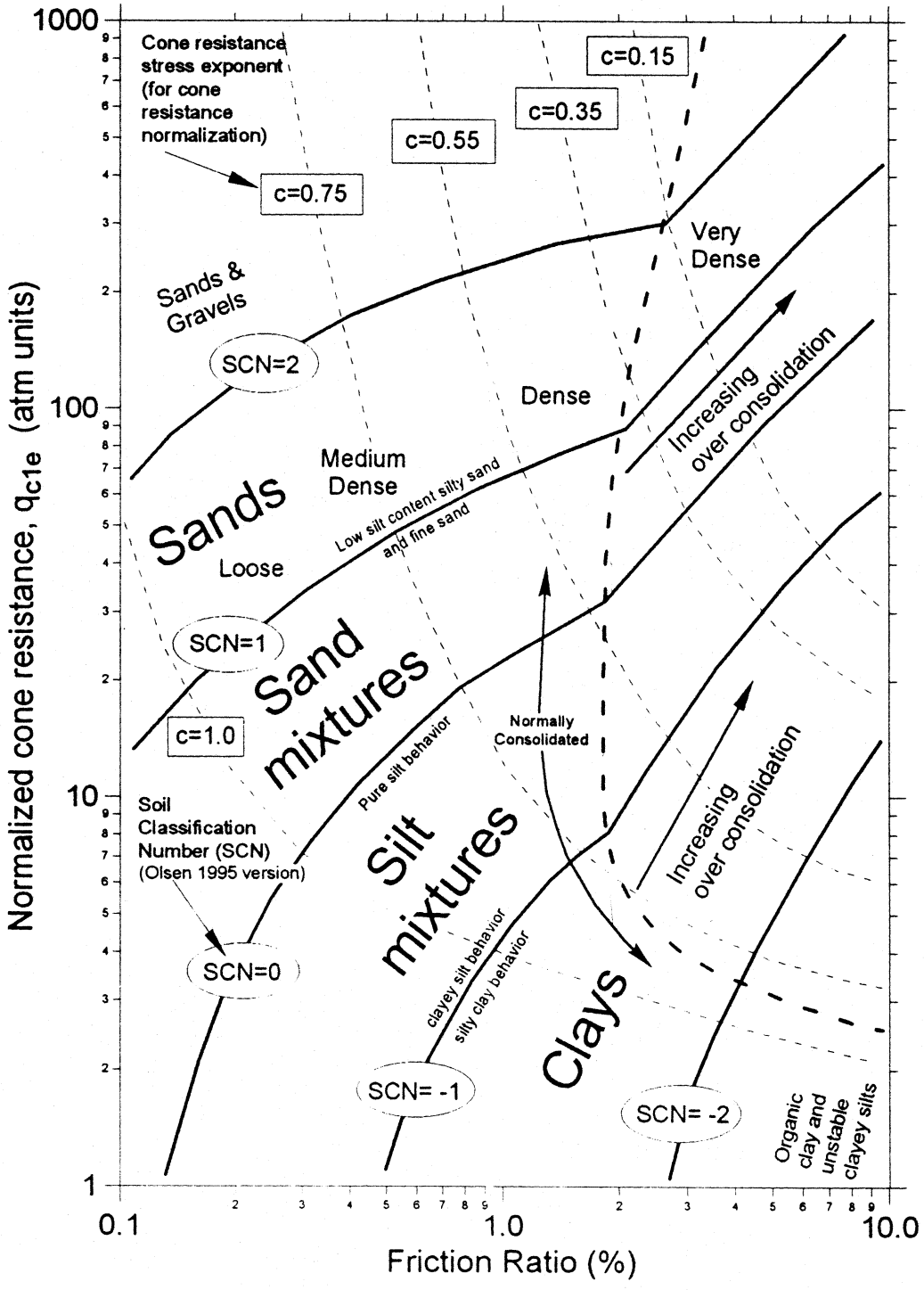


**Figure 2.13. Olsen & Mitchell (1995) Normalized Classification Chart**

different, which should be taken into consideration when determining layering profiles. Figure 2.14 displays four channels of data collected at a site in West Memphis, AR. This site was adjacent to a logged borehole with laboratory index testing at certain layers. Table 2.6 presents laboratory determined values of fines content as well as those estimated from empirical relations. Table 2.7 presents the manual visual classification, the visual method chosen for this study based on the Robertson et al. (1986) FR and $B_q$ charts, the Olsen & Mitchell (1995), as well as the Robertson (1990) normalized charts.

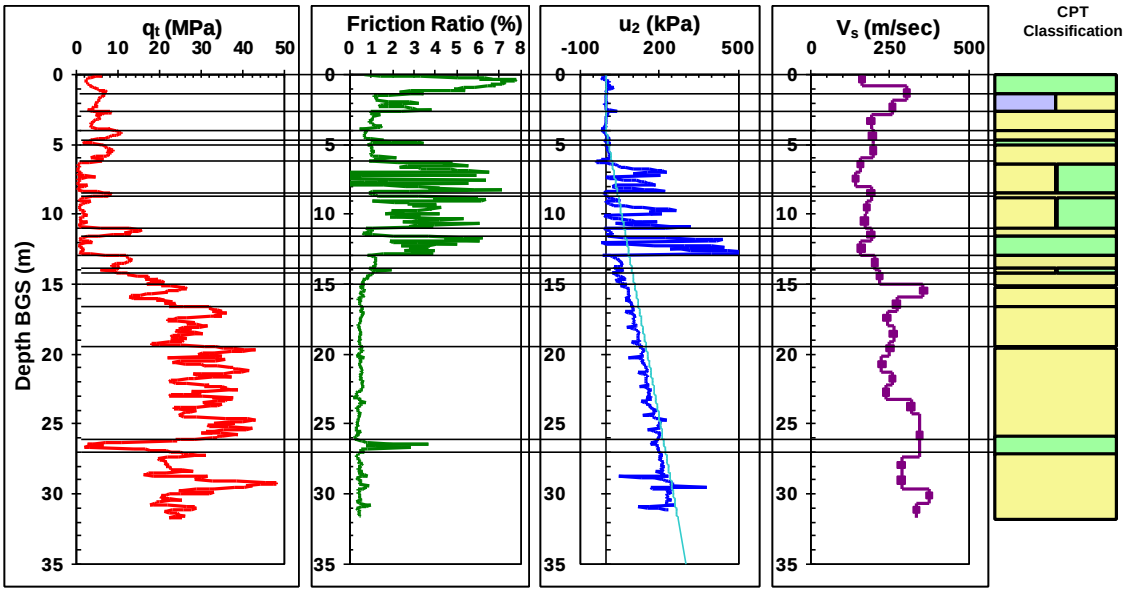


**Figure 2.14. Layering from SCPTu data at Monople Tower (W. Memphis, AR)**

As can be seen from Figure 2.14, the four channels of SCPTu data provide excellent stratagraphic detail for potential soil behavior, and good agreement with visual methods after about 2 m depth for normalized methods. Additional factors such as mineralogy, depositional environment, age, fabric, particle texture, stress state, pore fluid, plasticity,

and cementation may affect each reading to a certain degree. When trying to relate soil type to laboratory determined fines content, the results presented in Table 2.6 do not show good agreement. The Robertson & Wride (1997) fines content used the suggested best fit trend, but their range of trends show scatter that could result in up to a $\pm$ 15 discrepancy at a constant soil behavior index. The data presented in Suzuki et al. (1995) were from Japanese sites ($n \approx 100$ points), which resulted in a correlation coefficient, $r^2$, of about 0.69 for the correlation used. Additional scatter would likely arise when incorporating different penetrometers in different geologies, as shown by Arango (1997). Comparing a field measurement under in-situ stress conditions will likely not resemble a laboratory value taken on a dis-aggregated, remolded, oven dried specimen. Therefore CPT classification will likely resemble soil behavior type related to strength characteristics, rather than index soil type based on grain characteristics. The clean sand curve will be most conservative for a liquefaction evaluation, and can provide a preliminary estimation of liquefaction resistance for screening purposes if fines content is not known. It is recommended that companion borings be performed at sites where fines

**Table 2.6. Comparison of Empirical CPT Fines Content Predictions to Laboratory Index Testing Results at W. Memphis, AR site**

| Depth (m) | Laboratory Measured[1] | Average value from Robertson & Wride, 1997 | Average value from Suzuki et al., 1995 |
|---|---|---|---|
| 1.8 - 2.3 | 71 | 18 | 38 |
| 2.6 - 3.0 | 7 | 14 | 21 |
| 4.1 - 4.6 | 3 | 9 | 13 |
| 5.6 - 6.1 | 21 | 17 | 25 |

[1] Material passing No. 200 sieve from recovered drive samples in adjacent boring

**Table 2.7. Comparison of Manual Visual Classification and CPTu Classification Charts for MEMPH-K in West Memphis, AR (Figure 2.14)**

| Depth (m) | Visual Classification | Robertson, 1990[1] $Q_t$ vs. $F_r$ | Robertson, 1990[1] $Q_t$ vs. $B_q$ | Olsen & Mitchell[1], 1995 | Visual based on Robertson et al. (1986) |
|---|---|---|---|---|---|
| 0.30 - 0.75 | Brown clay | Clayey silt to silty clay (5) | Gravelly sand to sand (7) | Silty clay mixture (-0.5 to 0.5) | Clay |
| 1.0 - 1.5 | Brown silty clay | Silty sand to sandy silt (5/6) | Gravelly sand to sand (7) | Sand (2.0 to 1.0) | Clay |
| 1.8 - 2.3 | Brown clayey sandy silt | Silty sand to sandy silt (6/5) | Silty sand to silty clay (6/4) | Sand to sand mixture (0.5 to 1.5) | Silty sand |
| 2.6 - 3.0 | Brown Sand | Silty sand to sandy silt (6/5) | Silty sand to silty clay (6/4) | Sand to sand mixture (0.5 to 1.5) | Silt sand to sand |
| 4.1 - 4.6 | Brown Sand | Silty sand to sandy silt (6/5) | Silty clay to silty sand (4/6) | Sand (1.0 to 1.5) | Sand |
| 5.6 - 6.1 | Brown and gray clayey sand | Silty sand to sandy silt (6/5) | Clayey silt to silty clay (4) | Sand mixture (0.5 to 1.0) | Sand |
| 7.1 - 7.6 | Brown sand to gray clay | Clay to sandy silt (3/4/5) | Clay to silty clay (3/4) | Clay to sand (-2.0 to 1.2) | Sandy clay (layered) |
| 8.7 - 9.1 | Gray clayey silt | Silty clay to sandy silt (3/4/5) | Clayey silt to silty clay (4) | Clay to sand (-1.8 to 1.1) | Sand to sandy clay (layered) |
| 10.2 - 10.7 | Gray clayey silt | Silty clay to clayey silt (3/4) | Silty clay to clayey silt (3/4) | Clay mixture (-1.7 to 0) | Sandy clay to sand (layered) |
| 11.7 - 12.2 | Gray silty clay | Silty clay (3) | Silty clay to clayey silt (3/4) | Clay mixture (-1.7 to 0) | Clay |
| 13.3 - 13.7 | Gray silty sand | Silty sand to sandy silt (5/6) | Clayey silt to silty clay (4) | Sand to sand mixture (1.5 to 0.5) | Sand |
| 14.8 - 15.2 | Gray sand | Sand (6) | Clayey silt to silty clay (4) | Sand to sand mixture (0.5 to 1.5) | Sand |

[1] Numbers in parenthesis represent soil classification zones from appropriate chart as presented in Figures 2.12 (b) and 2.13

content is of concern. The effect of fines content on both liquefaction resistance and penetration test measurements should be considered during analysis.

## 2.5 Summary and Recommendations

The superior repeatability, speed, frequency of measurements, and number of measured parameters obtained from a seismic cone test makes it an optimal test for site characterization studies. Different penetrometers and load cell size did not seem to have a significant effect on the accuracy of readings in sands of concern. Due to gravel and hard cemented layers, a robust 15 $cm^2$ penetrometer is recommended for CPT soundings in the Mid-America Region.

The position of the piezocone filter provides differing results, with higher readings obtained at the mid-face location. The mid-face filter provided potential information about the location of dense layers. Since $u_1$ penetration porewater pressures in dense sands may be higher than those in soft clays (Fig. 2.11), this adds difficulty to soil stratification using the $u_1$ location. The $u_2$ filter location provides information on hydrostatic water pressure in sands, which allows the depth to the water table to be deduced. Since the location of the water table is of great importance for liquefaction evaluation, it is recommended that the pore water pressure filter be located behind the tip for liquefaction evaluation studies.

The Olsen & Mitchell (1995) normalization scheme based on soil type and consistency matches well with laboratory and field data. To avoid potential errors from normalization, the scheme adapted for each specific analysis method will be utilized.

The primary normalization used in this study are the Robertson & Wride (1997) methods for CPT parameters. For shear wave velocity, a stress exponent of 0.25 will be used for normalization.

Current soil classification schemes (e.g., Robertson et al, 1986; Robertson & Wride, 1997; Olsen & Mitchell, 1995) match well with visual classification methods in Mississippi Valley soils. Normalized methods tend to over predict tip resistance and misclassify soils in the upper 2 meters or so. Uncertainty in sleeve friction measurements leads to potential classification errors, and inaccuracy in fines content estimations. Due to the lack of pore pressure response at the $u_2$ position in sands leads to classification based solely on tip resistance when utilizing $B_q$ charts. Schemes utilizing friction ratio and tip resistance measurements seemed to be more reliable in the Mississippi River Valley, but utilization of all 3 parameters will provide a better indication of soil layering.

# CHAPTER 3

# SEISMIC HAZARDS AND GROUND MOTIONS IN MID-AMERICA

## 3.1 Seismic Hazards

Sandy sites located in proximity to the seismic regions of New Madrid, MO and Charleston, SC may liquefy if ground motions are sufficiently high. In this section, ground motion attenuation relationships are studied to estimate the peak horizontal acceleration at the ground surface ($a_{max}$). This peak ground acceleration (PGA) is used to assess the levels of cyclic shearing.

Two significant sets of events, the 1811-1812 New Madrid series and 1886 Charleston, SC earthquake, have shown that faults in Mid-America are active and can cause widespread damage. Due to lack of seismic considerations during the design of most existing structures in the Central and Eastern United States (CEUS), a severe event may cause considerable damage and loss of life. Studies of site amplification, attenuation relationships, recurrence intervals as well as soil and structural response can provide estimates of seismic risk. The socioeconomic ramifications of a severe event in New Madrid or Charleston, SC will be costly, deadly, catastrophic, and widespread.

The lack of strong motion data in CEUS leads to high uncertainty associated with ground motion studies. Existing seismometer arrays monitor the hypocentral locations of smaller earthquakes that have identified areas of seismic activity. The two main earthquake regions of this study are in different fault systems; therefore the New Madrid,

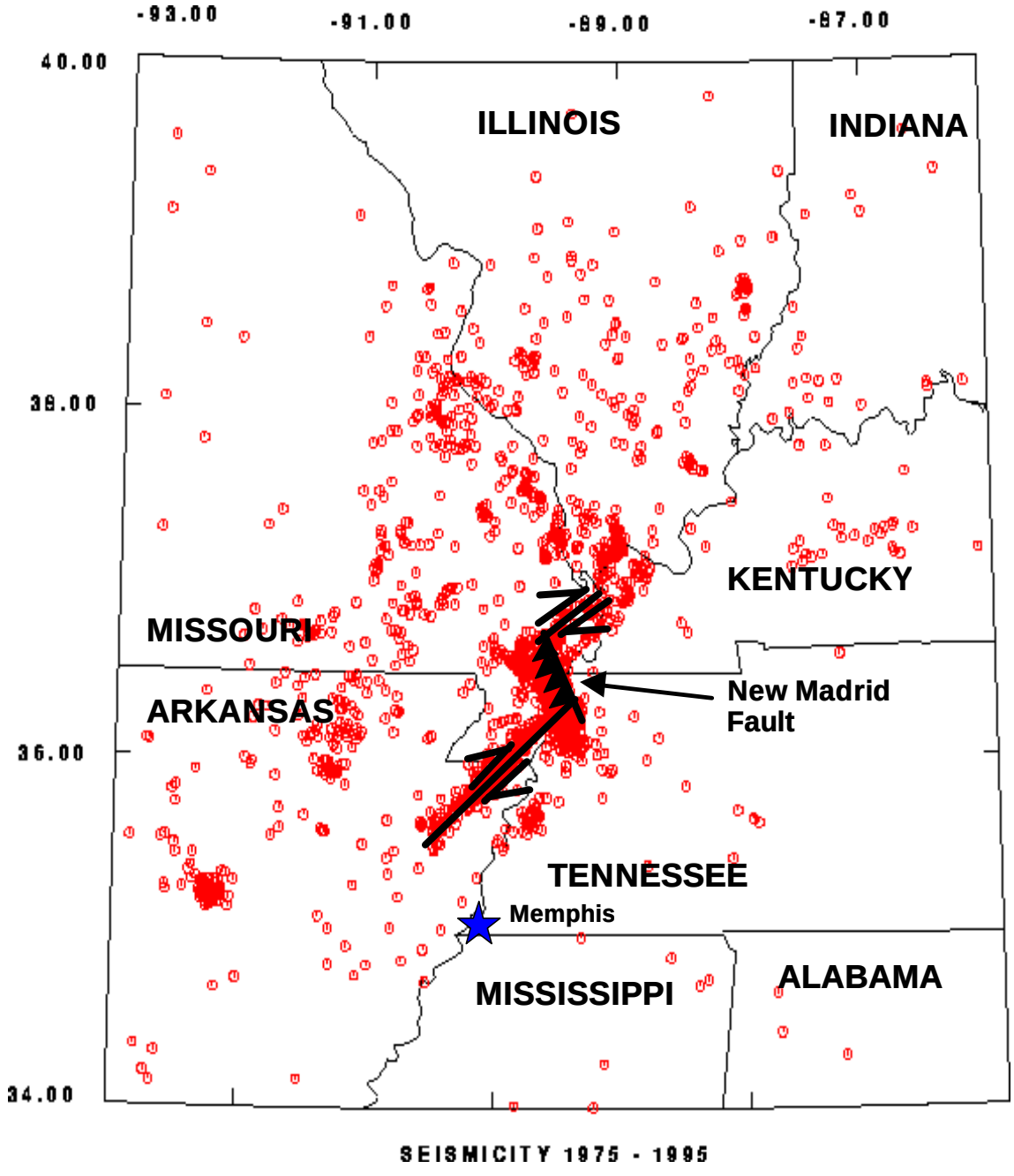


**Figure 3.1. Recent Seismicity (1975-1995) and Fault Structure in NMSZ (adapted from Schweig & VanArsdale, 1996; USGS & USNRC; http://www.eas.slu.edu/Earthquake_Center/newmadrid1975-1995.html)**

MO and Charleston, SC areas will be discussed separately.

3.1.1 New Madrid Seismic Zone (NMSZ)

Primary activity in the New Madrid Seismic Zone (NMSZ) occurs in the Reelfoot Rift system along the New Madrid Fault. The fault system consists of three legs, and has been identified as a left-stepping, right-lateral strike-slip fault zone (Schweig & Van Arsdale, 1996). Figure 3.1 displays recent (1975-1995) seismic activity in the NMSZ with the fault system sketched along areas of high seismicity.

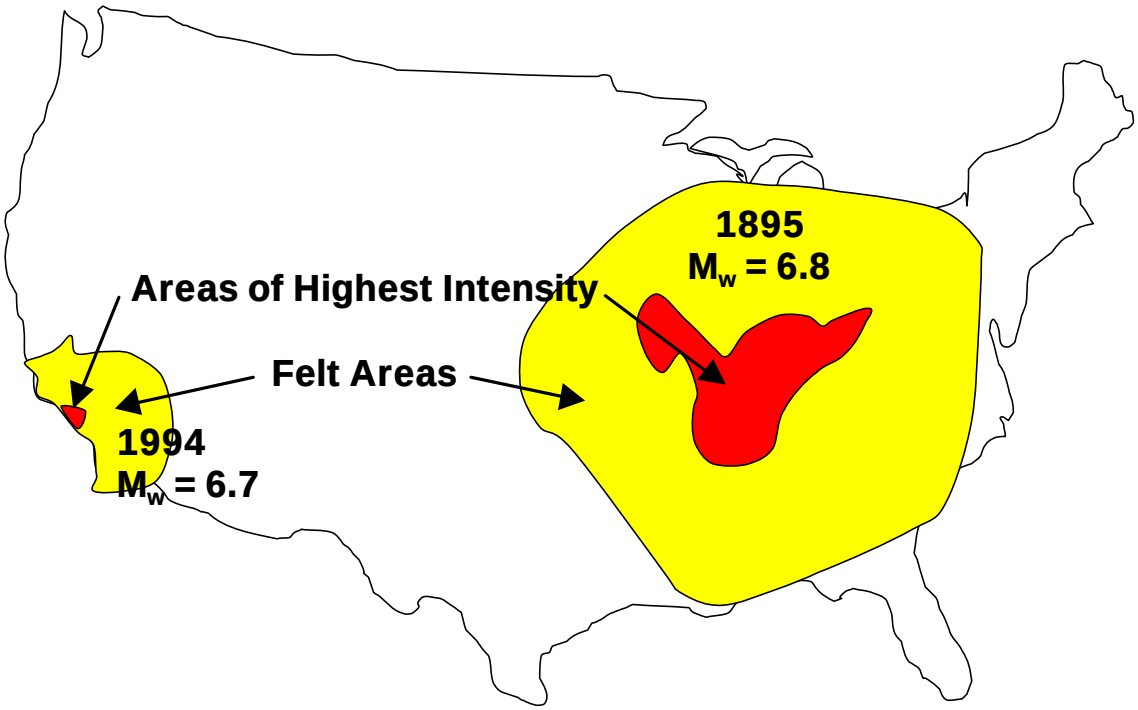


**Figure 3.2. Comparison of Felt Areas for Similar Magnitude Earthquakes in California (Northridge; 1994) and Central United States (Charleston, MO; 1895)**

**Table 3.1. Historic Large Earthquakes in the NMSZ**

| Date | Estimated Moment Magnitude, $M_w$[1] | Longitude[2] | Latitude[2] |
|---|---|---|---|
| December 16, 1811 | 7.9[1] | 35.6[2] | -90.4[2] |
| January 23, 1812 | 7.6[1] | 36.3[2] | -89.6[2] |
| February 7, 1812 | 8.0[1] | 36.5[2] | -89.6[2] |
| October 31, 1895 | 6.8[3] | 37.0[3] | -89.4[3] |

[1] from Johnston & Schweig, 1996 [2] from Stover & Coffman, 1993 [3] Nuttli & Brill, 1981

Over 200 minor events and three major shocks in 1811-1812 caused severe ground damage in the New Madrid, MO area. Table 3.1 presents the moment magnitude, $M_w$, and location of four severe historic events in the New Madrid area. The attenuation of motions in Mid-America are much lower than those on the West Coast, and thus different attenuation relationships will be necessary. Areas at greater distance from the potential fault regions may have a higher earthquake risk than previously anticipated. Current seismic hazard mapping studies (Frankel et al., 1996) utilize a return period of 1000 years for the maximum probable earthquake in the Central United States, but use of sand blow evidence, archeological artifacts, and radiocarbon dating for paleoliquefaction studies in the Mississippi Valley (e.g., Tuttle et al., 1998) have shown the presence of significant earthquakes between the dates of:

- 400 - 600 A.D.;
- 800 - 1000 A.D.;
- 1400 - 1600 A.D.

These events were large enough to cause sand boils and lateral spreading, but the potential short distance to alluvial sand sites could have resulted in high accelerations

from a moderate ($M_w < 7$) event. Determination of probable magnitudes, epicentral locations, and more accurate dating of these events are still ongoing at this time.

3.1.2 Charleston Seismic Region

The earthquake of 1886 in Charleston, SC was primarily a single event, preceded and followed by several days of small tremors (Dutton, 1889). While not as numerous as the shocks from the New Madrid series, the location of the event just west of the city led to increased loss of life and property damage. From historic seismicity, the Charleston fault system appears to be localized into point source areas. It can be inferred from field surveys that there exist at least two intersecting seismological structures composed of northwest trending dikes and faults, and a northeast trending dikes (Bollinger, 1983). Additional information on motion patterns and source mechanisms is available in Bollinger (1977) and Talwani (1982). Figure 3.2 shows historical seismicity in the Charleston area. Table 3.2 displays the magnitude and approximate location of the 1886 Charleston event.

## 3.2 Seismic Ground Hazard Analysis

Earthquake ground motion parameters, such as acceleration and magnitude, need to be evaluated before a liquefaction analysis can be performed. With knowledge of line

**Table 3.2. 1886 Earthquakes in Charleston, SC**

| Date | Estimated Magnitude[1] | Longitude[1] | Latitude[1] |
|---|---|---|---|
| September 1, 1886 | 7.0 | 32.9 | -80.0 |

[1] from Stover & Coffman, 1993

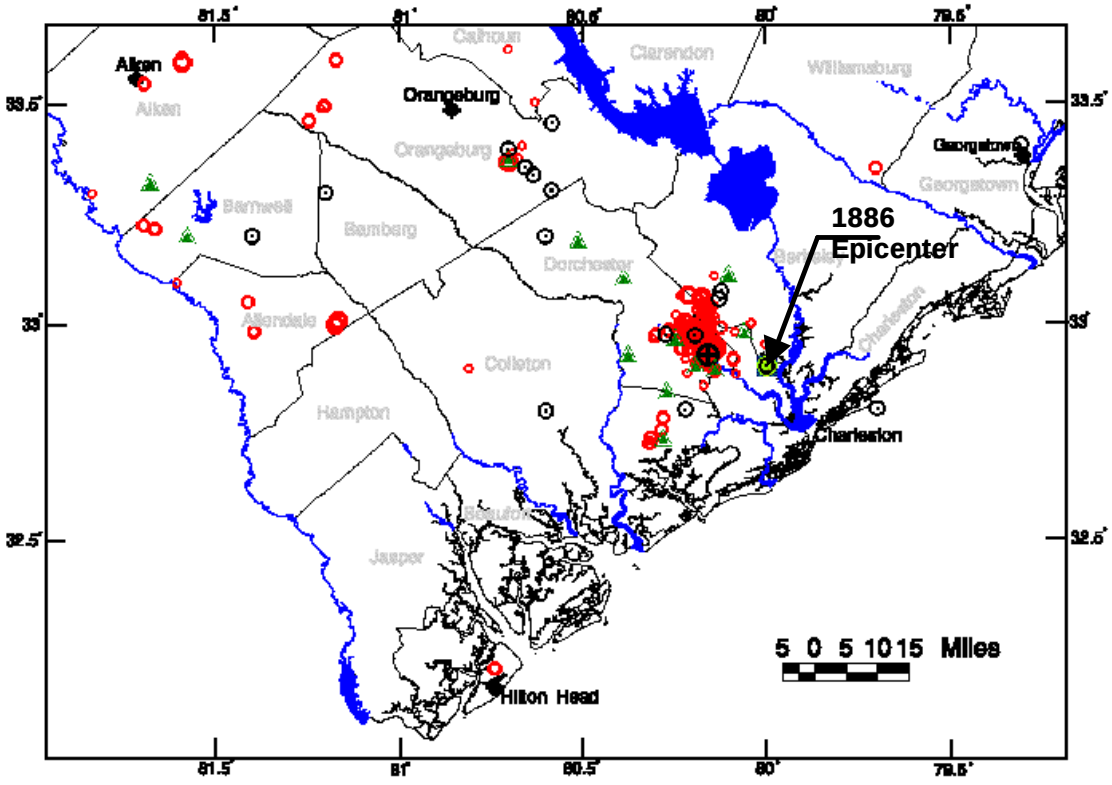


**Figure 3.3. Seismicity and in Charleston, S.C. Earthquake Region 1698-1995 (http://prithvi.seis.sc.edu/images/Map5H.gif)**

source or point source fault location (Figs. 3.1 and 3.3) Joyner-Boore distance to seismic hazards can be estimated. While Joyner-Boore distance is necessary for seismic analysis, hypocentral and epicentral distances will control the atenuation of motions from an actual event. For clarity in describing site distance, Figure 3.4 graphically defines source-to-site distance parameters.

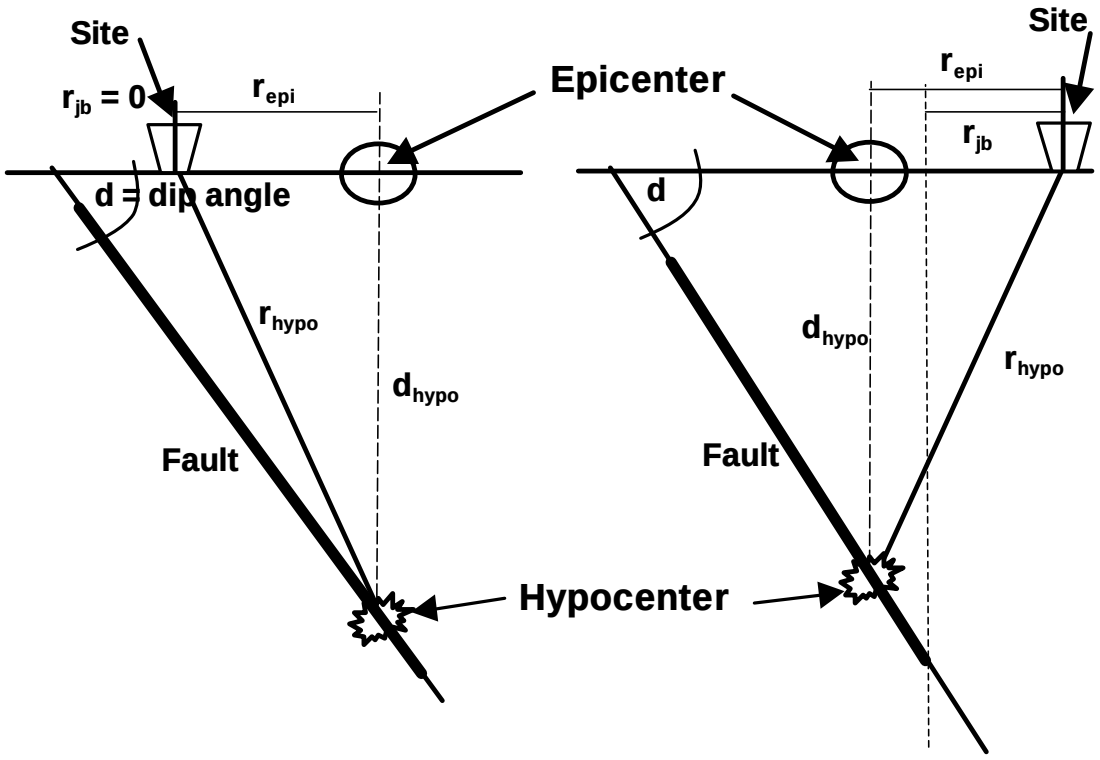


**Figure 3.4. Graphical Representation of Distance to Site from Dipping Faults**
**$r_{hypo}$ = hypocentral distance; $r_{epi}$ = epicentral distance; $r_{jb}$ = Joyner-Boore distance**

The hypocenter is the location on the fault where rupture occurs. Therefore, the hypocentral distance accounts for earthquake depth in its calculation. It should be mentioned that the modified Mid-America Deep Soil ground motion model under

development by Hermann & Akinci (1999) utilizes the input parameter of hypocentral distance ($r_{hypo}$) rather than epicentral ($r_{epi}$) or Joyner-Boore distance ($r_{jb}$). The expected hypocentral depth ($d_{hypo}$) needs be incorporated into the analysis to accurately assess attenuation of motions. Figure 3.5 displays a comparison of the measured hypocentral depths for earthquakes in both Mid-America and western United States. Considering that the data set was fairly limited, it does not appear that there is substantial difference between hypocentral depths of Mid-America and western U.S. earthquakes. Typical depths for Mid-America will range between about 4 km and 12 km, with typical depths

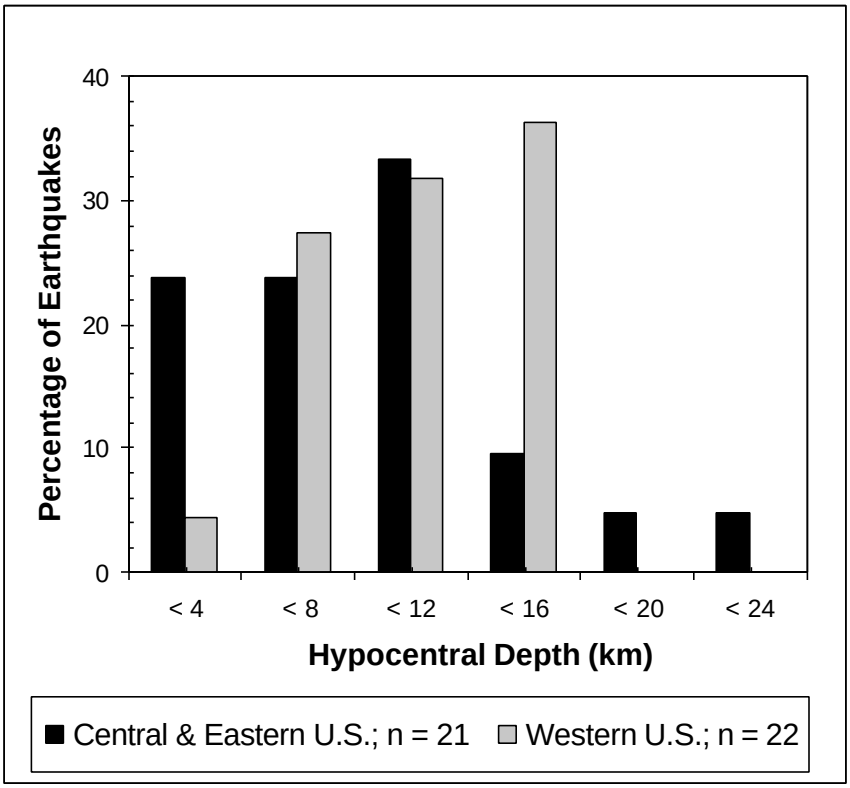


**Figure 3.5. Comparison of Hypocentral Depths for Mid-America and Western U.S. Earthquakes (data from Stover & Coffman, 1993)**

for the western U.S. between about 5 km and 16 km. Reviewing parameters affecting peak ground acceleration (PGA) as presented in Toro et al. (1997), hypocentral depths for Mid-continent earthquakes (NMSZ) can be estimated at 9.3 km, and hypocentral depths for gulf coastal plain earthquakes (Charleston, SC) can be estimated at 10.9 km. These reported parameters are at the upper end of the suggested range, and seem reasonable for conventional analysis. A parametric study using data from Stover & Coffman (1993) was performed to assess the effect of hypocentral depth may have on moment magnitude and felt area, but no trends were observed. Previous work by Nuttli (1983) noticed a relationship between minimum hypocentral depth and body wave magnitude ($m_b$; Appendix II) for Mid-American earthquakes:

$$\log h_{min} = (-1.730 + 0.456\, m_b) \sin d \qquad (3.1)$$

where $h_{min}$ is the minimum hypocentral depth in km, and $d$ is the angle the fault rupture plane dips at compared to horizontal. For a vertical fault, the angle will be $90^o$ and thus sin $d$ will be unity.

Due to uncertainty in the hypocentral depth, the epicentral or Joyner-Boore distance is commonly used. The relationship between epicentral and hypocentral distance is:

$$r_{hypo} = \sqrt{r_{epi}^{\ 2} + d_{hypo}^{\ 2}} \qquad (3.2)$$

where $d_{hypo}$ is the hypocentral depth, and other parameters are as shown in Figure 3.3. The exact location of the point of rupture for a future event will not be known, so the Joyner-Boore distance, or shortest distance to the surface projection of the fault, is commonly used for analyses. An approximation of hypocentral distance from Joyner-Boore distance is:

$$r_{hypo} = \sqrt{r_{jb}^{\ 2} + d_{hypo}^{\ 2}} \tag{3.3}$$

where $d_{hypo}$ is approximated as 9.3 km for mid-continent earthquakes and $d_{hypo}$ is approximated as 10.9 km for gulf coastal plain earthquakes when analyzing peak ground acceleration (PGA; $a_{max}$) (Toro et al., 1997).

To identify the most critical seismically-active areas that may result in significant ground motions, potential rupture zones across a specified area can be assessed to determine probability distributions for various distances. These values are available for major cities on the USGS web page at:

http://geohazards.cr.usgs.gov/eq

Tables 3.3 and 3.4 display the probability distribution of earthquake hazards with distance from Memphis, TN and Charleston, S.C., respectively. It should be noted that these tables are for the 2 percent chance of occurrence in 50 years, or the 2500-year earthquake. This will likely not be the design earthquake for typical structures, so additional judgement will be required during hazard analysis.

**Table 3.3. Probability Distribution for 2% Occurrence in 50 years Earthquake Hazards in Memphis, TN; PGA = 0.675 g (USGS, 1999)**

| $r_{jb} \leq$ (km) | Moment Magnitude, $M_w$ | | | | | | |
|---|---|---|---|---|---|---|---|
| | **5.0** | **5.5** | **6.0** | **6.5** | **7.0** | **7.5** | **8.0** |
| **25** | 3.23 | 4.25 | 4.02 | 3.15 | 1.50 | 1.10 | 0.00 |
| **50** | 0.10 | 0.33 | 0.74 | 1.19 | 0.82 | 0.96 | 52.26 |
| **75** | 0.00 | 0.01 | 0.05 | 0.17 | 0.20 | 0.36 | 16.72 |
| **100** | 0.00 | 0.00 | 0.01 | 0.04 | 0.07 | 0.18 | 8.35 |
| **125** | 0.00 | 0.00 | 0.00 | 0.01 | 0.03 | 0.09 | 0.00 |
| **150** | 0.00 | 0.00 | 0.00 | 0.00 | 0.01 | 0.04 | 0.00 |
| **175** | 0.00 | 0.00 | 0.00 | 0.00 | 0.00 | 0.01 | 0.00 |
| **200** | 0.00 | 0.00 | 0.00 | 0.00 | 0.00 | 0.01 | 0.00 |

It can be inferred from Table 3.3 that the most likely severe event over the next 2500 years in the Memphis, TN area will be a moment magnitude 8.0 at a distance between 25 km and 50 km. There also exists a smaller chance that the event may be between 50 km and 100 km. These distances match well with distance to the New Madrid Fault structure presented in Figure 3.1.

Review of Table 3.4 shows the most probabilistic event over the next 2500 years in the Charleston, SC area to be a moment magnitude 7.5 event at a distance of less than 25 km. Smaller probabilities also exist for a $M_w = 7.5$ event between 25 km and 75 km. These distances match well with the seismic activity presented in Figure 3.2.

**Table 3.4. Probability Distribution for 2% Occurrence in 50 years Earthquake Hazards in Charleston, SC; PGA = 0.758 g (USGS, 1999)**

| $r_{jb} \leq$ (km) | Moment Magnitude, $M_w$ | | | | | |
|---|---|---|---|---|---|---|
| | **5.0** | **5.5** | **6.0** | **6.5** | **7.0** | **7.5** |
| **25** | 3.11 | 4.49 | 4.64 | 3.93 | 2.16 | 57.55 |
| **50** | 0.07 | 0.24 | 0.57 | 1.02 | 0.99 | 15.82 |
| **75** | 0.00 | 0.01 | 0.03 | 0.10 | 0.15 | 3.77 |
| **100** | 0.00 | 0.00 | 0.00 | 0.01 | 0.03 | 0.84 |
| **125** | 0.00 | 0.00 | 0.00 | 0.00 | 0.01 | 0.37 |
| **150** | 0.00 | 0.00 | 0.00 | 0.00 | 0.00 | 0.09 |
| **175** | 0.00 | 0.00 | 0.00 | 0.00 | 0.00 | 0.01 |
| **200** | 0.00 | 0.00 | 0.00 | 0.00 | 0.00 | 0.00 |

## 3.3 Mid-America Deep Soil Models

The lack of strong ground motion data ($M_w > 5$) in the central and eastern United States causes difficulties when performing advanced analyses requiring input ground motions. Research has been undertaken in association with the Mid-America Earthquake (MAE) Center to develop synthetic ground motions to maintain consistency throughout MAE Center projects. At the time of this study, the Herrmann & Akinci (1999) model was considered to be the most appropriate. Model input data files are generated for use with the Boore (1996) simulated ground motion program. Time series are generated based on band limited white-noise stochastic simulations incorporated into random vibration theory (Herrmann & Akinci, 1999). A concern with performance of white noise ground motion models is that they do not accurately account for low frequency surface waves. Additional duration from these long period waves may be critical for earthquake analysis, as seen from field evidence presented in Youd (1999).

**Table 3.5. Mid-America Ground Motion Models (adapted from Herrman & Akinci, 1999)**

| Model | Spectral Source | Wave Propagation | Soil Condition | Reference |
|---|---|---|---|---|
| M1 | Atkinson & Boore (1995) | Atkinson & Boore (1995) | Eastern North America (ENA) hard rock | Atkinson & Boore (1995) |
| M2 | USGS 1996 - 150 Bar | Atkinson & Boore (1995) | Generic NEHRP B-C boundary ($V_s$ = 760 m/s) | Frankel et al. (1996) |
| M3 | USGS 1996 - 150 Bar | Atkinson & Boore (1995) | Deep Soil | Herrmann & Akinci (1999) |
| M4 | Atkinson & Boore (1995) | Mid-America (Herrmann & Akinci, 1999) | Deep Soil | Herrmann & Akinci (1999) |
| M5 | USGS 1996 - 150 Bar | Mid-America (Herrmann & Akinci, 1999) | Deep Soil | Herrmann & Akinci (1999) |

Two previously generated models (Atkinson & Boore, 1995; Frankel et al., 1996) along with three developing models may be used to generate time series. Table 3.5 summarizes key aspects of the origin of the models. Each of these models are permitted for use with MAE Center projects, but it has been suggested that the Modified USGS (M3) be used for current soil response studies (R. Herrmann, personal communication, 1999). The two existing models based on rock sites (M1; M2) are applicable for the NMSZ or Charleston, SC earthquake region. The three new models (M3; M4; M5) have been developed using shear wave velocity profiles for the central United States. Discussion of the details of each ground motion model is beyond the scope of this project and more information is available at the following web sites:

http://www.eas.slu.edu/People/RBHerrmann/MAEC/maecgnd.html

http://www.eas.slu.edu/People/RBHerrmann/GroundMotion/

http://www.eas.slu.edu/People/RBHerrmann/HAZMAP/hazmap.html

Input parameters necessary for the model will be discussed in the following paragraphs.

The main differences between current models (M1, M2) and the newly-proposed ground motion models (M3, M4, M5) is the depth of the soil column and effects of that overlying soil column on ground motions. Although linear aspects of the soil column are considered in the proposed models (M3, M4, M5), the nonlinear nature of soil is not taken into account. This will not be a concern for minor events, but high accelerations of a severe event will likely induce strain levels that exceed the threshold strain, and soil nonlinearity will be a concern during wave propagation. Studies by Idriss (1991) after the Loma Prieta earthquake showed the influence of soft sites on resulting surface accelerations. Figure 3.6 presents a summary of those results. Amplification of motions

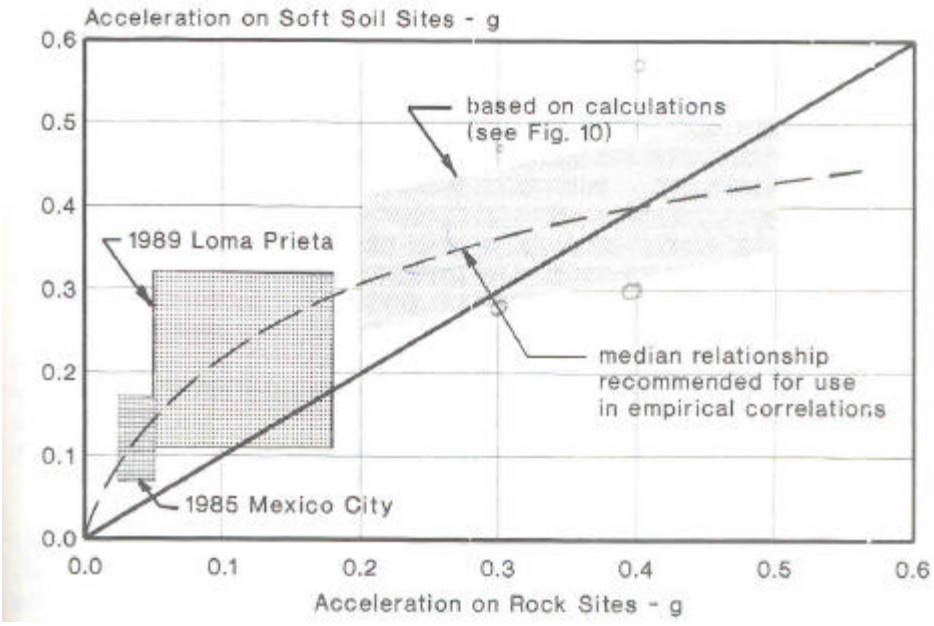


**Figure 3.6. Comparison of Acceleration at Soft Soil Sites to Rock Sites (Idriss, 1991)**

is apparent at low accelerations, and damping may decrease surface accelerations during a severe event. Application of these results to the Mississippi River Valley and Atlantic Coastal Plain sediments still needs to be verified.

A stiffness profile for the NMSZ was generated by Herrmann et al. (1999) using shallow shear wave velocities from previous studies. The stiffness of rock deposits was estimated from Street (personal communication to Bob Herrmann, 1999). The generated stiffness profile used in the Herrman and Akinci (1999) model is presented in Figure 3.5. The stiffness profile, as well as the output of models M3, M4, and M5, is a function of the depth of the soil column. A representation of the soil column depth was developed by Herrmann et al. (1999) and is seen in Figure 3.7. This figure shows the overall extent of thick sediments of the Mississippi River Valley, but does not provide the detail necessary for an exact input depth at a specific location. For this study, a 600-m vertical column of soil will be used in the Blytheville, AR and Steele, MO areas, and a 1000-m column of soil over rock will be used in the Memphis, TN area (R. Herrmann, personal communication, 1999). A linear soil-rock interface dipping relationship of 4 m per km between Blytheville, AR and Memphis, TN, was based on information presented in Figure 3.6, and will be assumed for model calculations. A generalized cross section of the Mississippi River Valley is presented in Figure 3.8.

In Charleston, SC, there will be extensive deposits of Atlantic Coastal Plain soils overlying a relatively insignificant thickness of Piedmont soils over bedrock. The Clubhouse Crossing boring logs presented in Figure 3.10 (Gohn et al., 1983; Yantis et al, 1983) have been used to estimated a bedrock depth of 770 m and dipping rates of 2-

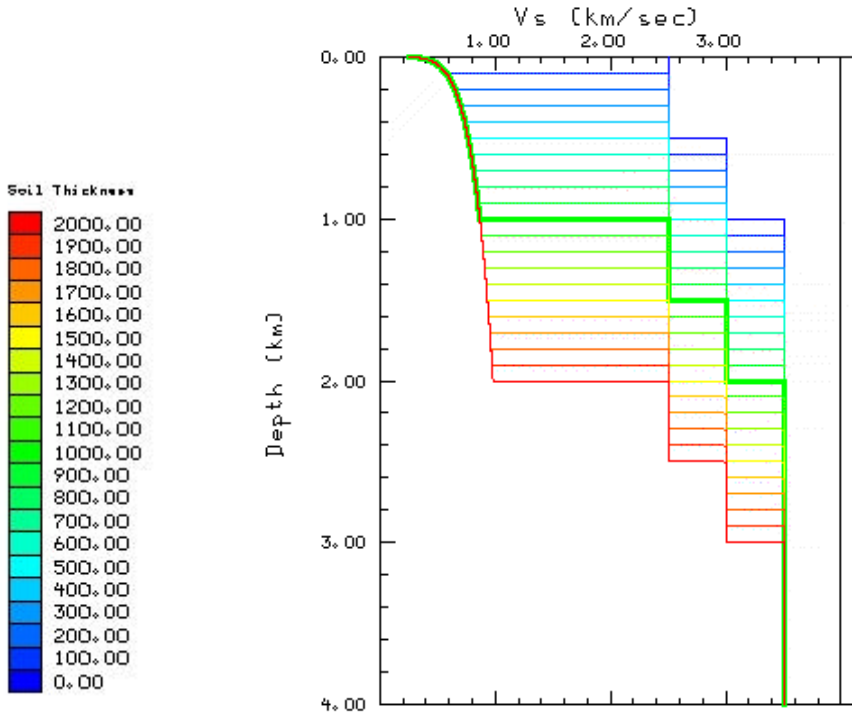


**Figure 3.7. Soil Column Depth-Dependent Shear Wave Velocity ($V_s$) Profile used in Herrmann and Akinci (1999) Soil Models (M3,M4,M5) (http://www.eas.slu.edu/People/RBHerrmann/HAZMAP/hazmap.html)**

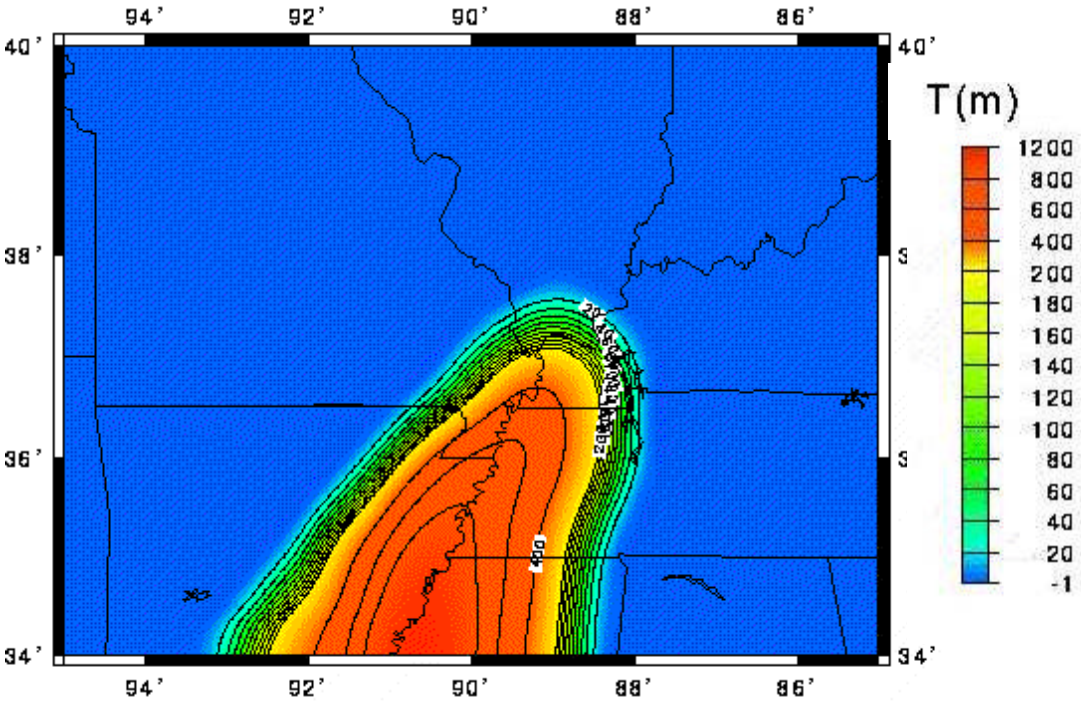


**Figure 3.8. Sediment Thickness Model of Mississippi River Valley (http://www.eas.slu.edu/People/RBHerrmann/HAZMAP/hazmap.html)**

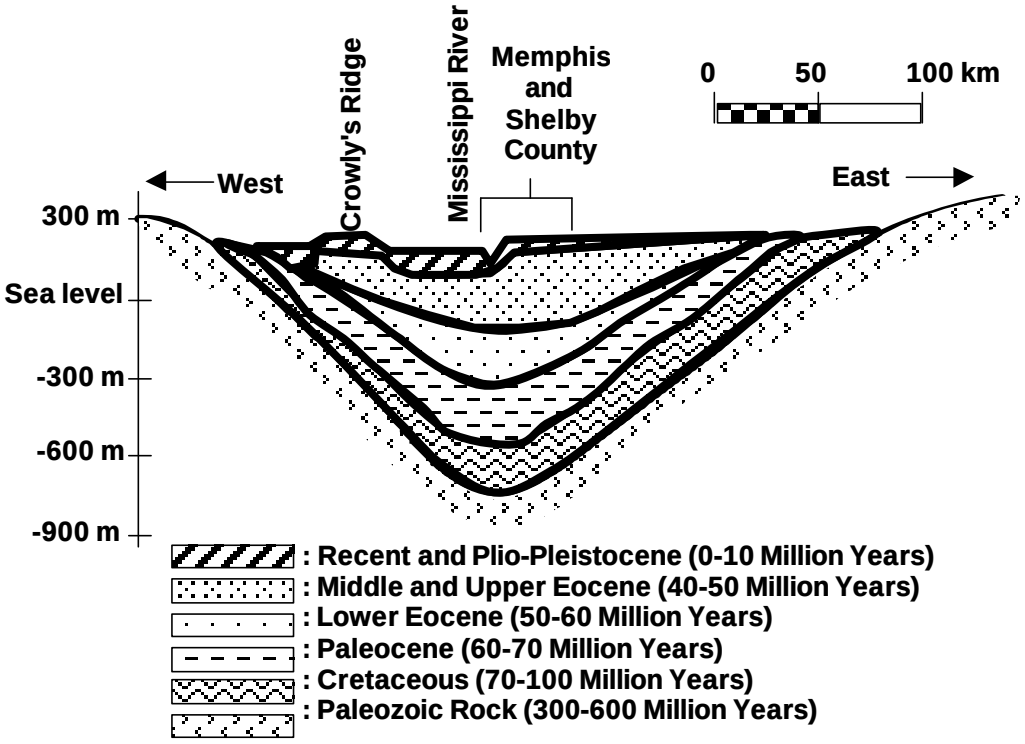


**Figure 3.9. Generalized Cross Section of Upper Mississippi River Valley (adapted from Whittenberg et al., 1977)**

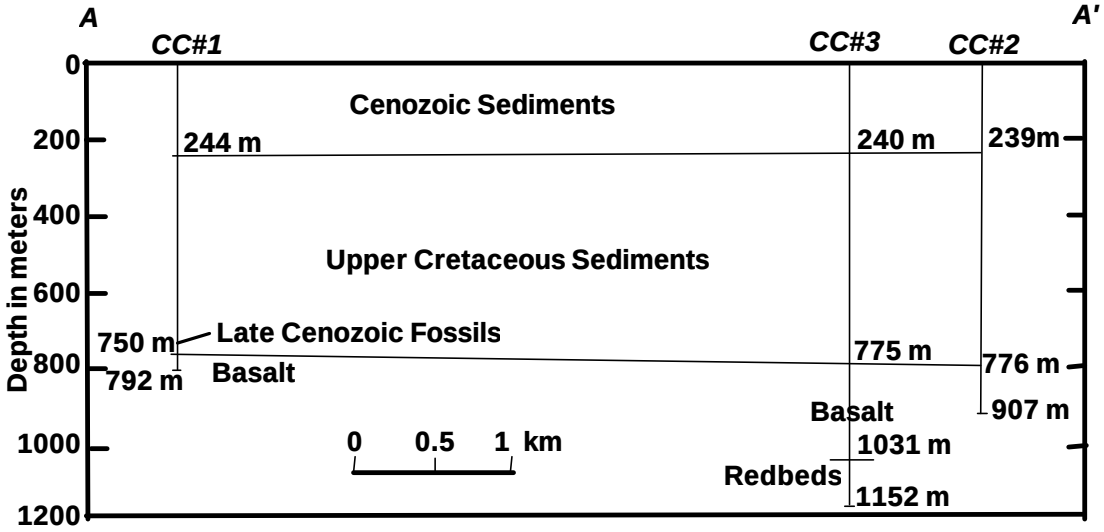


**Figure 3.10. Generalized Cross Section of Charleston, SC Stratigraphy from Clubhouse Crossroads Borings (Adapted from Gohn et al., 1983)**

m/km for the Piedmont formation below the Atlantic Coastal Plain in the Charleston, SC area. Using distances perpendicular to the Piedmont fall line, the Clubhouse Crossroads logs were performed about 15 km from the epicenter of the 1886 earthquake, and about 35 km from Charleston. For analysis, a bedrock depth of 800 m will be used at the epicenter, and the 2-m/km dipping rate will be used to produce a depth to bedrock of 840 m in Charleston.

A comparison of $a_{max}$ output by the five models for a magnitude 7.0 earthquake, is presented in Figure 3.11. The USGS (M1; Frankel, 1996) model is the most conservative. This model is based on rock sites (NEHRP B-C boundary) and does not account for damping in the overlying soil column. The modified USGS model (M3) accounts for damping through the depth of the soil column. This leads to lower anticipated accelerations than the USGS model at close distances, but the models converge at greater site distances (about 175 km). The Atkinson-Boore model (M2; 1995) is more conservative than the modified USGS (M3) at close distances. This model becomes less conservative after about 30 km, and does not seem to account for lower attenuation observed from events in the central and eastern United States. The two new Mid-America deep soil models (M4 & M5) with mid-continent site effects lead to lower accelerations than other models at close distances, and become more conservative at greater distances (about 150 km). These models are still being calibrated and modified, and may become more applicable after continued development.

Parametric studies show the differences in PGA responses obtained between an input thickness of 600 m of soil and 1000 m of soil, in Figure 3.12. The depth of the soils

column appears most important at close distance, and the models tend to converge after distances of about 100 km. When utilizing synthetic ground motions for liquefaction analysis, the depth of soil column will be determined using bedrock depth and dipping rates as presented above. Since the Herrmann & Akinci (1999) models were developed primarily for use in the NMSZ, their reliability in the Charleston EQ region is not yet verified.

Additional model input parameters for attenuation studies include moment magnitude, hypocentral site distance, oscillatory damping, and range of periods. Moment magnitude ($M_w$) can be varied between 3.0 and 8.5, and will be a function of the design earthquake. Additional aspects of magnitude are contained Appendix II. The hypocentral site distance can be varied from 1 km to 1000 km. This parameter will be a combination of epicentral distance and hypocentral depth, as described in the previous section. Oscillatory damping, *c*, is the critical damping of a single degree of freedom system, and is typically considered to be five percent (0.05). The models (M3; M4; M5) have three additional input parameters which can be used to control the primary range of output frequencies.

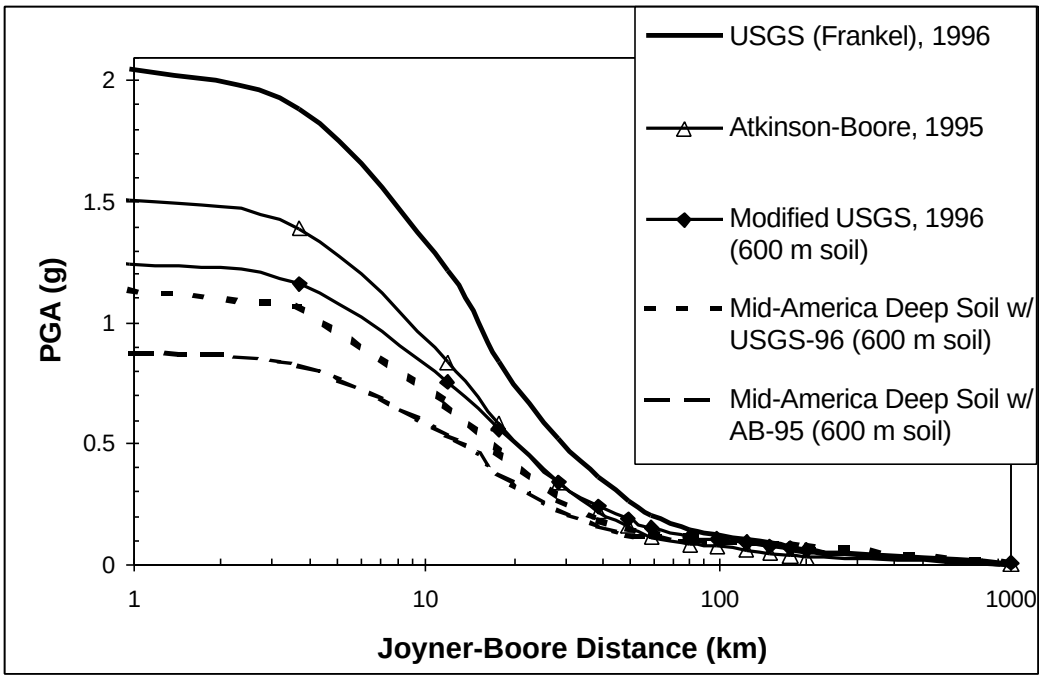


**Figure 3.11. Comparison of Accelerations Produced by Different Ground Motion Models available for Mid-American Soils; $M_w$ = 7.0**

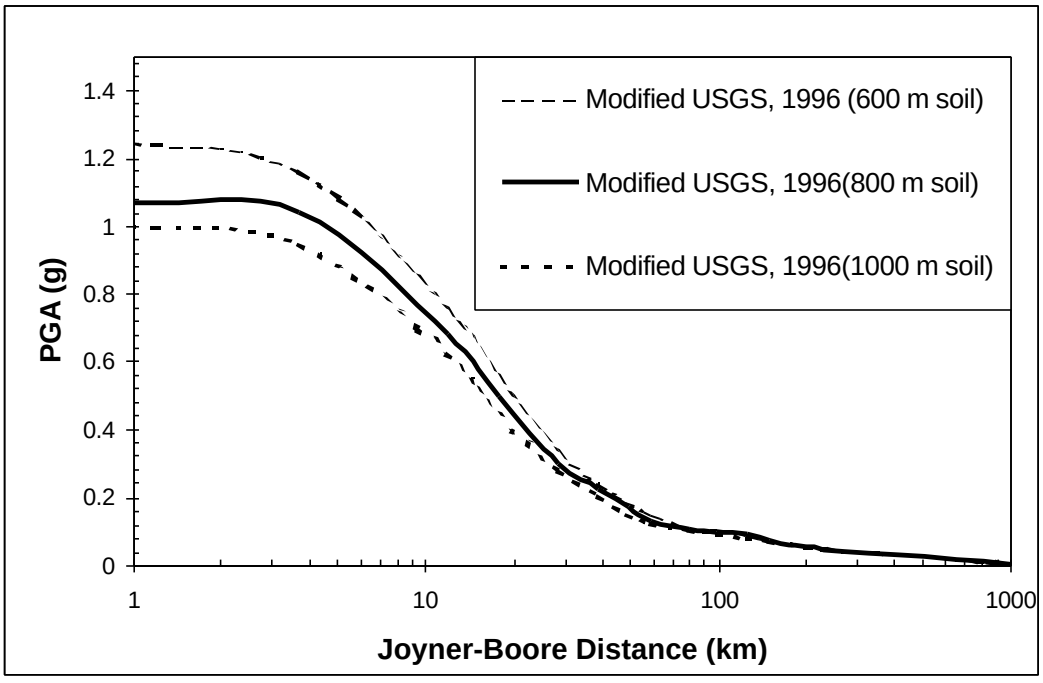


**Figure 3.12. Effects of Soil Column Depth on PGA as Predicted by Herrmann & Akinci (1999) Mid-America Deep Soil Model (M3); $M_w$ = 7.0**

## 3.4 Empirical Attenuation Relationships

To characterize an earthquake for geotechnical analysis, the peak horizontal ground acceleration (PGA; $a_{max}$) is required. Acceleration can be related to earthquake magnitude and distance through attenuation relationships. A number of separate empirical attenuation relationships for the eastern and central U.S. were reviewed in this study. Attenuation relationships generated by the Herrmann & Akinci (1999) model were previously discussed in Section 3.3 and displayed in Figures 3.11 and 3.12. These relationships will be compared to current models and earlier attenuation curves.

Areas of primary concern in this study are within 50 km of fault zones. The attenuation relationships will be carried out to 100 km to assess greater source-to-site distances, and presented on a semi-log scale to show increased detail at close distances. Since the analysis will be primarily compared to data produced from the Modified USGS deep soil model (M3), results from this model will be included in each of the figures for reference. Depths to bedrock and dipping relationships discussed in Section 3.2 will be used when generating attenuation relationships from the Herrmann & Akinci (1999) model. Hypocentral depths of 9.3 km and 10.7 km will be used for the NMSZ and Charleston, SC earthquake regions respectively (Toro et al., 1997).

Proposed attenuation relationships for Mid-American soils at a moment magnitude of 7.0 are presented in Figure 3.13. The Modified USGS (M3) model, that will be used in this study, generally agrees with the previous relationships. Current models (Herrmann & Akinci, 1999; Atkinson & Boore, 1997; Toro et al., 1997) predict higher accelerations at short distances than previous studies (Nuttli & Herrmann, 1984),

due to the higher source scaling used. It has also been noticed that relationships based on geotechnical investigations of historic liquefaction sites (e.g., Pond, 1996) generally predict lower accelerations than rock models at close source distances and higher accelerations at greater distance. This may be a result of increased damping due to the nonlinear properties of the soils at close distances (high accelerations), and amplification of soft sites at greater distances (low accelerations; as shown in Figure 3.6). Site specific effects are not accounted for in most attenuation models, but likely control attenuation relationships for specific geologic regions.

Figure 3.14 presents proposed attenuation relationships for Charleston, SC soils. For comparison with previous studies, attenuation of a moment magnitude 6.0 and moment magnitude 7.0 are reviewed. Field data from Martin (1990) is for moment magnitude 6.0 and moment magnitude 7.5, but the 1886 Charleston, SC earthquake on which the field data were based is generally considered to be a moment magnitude 7.0 event. The $M_w$ = 6.0 field data matches well with $M_w$ = 6.0 attenuation relationships at close distances. The $M_w$ = 7.5 field data matches well with the $M_w$ = 7.0 attenuation relationship at greater distances. This would support the hypothesis presented in the previous paragraph that accelerations are damped at close distances (high accelerations) and amplified at greater distance (low accelerations) at soft sites in Mid-America.

Figures 3.15 and 3.16 display magnitude effects on attenuation relations determined from the Modified USGS deep soil model (M3; Herrmann & Akinci, 1999) and Toro et al. (1997) rock motion model for sites in the NMSZ. Figures 3.17 and 3.18 display magnitude effects on attenuation relations using the same two models for the

Charleston, SC earthquake region. In both cases, the M3 deep soil model matches well with the Toro et al (1997) rock model at close distance, and predicts higher acceleration at greater distance. Nonlinear soil properties and the potential for increased damping or site amplification needs to be studied to better understand ground response at deep alluvial sites. The Herrmann & Akinci (1999) model is considered to provide conservatively high surface accelerations at close distance and reasonable surface acceleration at greater distance, when considering the work of Idriss (1991) and the Toro et al. (1997) rock model.

This study will also be concerned with Arias intensity (Appendix II) when evaluating liquefaction susceptibility. Attenuation relations for Arias intensity are not common in the literature, especially for the Mid-America region. Since integration of the entire acceleration-time history is required, the lack of strong ground motion data in the CEUS is a recurrent problem. Figure 3.19 displays Arias intensity attenuation relationships determined from 66 earthquake records in the western United States (Kayen & Mitchell, 1997) as compared to the results of Mid-America simulated earthquake model studies. Figure 3.17 is for a $M_w = 7.0$ earthquake, but Arias intensity will increase with magnitude. The equations for the Kayen & Mitchell (1997) attenuation relationships are:

$$\text{Log } I_h = M_w - 4.0 - 2 \cdot \text{Log } (r_{hypo}) \qquad \text{(Rock Sites)} \qquad (3.4a)$$

$$\text{Log } I_h = M_w - 3.8 - 2 \cdot \text{Log } (r_{hypo}) \qquad \text{(Alluvial Sites)} \qquad (3.4b)$$

$$\text{Log } I_h = M_w - 3.4 - 2 \cdot \text{Log } (r_{hypo}) \qquad \text{(Soft Sites)} \qquad (3.4c)$$

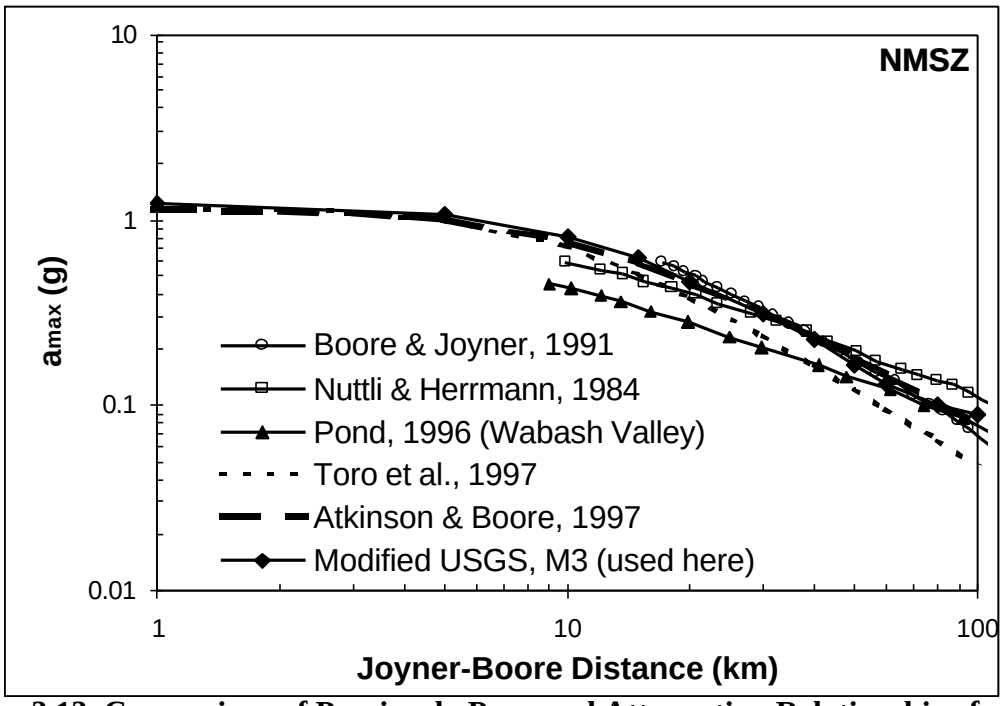


**Figure 3.13. Comparison of Previously Proposed Attenuation Relationships for New Madrid Seismic Zone and Results of Modified USGS model ($M_w$ = 7.0)**

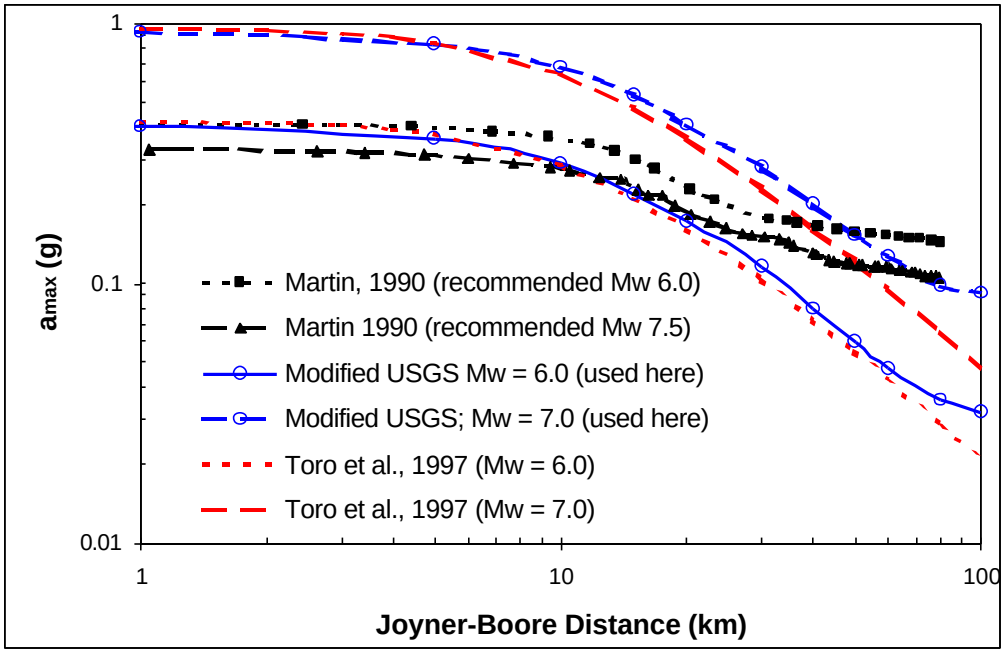


**Figure 3.14. Comparison of Previously Proposed Attenuation Relationships for Charleston, SC EQ Region and Results of Modified USGS model ($M_w$ = 7.0)**

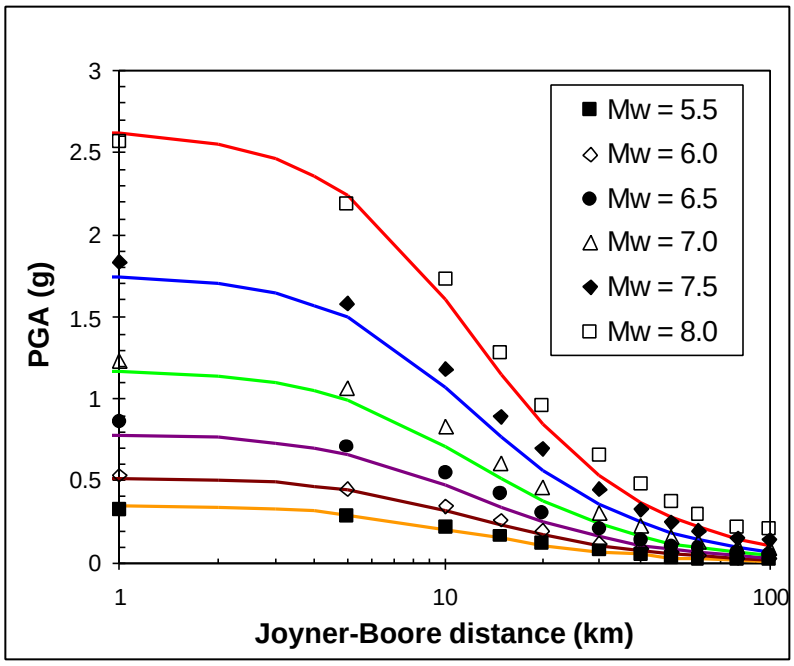


**Figure 3.15. Comparison of Toro et al. (lines; 1997) and Modified USGS (points) model for NMSZ on semi-log scale ($5.5 \leq M_w \leq 8.0$)**

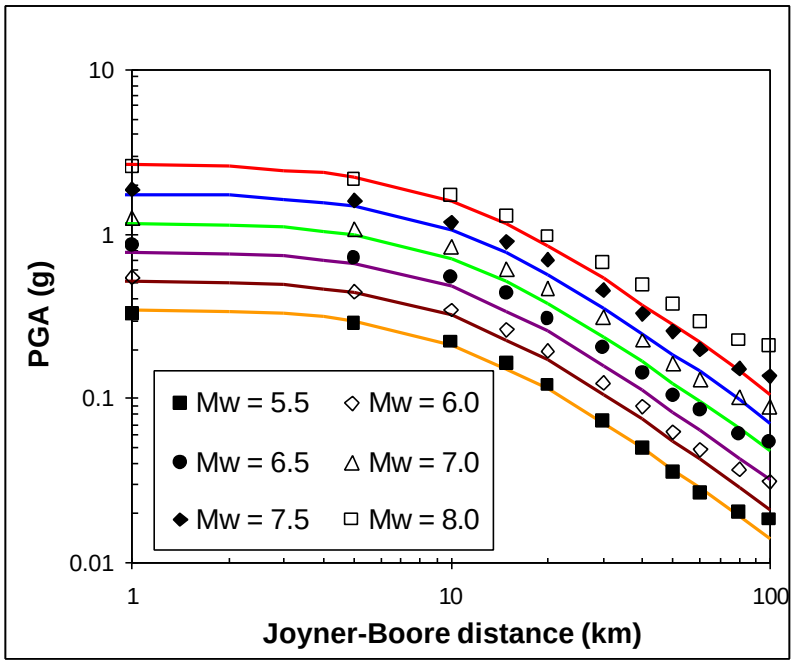


**Figure 3.16. Comparison of Toro et al. (lines; 1997) Relationship and Modified USGS model (points) for NMSZ on log-log scale ($5.5 \leq M_w \leq 8.0$)**

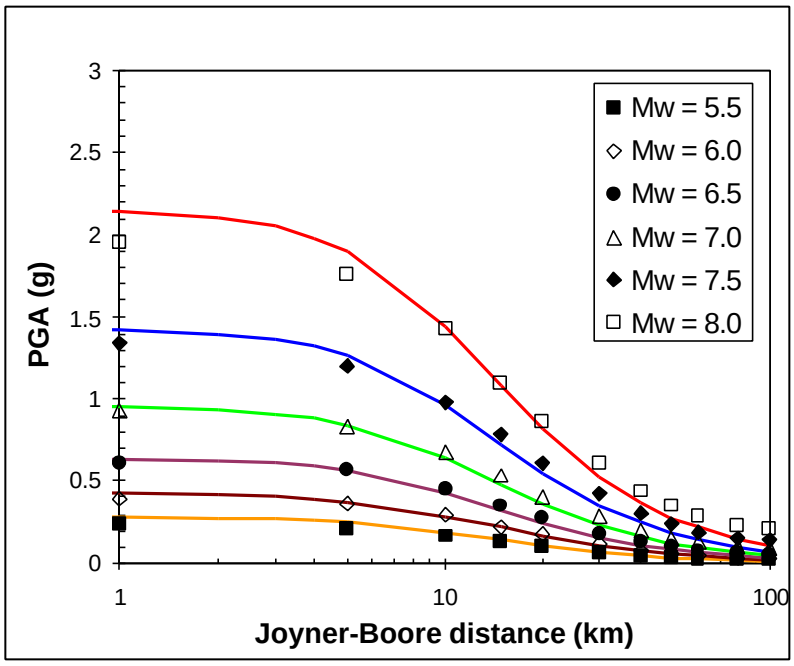


**Figure 3.17. Comparison of Toro et al. (lines; 1997) and Modified USGS model (points) for Charleston, SC on semi-log scale ($5.5 \leq M_w \leq 8.0$)**

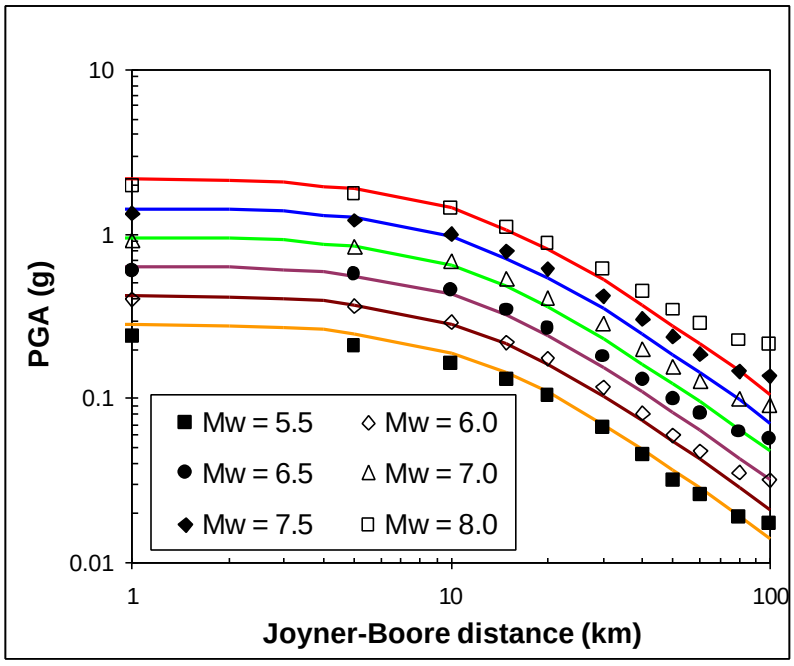


**Figure 3.18. Comparison of Toro et al. (lines; 1997) Relationship and Modified USGS model (points) for Charleston, SC on log-log scale ($5.5 \leq M_w \leq 8.0$)**

where $I_h$ is the averaged Arias intensity in the x- and y-directions, and $r_{hypo}$ is the hypocentral distance. Even though the Kayen & Mitchell relationships were determined for California Sites, the Mid-America models match well at close Joyner-Boore distances. At greater distance ($r_{jb}$ > 60 km), Arias intensity determined using the Mid-America deep soil model (M3) tends to decrease at a lower rate than the model for California sites. This will account for the lower attenuation rates observed in CEUS soils. The effects of soil column thickness and soil conditions are shown in Figure 3.19. The soil column thickness does not seem to have much effect, but potential for amplification and damping at alluvial sites should not be ignored. The three M3 model curves are more conservative than the Kayen & Mitchell (1997) relationship for alluvial soils at distances less than 90 km.

Figure 3.20 displays attenuation relationships in the Charleston, SC earthquake region, with the model studies providing an acceptable agreement with the Kayen & Mitchell (1997) curves up to Joyner-Boore distances of 100 km. Since this study is primarily concerned with earthquakes at close Joyner-Boore distance ($r_{jb} \leq$ 50 km), the Kayen & Mitchell (1997) relationship sites will be considered acceptable. For Mid-American sites at greater distances ($r_{jb}$ > 90 km), the specific Herrmann & Akinci (1999) M3 model studies should be performed.

## 3.5 Summary

Distinct zones of seismic activity are apparent in microseismic records from the New Madrid Seismic zone and Charleston, SC earthquake region. These areas are

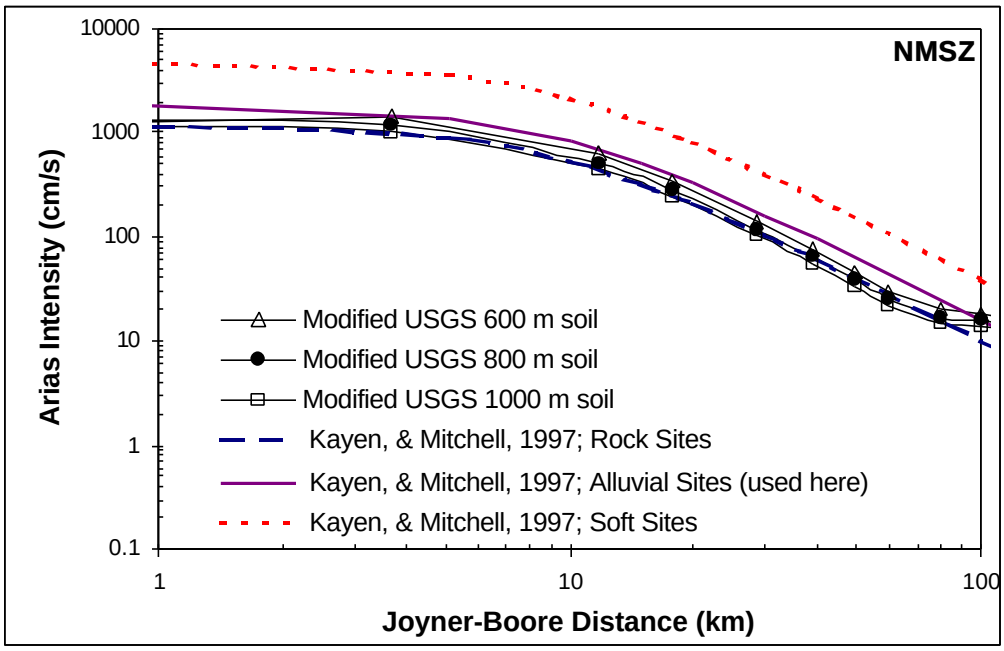


**Figure 3.19. Comparison of Previously Proposed Attenuation Relationships for New Madrid Seismic Zone and Results of Modified USGS model ($M_w$ = 7.0)**

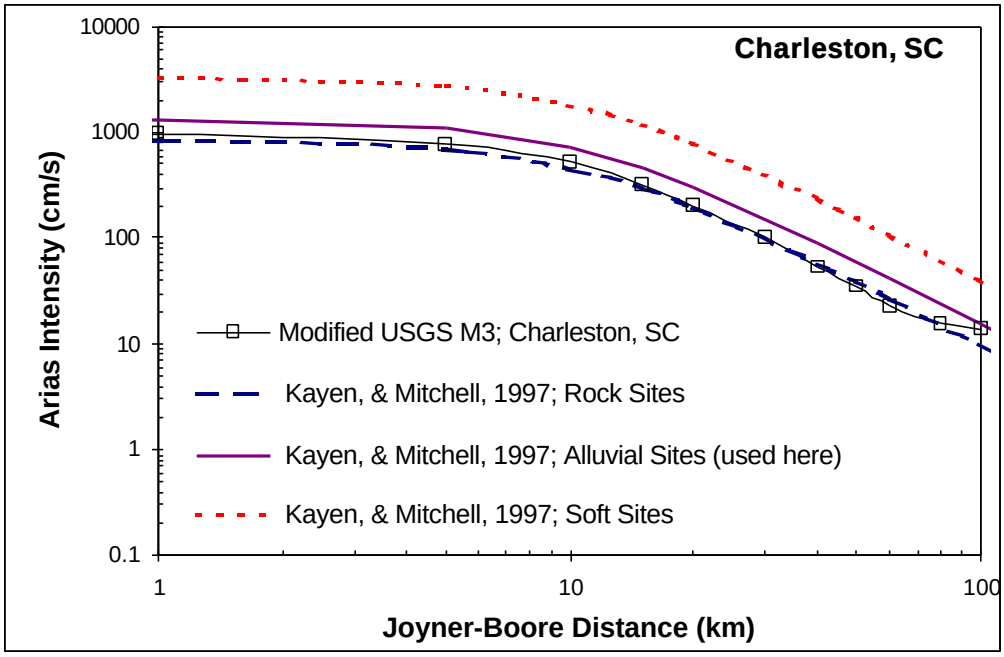


**Figure 3.20. Comparison of Previously Proposed Attenuation Relationships for New Madrid Seismic Zone and Results of Modified USGS model ($M_w$ = 7.0)**

interpreted as areas near the fault structures in these geologic formations. While large events have not occurred within the past 100 years, paleoseismic studies have shown a recurrence interval on the order of 200 to 250 years for a significant ($M_w > 7.0$) event. Depth and dipping rates of the soil column was estimated from model studies for the NMSZ, and estimated from deep boring logs in the Charleston, SC earthquake region.

A ground motion model which accounts for linear effects of the deep soil column in Mid-America is under development. Preliminary studies of this model have been compared to existing empirical attenuation relationships for rock as well as soil. While the model agrees well with data for small earthquakes ($Mw < 5.0$), it is expected that the nonlinear soil effects induced by a severe event should cause vast differences between soil and rock relationships. This may explain some of the differences between attenuation relationships determined from engineering data associated with paleoliquefaction studies, and models based on linear effects of the soil column calibrated to low magnitude events and extrapolated to higher magnitude earthquakes.

Since the non-linear effects of the soil column are still being studied, acceleration attenuation relationships generated by the modified USGS Mid-America deep soil model (M3) were used in this study. This model is based on depth of soil column, hypocentral distance, moment magnitude, and a generalized stiffness profile for the Mississippi River Valley. Arias intensity relationships from the M3 model matched well with California field performance data, and thus the Kayen & Mitchell (1997) attenuation relationship for alluvial sites was also used in this study.

# CHAPTER 4

# LIQUEFACTION RESPONSE OF SOILS

## 4.1 Overview

A number of methodologies are available for evaluating the cyclic response of soils. Liquefaction analyses performed in this study can be categorized under the:

- Cyclic stress approach (e.g., Seed & Idriss, 1971);
- Cyclic strain approach (e.g., Dobry et al., 1982);
- Arias intensity approach (e.g., Kayen & Mitchell, 1997).

The concepts of critical void ratio (e.g., Casagrande, 1936; Appendix I) and a critical state line for sands (e.g., Been, 1999; Appendix I) will be applied when evaluating these methods.

Cyclic-stress and cyclic-strain based methods were originally derived from laboratory tests performed to evaluate soil behavioral response to earthquake shaking. The cyclic response of soils is controlled by factors such as soil fabric, pre-straining, stress history, and aging effects (Seed, 1979) that cannot be replicated in the laboratory. Due to the difficulty and expense associated with obtaining undisturbed field samples of sandy and silty soils, empirical relations from in-situ test parameters are commonly compared to field performance of soil deposits which have been subjected to historic earthquakes. The Arias intensity approach for liquefaction evaluation has developed utilizing field performance databases as well as recorded earthquake seismograms. Since this method

utilizes the entire earthquake acceleration-time history, the uncertainties of simplified procedures and empirical magnitude scaling factors (MSF) can be minimized.

## 4.2 Cyclic Stress Approach

The cyclic stress approach is the most commonly used procedure in practice to estimate liquefaction resistance of sandy soils. To represent earthquake ground motions with a single parameter, a simplified procedure was developed by Seed & Idriss (1971). Liquefaction resistance is evaluated by comparison of a soil index property to the cyclic stress ratio (CSR). The CSR is the average cyclic shear stress in a layer ($\tau_{avg}$) normalized to the effective overburden stress ($\sigma'_{vo}$). It is a function of earthquake duration (magnitude), maximum surface acceleration ($a_{max}$), depth to soil element being analyzed (z), and total ($\sigma_{vo}$) and effective ($\sigma'_{vo}$) vertical stress. The maximum surface acceleration ($a_{max}$) can be determined from acceleration time histories or estimated from attenuation relationships (Fig. 3.13; Fig. 3.15; Toro et al., 1997). For a moment magnitude $M_w = 7.5$ earthquake, the CSR is generally presented as:

$$CSR = \frac{t_{avg}}{s_{vo}'} \approx 0.65 \cdot \left( \frac{a_{\max}}{g} \right) \cdot \left( \frac{s_{vo}}{s_{vo}'} \right) \cdot r_d \qquad (4.1)$$

where $r_d$ is a stress reduction factor with depth, and other variables are described above.

4.2.1 Stress Reduction Coefficient

Stress reduction factors, $r_d$, were initially presented in Seed & Idriss (1971) for sites with sand in the upper 15-meters, and may be approximated (Robertson & Wride, 1997):

$r_d = 1.0 - 0.00765\ z$ when $z < 9.15$ m (4.2a)

$r_d = 1.174 - 0.0267\ z$ when $9.15 \leq z < 23$ m (4.2b)

$r_d = 0.744 - 0.008\ z$ when $23 \leq z < 30$ m (4.2c)

$r_d = 0.5$ when $z > 30$ m (4.2d)

where z is depth in meters. Re-evaluation of improved data sets and interpretation led to the following expressions (Idriss, 1999):

$$r_d = \exp[a(z) + b(z) \cdot M_w] \quad (4.3a)$$

with

$$a(z) = -1.01 - 1.126 \cdot \sin[(z/11.73) + 5.133] \quad (4.3b)$$

$$b(z) = 0.106 + 0.118 \cdot \sin[(z/11.28) + 5.142] \quad (4.3c)$$

where z is depth in meters and $\leq 25$ m. Figure 4.1 compares the initial average relationship to revised relationships as well as expected uncertainty from preliminary field studies. The Idriss (1999) stress reduction factors will be used for this study.

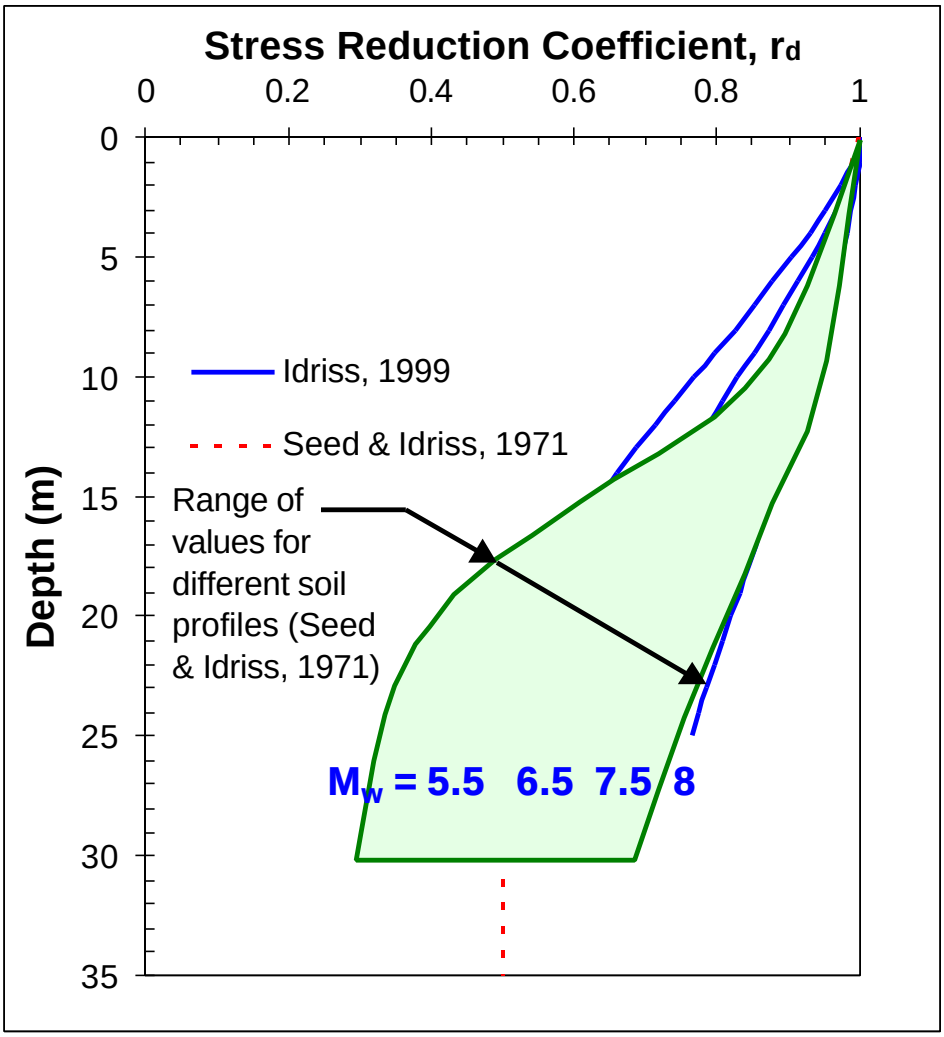


**Figure 4.1. Stress reduction Coefficients for Simplified Procedures**

4.2.2 Magnitude Scaling Factors

The moment magnitude of an earthquake will influence duration of shaking, and thus increase the number of significant stress cycles. With an increased number of significant stress cycles at the same stress ratio, the soil will exhibit a lower resistance to liquefaction. The effects of earthquake magnitude are not included in the cyclic stress ratio equation, Eq 4.1, so magnitude scaling factors (MSF) were developed. The reference magnitude for cyclic stress based analysis is 7.5.

Initially MSF trends were developed from a combination of field and laboratory data, based on relationships between magnitude and number of equivalent stress cycles. A relationship between moment magnitude, $M_w$, and significant stress cycles, $n_{eq}$, can be expressed as (Seed et al., 1985):

$$n_{eq} \approx 0.0007 \cdot M_w^{4.94} \qquad (4.4)$$

A number of studies concerning variation in magnitude scaling factors have been performed using combinations of theory and field data (Ambraseys, 1988; Arango, 1996; Andrus & Stokoe, 1997), with results and NCEER recommendations presented in Youd & Noble (1997).

Re-evaluation of field data sets and laboratory tests on frozen samples led to a revised magnitude scaling factor (Idriss, 1999):

$$MSF = 31.9\ (M_w)^{-1.72} \qquad (4.5)$$

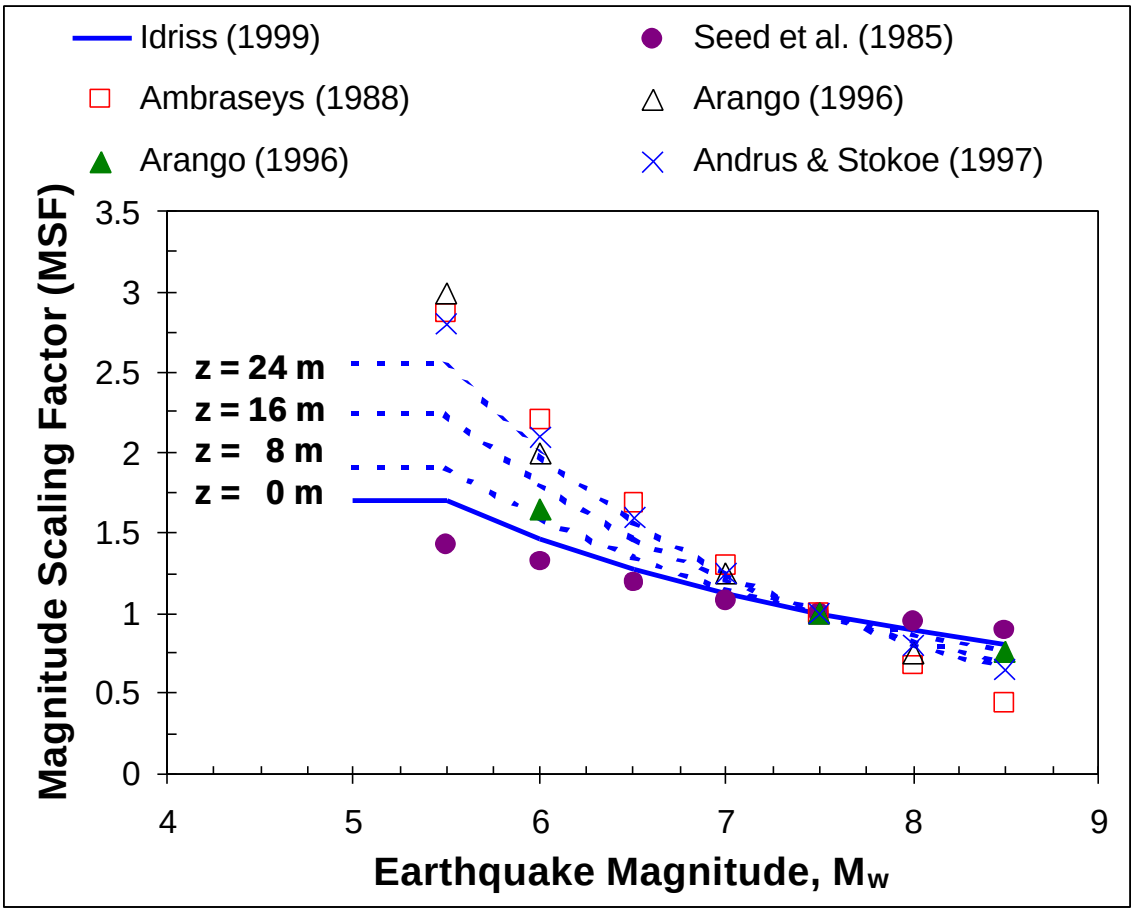


**Figure 4.2. Effect of Revised Stress Reduction Coefficients on Magnitude Scaling Factors (Idriss, 1999 factors used in this study)**

These studies also determined that the depth of liquefied layers affects the magnitude scaling factors through the stress reduction coefficient, $r_d$. Equation 4.3 displays the magnitude dependent stress reduction coefficient. Figure 4.2 presents the range of magnitude scaling factors determined from various studies. The magnitude scaling factors recommended by the NCEER (1997) workshop were between the lower bound of the Arango (1996) curves and the Andrus & Stokoe (1997) curve. The Idriss (1999) factors match well with the NCEER recommendations for depths between 8 and 16 m, and will be used in this study for simplified cyclic stress based analysis.

4.2.3 Cyclic Resistance Ratio

The CSR is a function of the earthquake motions, while the cyclic resistance ratio (CRR) represents the liquefaction resistance of the deposit. Databases from post-earthquake field investigations have been utilized to generate demarcation curves relating a stress normalized resistance parameter of an in-situ test [e.g., $(N_1)_{60}$, $V_{s1}$, $q_{c1}$; Section 2.3.2] to the soils resistance to cyclic loading from a magnitude 7.5 earthquake ($CRR_{7.5}$). Field performance data from earthquakes at magnitudes other than 7.5 are corrected to equivalent $CSR_{7.5}$ values as:

$$CSR_{7.5} = \frac{CSR}{MSF} \tag{4.6}$$

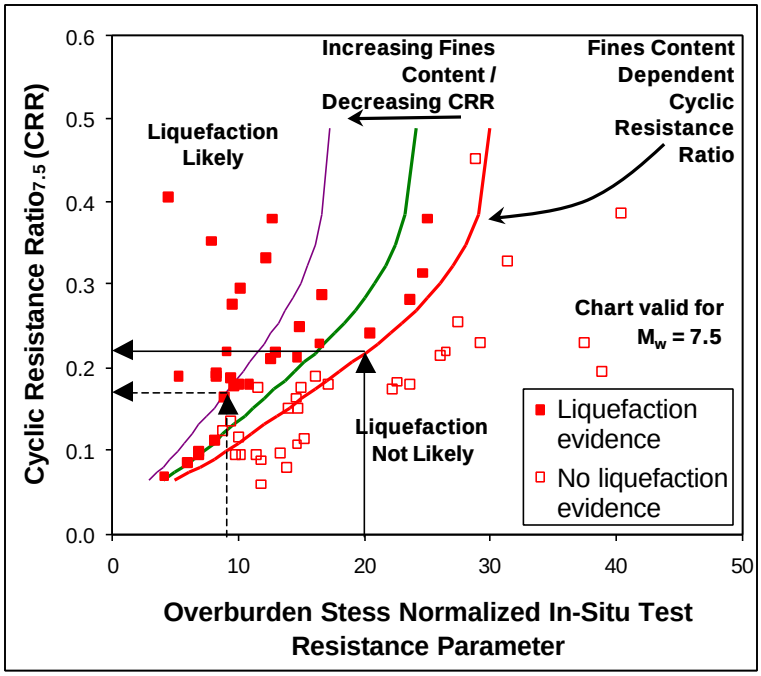


**Figure 4.3. Key Aspects of Simplified Cyclic Stress based Charts**

Field data are separated into sites that have or have not displayed surface manifestations of liquefaction behavior. A demarcation line, known as the $CRR_{7.5}$, is generated between the liquefaction and non-liquefaction sites. This line was originally estimated by hand, but mathematical representations are generally preferred for spreadsheet application. Figure 4.3 displays an example field case history data base, and notes key features of a typical chart.

Cyclic stress-based analysis consists of the following steps:

1. Determine $a_{max}$ and $M_w$ for design earthquake;
2. Determine the profile of cyclic stress ratio (CSR) with depth using equations 4.1 and 4.3 or a site specific analysis (e.g., SHAKE91; Idriss & Sun, 1992);

3. Evaluate critical layer resistance parameters from SPT, CPT, or $V_s$ profiles;
4. Estimate fines content from laboratory index tests or field correlations;
5. Determine cyclic resistance ratio from charts or simplified formulas as a function of in-situ test resistance parameter and fines content;
6. Calculate a factor of safety (FS) against liquefaction for the design earthquake as (Youd & Noble, 1997):

$$FS = \left( \frac{CRR_{7.5}}{CSR} \right) \cdot MSF \qquad (4.7)$$

where MSF is a magnitude scaling factor equal to one for earthquakes with moment magnitude ($M_w$) of 7.5.

4.2.4 Application to Paleoliquefaction Studies

For paleoliquefaction studies and backcalculation of accelerations, the calculated FS will be close to unity in cases of marginal liquefaction, and below unity for extensive liquefaction. Questions arise concerning the validity of using of post-earthquake field data to estimate pre-earthquake in-situ state, and thus backcalculation of prehistoric accelerations. The use of field performance data in liquefaction studies became popular because sampling destroyed structure and aging effects, which are known to increase liquefaction resistance. At a location of surface evidence of liquefaction, such as sand boils and lateral spreads, it would be expected that the post-earthquake soil conditions would be extremely disturbed with a loss of structure and aging effects.

It has been shown that sites that liquefy during an earthquake event will likely liquefy in subsequent events (Youd, 1984; Yasuda & Tohno, 1988). This process has been termed re-liquefaction. Earthquakes have been occurring throughout the evolution of the planet, so at liquefaction sites in seismically-active regions it would be expected that soils have undergone more than one liquefaction event over the history of the deposit. Younger sand dikes erupting through older sand dikes have been noticed in the NMSZ, but are not common. These previous events would destroy the natural alluvial deposition structure, and replace it with a loose pluvial structure resembling that of water sedimentation (Pond, 1996). With time, the soil structure and aging effects would form in a similar manner as they had before the previous liquefaction event. It has been shown that strength increase in sands from aging is a log-linear process (logarithm for time, and linear for strength increase; Seed, 1979). A majority of the strength increase occurs within the first 100 years after deposition, and then the effects level off. If sites with pre-earthquake field data are not available, it would be desirable to test the properties of the soil after a time period where aging would better resemble the pre-earthquake structure.

4.2.5 Liquefaction Evaluation from Standard Penetration (SPT) Test Data

Seed et al. (1983) developed a field performance database for liquefaction analysis using uncorrected standard penetration test (SPT) N-value. This study was comprised of sites where surface manifestations of liquefaction (e.g. sand boils, lateral spreading, etc.) were either evident or not evident during post-earthquake field reconnaissance investigations. SPT values were plotted against the $CSR_{7.5}$ (Eq. 4.1; Eq. 4.6) from the earthquake event, and a demarcation line ($CRR_{7.5}$) was determined from the boundary

between sites where liquefaction was evident and other sites where no surface evidence of liquefaction was observed. Some data were also classified as "marginal evidence," and these points were expected to lie closer to the cyclic resistance ratio curve.

Since this database was generated from different studies throughout the world, the variation in N-value from SPT procedures was recognized to influence the position of the CRR curve (Seed et al., 1985). Current simplified curves using SPT data are compared to the $(N_1)_{60}$ value, which has been corrected to an energy efficiency of 60 percent for procedural variation, and normalized to an overburden stress of 1-atmosphere (Chapter 2). Additional case histories have been used to slightly modify the position of the CRR, but due to the variability in the SPT, additional analyses should be performed on borderline cases to reduce the inherent uncertainty. An empirical equation for the cyclic resistance ratio adapted by NCEER (1997) is:

$$CRR_{7.5} = \frac{a + cx + ex^2 + gx^3}{1 + bx + dx^2 + fx^3 + hx^4} \qquad (4.8)$$

where the parameter $x = (N_1)_{60cs}$, and the empirical constants consist of: a = 4.844·E-2, b = -1.248·E-1, c = -4.721·E-3, d = 9.578·E-3, e = 6.136E-4, f = -3.285E-4, g= -1.673E-5, and h = 3.714E-6. The parameter $(N_1)_{60cs}$ is the stress normalized SPT blowcount corrected for energy efficiency and fines content. The fines content correction can be estimated by (Robertson & Wride, 1997):

$$(N_1)_{60cs} = K_s \cdot (N_1)_{60} \quad (4.9a)$$

$$K_s = 1 + \left[ \left( \frac{0.75}{30} \right) \cdot (FC - 5) \right] \quad (4.9b)$$

Figure 4.3 displays the Seed et al. (1985) SPT database along with the NCEER (1997) curves. Four charts are presented: (a) clean sand data with fines content (FC) less than 5 percent; (b) silty sand data with fines content between 5 and 15 percent; (c) sandy silt data with fines content between 15 and 35 percent; and (d) silt data with fines content greater than 35 percent.

The SPT case history data and the mathematical representation of the cyclic resistance ratio curves match well. For clean sands, there is sufficient data that suggests a relatively linear relationship between CRR and N-value for low N-value soils, which trends towards a vertical asymptote at about 30 blows per foot. The silty sand (FC=15%) curve matches well with the case histories, but there are insufficient data to support a vertical asymptote. The data for sandy silt (FC between 15 and 35%) match well with the proposed trends, but there are insufficient data to support a vertical asymptote. The data for the silty soils (FC > 35%) match well with the proposed trends. While there is only 1-point at a high cyclic stress ratio (0.6), this point supports the concept of a vertical asymptote at an N-value of about 17.

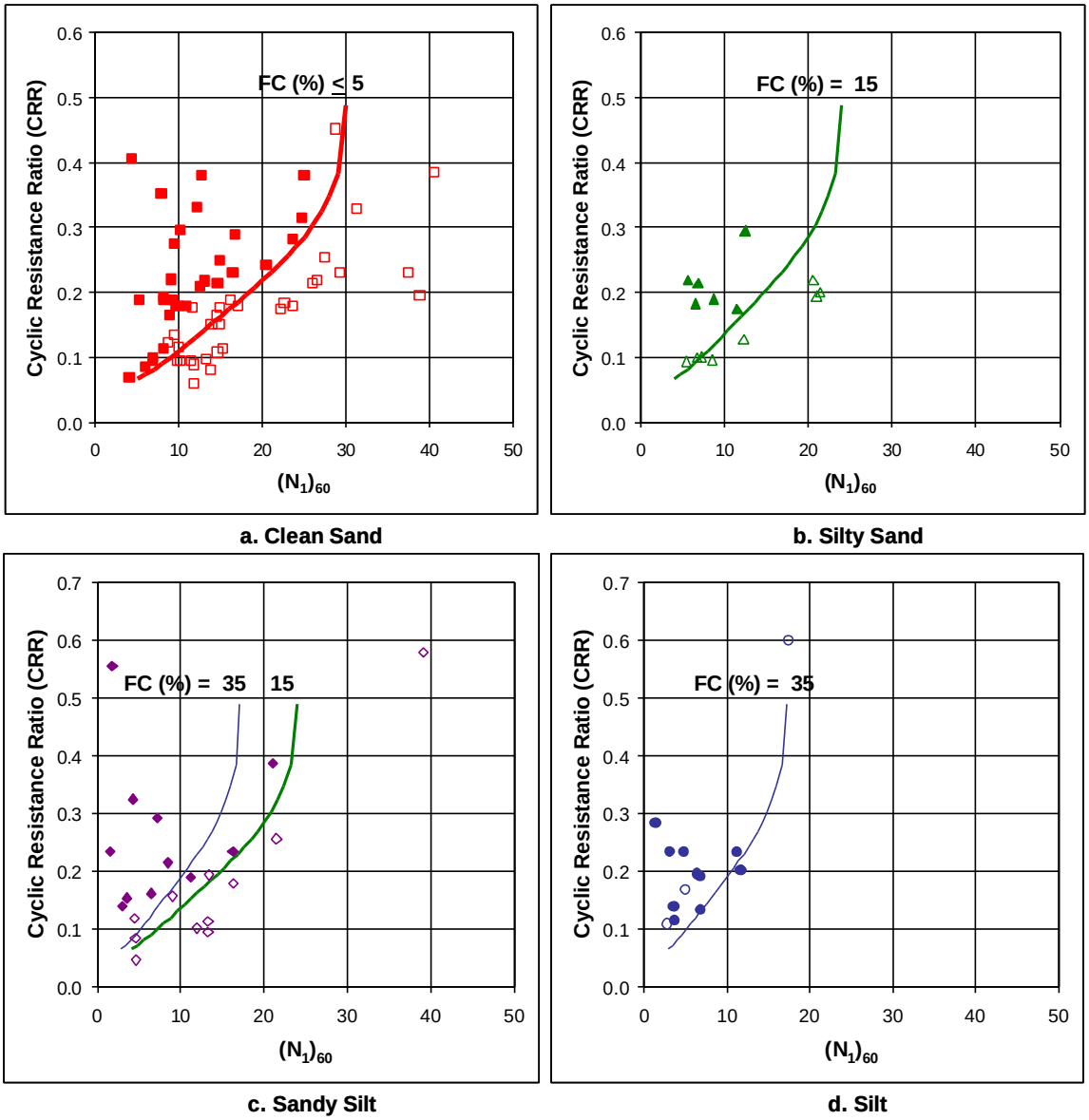


**Figure 4.4. SPT Liquefaction Site Database and NCEER CRR curves (a) FC (%) ≤ 5; (b) 5 < FC (%) ≤ 15; (c) 15 < FC (%) ≤ 35; (d) FC (%) > 35 (adapted from Seed et al., 1986; Robertson & Wride, 1997)**

It can be expected that CRR trends for various levels of fines content will be similar. The concept of a limiting vertical asymptote makes sense when considering the existence of a critical void ratio (Casagrande, 1936) and a critical state line for sands (Been, 1999). More detail on the critical state parameters for sands is presented in Appendix I. The currently recommended curves by NCEER (1997) have good agreement with the field data as well as concepts relating to the shear behavior of sands.

4.2.6 Liquefaction Evaluation from Cone Penetration Test (CPT) Data

Since the CPT is more reliable than the SPT, a simplified cyclic-stress based procedure using the cone penetration test was formed. When the CPT method was initially developed, there were only a limited number of case histories with available cone tip resistance data. Therefore, correlations between SPT N-value and CPT tip resistance were used along with the SPT liquefaction case history database presented in the previous section (Robertson & Campanella, 1985; Seed & DeAlba, 1986). To reduce uncertainty from the SPT-CPT correlation, a CPT only database was developed by Shibata & Teparaksa (1988). New field data have been added by Stark & Olson (1995) and Olson & Stark (1998). The CPT database now contains 172 independent case histories of seismic sites where surface evidence of liquefaction has or has not been evident.

With the cone penetration test, a soil specimen is not retrieved, resulting in questions as to the soil type and fines content. Many different classification schemes are currently available for cone testing based on tip resistance and friction ratio, FR, or tip resistance and pore pressure parameter, $B_{q.}$ These schemes are discussed in detail in Section 2.3.3. In addition to tip resistance data, it is necessary to estimate fines content in sandy layers.

Correlations between fines content and Friction Ratio (FR = $f_s/q_t \cdot 100$) have been presented in Suzuki et al. (1995a; 1995b), Robertson & Wride (1997), as well as Olsen (1997). In contrast, and a lack of correlation between Friction Ratio and fines content has been shown in Arango (1997). Confirmation of CPT fines content correlations by sampling and index testing is recommended (Mitchell & Brandon, 1998). In clean sands, the penetration pore water pressures will be close to hydrostatic. The pore pressure reading behind the tip will also be useful in estimating water table depth as well as soil strata demarcations.

The cyclic resistance ratio for CPT $q_c$ has been represented as a numerical approximation by Robertson & Wride (1997; 1998) and Olsen (1997). The NCEER (1997) workshop participants reviewed these methods and recommend the following expression from Robertson & Wride (1997):

$$\text{if } 50 \le (q_{c1N})_{cs} < 160 \qquad CRR_{7.5} = 93 \cdot \left( \frac{(q_{c1N})_{cs}}{1000} \right)^3 + 0.08 \qquad (4.10a)$$

$$\text{if } (q_{c1N})_{cs} < 50 \qquad CRR_{7.5} = 0.83 \left( \frac{(q_{c1N})_{cs}}{1000} \right) + 0.05 \qquad (4.10b)$$

where $(q_{c1N})_{cs}$ is the stress-normalized cone tip resistance corrected for apparent fines content. Appropriate normalization factors for this method were presented earlier in Table 2.4. The concept of a clean sand corrected tip resistance has not been

recommended by the NCEER (1996) committee, but it is based on a similar concept as presented for the SPT where:

$$(q_{c1N})_{cs} = K_c \cdot q_{c1N} \tag{4.11}$$

with methods to estimate $K_c$ based on grain characteristics as presented in Robertson & Wride (1997; 1998). Figure 4.5 displays the Olson & Stark (1998) database along with the NCEER (1997) cyclic resistance ratio curves. Four charts are presented: (a) clean sand data; (b) silty sand data; (c) sandy silt data; (d) all 3 NCEER curves. The CRR curves for 15 percent and 35 percent fines content were calculated using the $K_c$ clean sand correction factor. The cone tip resistance presented in Olsen & Stark (1998) was normalized using the Kayen et al (1992) method, with the resulting units presented in megapascals (MPa). The CRR calculated from the Robertson & Wride (1997) formula was converted to MPa as:

$$q_{cq} = q_{c1} \cdot \frac{0.1013 \cdot MPa}{atm} \tag{4.12}$$

where $q_{c1}$ is the Kayen et al. (1992) normalized tip resistance, and $q_{c1N}$ in the Robertson & Wride (1997; 1998) normalized tip resistance.

The proposed curves and field performance match well for the CPT data, but the Robertson & Wride (1997; 1998) curve appears to be slightly unconservative for all soil types. There are no CPT field data supporting a vertical asymptote for any of the soil

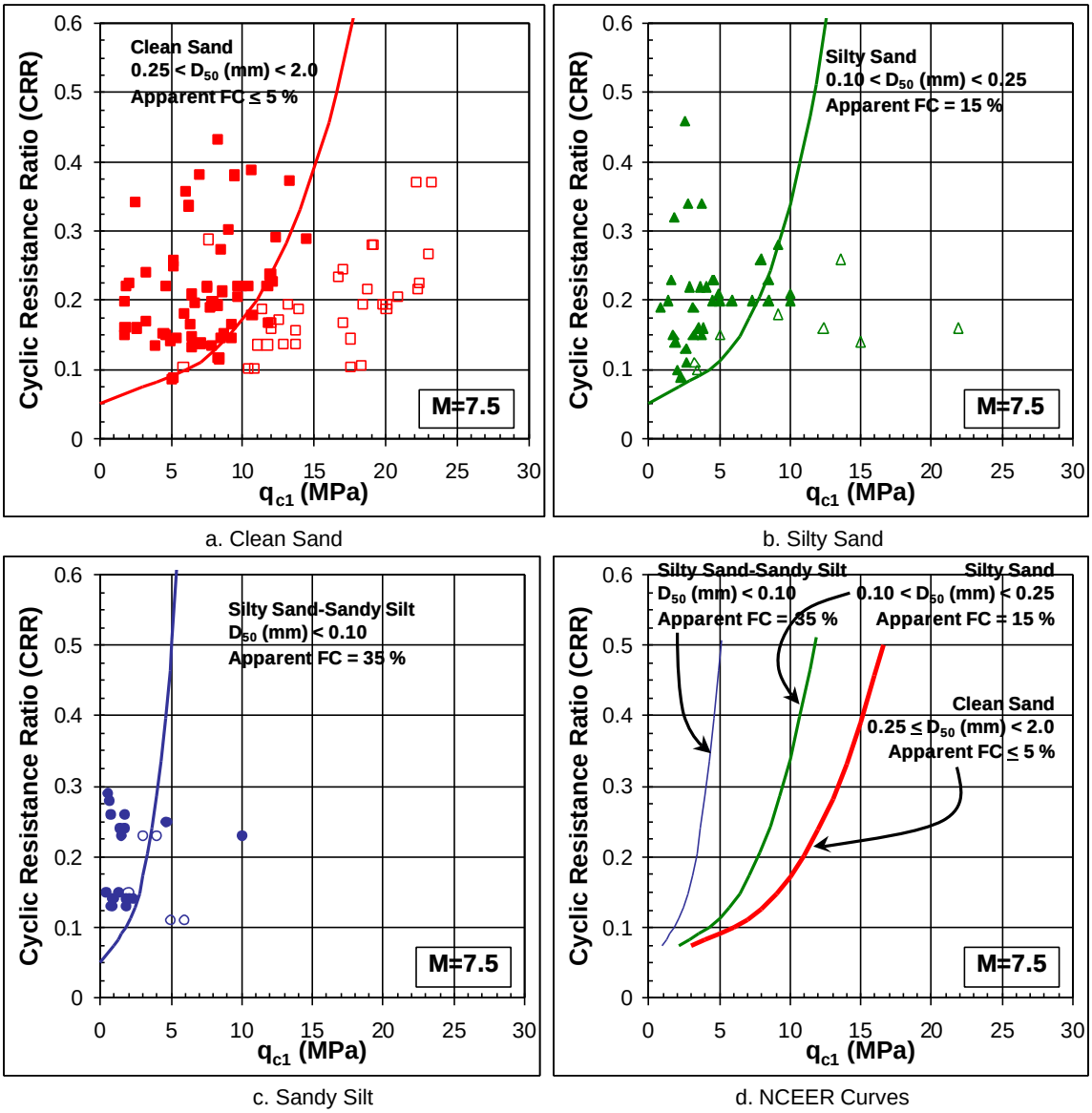


**Figure 4.5. CPT Liquefaction Database and NCEER Recommended CRR (a) Clean Sand; (b) Silty Sand; (c) Sandy Silt; (d) NCEER Curves (Adapted from Olson & Stark, 1998; Robertson & Wride, 1997)**

types. While the Robertson & Wride (1997; 1998) curve is recommended up to a CSR of 0.5, additional data from sites that have not liquefied at high CSR values would lead to more confidence in the suggested CRR curve.

4.2.7 Liquefaction Evaluation from Shear Wave Velocity ($V_s$) Data

Cyclic stress-based procedures were based on the premise that liquefaction resistance is governed by relative density. Since in-situ penetration test resistance parameters are also strongly influenced by relative density, a correlation between in-situ test parameters and liquefaction resistance should exist. The work of Dobry et al (1982) determined that seismically-induced shear strains are more important than seismically-induced stresses in the liquefaction response of soils. To adapt the cyclic strain-based procedures to the well-known simplified cyclic stress based methods, shear stress is related to shear strain using the shear modulus. Since the shear modulus is directly related to shear wave velocity through the fundamental equation $G = \rho V_s^2$, a theoretical basis exists for the development of cyclic resistance ratio curves using shear wave velocity data. Andrus & Stokoe (1997) present the derivation of a shear wave velocity dependent CRR for relatively small strains (e.g., less than about $5 \times 10^{-1}$ %). For higher strain levels, a limiting value of shear wave velocity is expected to be approached. Shear wave velocity is strongly influenced by void ratio and the coordination number of the soil fabric (e.g., Robertson et al., 1995; Santamarina et al., 1999). Therefore, the concepts of critical void ratio (Casagrande, 1936) and a unique critical state line for sands (Been, 1999) can be incorporated into the derivation of this CRR equation.

As in the case of the SPT, and CPT, a database of field case histories has been developed comparing shear wave velocity at seismically-active sites that have or have not shown surface manifestations of liquefaction. The database contains over 75 sites subject to 25 earthquakes between 1906 and 1995 (Andrus et al., 1999). Most of the shear wave velocity data is from post earthquake field investigations, so the soil fabric is likely disturbed from its pre-earthquake sate. This may increase shear wave velocity from additional cyclic pre-straining, or reduce shear wave velocity if aging and cementation affects were destroyed by excessive cyclic straining. Since the same shear wave velocity measurements at a site were used for multiple earthquakes, additional scatter is expected when comparing the database results to theoretical curves.

The cyclic resistance ratio for overburden stress normalized shear wave velocity ($V_{s1}$) has been represented as a numerical approximation by Andrus & Stokoe (1997) and updated by Andrus et al. (1999):

$$CRR_{7.5} = a \cdot \left( \frac{V_{s1}}{100} \right)^2 + b \cdot \left( \frac{1}{V_{s1}^{*} - V_{s1}} - \frac{1}{V_{s1}^{*}} \right) \qquad (4.13)$$

where $V_{s1}=V_s / (\sigma_{vo}')^n$ and is the stress normalized shear wave velocity using a stress exponent n = 0.25 and $\sigma_{vo}'$ is in atmospheres (Robertson et al., 1992b), $V_{s1}^{*}$ is the limiting upper value of $V_{s1}$ for liquefaction occurrence, and *a* and *b* are curve fitting parameters equal to 0.022 and 2.8 respectively. The limiting value of shear wave velocity in sandy soils has been estimated to be:

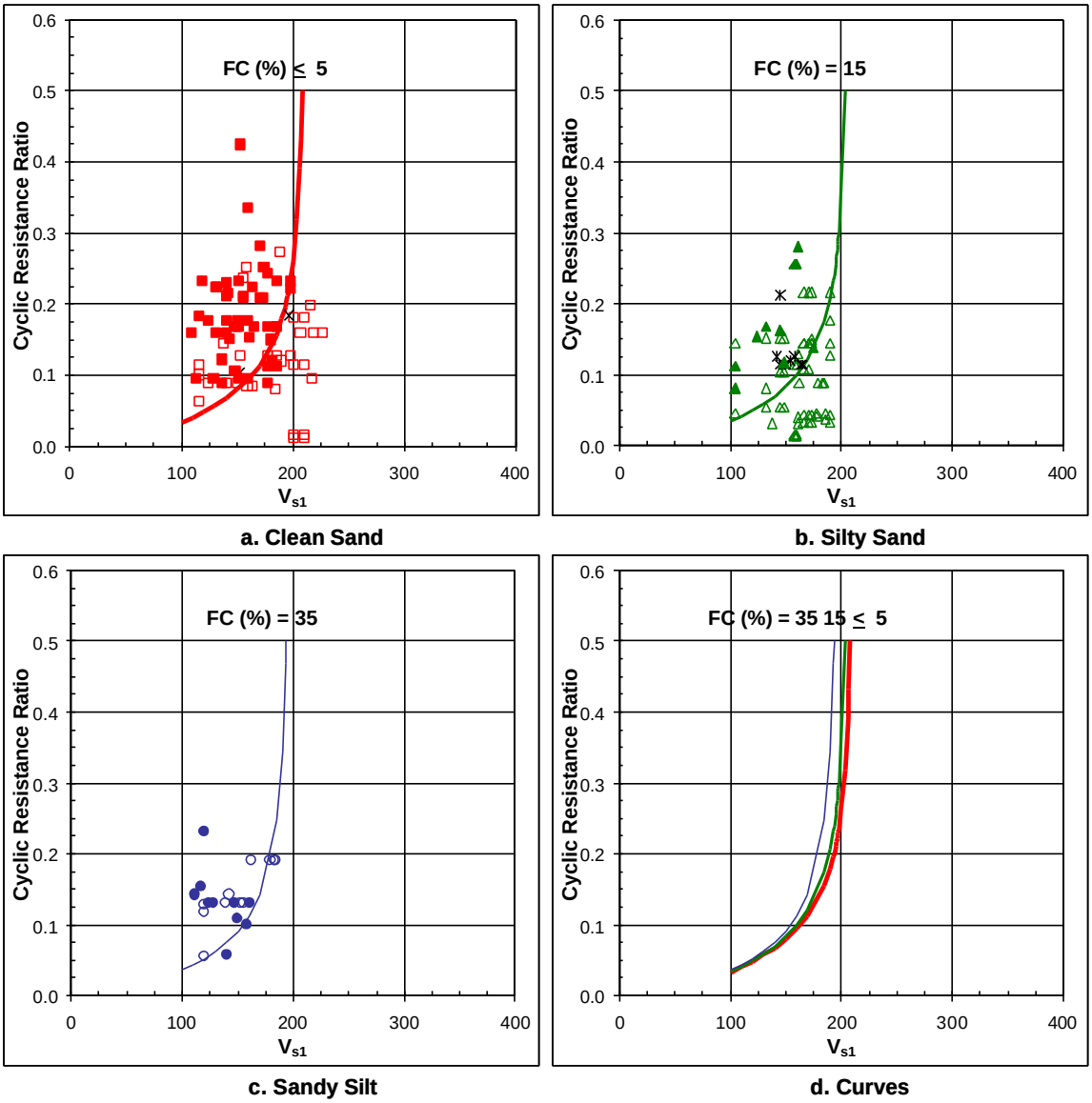


**Figure 4.6. $V_s$ Liquefaction Site Database and Recommended CRR Curves (a) Clean Sand; (b) Silty Sand; (c) Sandy Silt; (d) Andrus et al. (1999) Curves (adapted from Andrus & Stokoe, 1997; Andrus et al., 1999)**

$V_{s1}^{*}$ = 215 m/s  FC (%) ≤ 5  (4.14a)

$V_{s1}^{*}$ = 215 - 0.5·(FC-5) m/s  5 < FC (%) < 35  (4.14b)

$V_{s1}^{*}$ = 200 m/s  FC (%) ≥ 35  (4.14c)

Figure 4.6 displays the Andrus & Stokoe (1997) database along with the Andrus et al. (1999) cyclic resistance ratio curves. Four charts are presented: (a) clean sand data; (b) silty sand data; (c) sandy silt data; (d) all 3 NCEER curves. The data agree well with the proposed CRR curves, but the Andrus et al. (1999) curve appears to be slightly unconservative for all soil types. There are limited $V_s$ field data supporting a vertical asymptote for any of the soil types, so additional data from sites that have not liquefied at high CSR values would lead to greater confidence in the CRR curves.

4.2.8 Extrapolation to High CSR

It is anticipated that an extreme event in Mid-America could result in cyclic stress ratios on the order of 1.0 or higher at close epicentral distances (Toro et al., 1997). Current field performance data are is limited to CSR values typically below 0.4, with most data in the 0.1 to 0.2 range. Laboratory tests on reconstituted specimens can not fully replicate soil fabric, which contributes significantly to liquefaction resistance. Advances in sampling of granular soils by freezing techniques allows in-situ soil fabric to remain relatively undisturbed prior to laboratory testing. Therefore, the cyclic resistance of a deposit may be more accurately determined from laboratory testing.

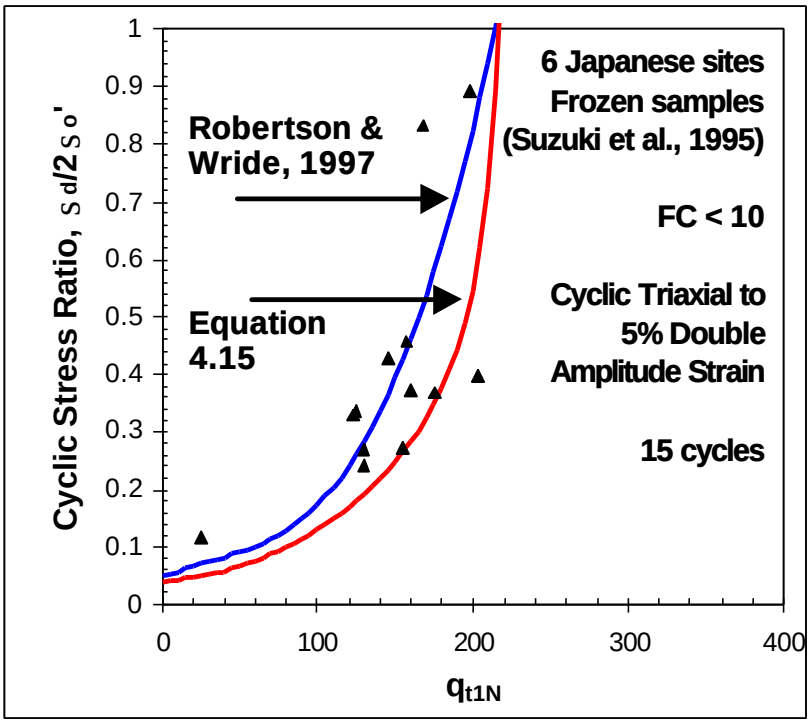


**Figure 4.7. Comparison of CRR curves and Laboratory Frozen Specimens**

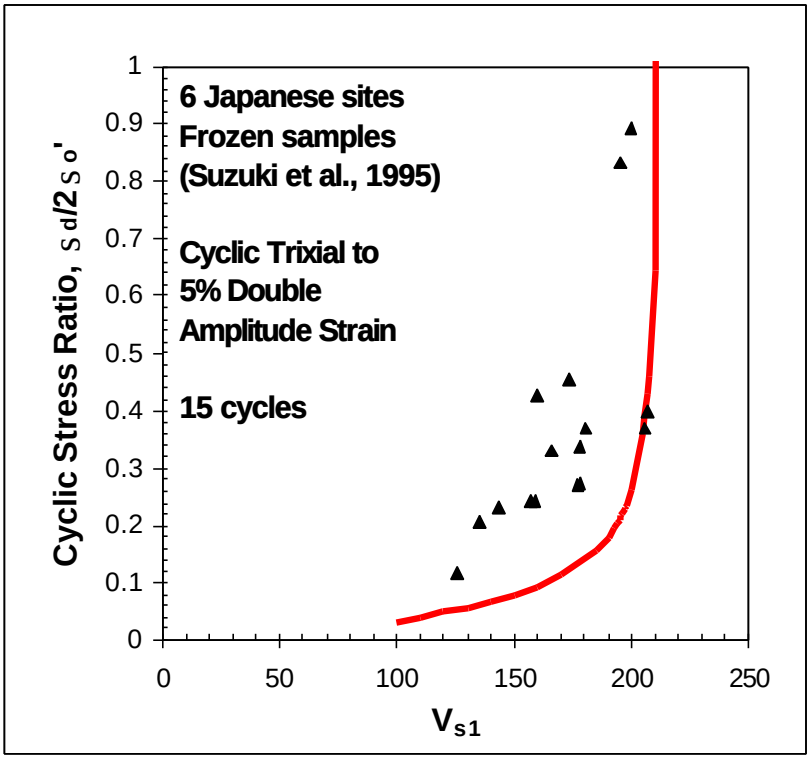


**Figure 4.8. Comparison of $V_{s1}$ CRR curve and Laboratory Frozen Specimens**

Field performance based CRR curves can be validated by comparison of laboratory based cyclic resistance from frozen specimens to in-situ test parameters taken adjacent to the sample location. A study by Suzuki et al (1995b) presents field shear wave velocity and cone tip resistance data as compared to laboratory cyclic resistance from frozen specimens. Figures 4.7 and 4.8 display the data compared to $q_{c1}$ and $V_{s1}$ respectively. The Robertson & Wride (1997; 1998) curves match the average value of the data presented in Suzuki et al. (1995) study, but a number of points are misclassified. The uncertainty inherent when using simplified curves should result in a conservative estimate of liquefaction resistance, such as the Seed et al. (1985) SPT-type CRR curves. The Robertson & Wride (1997; 1998) curves do not approach an asymptotic value at high values of CSR. Considering the concepts of a critical void ratio and critical state for sands, an asymptotic value is expected for CRR curves.

The work of Andrus & Stokoe (1997) and Andrus et al. (1999) present an equation for the CRR based on shear wave velocity data. The format of this equation leads to an asymptotic value of shear wave velocity at high values of CSR. A similar form will be adapted for the CRR determined from CPT $q_{c1N}$ data:

$$CRR = a \cdot \left( \frac{q_{c1N}}{350} \right) + \frac{b}{\left( q_{c1N}{}^{*} - q_{c1N} \right)} \qquad (4.15)$$

where *a* and *b* are curve fitting parameters equal to 0.7 and 9.33 respectively. The Andrus & Stokoe (1997) term $-b/V_{s1}{}^{*}$ (or in this case $-b/q_{c1N}{}^{*}$) is left out of the

equation since it is accepted that the CRR does not pass through the origin (NCEER, 1997). The limiting value of normalized cone tip resistance in clean sands has been estimated to be 230 from cyclic triaxial test data. To validate this curve for field performance data, Figure 4.8 compares Equation 4.15 and the Robertson & Wride (1997; 1998) CRR equation (Eq. 4.10) for the Olson & Stark (1998) CPT field performance database. Equation 4.15 is more conservative than currently-recommended methods, but seems to better fit all of the field data. It incorporates critical state concepts for sands with a limiting value of normalized CPT tip resistance.

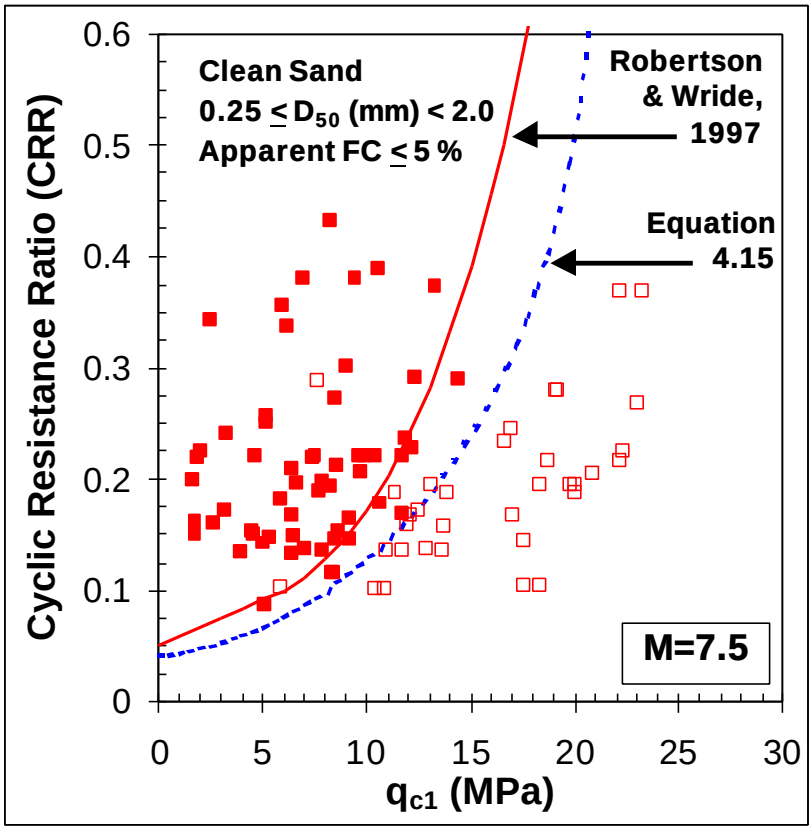


**Figure 4.9. Comparison of CRR curves with CPT Field Performance data**

## 4.3 Cyclic Strain Approach

The cyclic strain approach was developed by Dobry et al. (1982) as a more rational means to accommodate that the liquefaction resistance of soils is controlled not only by relative density, but also by soil fabric, level of prestraining, lateral stress coefficient ($K_o$), overconsolidation ratio (OCR), and aging effects. Strain-controlled cyclic triaxial tests to evaluate porewater pressure generation due to cyclic straining are apparently not affected by relative density, fabric effects, prestraining, and aging, as seen in Figure 4.10 (Dobry et al., 1982). The soil stiffness (G) increases with increased relative density, and decreased in void ratio (Hardin and Drnevich, 1972). This will in turn reduce shear-induced strains, and increase liquefaction resistance. The generality of the cyclic strain approach is appreciated further because cyclic generation of porewater pressures has been shown to be dependent on lateral stress and OCR (Vasquez-Herrera et al., 1988), but relatively independent of the sand tested (Ladd et al., 1989).

The cyclic strain method consists of the following steps (Dobry et al., 1982):

1. Determine strain level ($\gamma_c$) with depth;
2. Compare induced-strain level to the plastic threshold strain level ($\gamma_t^p = 10^{-2}\%$);
3. Evaluate porewater pressure buildup using normalized curves;
4. Decide if the pore pressures in the soil will cause initial liquefaction ($u = \sigma_{vo}$).

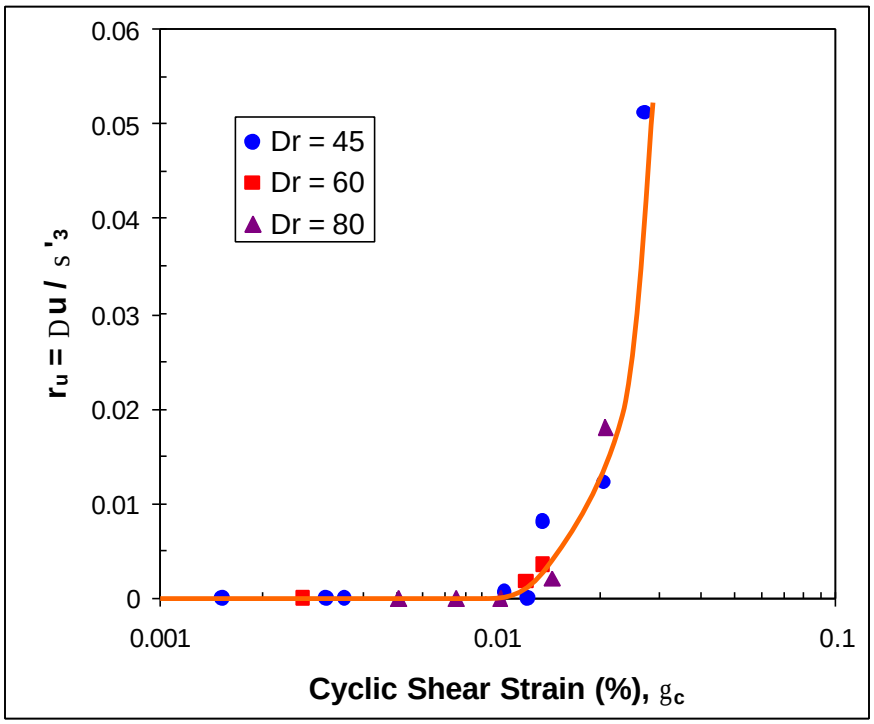


**Figure 4.10. Density Independence of Initial Porewater Pressure Generation During Cyclic Strain Controlled Tests on Some Sand (after Ladd et al., 1989)**

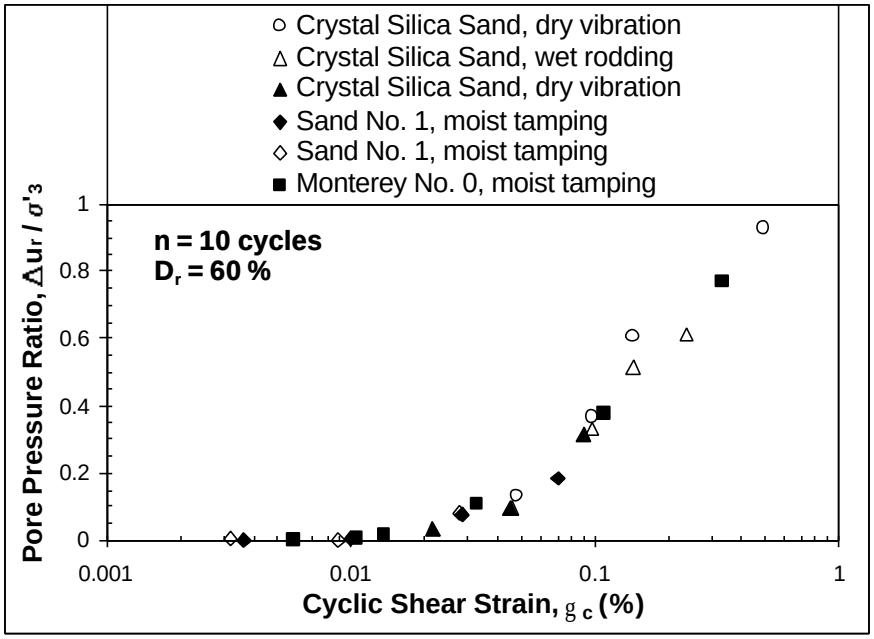


**Figure 4.11. Sand Type and Preparation Method Independence of Porewater Pressure Generation in Cyclic Strain Controlled Tests (after Ladd et al., 1989)**

4.3.1 Shear Strain Level with Depth

The strain level with depth can be estimated by using two primary methods:

1. Simplified procedures developed by Seed & Idriss (1971) can be modified using maximum shear modulus ($G_o = G_{max}$) and normalized $G/G_{max}$ degradation schemes;
2. Site-specific analysis, such as SHAKE91 (Idriss & Sun, 1992).

This study will only be concerned with modified simplified procedures. The equations necessary for the simplified analysis utilize the definition of shear modulus (Eq. 4.16) to modify the simplified CSR equation (Eq. 4.1):

$$g = \frac{t}{G} \tag{4.16}$$

$$g = 0.65 \cdot \frac{a_{\max}}{g} \frac{s_{vo}}{G_{\max}\left(G/G_{\max}\right)_g} r_d \tag{4.17}$$

where $\gamma$ is strain level, $\tau$ is the earthquake induced stress level, G is the strain level dependent shear modulus, $a_{max}$ is the maximum horizontal surface acceleration, g is the acceleration due to gravity, $\sigma_{vo}$ is the total vertical stress, $r_d$ is the stress reduction coefficient presented in Equation 4.3, $G_{max}$ is the maximum small strain shear modulus, and $(G/G_{max})_\gamma$ is the modulus reduction factor at the appropriate strain level. The effective vertical stress ($\sigma_{vo}'$) cancels out of this equation, since it is on both sides of Equation 4.1. The maximum small strain shear modulus, $G_{max}$, can be directly obtained from the shear wave velocity determined from SCPTu soundings as:

$$G_{max} = \rho \cdot V_s^2 \qquad (2.3; 4.18)$$

The mass density ($\rho$) can be estimated from shear wave velocity and depth (Mayne et al., 1999):

$$r \approx 1 + \frac{1}{0.614 + 58.7 \cdot (\log z + 1.095)/V_s} \qquad (2.4; 4.19)$$

where $z$ is depth in m, and $V_s$ is in m/s. Typical modulus reduction schemes have been presented by Seed & Idriss (1970) and Vucetic & Dobry (1991) among others. Laboratory data matched well with normalized reduction curves related to effective confining stress presented in Ishibashi (1992). A modified hyperbola (Eq. 2.6) will be used for modulus reduction in cyclic strain analysis.

4.3.2 Initial Porewater Pressure Generation

Strain controlled cyclic test results on sands from Dobry et al. (1982) show two threshold shear strains that should be noted for liquefaction analysis:

1. the elastic threshold shear strain, $\gamma_t^e$;
2. the plastic threshold shear strain, $\gamma_t^p$.

In sandy soils, the elastic threshold shear strain, $\gamma_t^e$, will be a function of confining stress, as discussed in section 2.3.1. For depths of concern for liquefaction evaluation (z

< 20 m), the overburden stresses should be within the 0.5- to 2-atmosphere range. This will result in an elastic threshold strain on the order of $1x10^{-3}$ percent.

Once the plastic threshold shear strain ($\gamma_t^p$) is exceeded, pore pressures will be induced by undrained cyclic loading. Figures 4.7 and 4.8 display the independence of plastic threshold strain with regards to sand type, preparation method (fabric), and relative density. The plastic threshold shear strain in sands is considered to be equal to $1x10^{-2}$ percent (Dobry et al., 1982).

If the plastic threshold shear strain is not reached, cyclic pore pressures will not be induced and liquefaction will not occur. The reduced shear modulus at $\gamma_t^p$ will be approximately equal to $0.8 \cdot G_{max}$. Therefore the following screening equation can be generated from Equations 4.17:

$$g = \frac{a_{max}}{g} \cdot \frac{s_{vo}}{1.23 \cdot G_{max}} \cdot r_d \qquad (4.20)$$

where all terms are as defined above. If $\gamma$ induced by the earthquake is less than $1x10^{-2}$ ($\gamma_t^p$), liquefaction will not occur.

4.3.3 Cyclic Pore Pressures from Normalized Curves

For induced strain levels higher than the plastic threshold shear strain ($\gamma_t^p$), an evaluation of cyclic pore pressure generation will be desired. Vasquez-Herrera et al. (1988) developed an empirical method relating the stress state of the soil to the shape of the pore pressure generation curve. This method was developed for flow liquefaction of

embankments, but will be adapted for use with cyclic liquefaction. The key soil and empirical parameters used in the development of this method are:

- soil liquefaction will occur at a critical pore pressure ratio ($r_u = \Delta u/\sigma_{vo}$');
- a threshold pore pressure ($r_{ut}$) may exist below initial liquefaction ($r_u = 1$);
- $r_{ut}$ is a function of $K_c$ and $\alpha'_{up}$;
- $K_c$ is the ratio of vertical stresses to horizontal stresses ($\sigma_{1c}' / \sigma_{3c}'$);
- $\alpha'_{up}$ is a flow liquefaction failure surface where loss of contact points between soil grains will leads to structural collapse, rapid increase in pore pressure, and flow to a critical void ratio (Alarcon-Guzman et al., 1988);
- the number of cycles to liquefaction is a function of $r_{ut}$, $\gamma_t^p$, induced cyclic strains ($\gamma_{cy}$), and the empirical coefficients $\alpha$ and $\beta$;
- The empirical curve fitting parameter $\alpha = 4.78 - 1.91 \cdot K_c$;
- The empirical curve fitting parameter $\beta = 2.96 - 0.78 \cdot K_c$;

The normalized pore pressure generation curves will be adapted for free field level ground cyclic liquefaction by using the following:

- the threshold pore pressure generation coefficient ($r_{ut}$) will be equal to one (Seed, 1979);
- the in-situ coefficient of lateral stress, $K_o = \sigma_{ho}' / \sigma_{vo}'$, will be equivalent to $1 / K_c$;
- the flow surface will not contribute to level ground liquefaction.

For evaluation of pore pressure generation, the in-situ coefficient of lateral stress ($K_o$) will need to be estimated. Analysis procedures for determining in-situ state was shown in

Chapter 2, and recommended correlations will be presented here. To estimate the lateral stress coefficient from CPT data in clean sands, $K_o$-OCR-$\phi'$ relationships presented in Mayne & Kulhawy (1982) will be utilized:

$$K_o = (1-\sin\phi')\cdot OCR^{\sin\phi'} \qquad (4.21)$$

The friction angle ($\phi'$) can be estimated from cone tip resistance ($q_t$) data as (Kulhawy & Mayne, 1990):

$$\phi' = 17.6^o + 11\cdot\log(q_t\cdot(p_a/\sigma_{vo}')^{0.5}) \qquad (4.22)$$

where $p_a$ is atmospheric pressure and $\sigma_{vo}'$ is the effective overburden stress. The estimation of $K_o$ in clean unaged quartz sands is obtained with Equations 4.21 and 4.22 in an iterative solution using the following expression based on calibration chamber test data (Mayne, 1995):

$$K_o = 0.192\left(\frac{q_t}{P_a}\right)^{0.22}\left(\frac{s_{vo}'}{P_a}\right)^{-0.31}\cdot OCR^{0.27} \qquad (4.23)$$

Three additional equations will be used to estimate the shape of pore pressure generation curves. The number of cycles to failure ($n_t$) can be represented as:

$$n_t = \frac{r_{ut}}{a\left(g_c - g_t^{\,p}\right)^b \cdot \left(2 - r_{ut}\right)} \tag{4.24}$$

where $r_{ut}$ is the threshold pore pressure ratio equal to one, and the other terms are as defined previously. The number of cycles generated by a seismic event will be a function of the earthquake magnitude, as discussed in section 4.2.2 on magnitude scaling factors:

$$n_{eq} \approx 0.0007 \cdot M_w^{\,4.94} \tag{4.4}$$

Therefore, the pore pressure ratio ($r_u = \Delta u/\sigma_3'$) for level ground earthquakes as a function of strain cycles can be expressed as:

$$r_u = \frac{1.02\left(\frac{n_{eq}}{n_t}\right)}{1 + 2.18 \cdot \left(\frac{n_{eq}}{n_t}\right)} + 0.68 \cdot \left(\frac{n_{eq}}{n_t}\right)^8 \tag{4.25}$$

with all parameters as defined above. If $r_u$ equals unity for an earthquake of n cycles, initial liquefaction will occur. Figure 4.12 displays the shape of porewater pressure generation curves set by $\phi$' as a function of the ratio of number of cycles to number of cycles to failure.

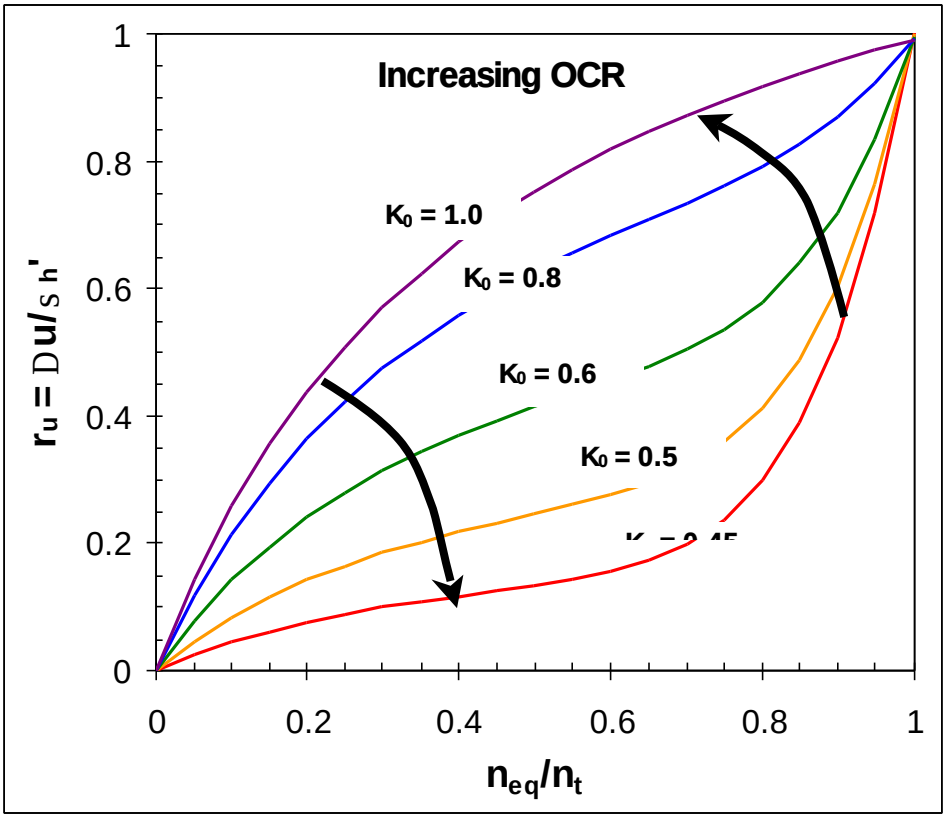


**Figure 4.12. Normalized Pore Pressure Generation Curves as a Function of $K_o$ (adapted from Vasquez-Herrera et al., 1989)**

## 4.4 Arias Intensity Method

A developing method for liquefaction analysis based on Arias intensity of earthquake records has the advantage that it does not require magnitude scaling factors. Although this method seems promising, lack of strong motion data in the Mid-America Earthquake region area leads to increased reliance on ground motion models. Arias intensity represents the cumulative energy per unit weight in a given direction that is absorbed by a set of single degree of freedom oscillators (Arias, 1970). Arias intensity ($I_h$) can be calculated as the sum of Arias Intensity in the x- ($I_{xx}$) and y- ($I_{yy}$) directions as (Kayen & Mitchell, 1997):

$$I_h = I_{xx} + I_{yy} = \frac{p}{2g}\int_0^{t_o} a_x{}^2(t)dt + \frac{p}{2g}\int_0^{t_o} a_y{}^2(t)dt \qquad (4.26)$$

where $g$ is the acceleration due to gravity, $a_x(t)$ is the horizontal acceleration time history in one direction, and $a_y(t)$ is the horizontal acceleration time history in the direction perpendicular to $a_x(t)$. The numerical integration of acceleration time histories to determine intensity should be performed on corrected acceleration time histories using trapezoidal integration (Youd et al., 1997).

Similarly to the CSR from the Seed & Idriss (1971) simplified procedure, the Arias intensity will typically decrease with depth. Depending upon the depth where the time history was recorded and the depth of the liquefied layer, it may be necessary to apply a depth correction factor, $r_b$:

$$I_{hb} = I_h \cdot r_b \qquad (4.26)$$

The Arias intensity depth correction factor was primarily determined from analysis of synthetic seismograms propagated through soil profiles using the SHAKE 1-D equivalent linear program. Significant scatter existed within the data (as is also evident in the $r_d$ correction factor for the simplified cyclic stress procedure), with average values as:

$r_b = 1.0 - 0.07z$ when $z \leq 6$ m (4.27a)

$r_b = 0.76 - 0.03z$ when $6 \text{ m} < z \leq 10$ m (4.27b)

$r_b = 0.46$ when $z > 10$ m (4.27c)

where z is in meters. Field data from the Superstition Hills and Elmore Ranch (California) earthquakes of 1987 lie between the averages presented above and one standard deviation below the averages (Kayen & Mitchell, 1997).

Simplified liquefaction resistance curves have been generated comparing Arias Intensity ($I_{hb}$) to penetration resistance [$(N_1)_{60}$ and $q_{c1}$] for field case histories where strong ground motion data have been readily available (Kayen & Mitchell, 1997). These curves are based on limited field data from California (n=28), and thus Arias Intensity Resistance to liquefaction curves ($I_{hb}R$) are considered quite approximate. Considering Arias intensity field performance data for the CPT, cyclic stress-based field data for the CPT, stress-based laboratory tests on frozen specimens compared to CPT tip resistance,

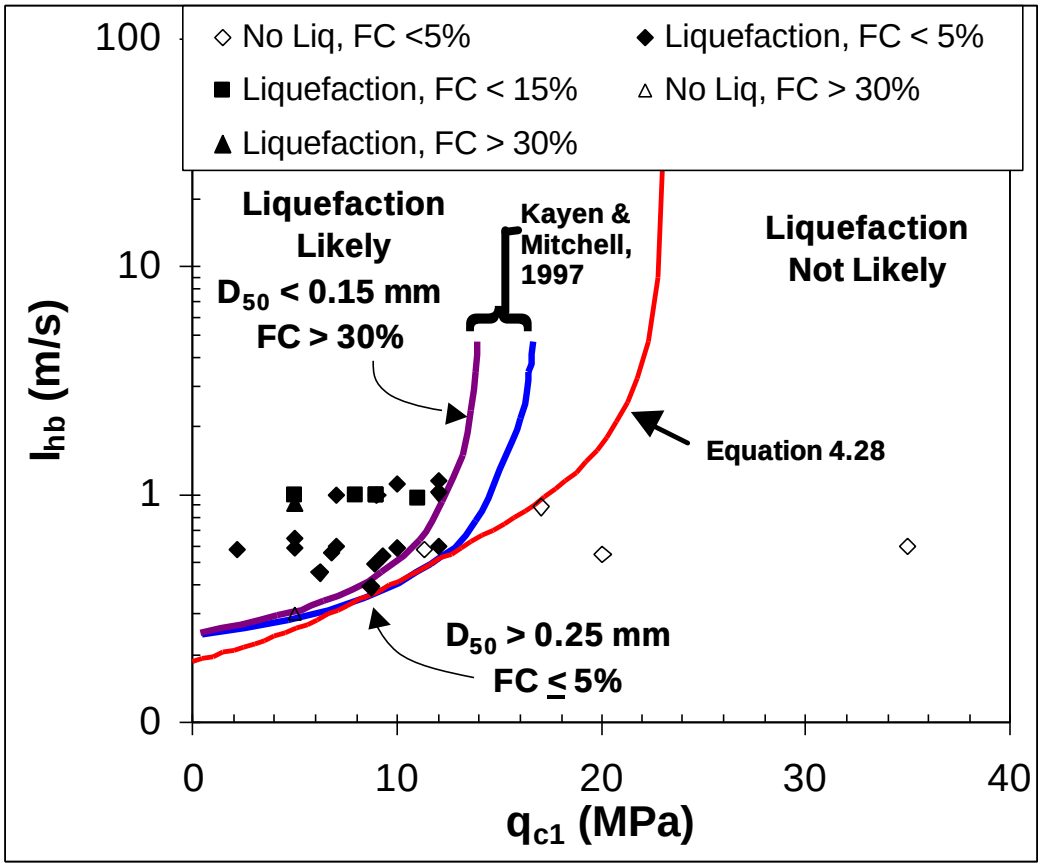


**Figure 4.13. Arias intensity Liquefaction Field Data compared to curves from Kayen & Mitchell (1997) and Equation 4.28**

and critical state concepts for sands, the CPT-based liquefaction resistance curve should approach a vertical asymptote. To maintain consistency in analysis, this asymptote should be equal to that presented for cyclic stress-based procedures in clean sands: $q_{c1n}^{*}$ = 230. Alteration of the curve fitting coefficients to account for differences between Arias intensity and cyclic stress ratio analyses, yields the following equation:

$$I_{hb}R = a \cdot \left( \frac{q_{c1N}}{350} \right)^2 + \frac{b}{\left( q_{c1N}^{*} - q_{c1N} \right)} \qquad (4.29)$$

where a = 1.1 and b = 42.7. Figure 4.13 displays field performance data and the simplified curves from (Kayen & Mitchell, 19997) and Equation 4.29 relating Arias intensity and normalized cone penetration resistance to liquefaction resistance. To maintain consistency with data presented in Kayen & Mitchell (1997), $q_{c1N}$ was converted to the units of MPa for Figure 4.13. Both sets of curves match well with the field data, but Equation 4.29 approaches a more reasonable asymptote at $q_{c1N}^{*}$ = 230.

## 4.5 Summary

Current liquefaction evaluation procedures that utilize SCPTu parameters directly, or indirectly through a rational framework, have been discussed. These methods and their associated controlling parameters include:

1. Cyclic stress-based framework
    - based solely on cone tip resistance ($q_t$)

- base solely on shear wave velocity ($V_s$)

2. Arias intensity based framework
    - based solely on cone tip resistance ($q_t$)
3. Cyclic strain based method
    - based on engineering parameters ($K_o$, OCR, $\phi$', $D_r$) determined from shear wave velocity ($V_s$) and cone tip resistance ($q_t$)

Anticipated cyclic stress ratio (CSR = $\tau$ / $\sigma_{vo}$') and Arias intensity ($I_{hb}$) from a severe event in Mid-America are anticipated to be much higher than current curves have been validated in China, Japan, and California. Utilization of the concepts of critical state for sands in association with data from cyclic tests on frozen specimens has been used to determine cyclic resistance ratio curves that progress to an asymptotic value. These curves have been validated as a conservative lower bound for clean sand field data from liquefaction sites. The same curve format with altered empirical coefficients (a & b) has been applied to Arias intensity based field data. These proposed curves are more internally consistent, and encompass the available liquefaction case data. This provides a conservative curve for simplified analysis.

# CHAPTER 5

# GEOTECHNICAL SITE CHARACTERIZATION OF SOILS IN MID-AMERICA

## 5.1 Overview

Proper classification and characterization of soils are necessary for a reliable liquefaction analysis. Soil behavior type classification methods based on CPT test results have been discussed previously, and verification through laboratory index testing is desirable. This chapter will present results from field and lab tests on soils in Mid-America. Simple laboratory index tests were performed on surface samples obtained from select sites. Field testing by seismic piezocone tests (SCPTu) are utilized to determine stratigraphic layering and stiffness profiles with depth at 12 test sites located in the New Madrid seismic zone and Charleston, SC earthquake region. These sites are generally associated with seismic events, and most have shown surface evidence of liquefaction.

## 5.2 Laboratory Index Testing

Grain characteristics of sands have been shown to influence soil susceptibility to liquefaction (e.g., Yamamuro et al., 1999) as well as steady state characteristics (e.g., Poulos et al., 1985). A study of index properties associated with granular soils of Mid-America was undertaken as part of this research. A limited series of laboratory index testing of soils from the Memphis, TN area and Blytheville, AR has been conducted at

Georgia Tech. Soil index properties from liquefaction sites in the Charleston, SC area (Cullen, 1985) and the Shelby Forest site (Liu et al., 1997) are also reviewed. The parameters studied and associated laboratory tests are:

- Grain Size Distribution (Sieve Analysis - ASTM D422);
- Fines Content (Percent finer than U.S. No. 200 Sieve - ASTM D422);
- Limiting Void Ratios ($e_{max}$ - ASTM D4254: $e_{min}$ - ASTM D4253);
- Specific Gravity, ($G_s$ - ASTM D854);
- Roundness (Visual inspection of magnified particles).

Figure 5.1 shows characteristic values of roundness (R) and associated particle shapes (Youd, 1973). Well-rounded particles are often associated with aged, water-borne sediment. Very angular ($R<0.15$) particles are characteristic of freshly crushed aggregates from rock quarries. Figures 5.2 through 5.5 display images of sands from Shelby County, TN, and Blytheville, AR captured using a microscope and digital image analysis software. These images will be used for visual determination of roundness characteristics. Figure 5.6 displays grain size distributions for Mid-America sands determined from laboratory testing. Table 5.1 presents grain characteristics of sands from this study (Memphis, TN & Blytheville, AR), West Memphis AR (personal communication Marshall, 1998), Shelby Forest TN (Liu et al., 1997), and Charleston SC (Cullen, 1985). In addition, indices from standard reference sands (Been et al., 1987; Mayne & Kulhawy, 1991) are presented in this table for comparison.

Index properties from four primary Mid-America depositional geologies are presented:

- Mississippi River Valley - WRMS, Memphis TN; B-1, West Memphis AR; Yarbro Excavation, Blytheville AR;
- Loess Bluffs - Shelby Forest, north Memphis TN;
- Wolf River - Shelby Farms and Houston Levee, east Memphis TN;
- Atlantic Coastal Plain - North-South and East-West trenches, Charleston SC;

Grab samples were taken at shallow surface depths from exposed layers, in most cases. Sands from West Memphis, AR and Shelby Forest, TN were sampled at depth using SPT methods. The tested soils are uniformly graded, relatively clean (low fines content) fine quartz sands. The sands from Mississippi River Valley were finer than the Wolf River sands. The Atlantic Coastal plain sediments were of similar median grain size to the Mississippi Valley deposits, but were more uniform with no fines. Each of the soils analyzed in this study were subangular from visual classification. Drawings of particles presented in Cullen (1985) appeared to be more angular than the magnified pictures presented in Figures 5.2 to 5.6.

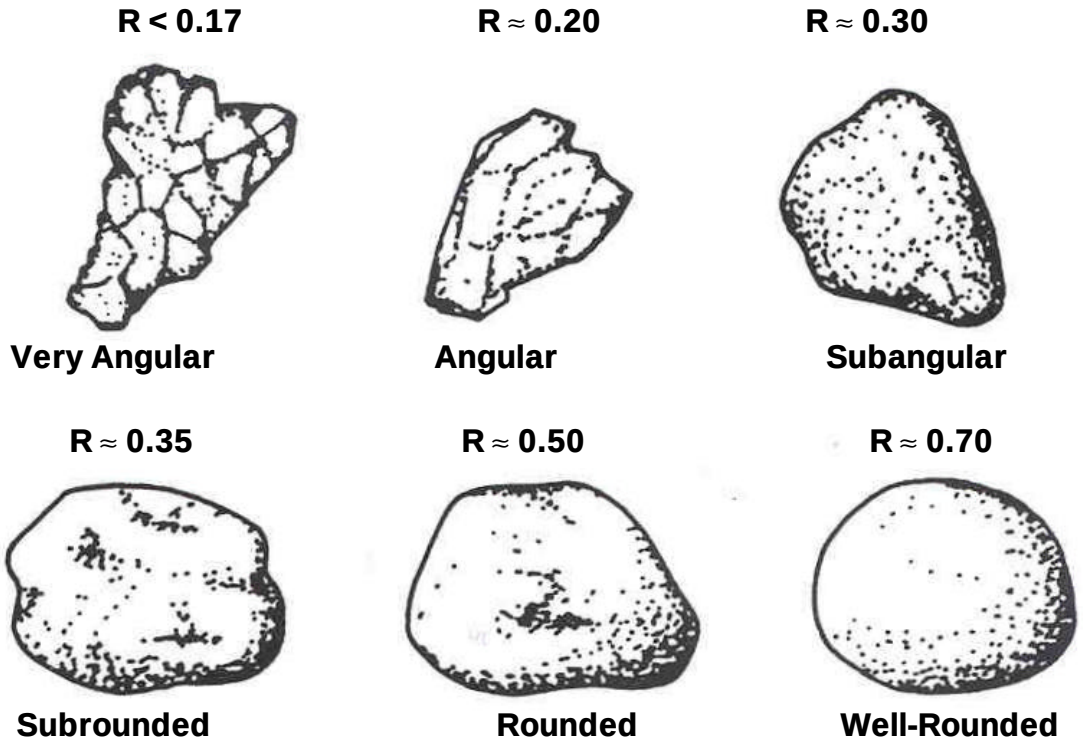


**Figure 5.1. Characteristic Values of Roundness (adapted from Youd, 1973)**

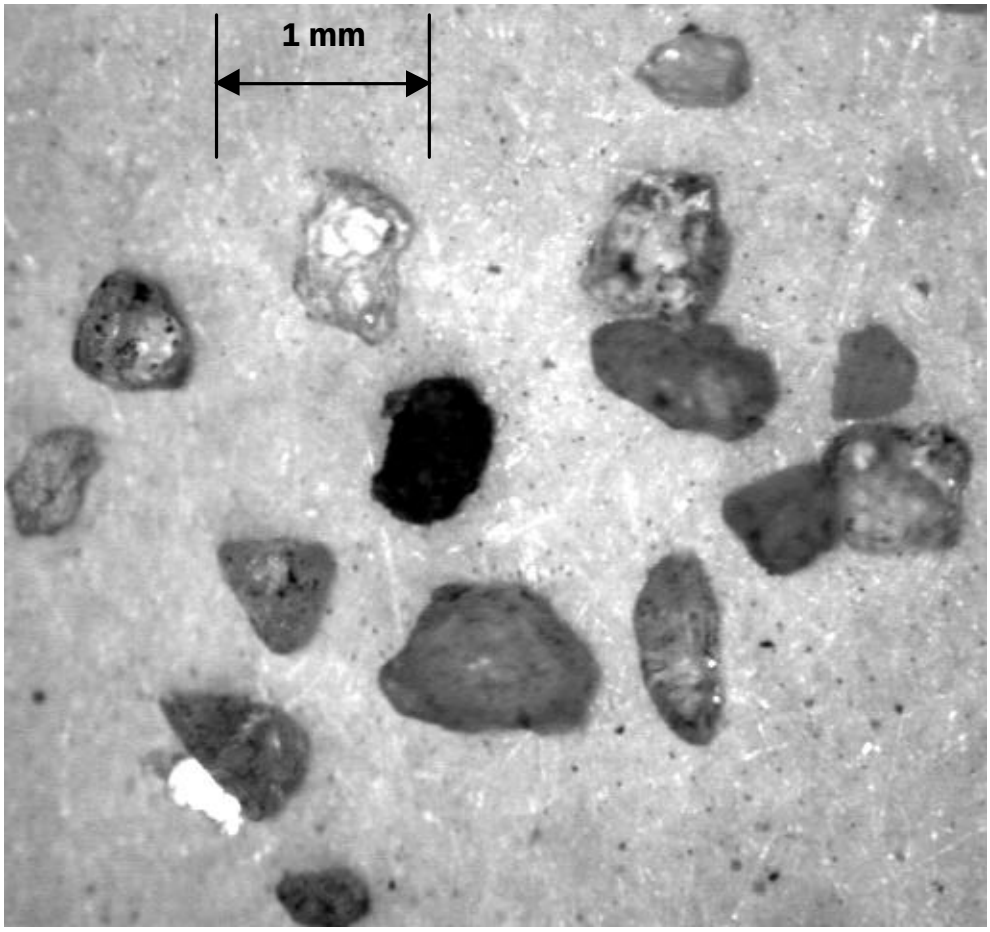


**Figure 5.2. Magnified View of Particles from Shelby Farms (SF)**

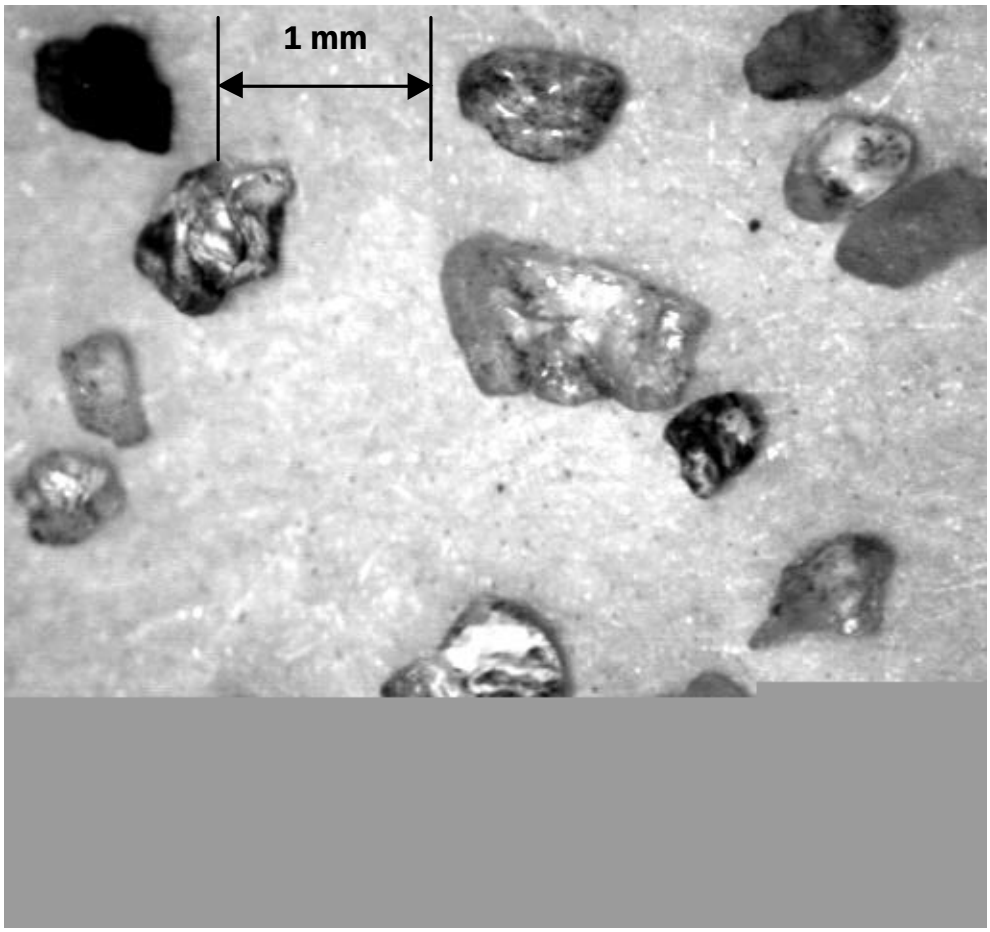


**Figure 5.3. Magnified View of Particles from Houston Levee (HL)**

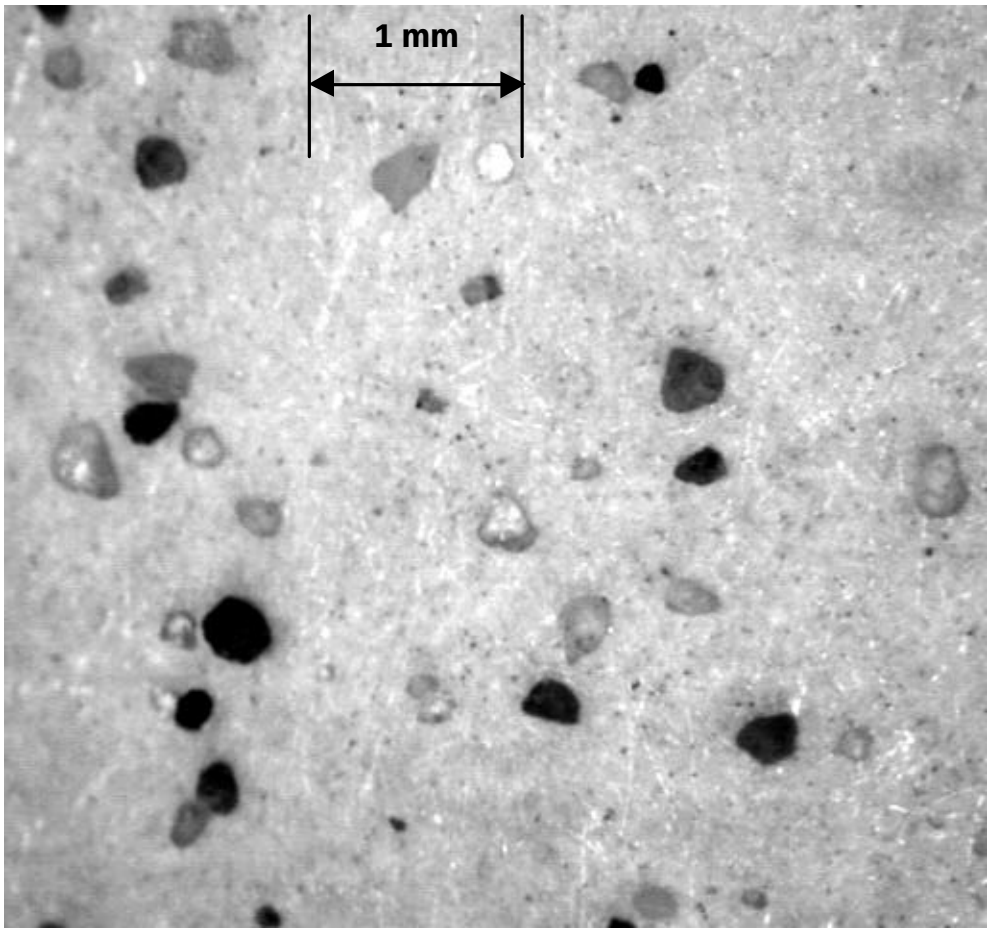


**Figure 5.4. Magnified View of Particles from Wolf River at Mississippi River (WRMS)**

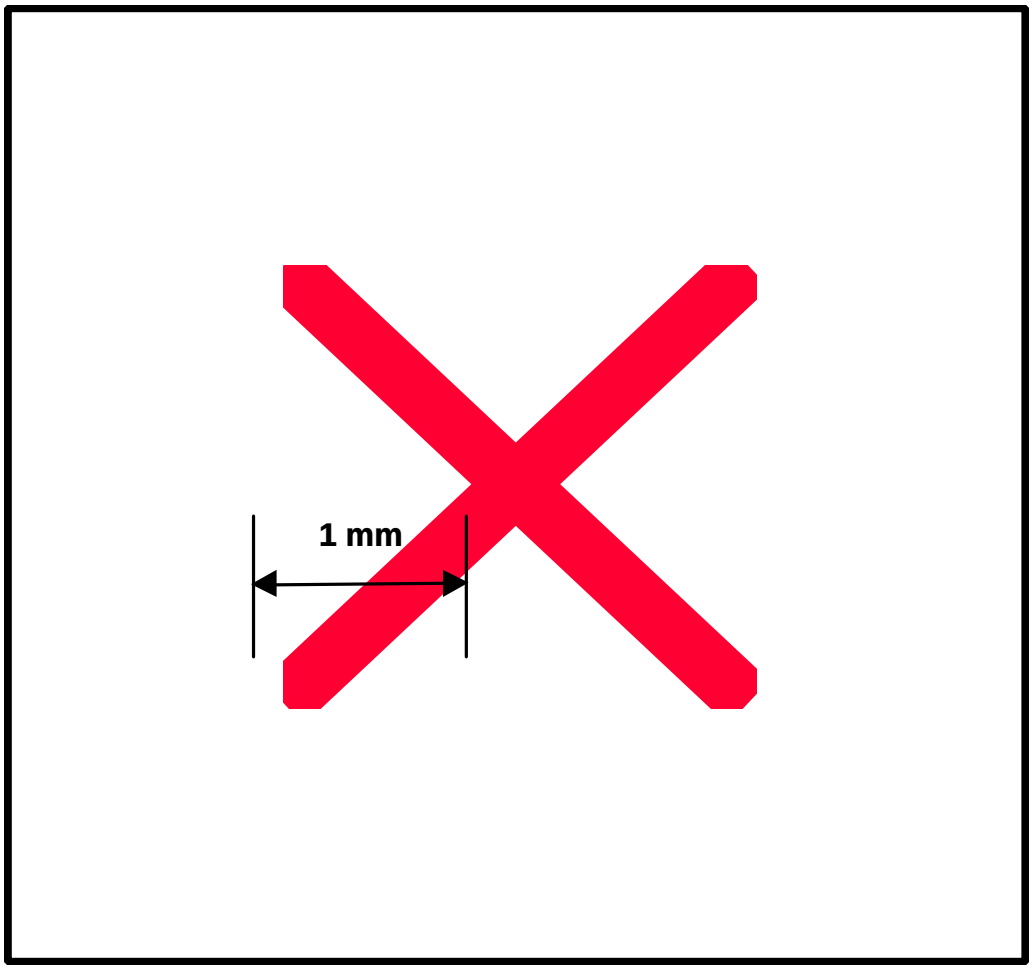


**Figure 5.5. Magnified View of Particles from Yarbro Excavation (YE)**

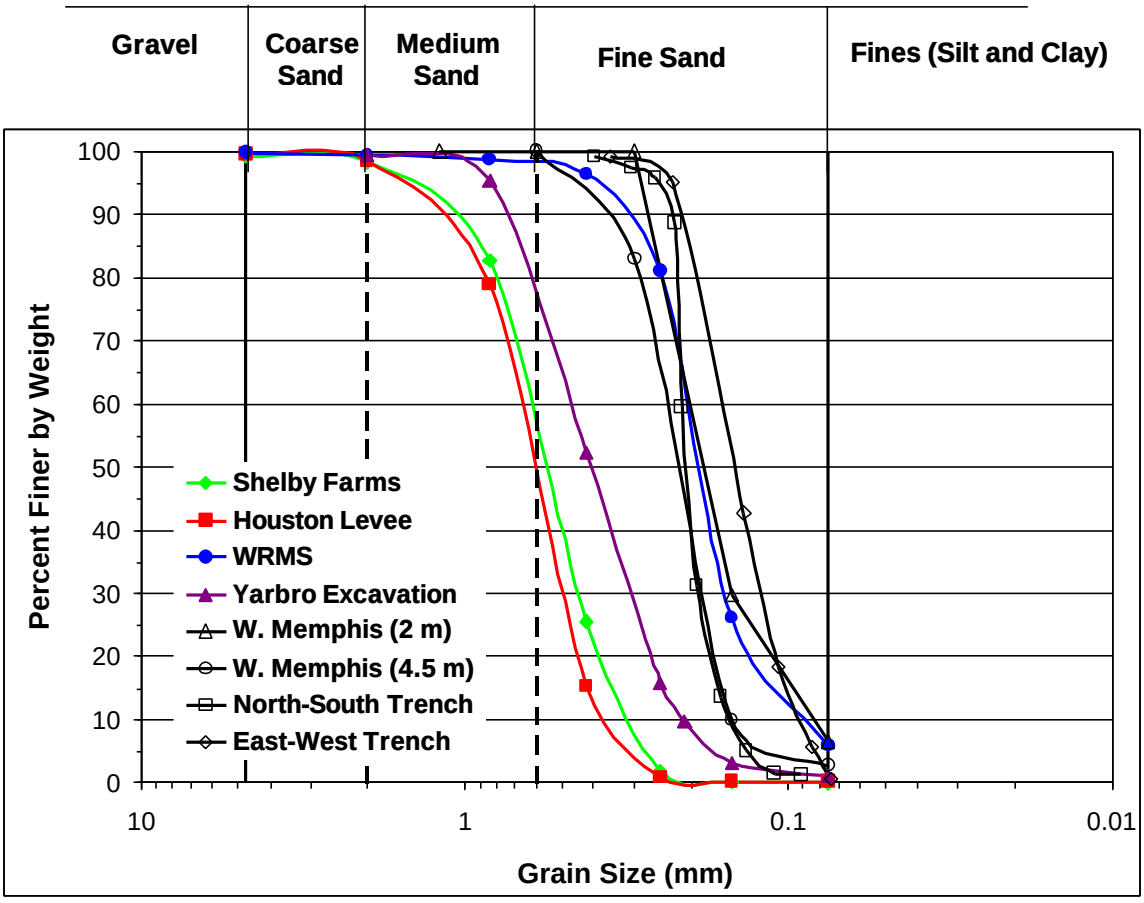


**Figure 5.6. Grain Size Curves for Mid-America Sands**

**Table 5.1. Grain Characteristics for Sands from Mid-America and Standard Reference Sands**

| Sand | $D_{50}$ (mm) | $D_{10}$ (mm) | Uniformity Coefficient | Percent Fines | Specific Gravity | Roundness | Description | $e_{max}$ | $e_{min}$ |
|---|---|---|---|---|---|---|---|---|---|
| Shelby Farms (Memphis, TN) | 530 | 310 | 2.0 | 0 | 2.66 | ≈ 0.30 | Subangular | 0.76 | 0.53 |
| Houston Levee (Memphis, TN) | 600 | 400 | 1.6 | 0 | 2.66 | ≈ 0.30 | Subangular | 0.80 | 0.57 |
| WRMS (Memphis, TN) | 190 | 90 | 2.3 | 5-7 | 2.64 | ≈ 0.30 | Subangular | 0.88 | 0.59 |
| Yarbro Ex. (Blytheville, AR) | 410 | 210 | 2.3 | 1 | 2.62 | ≈ 0.30 | Subangular | 0.79 | 0.51 |
| B-1 @ 2 m (W. Memphis, AR) | 180 | 80 | 2.5 | 6.7 | NA | NA | NA | NA | NA |
| B-1 @ 4.5 m (W. Memphis, AR) | 210 | 140 | 1.7 | 2.7 | NA | NA | NA | NA | NA |
| Shelby Forest (Shelby Co., TN)[4] | NA | NA | NA | NA | 2.62 | NA | NA | 0.88 | 0.47 |
| North-South Trench (Charleston, SC)[1] | 200 | 140 | 1.3 | 0 | 2.66 | ≈ 0.25 | Subangular | 0.91 | 0.62 |
| East-West Trench (Charleston, SC)[1] | 150 | 95 | 1.8 | 0 | 2.67 | ≈ 0.25 | Subangular | 0.96 | 0.67 |
| Ticino[2] (Italy) | 530 | 360 | 1.6 | 0 | 2.67 | 0.38 | Subrounded | 0.89 | 0.60 |
| Toyoura[3] (Japan) | 160 | 130 | 1.46 | - | 2.64 | - | Subangular | 0.98 | 0.61 |
| Ottawa[2] (United States) | 530 | 350 | 1.7 | 0 | 2.66 | 0.55 | Rounded | 0.79 | 0.49 |
| Monterey No. 0[2] (United States) | 370 | 250 | 1.6 | 0 | 2.65 | 0.35 | Subrounded | 0.82 | 0.54 |

[1] Cullen, 1985 [2] Been et al., 1987 [3] Mayne & Kulhawy, 1991 [4] Liu et al., 1997

## 5.3 Seismic Piezocone Test Results

Field-testing for this study concentrated on a total of 12 sites, with six sites located in the New Madrid seismic zone, four sites in Memphis, TN, and two sites in Charleston, SC. One or more SCPTu sounding was performed at each site. A majority of the sites and sounding locations selected were in coordination with the work of previous paleoliquefaction studies (Tuttle et al., 1998; Tuttle et al., 1996; Wolf et al., 1998; Collier, 1998; Van Arsdale, 1998a; Schweig, 1998; Martin, 1990). Most of the sites have shown evidence of prior liquefaction, such as sand blows, feeder dikes, lateral spreads, settlement, subsidence, or cracks. This study is meant to complement paleoliquefaction investigations and evaluate deeper source soils and site effects. Site maps, photos, and descriptions are available in Appendix IV.

Figure 5.7 displays the main areas of testing for this study. The test sites are broken up into three different sections:

- *Shelby County, TN area*: Representing test sites in Memphis and surrounding areas associated with a Joyner-Boore distance of approximately 50-km and 1000-m thickness of sediments over bedrock. Epicentral distances from the New Madrid 1811 event ranged from 40- to 90-km, and were greater than 100-km for other historic events.
- *Northeast Arkansas and Southeast Missouri*: Representing test sites in Blytheville AR, Steele MO, and Caruthersville MO areas with a Joyner-Boore distance of less than 15 km and 600-m thickness of sediments overlying bedrock. Epicentral distances ranged from 40- to 65-km for events in 1811 to 1812.

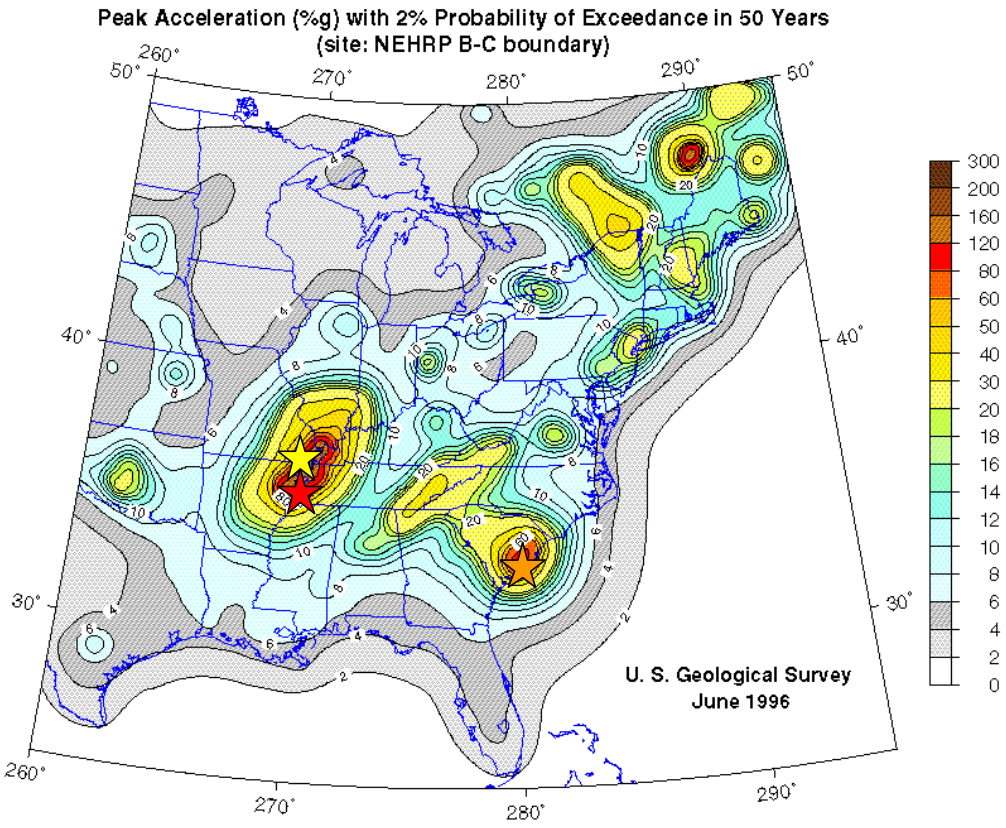


**Figure 5.7. Test areas presented on USGS 1996 2% PE in 50 year Central and Eastern U.S. Hazard Map; Memphis★ ; NE AR / SE MO☆ ; Charleston, SC ☆. (http://www.geohazards. cr.usgs.gov/eq/hazmaps/250pga.gif)**

- Charleston, SC area: Representing test sites in the Charleston SC area with a Joyner-Boore distance of about 25 km to the center of the city and 820-m thickness of sediments overlying bedrock. Epicentral distances ranged between 5- and 10-km for the earthquake of 1886.

5.3.1 SCPTu Profiles

Table 5.2 displays the list of seismic piezocone test soundings that are analyzed, along with pertinent site and sounding information. Unless noted, longitude and latitude measurements were recorded with a Garmin hand-held unit with an accuracy of about $\pm$ 0.001 degrees (15 m). Figure 5.8 displays a legend used for the soil profiles generated from SCPTu data using methods discussed in Chapter 2. Figures 5.9 through 5.23 display soundings that will be discussed for liquefaction analysis of Mid-American soils. Additional seismic cone profiles generated by this study, with termination depths greater than 10-m are contained in Appendix V.

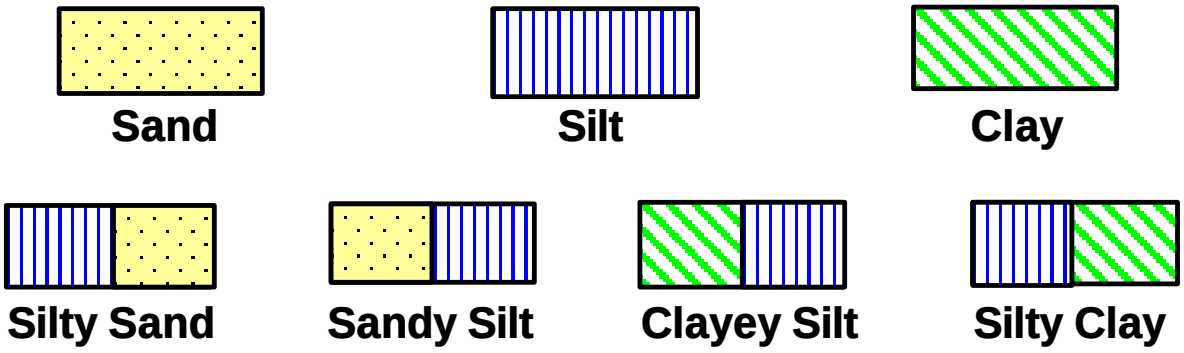


**Figure 5.8. General soil classification legend for profiles depicted**

**Table 5.2. Seismic Piezocone Testing in Mid-America Earthquake Region**

| Location | Type of Test[2,3,4] | Sounding I.D. | Longitude North (degrees) | Latitude[5] East (degrees) | Max Test Depth (m) |
|---|---|---|---|---|---|
| ***Shelby County, TN Area*** | | | | | |
| Shelby Farms (SF) | 10T SCPT$u_2$ | MEMPH-G | 35.1172 | -89.8055 | 31.40 |
| SF Shooting Range | 10T SCPT$u_2$ | SFSR-01 | 35.1292 | -89.8416 | 30.40 |
| Houston Levee (HL) | 10T SCPT$u_2$ | MEMPH-H | 35.1083 | -89.7305 | 20.40 |
| Shelby Forrest | 10T SCPT$u_2$ | SFOR-01 | 35.3578 | -90.0188 | 21.40 |
| ***Northeast Arkansas and Southeast Missouri Area*** | | | | | |
| Yarbro Excavation | 10T SCPT$u_2$ | YARB-01 | 35.9823 | -89.9331 | 28.00 |
| Bugg 40 | 10T SCPT$u_2$ | BUGG-01 | 35.9728 | -89.9078 | 38.50 |
| Bugg 40 | 10T SCPT$u_2$ | BUGG-02 | 35.9723 | -89.9079 | 34.20 |
| 3MS617 | 15T SCPT$u_2$ | 3MS617-A | 35.9926 | -89.8356 | 32.50 |
| Huey House | 15T SCPT$u_2$ | HUEY-01 | 35.9835 | -89.8865 | 26.00 |
| Dodd Farm | 15T SCPT$u_2$ | DODD-01 | 36.0949 | -89.8483 | 30.85 |
| Dodd Farm | 15T SCPT$u_2$ | DODD-02 | 36.0946 | -89.8483 | 25.35 |
| Dodd Farm | 15T CPT$u_2$ | DODD-03 | 36.0942 | -89.8482 | 32.30 |
| Johnson Farm | 15T SCPT$u_2$ | JOHN-01 | 36.1192 | -89.8439 | 25.15 |
| ***Charleston, SC*** | | | | | |
| Hollywood Ditch[1] | SCPT$u_2$ | HW-4 | 32.739 | -80.240 | 19.20 |
| Thompson Industrial[1] | SCPT$u_2$ | TIS-01 | 32.919 | -80.047 | 14.4 |

[1] Longitude and latitude determined from street address using http://www.mapblast.com
[2] 10 T refers to a load cell with a maximum capacity of 10 tons
[3] 15T refers to a load cell with a maximum capacity of 15 tons
[4] $u_2$ refers to penetration pore pressure measurements taken behind the tip
[5] negative values of latitude refer to west

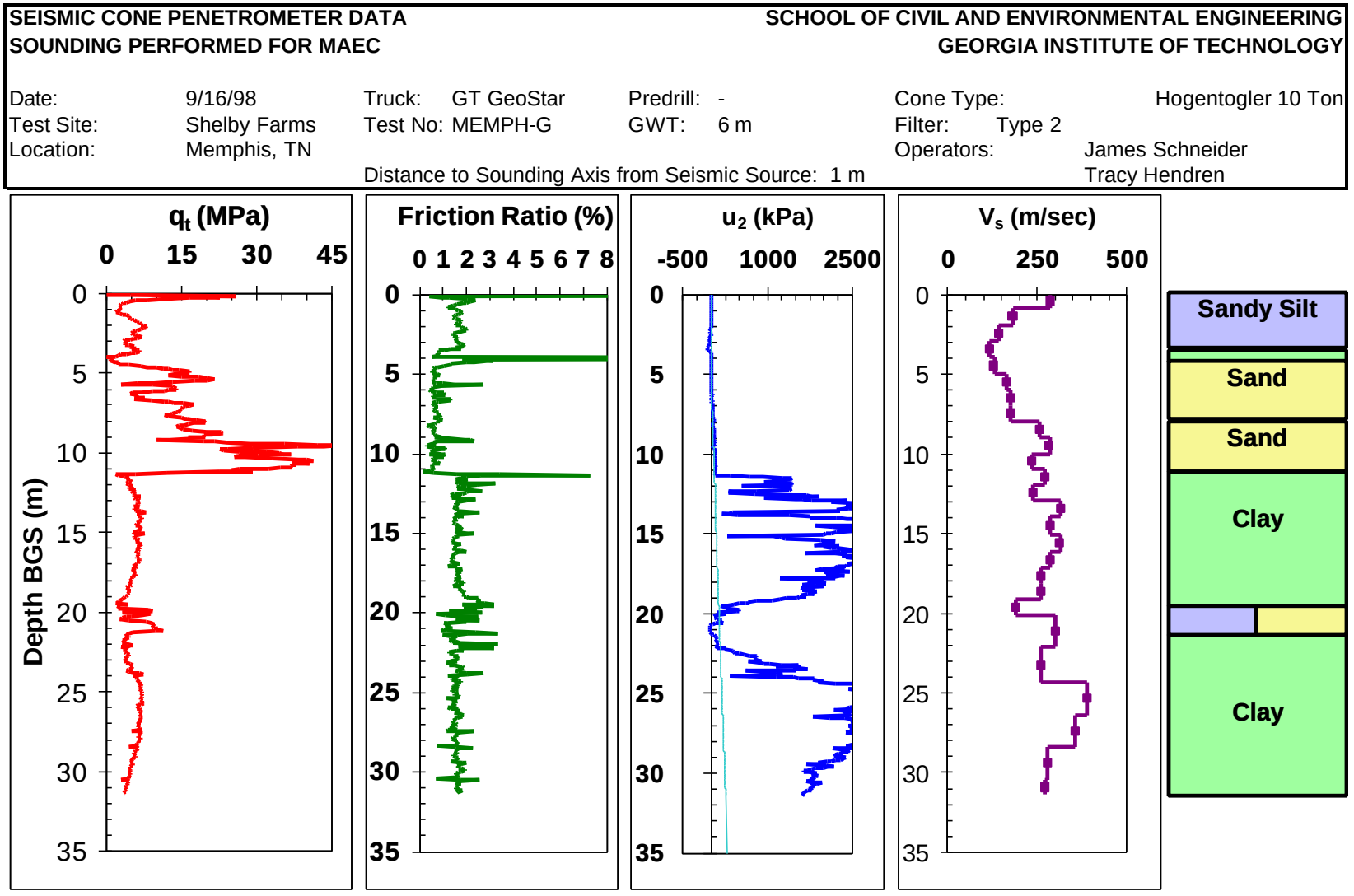


**Figure 5.9. Seismic Piezocone Test Results from Shelby Farms, TN (MEMPH-G)**

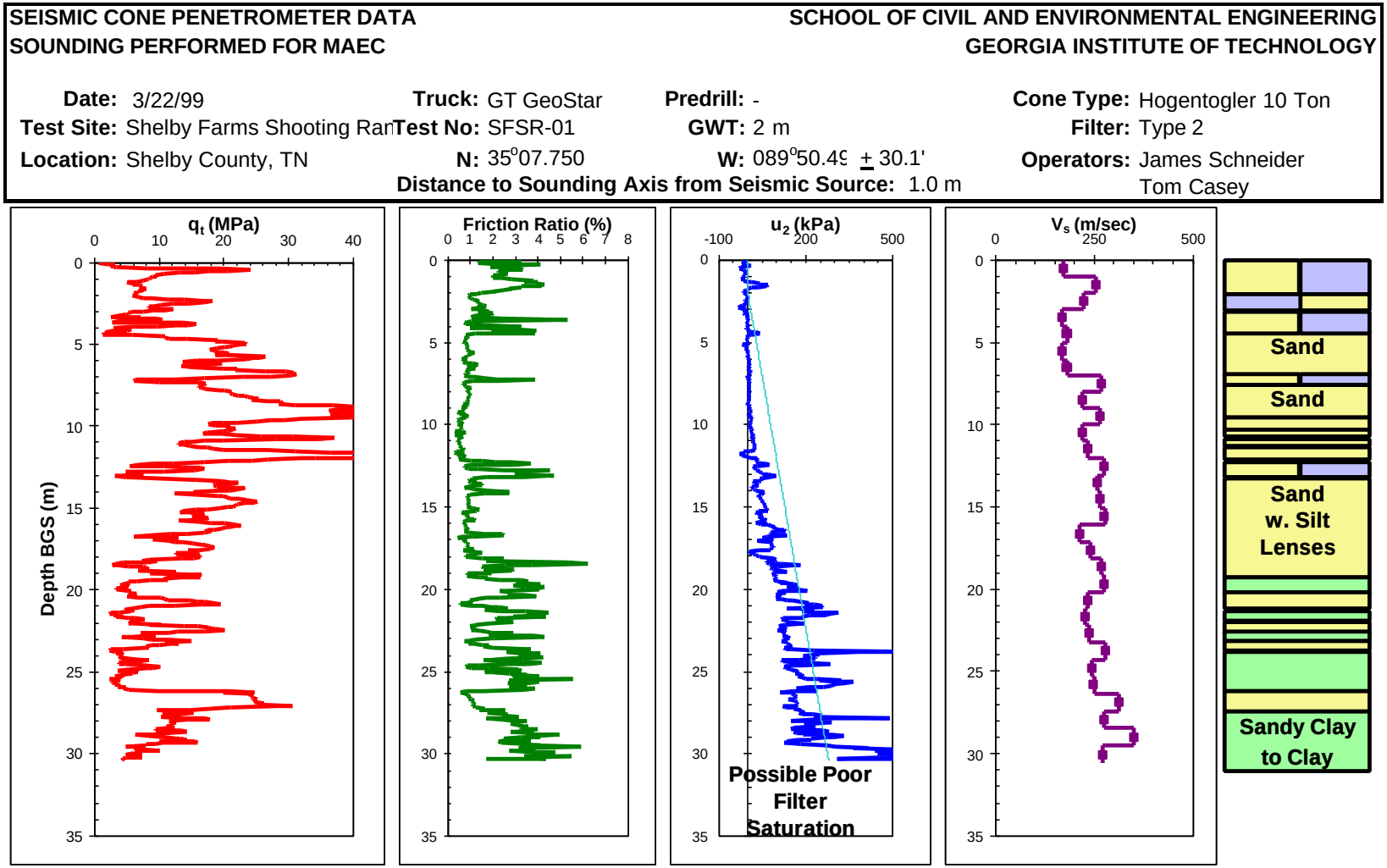


**Figure 5.10. Seismic Cone Test Results from Shelby Farms Shooting range, TN (SFSR-01)**

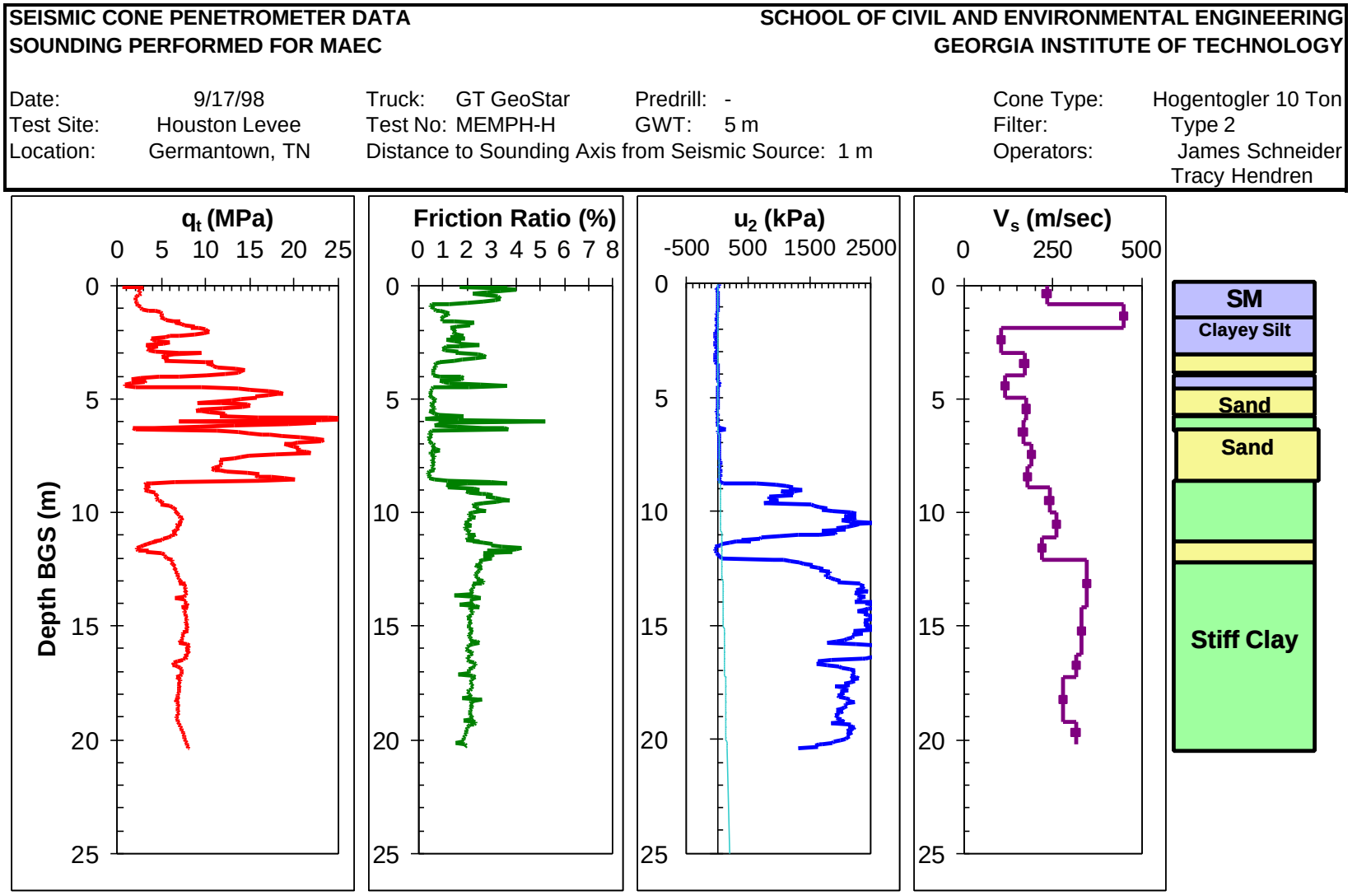


**Figure 5.11. Seismic Piezocone Test Results from Houston Levee, TN (MEMPH-H)**

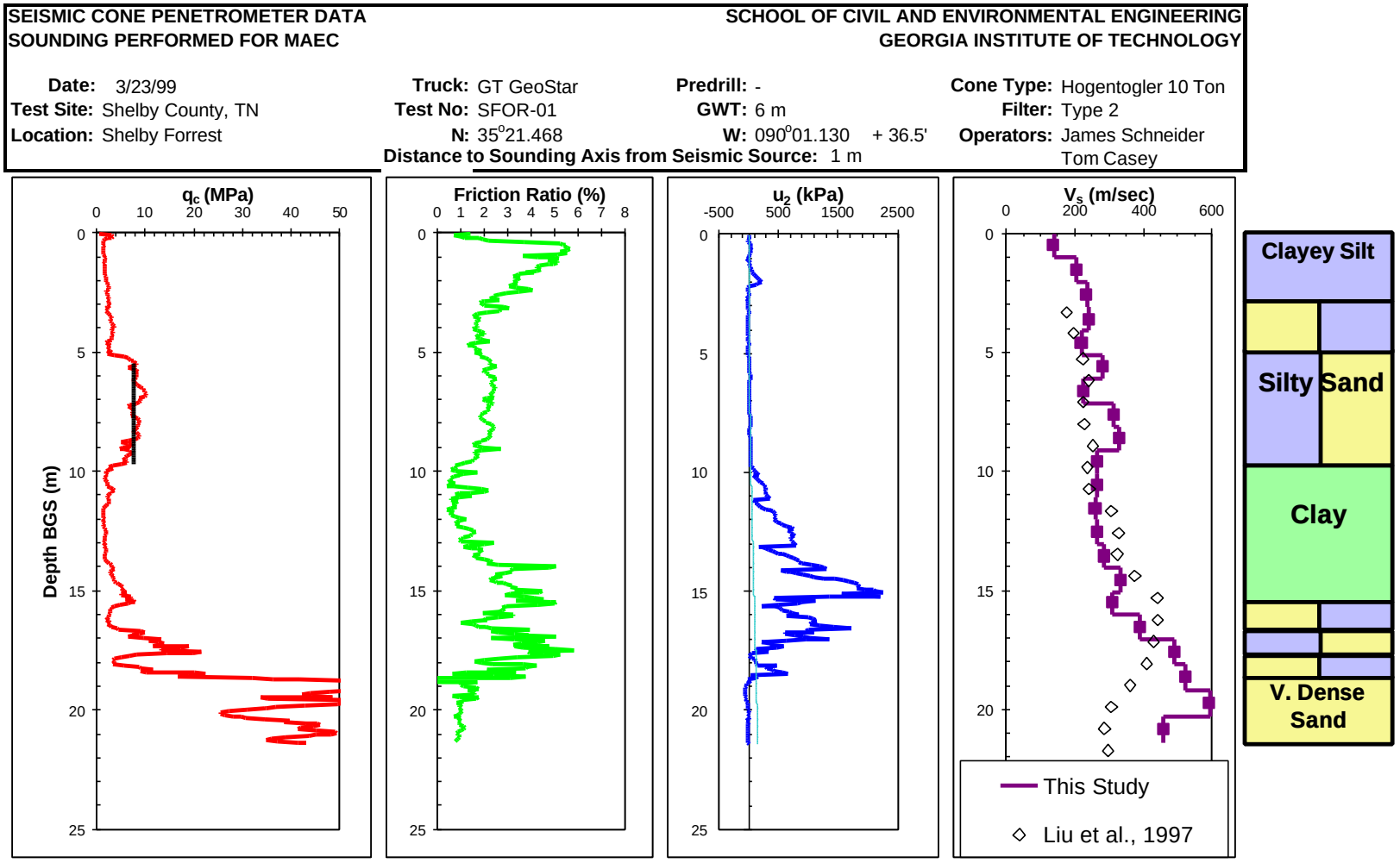


**Figure 5.12. Seismic Piezocone Test Results from Shelby Forrest, TN (SFOR-01)**

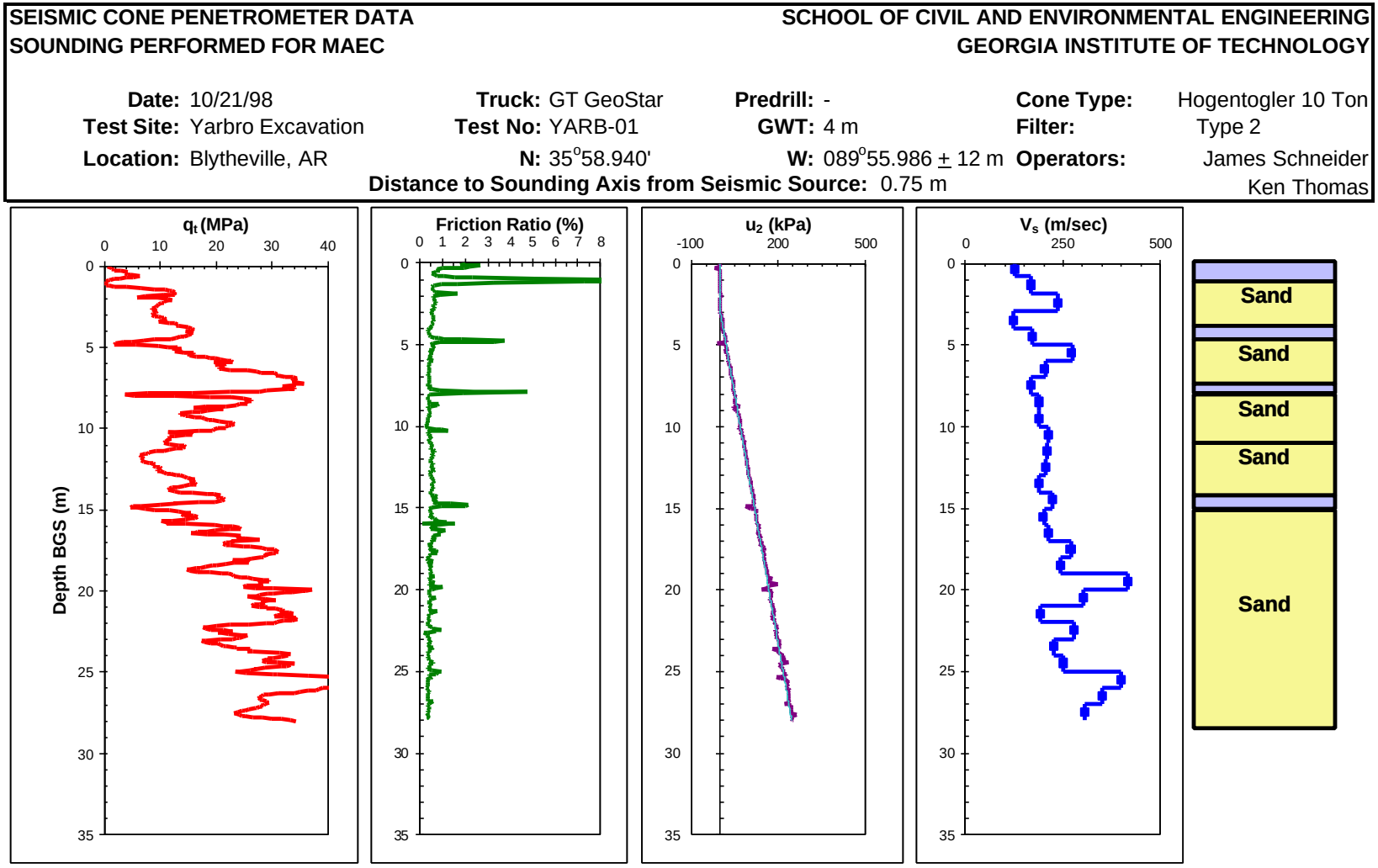


**Figure 5.13. Seismic Piezocone Test Results from Yarbro Excavation, AR (YARB-01)**

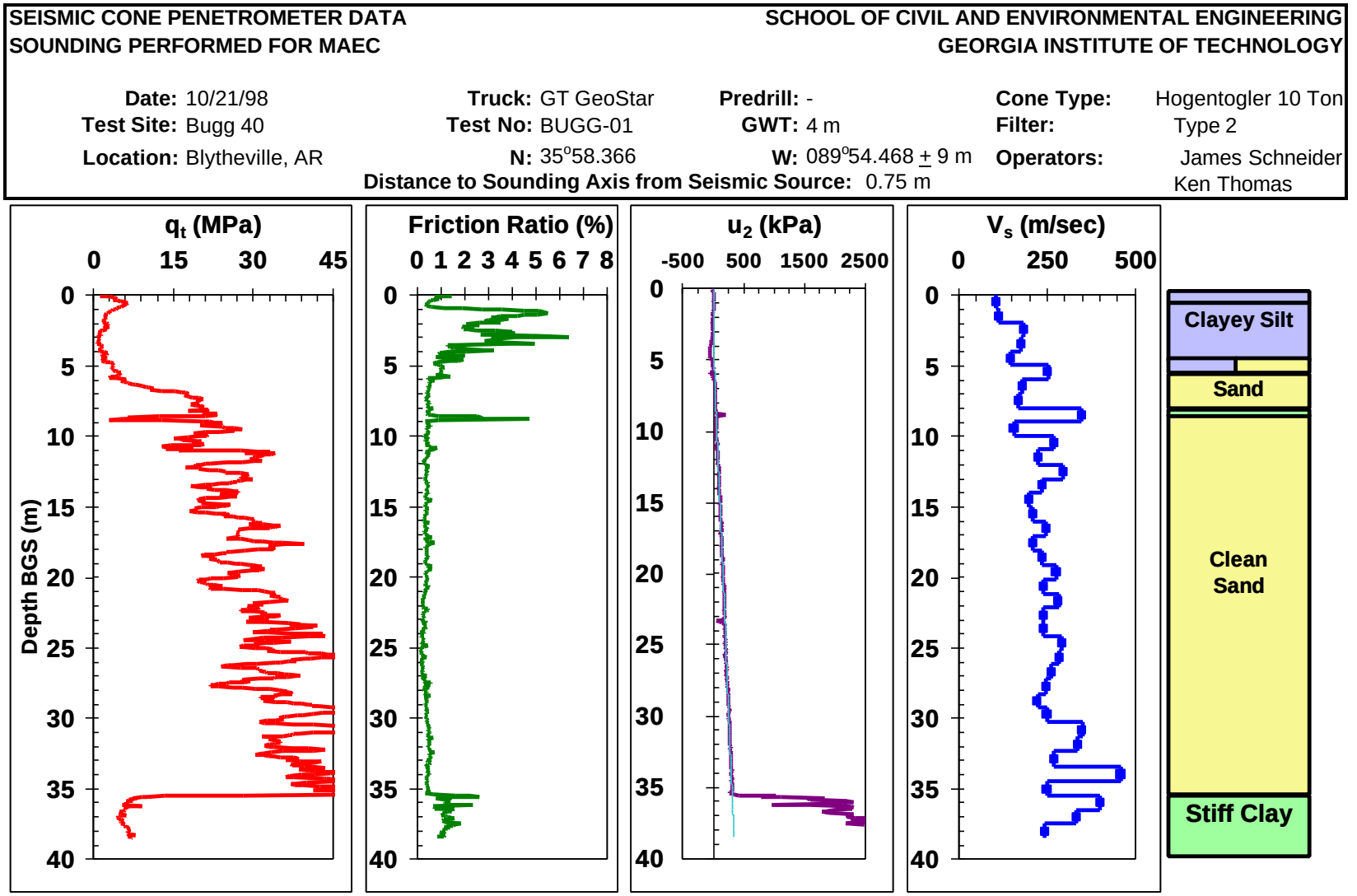


**Figure 5.14. Seismic Piezocone Test Results from Bugg 40, AR (BUGG-01)**

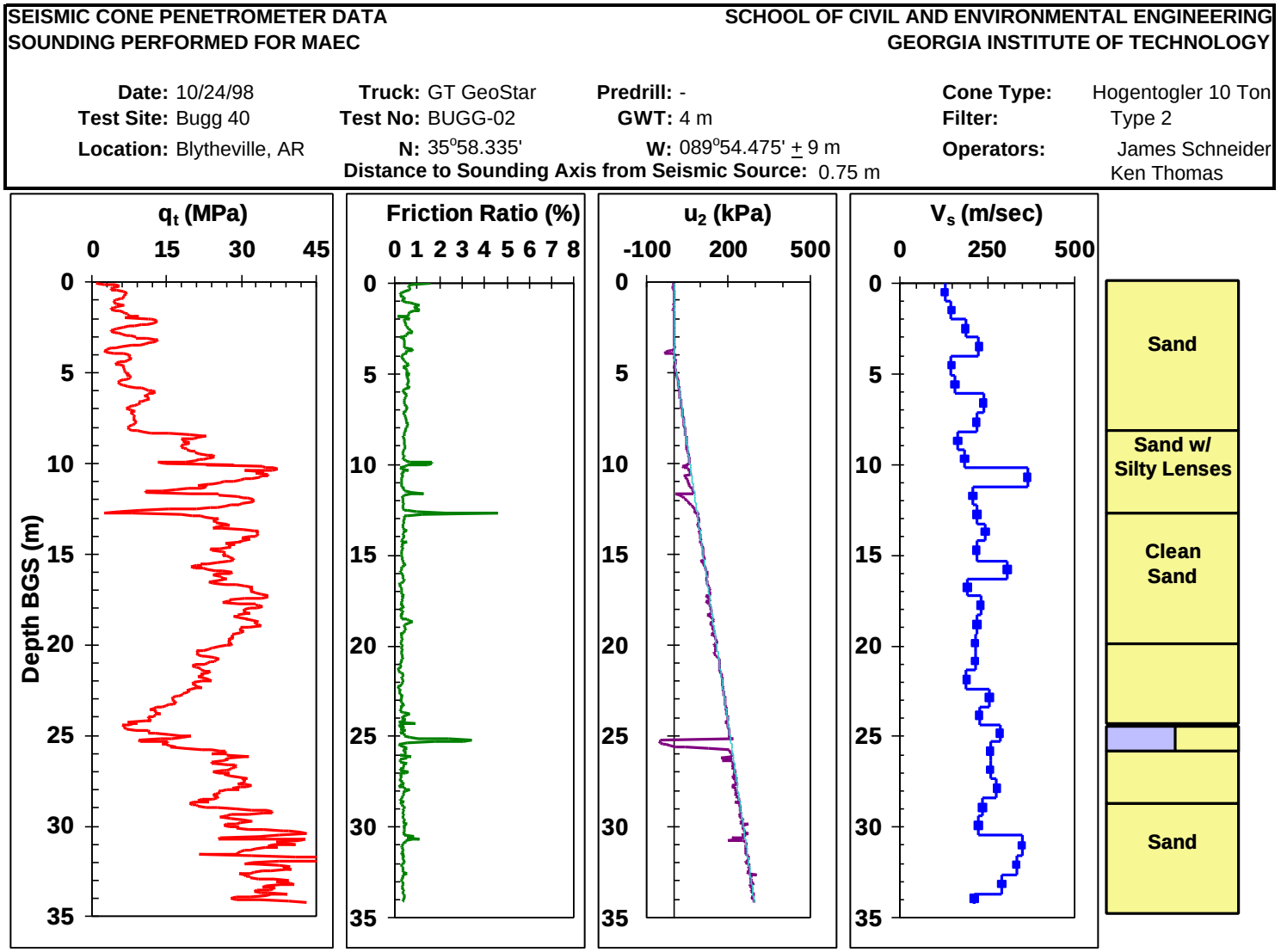


**Figure 5.15. Seismic Piezocone Test Results from Bugg 40, AR (BUGG-02)**

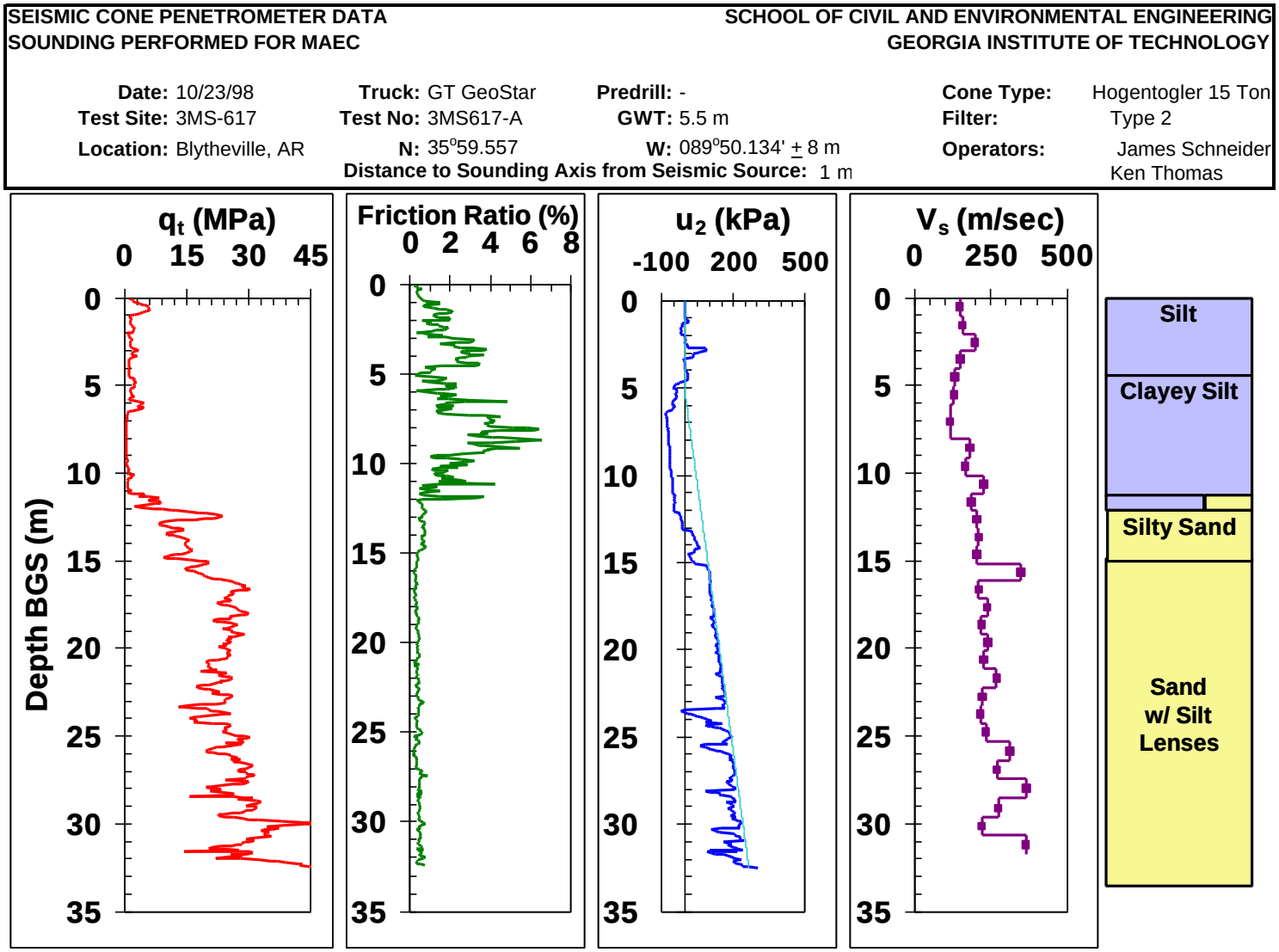


**Figure 5.16. Seismic Piezocone Test Results from 3MS617, AR (3MS617-A)**

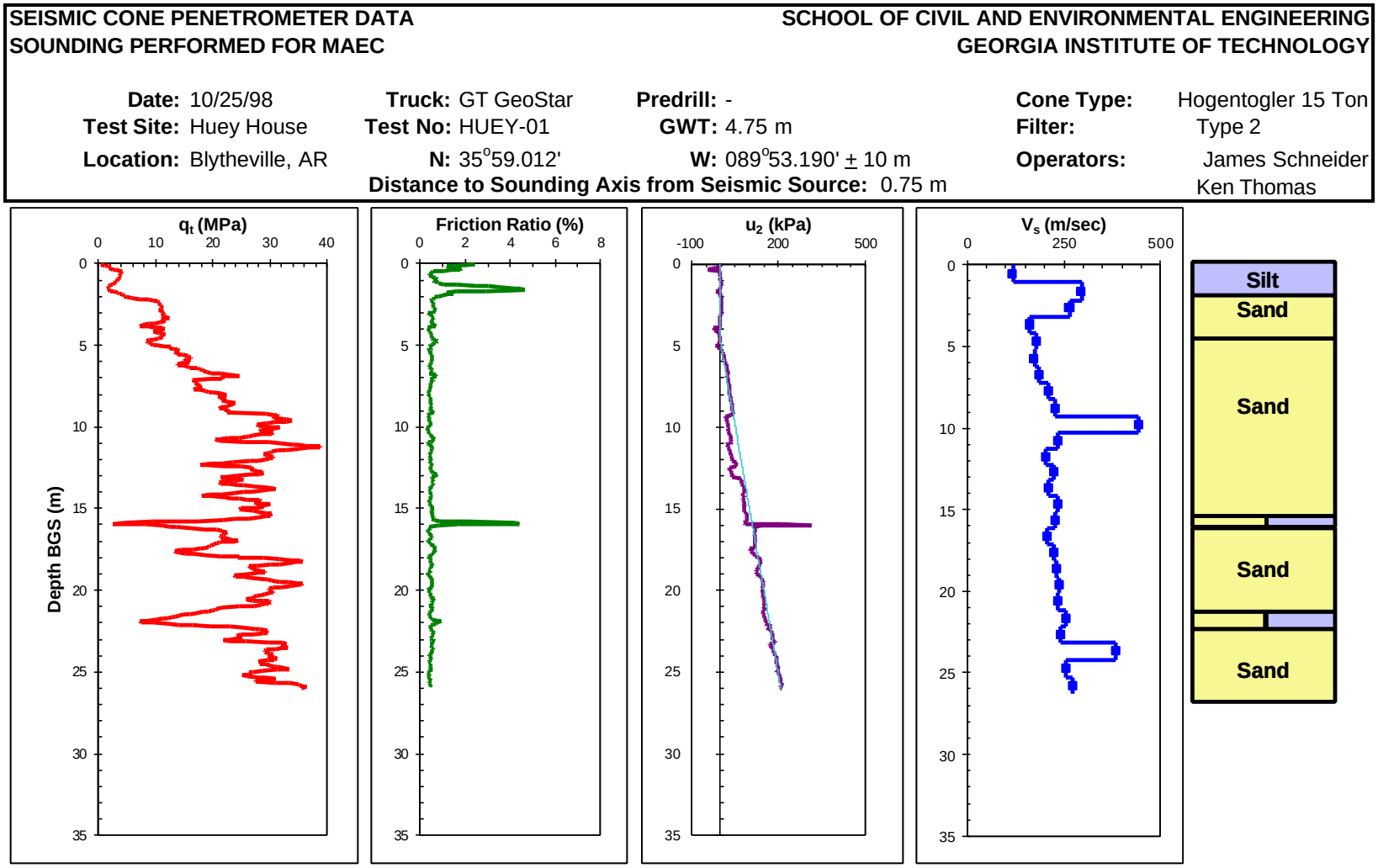


**Figure 5.17. Seismic Piezocone Test Results from Huey House, AR (HUEY-01)**

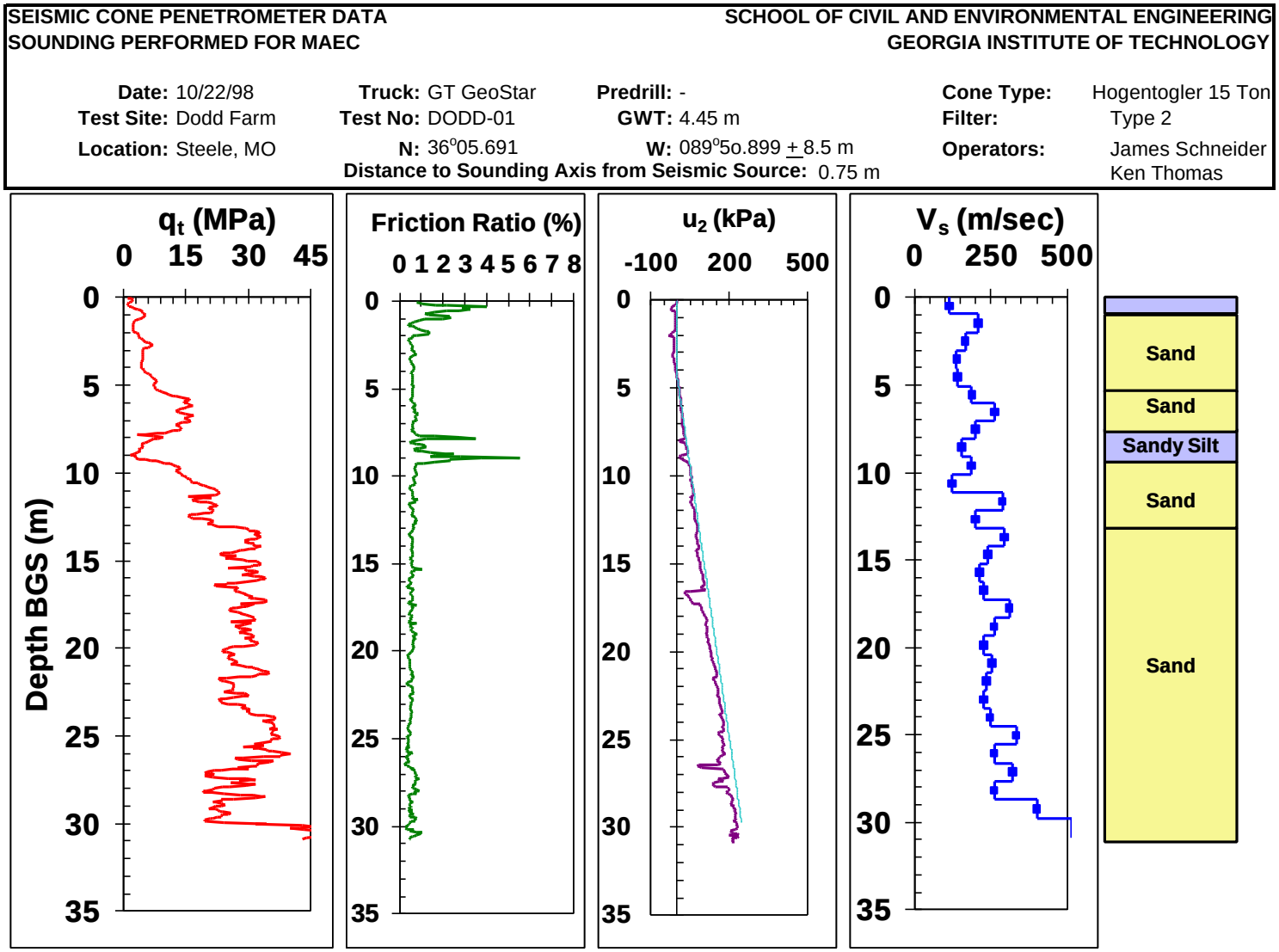


**Figure 5.18. Seismic Piezocone Test Results from Dodd Farm, MO (DODD-01)**

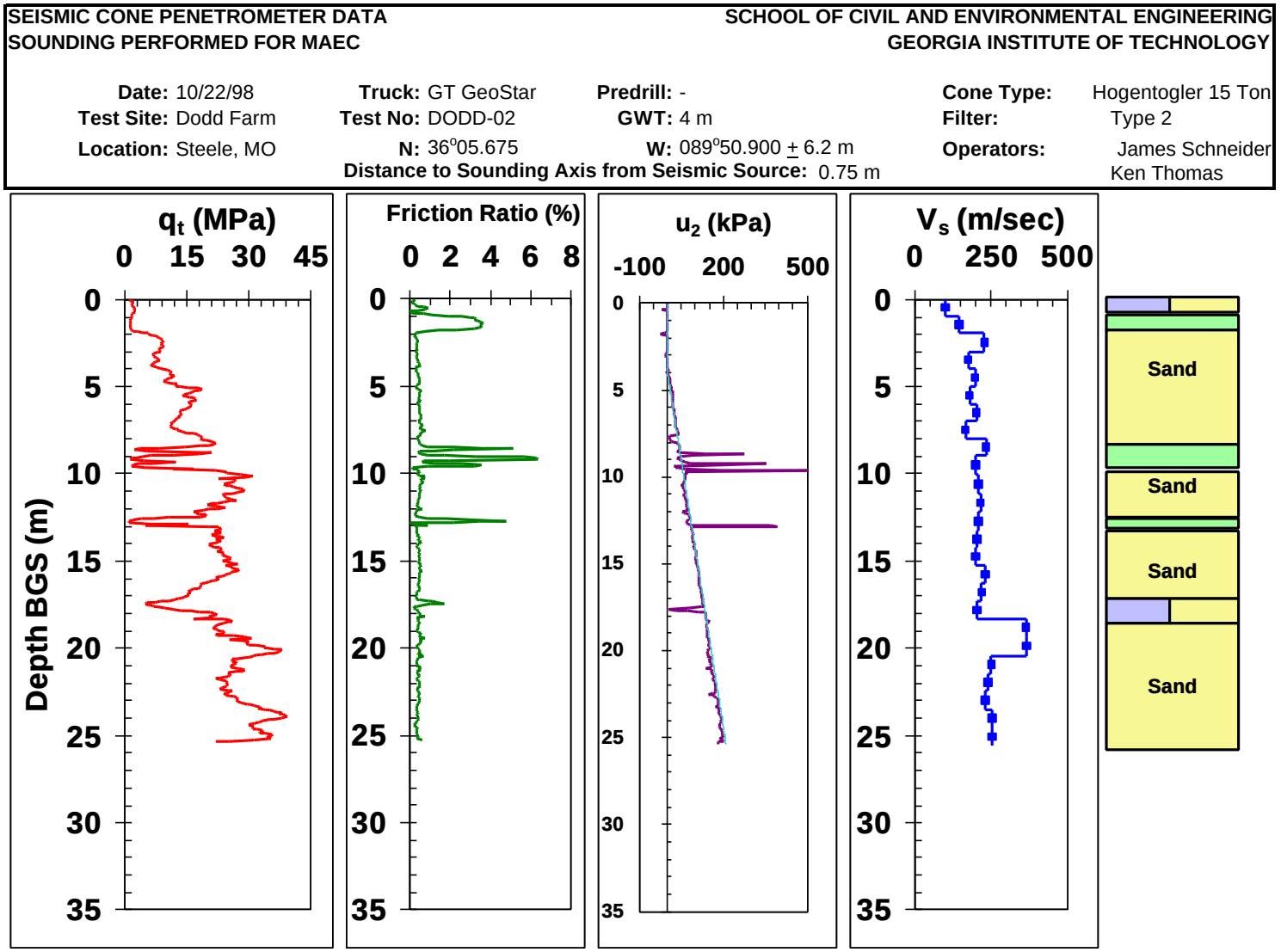


**Figure 5.19. Seismic Piezocone Test Results from Dodd Farm, MO (DODD-02)**

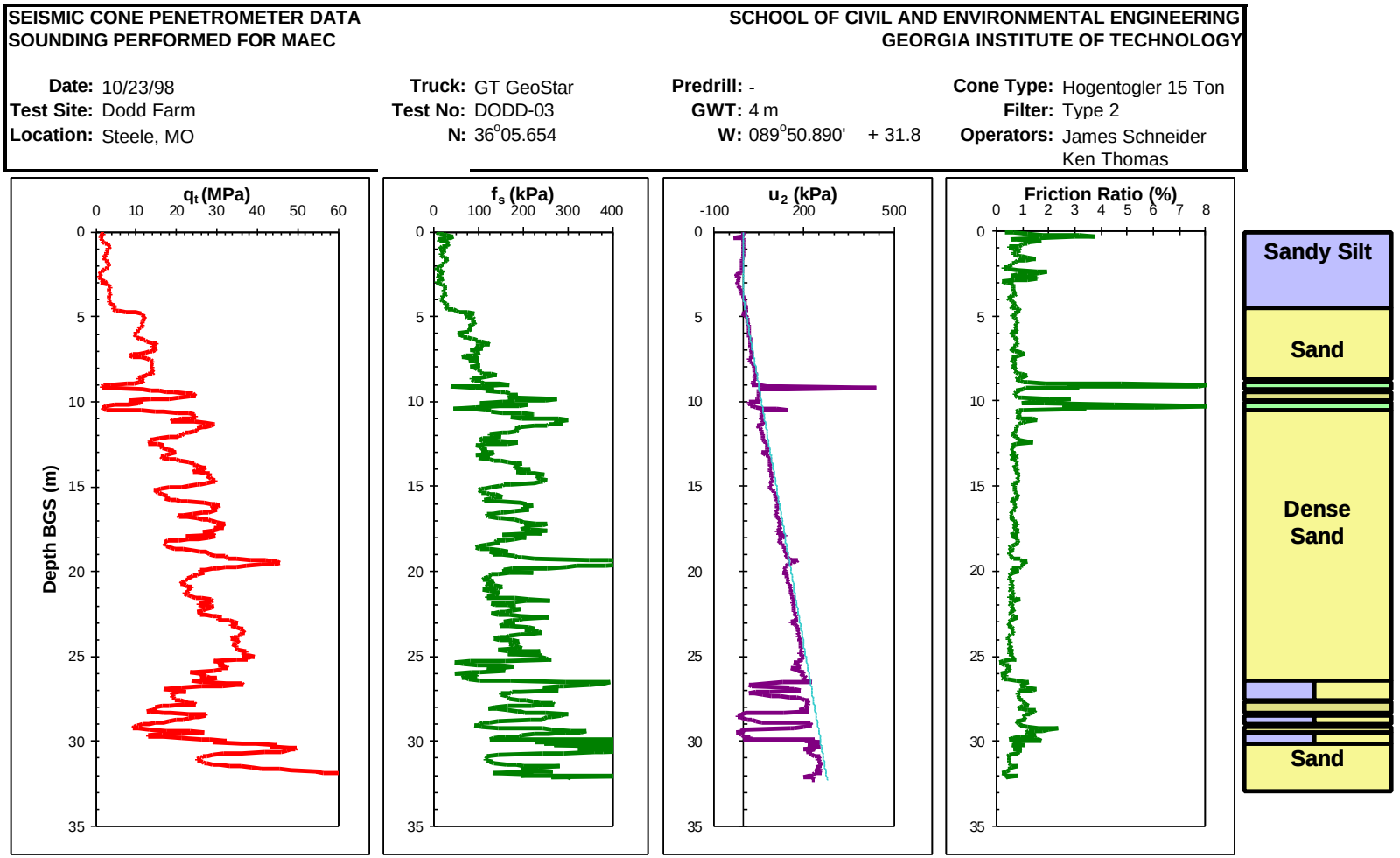


**Figure 5.20. Piezocone Test Results from Dodd Farm, MO (DODD-03)**

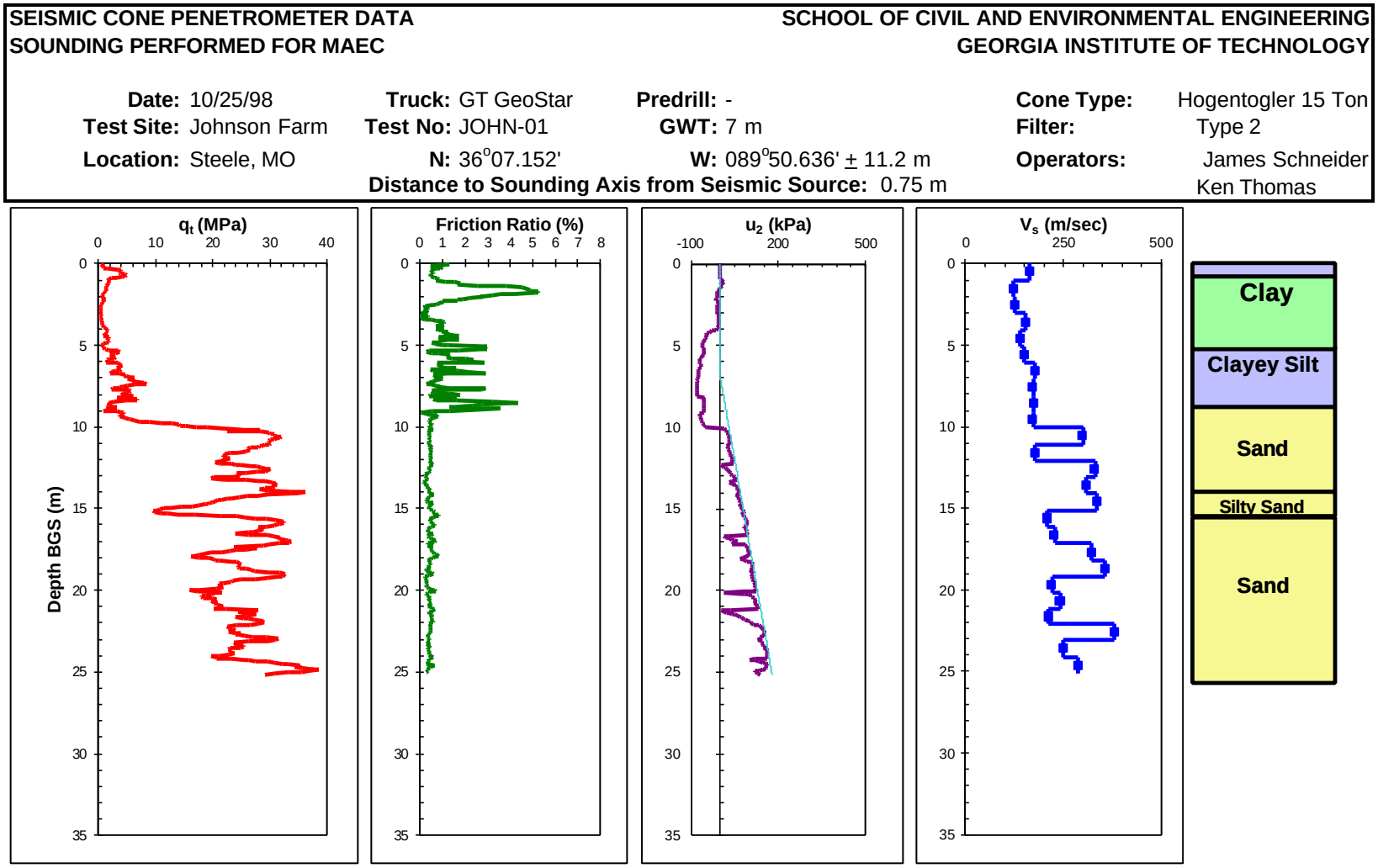


**Figure 5.21. Seismic Piezocone Test Results from Johnson Farm, MO (JOHN-02)**

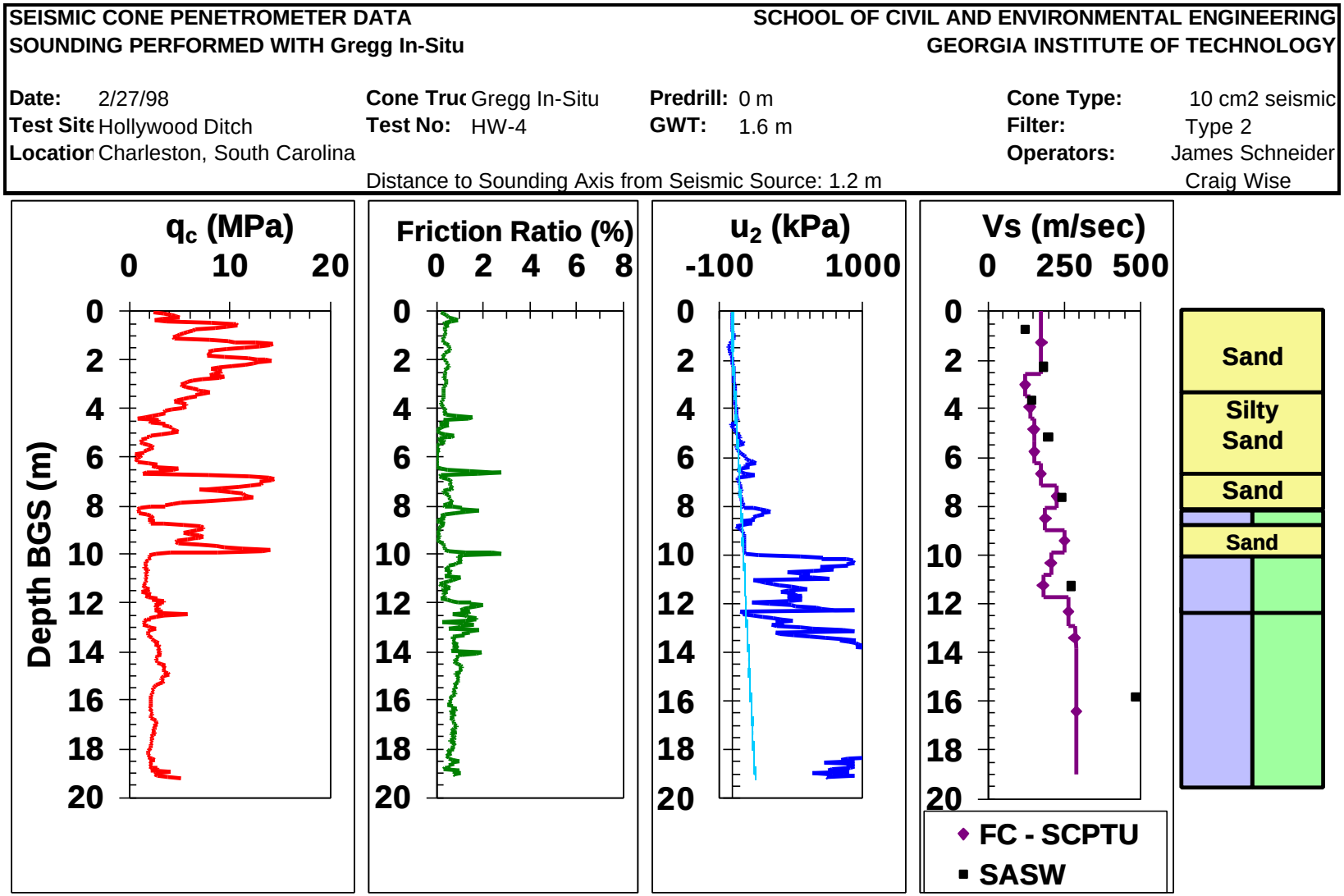


**Figure 5.22. Seismic Piezocone Test Results from Hollywood Ditch, SC (HW-4)**

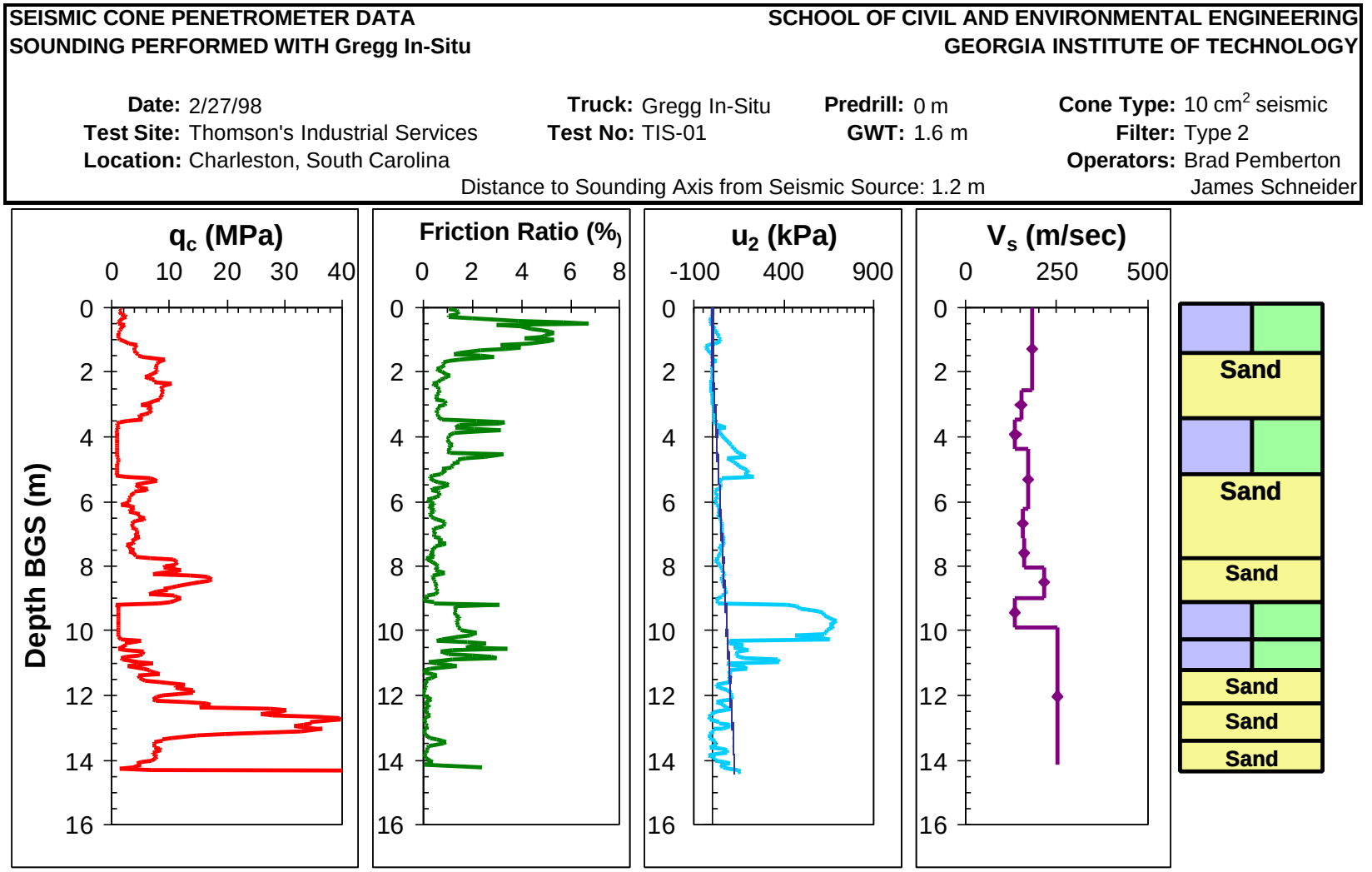


**Figure 5.23. Seismic Piezocone Test Results from Thompson Industrial Services, SC (TIS-1/3)**

The Shelby Farms (Fig. 5.9) and Houston Levee (Fig. 5.11) sites were located within the Wolf River alluvial deposits in Shelby County, which resulted in similar soundings in silty sand to sand, overlying stiff clay of the Jackson Formation. The Shelby Farms Shooting Range site (Fig. 5.10) was about 2-km north of the Wolf River, and has more alternating layers of sand and clay than the other two sites. It was interpreted that gravel was intermixed with the sandy layers, which is consistent with geologic profiles presented in Saucier (1994). The Shelby Forest site (Fig. 5.12) is located north of Memphis and within the loess bluffs, yet closer to the Mississippi River.

Shear wave velocity was also available at the Shelby Forest site from downhole studies performed by Liu et al. (1997), which are displayed on Figure 5.12. The velocities from both studies matched well until a depth of 15-m, where the Liu et al. data were higher from 15- to 17-m and the data from this study were higher after 17-m. It is expected that the stiff layer started at a greater depth and was more extensive in the sounding from this study.

Sites in the Northeast Arkansas and Southeast Missouri (Fig. 5.13 to 5.21) areas generally consisted of soundings with a thin clay to silt surface layer, over medium dense to dense sands. At a depth of about 35-m in the Bugg-40 site, tertiary clay deposits were encountered. These deposits had similar tip resistance and pore pressure response as did the clays at depth from Shelby Farms and Houston Levee. The depth that the clays soils were encountered matched well with generalized cross sections presented in Saucier (1994). Figure 5.8 displays a generalized cross section from Saucier (1994) with the location and approximate depths of soundings performed in this study.

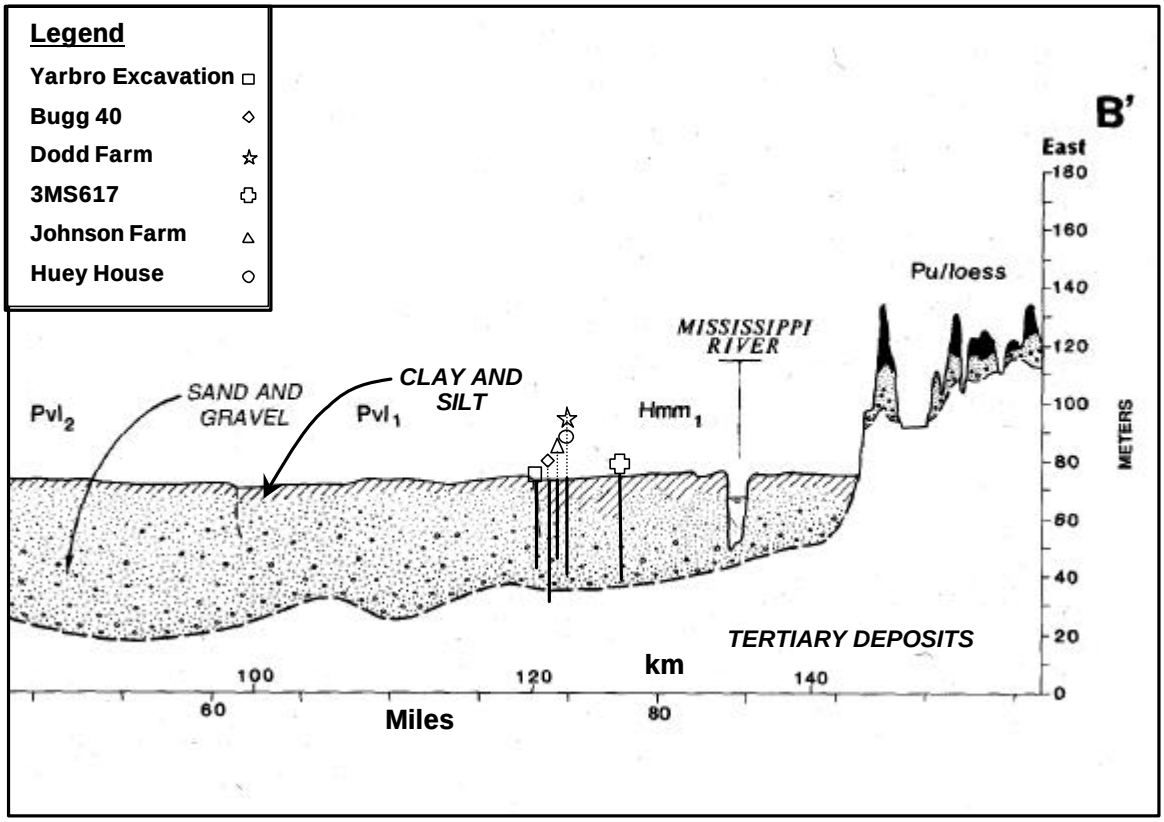


P - Pleistocene deposits
H - Holocene deposits

**Figure 5.24. Typical Mississippi Valley Cross Section in NE Arkansas and SE Missouri (from Saucier, 1994) with Approximate Locations and Depths of Seismic Piezocone Soundings**

The soundings in Charleston, SC penetrated into relatively loose clean to silty sands over a thick layer of overconsolidated silty clay (Cooper Marl). At Thompson Industrial Services (Fig. 5.23), the sounding did not reach the thick marl at depth, but two thin layers were noticed at about 4- to 5-m and 9- to 10-m. Cooper marl was encountered at 10-m during testing at the Hollywood ditch site (Fig. 5.22).

Surface wave testing was performed along Hollywood Ditch and presented in Indridason (1992). In Figure 5.22, SASW and SCPTu shear wave velocity results are presented. The two testing methods agree well up to a depth of 15-m, with the SASW determining slightly higher shear wave velocities.

5.2.2 Site Variation

The sites in the Mississippi River Valley are braided bar deposits, which are considered to be quite variable. In this study a large number of sites have been visited, but typically only one or two soundings have been performed in each location. This leads to concern with the potential variability inherent at each location, and how it may affect data interpretation. Since each of the sites in this chapter have been examined as part of paleoliquefaction studies, the soundings were either performed adjacent to surface manifestations of liquefaction (e.g., sand boils) or in areas of no liquefaction apparent features. Two sets of soundings will be discussed in this section to compare SCPTu data in the area of liquefaction features to that at distances over 30-m away.

While surface evidence of liquefaction features may not be apparent near each sounding within a site, liquefaction likely occurred if the soil conditions were similar. The area near the surface liquefaction feature may be the most disturbed, and thus soil in

that area may be the least suitable for estimating pre-earthquake state. Loose zones that have liquefied are potentially denser due to settlement, and dense zones that have liquefied are potentially looser due to migration of pore water from the liquefied zones (Youd, 1984). Frost et al. (1993) and Chameau et al. (1998) examine data in fills soils that liquefied during the 1989 Loma Prieta earthquake. Their studies showed significant increase in both $V_s$ and $q_c$ in the post-earthquake soils as compared to pre-earthquake studies.

To investigate local site variability, three soundings were performed at the Dodd farm site in Steele, MO: one sounding was advanced adjacent to a liquefaction feature (DODD-01), a second 30-m due south (DODD-02), and a third an additional 30-m to the south (DODD-03). All three SCPTu soundings used the same penetrometer and are shown plotted together on Figure 2.25. Mapped liquefaction features at this site correlated with areas of high resistivity from surface studies (Wolf et al., 1998). While no trenching was performed in the areas of DODD-02 and DODD-03, these soundings were in areas of low resistivity and thus inferred not to have surface liquefaction features. DODD-01 and DODD-03 had essentially the same profile for tip resistance, friction ratio, and $u_2$ penetration porewater pressure. DODD-02 had slightly high tip resistance up to 11-m, and contained thin clay seams at 13- and 17.5-m. The shear wave velocity comparison between DODD-01 and DODD-02 was quite scattered through most of the sounding. Shear wave arrival times were not recorded for DODD-03. The velocity at shallow depth, up to 11-m, was generally higher in DODD-02, which matches trends expected from cone tip resistance. This comparison of shear wave velocity profiles

displays the uncertainty associated with the pseudo interval analysis procedure, rather than distinct differences in stiffness.

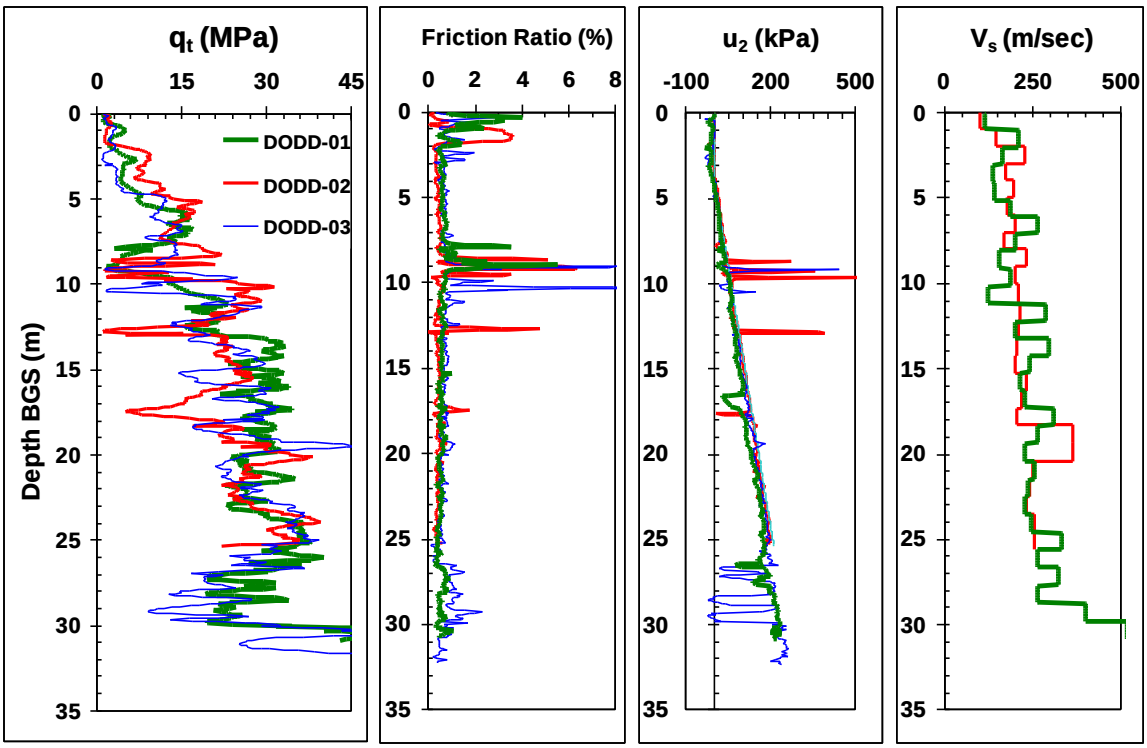


**Figure 2.25. Comparison of Site Variability at Dodd Farm**

In another brief look at site variation, two soundings were performed at the Bugg-40 site in Blytheville, AR: one adjacent to a mapped liquefaction feature (BUGG-01) and a second 40-m due south adjacent to a mapped area with no apparent evidence of liquefaction (BUGG-02). The two soundings are presented in Figure 2.26. The soils consist of medium dense sands grading to dense sands with clay lenses, over a stiff clay layer at about 35-m. These two soundings are fairly similar in tip resistance, penetration pore pressure response, friction ratio, as well as shear wave velocity. A noticeable

differences is that BUGG-01 has a 5-m thick silty clay crust, while BUGG-02 has essentially clean sands through the entire deposit. Migrating seismically induced porewater pressure may have become trapped under the low permiability cap at BUGG-01, while porewater pressures may have been free to dissipate in the area of BUGG-02.

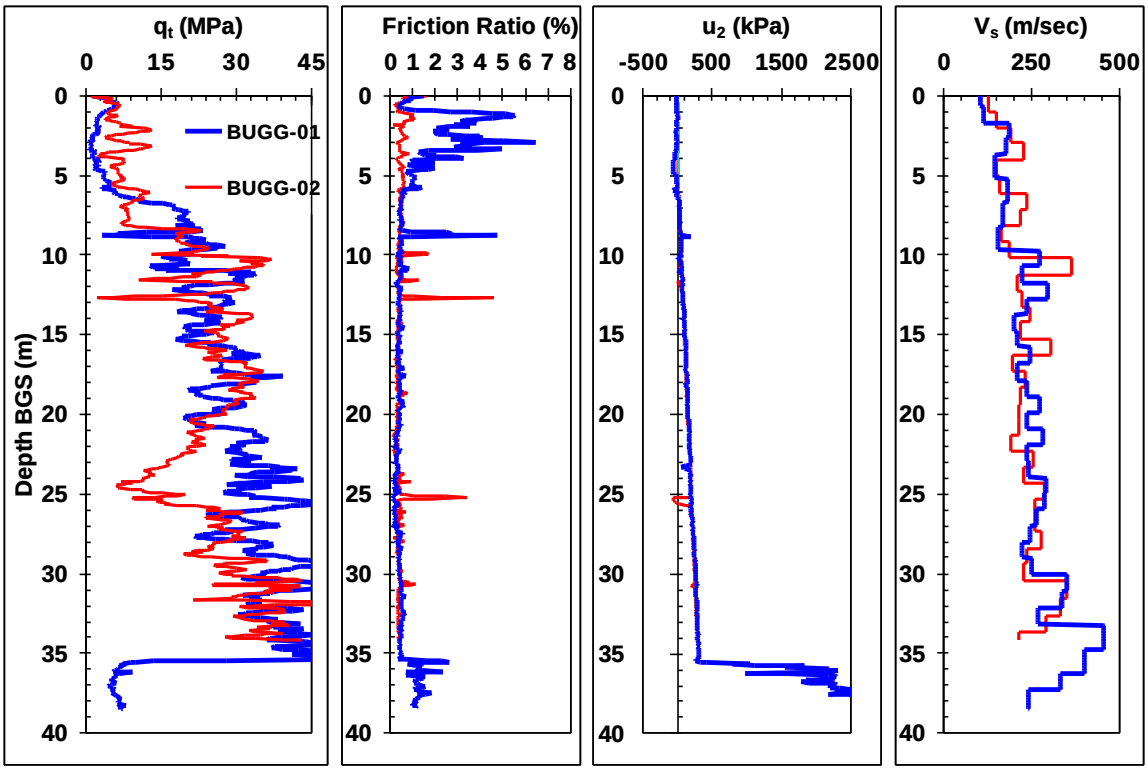


**Figure 2.26. Site Variability at Bugg-40 Site**

5.4 Summary

A number of observations were determined from laboratory and field testing of soils in Mid-America:

- Near surface sands from Mid-America classify as uniformly graded, subangular, clean, fine sands by laboratory index testing methods.

- Fourteen seismic piezocone soundings are displayed in this chapter. These soundings were used to generate layering and stiffness profiles, as well as assess local variability of site conditions.
- Local variation across a site did not appear to be significant. Variability inherent in Mississippi Valley braided bar deposits exists primarily in the vertical direction, rather than horizontally. Since this analysis was based on a limited number of soundings at a limited number of sites, additional study of site variability is recommended.
- The presence of silty clay layers may be a significant feature when considering porewater pressure build-up and sand boil formation.

# CHAPTER 6

# ANALYSIS OF SOIL LIQUEFACTION RESPONSE USING SEISMIC CONE DATA

## 6.1. Overview

The application of current liquefaction methodologies to Mid-American soils will be compared and assessed in regards to historical earthquakes using seismic piezocone data. Sites related to three historic earthquakes (Stover & Coffman, 1993) and three earthquakes dated by paleoliquefaction studies (Tuttle et al., 1998) are analyzed in this section. Liquefaction assessment of soils in this study will be performed by direct methods using simplified cyclic stress procedures and Arias Intensity estimations. Soil properties and in-situ stress state will be evaluated utilizing the four independent readings obtained from the SCPTu: $q_c$, $f_s$, $u_2$, and $V_s$. Strain levels, pore pressure generation, and indirect liquefaction analysis will be evaluated under the cyclic strain framework.

Table 6.1 displays the sites and soundings that are assessed, the associated earthquakes, previous estimates of moment magnitude, estimated epicentral distance, as well as the presence or absence of surface liquefaction features. If the epicentral distance is unknown, an assumed 15-km and 25-km will be used for analyses. A range of magnitude between 6.5 and 8.0 will be studied for earthquakes in the NMSZ, and a range of earthquake magnitude between 6.0 and 7.5 will be studied for the 1886 Charleston, SC

**Table 6.1. Sites and Associated Earthquakes**

| Site (Sounding) | Event(s) (Year A.D.) | Estimated Moment Magnitude | Epicentral Distance (km) | Evidence of Liquefaction |
|---|---|---|---|---|
| ***New Madrid Seismic Zone*** | | | | |
| Shelby Farms (SF) (MEMPH-G) | 1811 | 7.9 | 75 | Sand Boil |
| SF Shooting Range (SFSR-01) | 1811 | 7.9 | 70 | None |
| Houston Levee (MEMPH-H) | 1811 | 7.9 | 90 | None |
| Shelby Forest (SFOR-01) | 1811 | 7.9 | 40 | None |
| Yarbro Excavation (YARB-01) | 1400-1600<br>1811<br>1812a<br>1812b | ?<br>7.9<br>7.6<br>8.0 | ?<br>60<br>45<br>65 | Sand Boils; 6-m deep subsidence |
| Bugg-40 (BUGG-01) | 800-1000 | ? | ? | Sand Boil |
| 3MS617 (3MS617-A) | 1811<br>1812a<br>1812b | 7.9<br>7.6<br>8.0 | 65<br>40<br>60 | Sand Boils |
| Huey House (HUEY-01) | 880-1000 | ? | ? | Sand Boil |
| Dodd Farm (DODD-01) | 1400-1670 | ? | ? | Sand Boil |
| Johnson Farm (JOHN-01) | 770-1200 | ? | ? | Sand Boil |
| ***Charleston, SC Earthquake Region*** | | | | |
| Hollywood Ditch (HW-4) | 1886 | 7.0 | 10 | Sand Boils |
| Thompson Industrial (TIS-01) | 1886 | 7.0 | 5 | None |

1812a - January 23, 1812
1812b - February 7, 1812

event. To analyze a number of sites for various earthquake scenarios, it was necessary to determine critical layers for liquefaction analysis.

## 6.1 Critical Layer Selection

One sounding from each site listed in Table 6.1 will be evaluated under theliquefaction susceptibility frameworks. For each of the soundings, two critical layers were determined; (1) loose granular layer with high liquefaction potential, and (2) a dense granular layer with lower liquefaction potential. Only one critical layer was found at Shelby Forest, since this site primarily consisted of uniform silts over clay. Only one critical loose layer was selected at Shelby Farms Shooting Range, due to the predominance of high tip resistance layers recorded at this site.

Methods for determining the location and thickness of liquefiable layers using continuous CPT techniques have been presented in Olsen (1997) and Robertson & Wride (1998). These methods compare the anticipated cyclic stress ratio of an earthquake to the empirical cyclic resistance ratio determine from in-situ tests. For this study, a number of earthquake magnitudes have been analyzed with associated acceleration as a function of distance. Due to the uncertainty associated with ground motions and location of the earthquakes, it is desirable to estimate the depth and in-situ test parameters of liquefiable layers using a procedure independent of earthquake magnitude and acceleration. To determine critical layers, techniques discussed in Olsen (1994) were combined with field performance analysis of sites that have liquefied during previous earthquakes.

In a study of historical California earthquakes, Youd (1984) discusses how expelled porewater from a liquefied deposit can be trapped beneath low permeability layers. This creates a loose layer that is susceptible to liquefaction during future events. Figure 6.1 displays SPT and CPT resistance at a site having a loose liquefied layer over densified sand. The slope of tip resistance at this site increases rapidly with depth in the loosened layer, while tip resistance is less affected by depth in denser layers (z>6.5 m).

The rate of increasing tip resistance with depth was used to develop the Olsen & Mitchell (1995) CPT soil behavior classification charts (presented earlier in Fig. 2.13). Their data analysis procedure involved plotting CPT tip resistance and sleeve friction measurements compared to effective overburden stress on a log-log plot. Layers of constant soil type and consistency increase with effective confinement on a slope of *1/c*, where *c* is the stress exponent for normalization (Table 2.4). Very dense, overconsolidated soils were determined to have a relatively vertical slope of log $\sigma_{vc}$' vs. log $q_c$, and thus a small value stress exponent, *c*, on the order of 0.15 or lower. Loose, soft soils were determined to have flatter slopes, and thus a *c-value* on the order of 1.0 or higher. Olsen & Mitchell (1995) do not discuss stress exponents higher than unity, but data from unstable deposits has been presented with a *c-value* of 1.5 (Olsen, 1994).

Stress exponents and overburden stress normalized tip resistance, $q_{t1}$, were determined using graphical techniques. Stress normalized tip resistance is expressed as:

$$q_{t1} = \frac{(q_t - s_{vo})}{(s_{vo}')^c} \qquad (6.1)$$

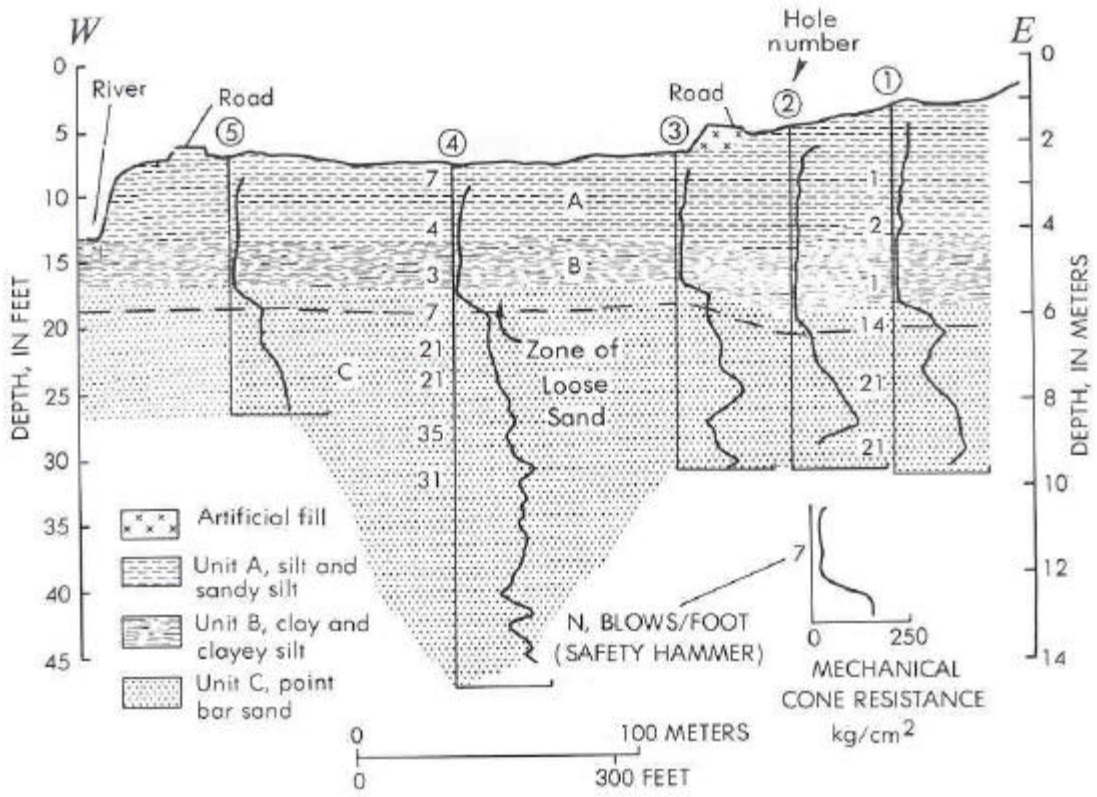


**Figure 6.1. Mechanical Cone Resistance in Loose Layers at a Site of Re-liquefaction in Brawley, California (Youd, 1984)**

where $q_t$ is cone tip resistance, $\sigma_{vo}$ is total overburden stress, and $\sigma_{vo}'$ is effective overburden stress, all in units of atmospheric pressure.

The method for determining normalized tip resistance and stress exponent as presented in Olsen (1994) is shown in Figure 6.2, with tip resistance compared to effective overburden stress on a log-log scale using data from the Huey House sounding in Blytheville, AR. The same sounding is also plotted in the conventional form in Figure 6.3, with tip resistance as compared to depth on an arithmetic scale. Figure 6.3 displays all four channels of the record. Tip resistance, as a function of effective overburden stress and stress exponent, is presented as solid lines through the critical layers. These lines were determined by rearranging Equation 6.1 to get:

$$q_t = q_{t1} \cdot \left(s_{vo}'\right)^c + s_{vo} \qquad (6.2)$$

Due to uncertainties associated with stress exponent values (c) greater than unity, averaged seismic cone data over the selected layer will be presented along with normalization parameters based on the Olsen (1994) method. Figures 6.4 (a-f) and 6.5 (a-f) display the location of the 22 critical layers selected for this study. Each critical layer is marked on the particular $q_c$ profile from individual soundings. Table 6.2 lists each layer location and associated parameters necessary for liquefaction analysis. Table 6.3 displays the averaged SCPTu parameters for each selected layer.

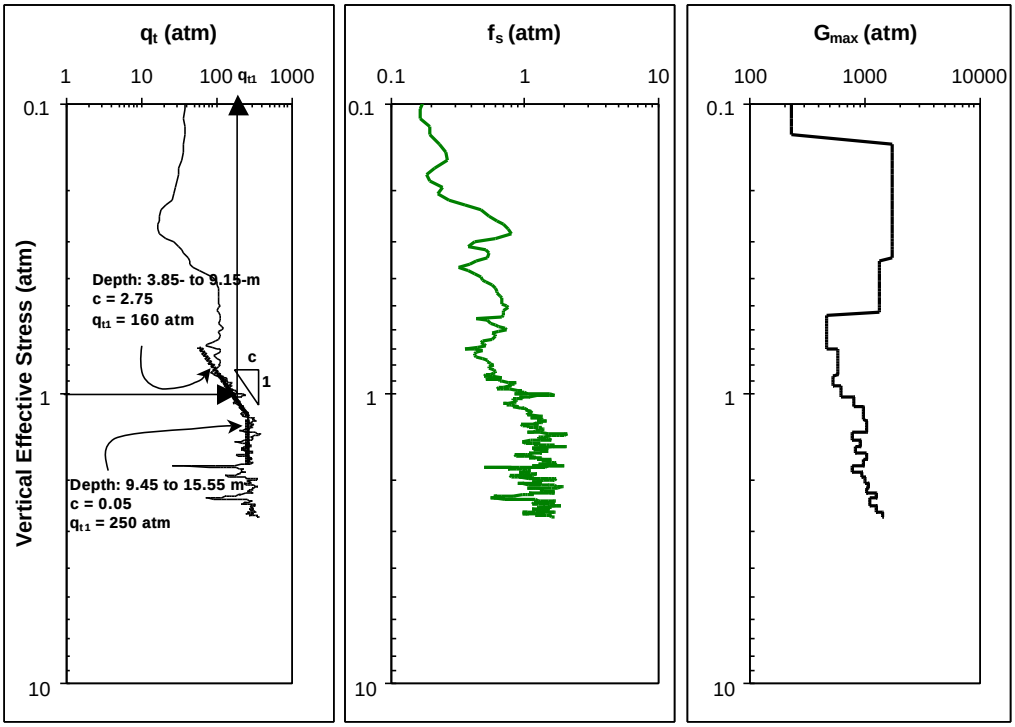


**Figure 6.2. Normalization of Uniform Loose and Dense Sand Layers at Huey House, Blytheville, AR (log-log stress scale)**

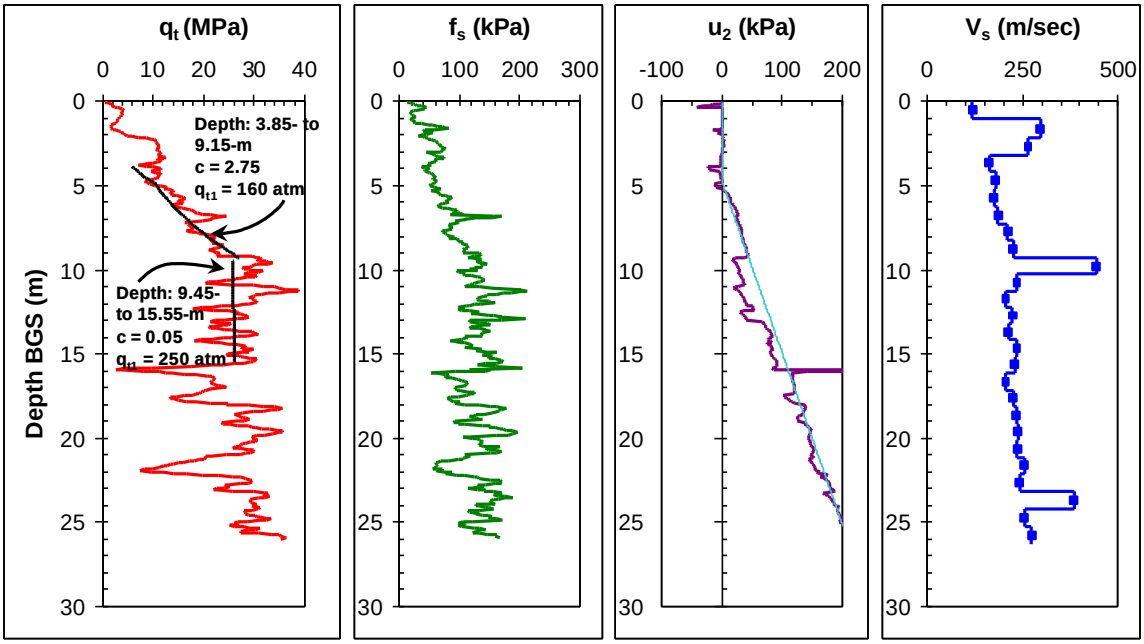


**Figure 6.3. Normalization of Uniform Loose and Dense Sand Layers at Huey House, Blytheville, AR (based on standard plotting scales)**

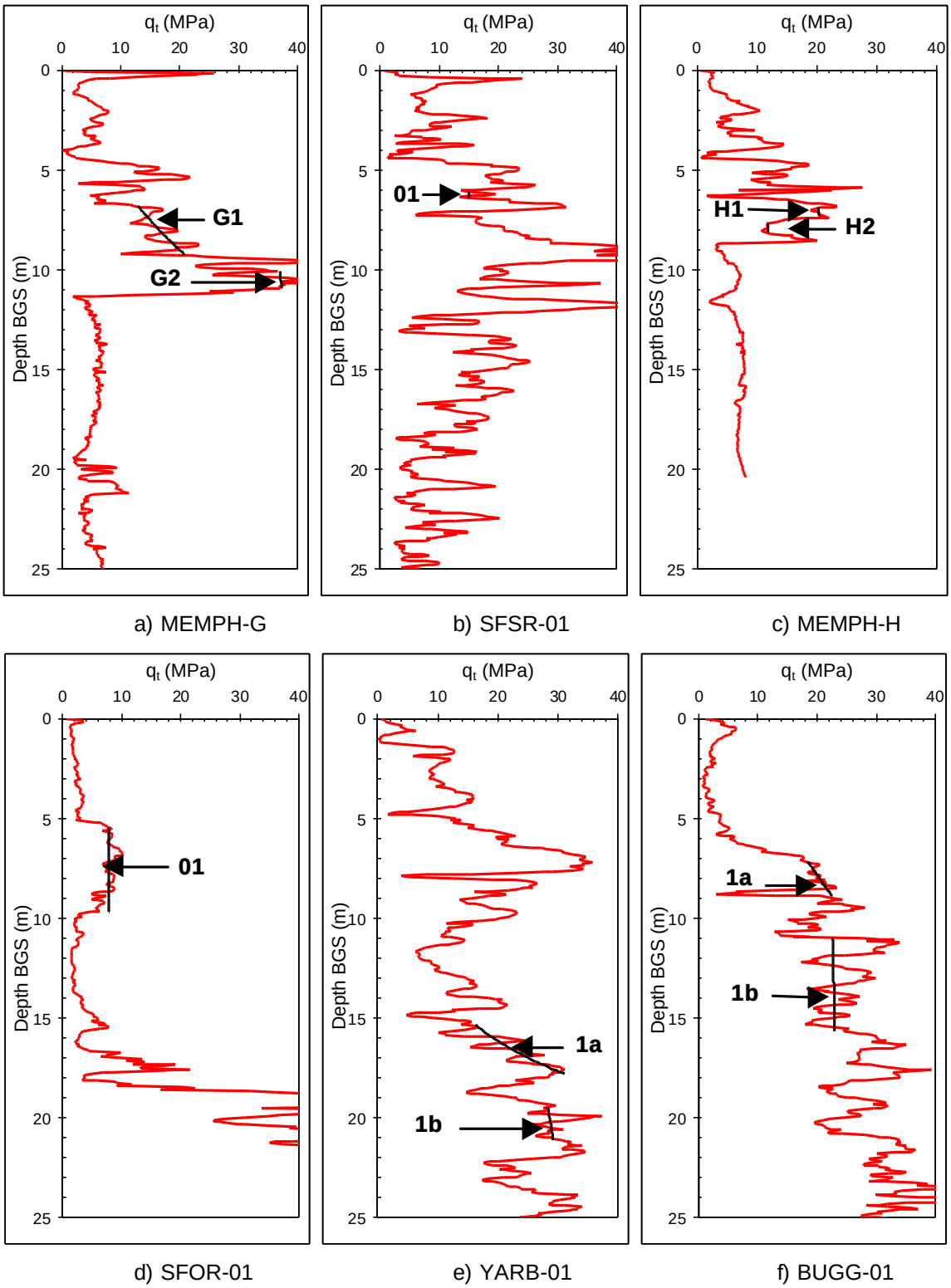


**Figure 6.4. Ten Critical Layers Selected for Liquefaction Analysis**

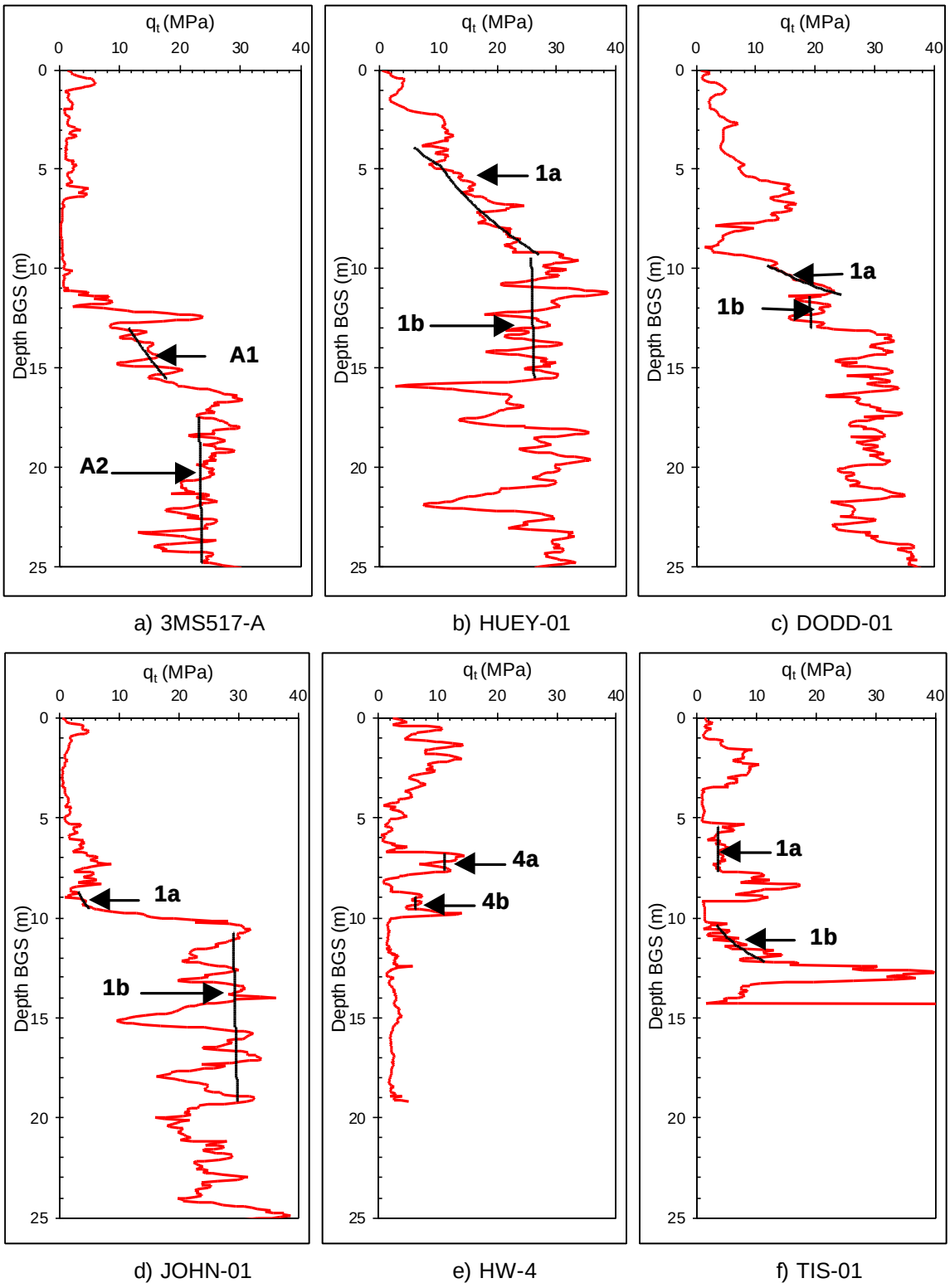


**Figure 6.5. Twelve Critical Layers Selected for Liquefaction Analysis**

**Table 6.2. Layer Parameters used for Simplified Analyses**

| sounding | site lique-faction (Y/N) | Dense or Loose (D/L) | water table (m) | top of layer (m) | layer thick-ness (m) | $\sigma_{vo}$ (kPa) | $\sigma_{vo}'$ (kPa) | $u_o$ (kPa) | soil type |
|---|---|---|---|---|---|---|---|---|---|
| MEMPH-G1 | Y | L | 6 | 6.8 | 2.5 | 139 | 119 | 20 | CS |
| MEMPH-G2 | Y | D | 6 | 10.1 | 0.85 | 183 | 139 | 44 | CS |
| SFSR-01 | N | D | 2 | 6.1 | 0.35 | 112 | 71 | 41 | CS |
| MEMPH-H1 | N | D | 5 | 6.9 | 0.45 | 126 | 105 | 21 | CS |
| MEMPH-H2 | N | D | 5 | 7.7 | 0.5 | 140 | 112 | 28 | CS |
| SFOR-01 | N | D | 5.5 | 5.5 | 4.25 | 140 | 120 | 20 | Loess |
| YARB-01a | Y | L | 4 | 15.35 | 2.5 | 297 | 164 | 133 | CS |
| YARB-01b | Y | D | 4 | 19.45 | 1.7 | 368 | 199 | 169 | CS |
| BUGG-01a | Y | L | 4 | 7.15 | 1.8 | 138 | 98 | 40 | CS |
| BUGG-01b | Y | D | 4 | 11 | 4.7 | 235 | 143 | 92 | CS |
| 3MS617-A1 | Y | L | 5.5 | 13 | 2.6 | 248 | 162 | 86 | CS |
| 3MS617-A2 | Y | D | 5.5 | 17.45 | 7.45 | 375 | 221 | 154 | CS |
| HUEY-01a | Y | L | 4.75 | 3.85 | 5.3 | 117 | 99 | 18 | CS |
| HUEY-01b | Y | D | 4.75 | 9.45 | 6.1 | 226 | 151 | 75 | CS |
| DODD-01a | Y | L | 4.45 | 9.85 | 1.5 | 185 | 125 | 60 | CS |
| DODD-01b | Y | D | 4.45 | 11.4 | 1.65 | 215 | 139 | 76 | CS |
| JOHN-01a | Y | L | 7 | 8.75 | 0.85 | 157 | 136 | 21 | SM-ML |
| JOHN-01b | Y | D | 7 | 10.75 | 8.5 | 265 | 187 | 78 | CS |
| HW-4a | Y | D | 1.6 | 6.8 | 0.9 | 125 | 70 | 55 | CS |
| HW-4b | Y | D | 1.6 | 8.95 | 0.7 | 162 | 87 | 75 | CS |
| TIS-01a | N | D | 1.6 | 5.45 | 2.3 | 115 | 66 | 49 | CS |
| TIS-01b | N | L | 1.6 | 10.4 | 1.85 | 199 | 104 | 95 | CS |

CS: Clean Sand
SM-ML: Silty Sand to Sandy Silt
Loess: Cemented sandy silt
Site Liquefaction - Was surface liquefaction evident at the site? (Yes / No)
Dense or Loose- Layers of differing consistency were selected using the Olsen (1994) method. Loose layers (L) have a stress exponent, c, greater than 1.
$\sigma_{vo}$ - total overburden stress averaged over layer at time of in-situ testing taken at midpoint of layer
$\sigma_{vo}'$ - effective overburden stress averaged over layer at time of in-situ testing taken at midpoint of layer
$u_o$ - hydrostatic water pressure averaged over layer at time of in-situ testing taken at midpoint of layer

**Table 6.3. Seismic Piezocone Parameters used for Simplified Analyses**

| Sounding | $q_{t1}$* c Olsen (1994) | | $q_{t,avg}$ (atm) | $F_{s,avg}$ (atm) | $FR_{avg}$ (%) | $u_{2,avg}$ (atm) | $B_{q,avg}$ | $V_{s,avg}$ (m/s) | $V_{s1}$ (m/s) |
|---|---|---|---|---|---|---|---|---|---|
| MEMPH-G1 | 100 | 3 | 160 | 1.2 | 0.75 | 0.31 | 0.001 | 172 | 165 |
| MEMPH-G2 | 360 | 0.05 | 350 | 2.4 | 0.69 | 0.75 | 0.001 | 261 | 241 |
| SFSR-01 | 150 | 0.05 | 161 | 1.5 | 0.93 | 0.07 | -0.002 | 181 | 198 |
| MEMPH-H1 | 200 | 0.05 | 199 | 1.3 | 0.65 | 0.3 | 0.000 | 189 | 187 |
| MEMPH-H2 | 115 | 0.05 | 113 | 0.7 | 0.62 | 0.36 | 0.001 | 180 | 176 |
| SFOR-01 | 75 | 0 | 77 | 1.6 | 2.08 | 0.19 | 0.000 | 271 | 260 |
| YARB-01a | 20 | 5 | 213 | 1.4 | 0.66 | 0.21 | -0.005 | 234 | 207 |
| YARB-01b | 215 | 0.4 | 288 | 1.4 | 0.49 | 0.315 | -0.005 | 310 | 262 |
| BUGG-01a | 210 | 1.5 | 180 | 1.1 | 0.61 | 0.43 | 0.000 | 165 | 166 |
| BUGG-01b | 220 | 0.05 | 244 | 1 | 0.41 | 0.89 | 0.000 | 234 | 215 |
| 3MS617-A1 | 30 | 3.3 | 142 | 0.8 | 0.56 | 0.41 | -0.003 | 206 | 183 |
| 3MS617-A2 | 220 | 0.05 | 232 | 0.85 | 0.37 | 1.28 | -0.001 | 234 | 193 |
| HUEY-01a | 160 | 2.75 | 164 | 0.8 | 0.49 | 0.18 | 0.000 | 195 | 196 |
| HUEY-01b | 250 | 0.05 | 272 | 1.3 | 0.48 | 0.52 | -0.001 | 224 | 203 |
| DODD-01a | 28 | 8.5 | 177 | 1.1 | 0.62 | 0.56 | 0.000 | 156 | 148 |
| DODD-01b | 185 | 0.05 | 194 | 1.2 | 0.62 | 0.65 | -0.001 | 246 | 227 |
| JOHN-01a | 2 | 10 | 34.3 | 0.3 | 0.87 | -0.63 | -0.026 | 172 | 160 |
| JOHN-01b | 280 | 0.05 | 252 | 1.1 | 0.44 | 0.64 | -0.001 | 280 | 240 |
| HW-4a | 110 | 0 | 113 | 0.55 | 0.49 | 0.5 | 0.000 | 205 | 225 |
| HW-4b | 60 | 0 | 61 | 0.07 | 0.11 | 0.8 | 0.001 | 238 | 247 |
| TIS-01a | 35 | 0.05 | 38.4 | 0.2 | 0.52 | 0.4 | -0.002 | 163 | 181 |
| TIS-01b | 50 | 8 | 65.2 | 0.3 | 0.46 | 1.2 | 0.004 | 253 | 251 |

$q_{t1}$ - normalized tip resistance based on uniform layer using stress exponent *c* (Eq. 6.1)
*c* - stress exponent for normalization of tip resistance from graphical procedures (Eq. 6.1)
$q_{t,avg}$ - tip resistance averaged over layer presented in Table 6.2
$f_{s,avg}$ - sleeve friction averaged over layer presented in Table 6.2
$FR_{avg}$ - average friction ratio, $f_{s,avg} / q_{t,avg} \cdot 100$
$u_{2,avg}$ - average penetration porewater pressure for layer taken behind the tip
$B_{q,avg}$ - average pore pressure parameter, $(u_{2,avg} - u_{o,avg})/(q_{t,avg} - \sigma_{vo})$
$V_{s,avg}$ - shear wave velocity averaged over layer presented in Table 6.2
$V_{s1}$ - normalized shear wave velocity, $V_{s,avg} / (\sigma_{vo}')^{0.25}$

* while $q_{t1}$ is a normalized value, averaged parameters are presented due to uncertainty associated with c values greater than 1.0

## 6.3 Cyclic Stress based Methods

Cyclic stress-based methods for liquefaction evaluation using the Seed & Idriss (1971) simplified procedure are available for the normalized seismic piezocone parameters of $q_{c1N}$ and $V_{s1}$ (NCEER, 1997). This section will present methods and results from cyclic stress based analysis on the 22 critical layers presented in the previous section. Normalization schemes used for the parameters are as recommended by NCEER (1997) and are expressed as:

$$q_{c1N} = q_c / (\sigma_{vo}')^n \quad (6.3)$$

$$V_{s1} = V_s / (\sigma_{vo}')^n \quad (6.4)$$

For the normalized CPT tip resistance ($q_{c1N}$), the stress exponent (n) is 0.5 in sands and 0.75 in sandy silts (Robertson & Wride 1997). For the normalized shear wave velocity ($V_{s1}$), the stress exponent (n) is 0.25 (Robertson et al., 1992b).

Earthquakes and associated sites to be evaluated are presented in Table 6.l. A range of magnitudes between 6.5 and 8.0 will be studied for earthquakes in the NMSZ, and a range of earthquake magnitude between 6.0 and 7.5 will be studied for the 1886 Charleston, SC event. Table 6.4 displays ground surface accelerations determined from the Herrmann & Akinci (1999) deep soil model as a function of hypocentral distance, moment magnitude, and depth of soil column. A hypocentral depth of 9.3-km is used in the NMSZ and a hypocentral depth of 10.9-km is used in the Charleston, SC earthquake region (Toro et al., 1997).

Results of cyclic stressed-based analysis will be presented on charts comparing normalized in-situ test parameters ($q_{c1N}$ and $V_{s1}$) to cyclic stress ratio (CSR). Sites and analyzed data will be presented on figures separated into earthquake events. Cone tip resistance based analysis and shear wave velocity analysis will be presented on individual charts. Figure 6.6 shows a sample cyclic stress based analysis chart from this study, with pertinent information.

Utilizing the data and curves as presented in Figure 6.6, a critical moment magnitude ($M_w$) will be selected for each method, each site, and each earthquake. Critical layers are analyzed at constant source-to-site distance. Utilizing magnitude and distance dependent acceleration attenuation relationships, the induced CSR becomes solely a function of earthquake magnitude. A cyclic stress ratio line will be vertically increasing for a critical soil layer of constant properties. The critical magnitude represents the intersection of the cyclic stress ratio line with the cyclic resistance ratio. This critical magnitude represents a factor of safety near unity that would cause borderline liquefaction.

For cyclic stress based analyses utilizing normalized cone tip resistance ($q_{c1N}$), two CRR curves have been previously presented in Chapter 4:

1. Equation 4.10; 1997 NCEER recommended curve presented in Robertson & Wride (1997; 1998);
2. Equation 4.15; asymptotic curve with a limiting $q_{c1N}$ of 230.

When determining critical lower bound magnitudes, the curve generated by Equation 4.15 will be used. This curve is more conservative than Equation 4.10 up to CSR values

**Table 6.4. Peak Ground Acceleration (g) for Earthquake Scenarios (M3 Model)**

| New Madrid Earthquake of 800 -1000 (Bugg-40, Huey House, Johnson Farm)<br>New Madrid Earthquake of 1400-1600 (Yarbro Excavation, Dodd Farm) | | |
|---|---|---|
| Moment Magnitude | Epicentral Distance (km) | |
| | 15[b] | 25[b] |
| 6.5 | 0.43 | 0.27 |
| 7.0 | 0.61 | 0.38 |
| 7.5 | 0.84 | 0.54 |
| 8.0 | 1.30 | 0.83 |

| New Madrid Earthquake of 1811 (Shelby Farms, SF Shooting Range, Houston Levee, Shelby Forest, Yarbro Excavation, 3MS617) | | | | | | |
|---|---|---|---|---|---|---|
| Moment Magnitude | Epicentral Distance (km) | | | | | |
| | 40[a] | 60[b] | 65[b] | 70[a] | 75[a] | 90[a] |
| 6.5 | 0.13 | 0.09 | 0.09 | 0.07 | 0.07 | 0.06 |
| 7.0 | 0.19 | 0.14 | 0.13 | 0.10 | 0.10 | 0.09 |
| 7.5 | 0.28 | 0.21 | 0.20 | 0.15 | 0.15 | 0.14 |
| 7.9 | 0.39 | 0.29 | 0.26 | 0.20 | 0.20 | 0.18 |

| New Madrid Earthquake of January 23, 1812 (Yarbro Excavation, 3MS617) | | |
|---|---|---|
| Moment Magnitude | Epicentral Distance (km) | |
| | 40[b] | 45[b] |
| 6.5 | 0.15 | 0.13 |
| 7.0 | 0.23 | 0.20 |
| 7.6 | 0.36 | 0.33 |
| 8.0 | 0.49 | 0.43 |

| New Madrid Earthquake of February 7, 1812 (Yarbro Excavation, 3MS617) | | |
|---|---|---|
| Moment Magnitude | Epicentral Distance (km) | |
| | 60[b] | 65[b] |
| 6.5 | 0.09 | 0.09 |
| 7.0 | 0.14 | 0.13 |
| 7.5 | 0.21 | 0.20 |
| 8.0 | 0.31 | 0.28 |

| Charleston Earthquake of 1886 (Hollywood Ditch, Thompson Industrial Services) | | | |
|---|---|---|---|
| Moment Magnitude | Epicentral Distance (km) | | |
| | 5[c] | 10[c] | 20[c] |
| 6.0 | 0.36 | 0.28 | 0.16 |
| 6.5 | 0.50 | 0.39 | 0.25 |
| 7.0 | 0.79 | 0.62 | 0.39 |
| 7.5 | 1.10 | 0.87 | 0.55 |

[a] 1000-m of soil over bedrock
[b] 600-m of soil over bedrock
[c] 810- to 840-m of soil over bedrock (depth of soil = 800 (m) + 2·$r_{epi}$ (km))
$r_{epi}$ = epicentral distance

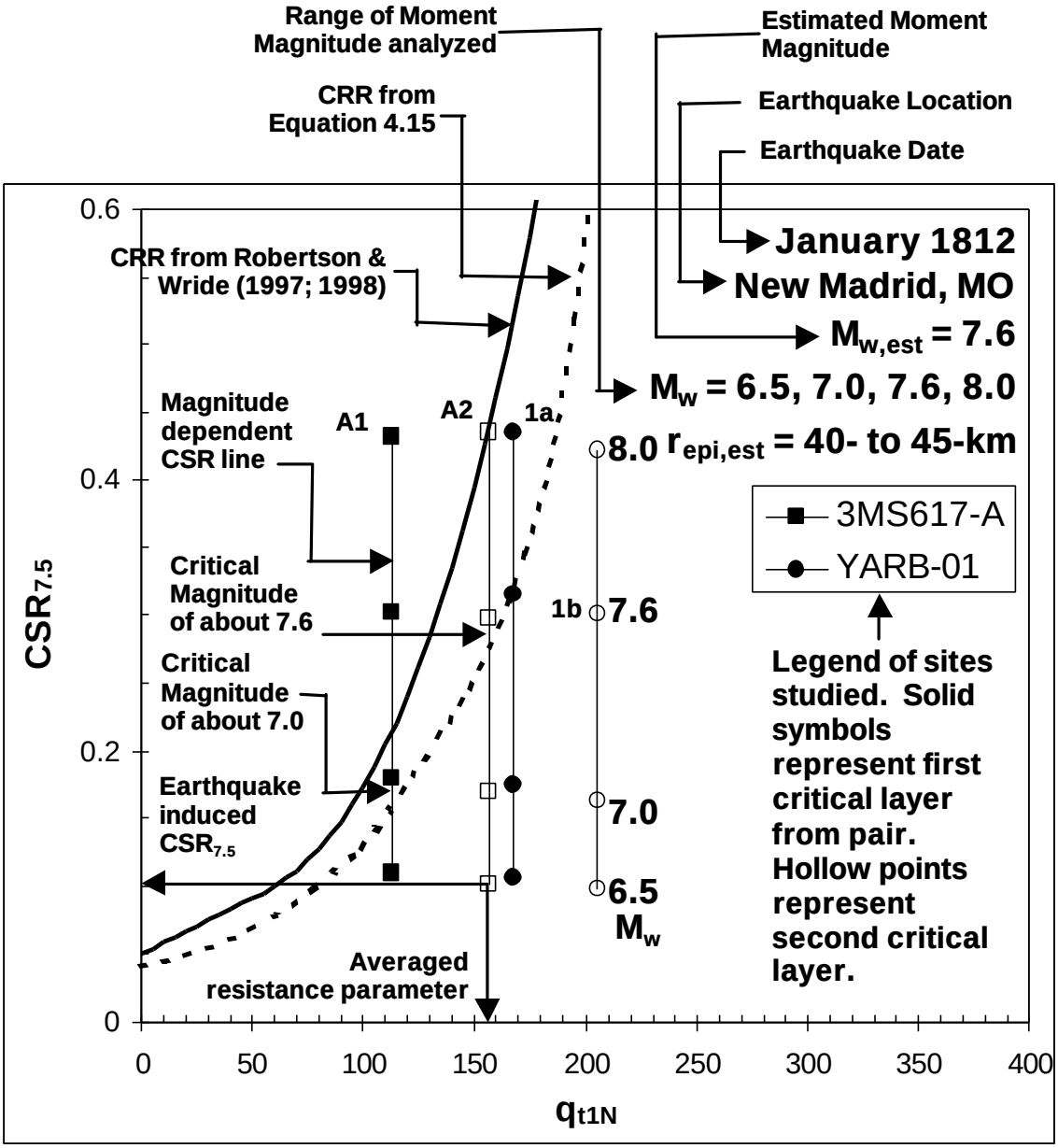


**Figure 6.6. Key Aspects of Cyclic Stress based Analysis Charts for This Study**

of 1.0, and will provide a lower bound estimate of magnitude required to induce liquefaction. For cyclic stress based analysis utilizing normalized shear wave velocity ($V_{s1}$), the Andrus et al. (1999) CRR curve will be used (Eq. 4.13). Figures 6.7 through 6.12 display the results of cyclic stress based analyses for six different earthquakes.

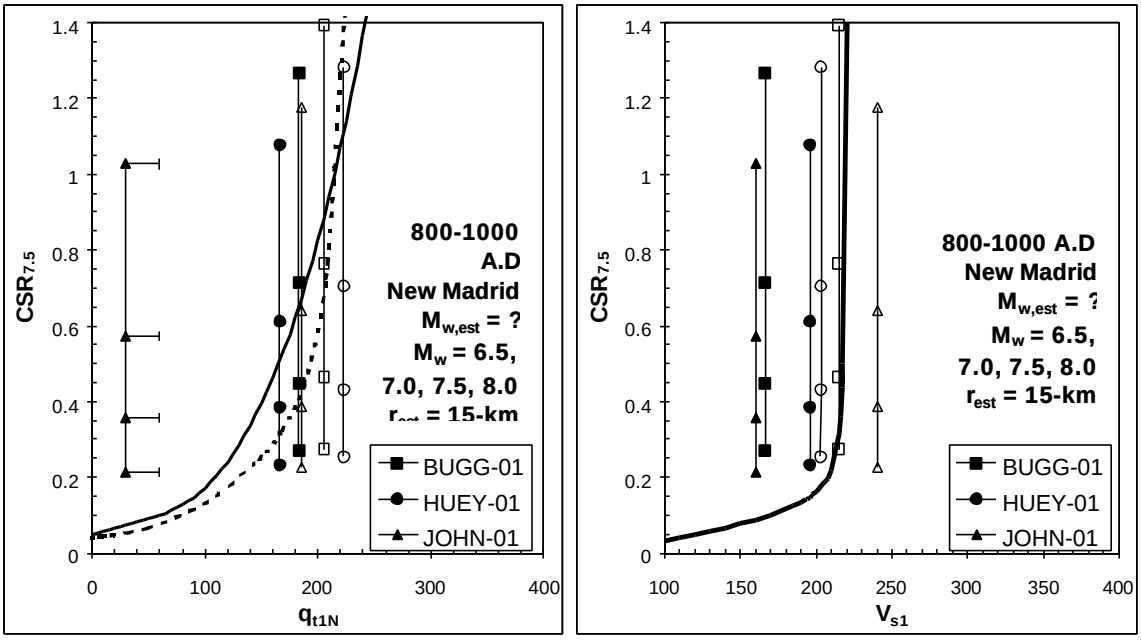


**Figure 6.7 (a) Liquefaction Plots for 800-1000 New Madrid Earthquake at $r_{epi}$ = 15km**

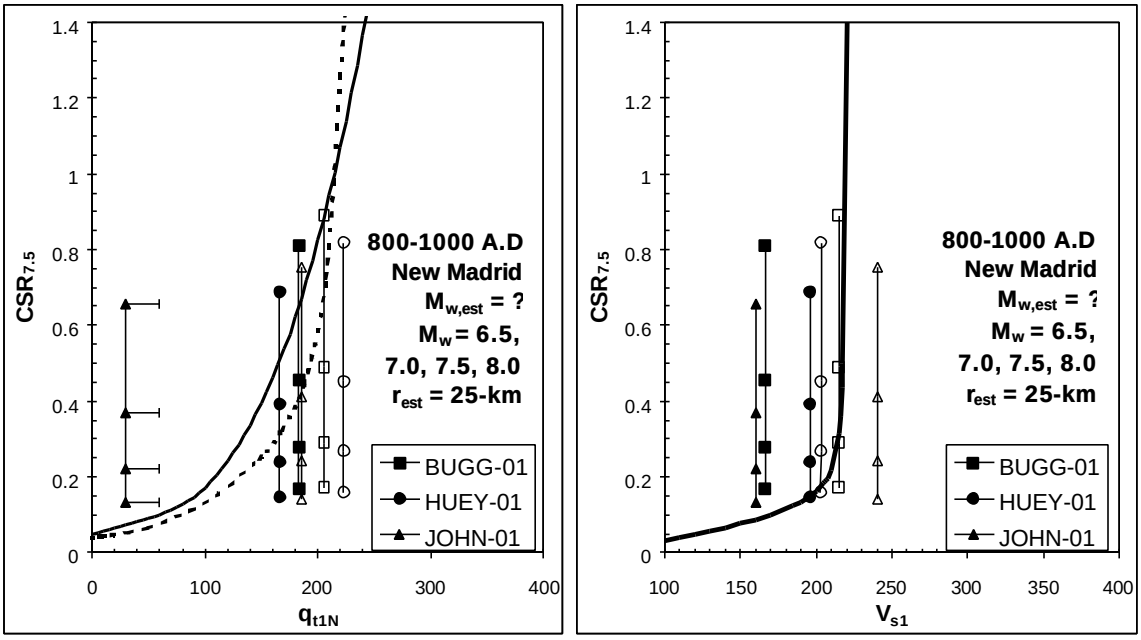


**Figure 6.7 (b) Liquefaction Plots for 800-1000 New Madrid Earthquake at $r_{epi}$ = 25 km**

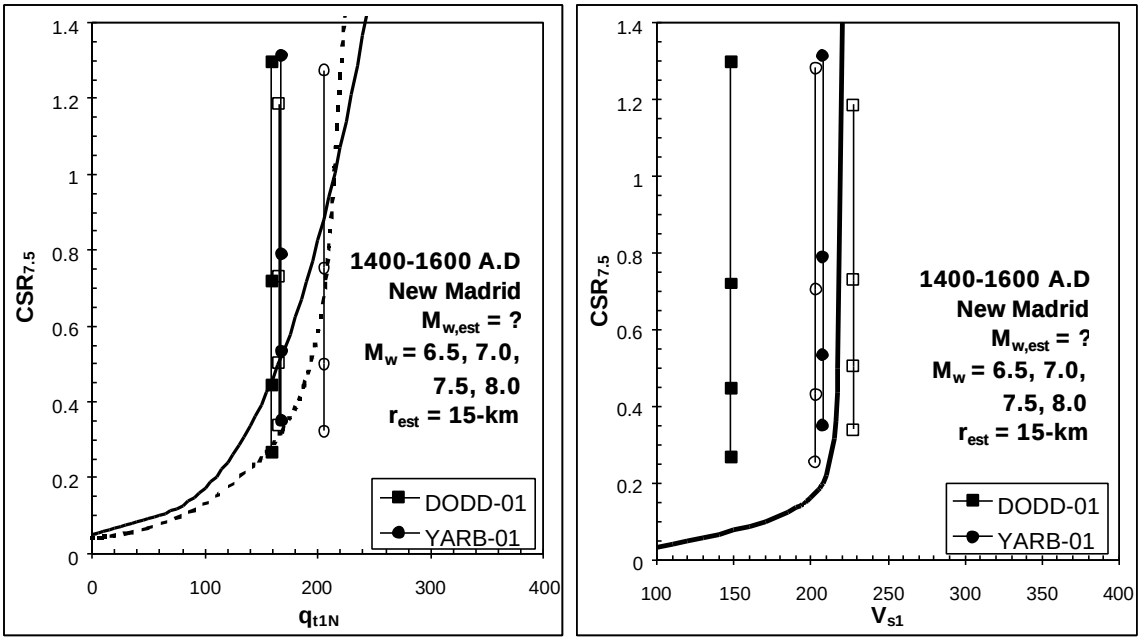


**Figure 6.8 (a) Liquefaction Plots for 1400-1600 New Madrid Earthquake at $r_{epi}$ = 15km**

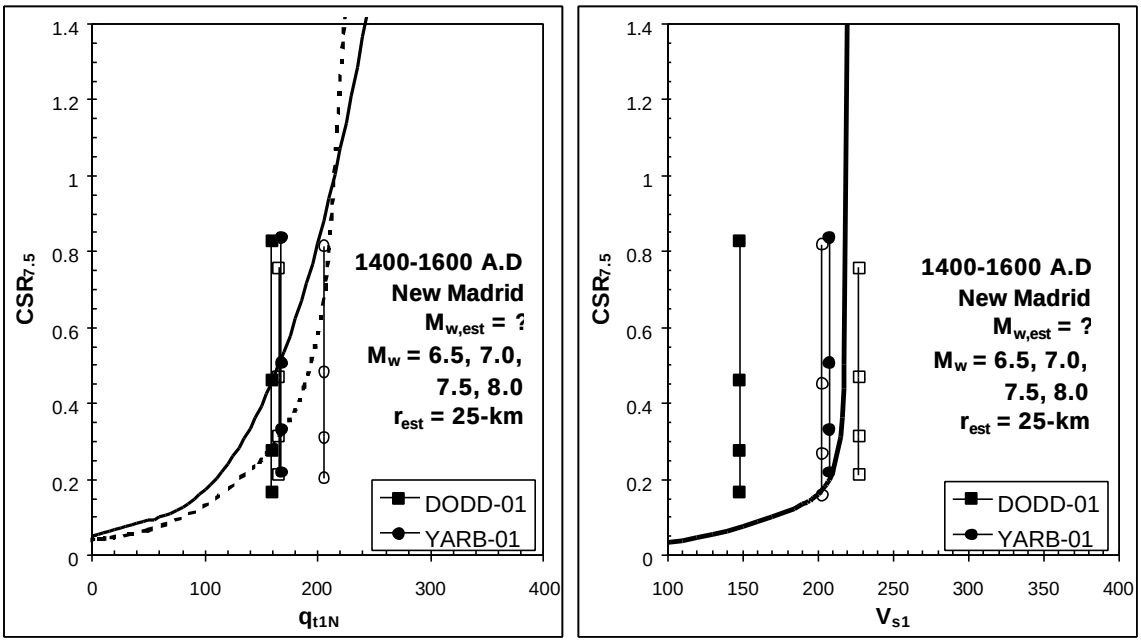


**Figure 6.8 (b) Liquefaction Plots for 1400-1600 New Madrid Earthquake at $r_{epi}$ = 25 km**

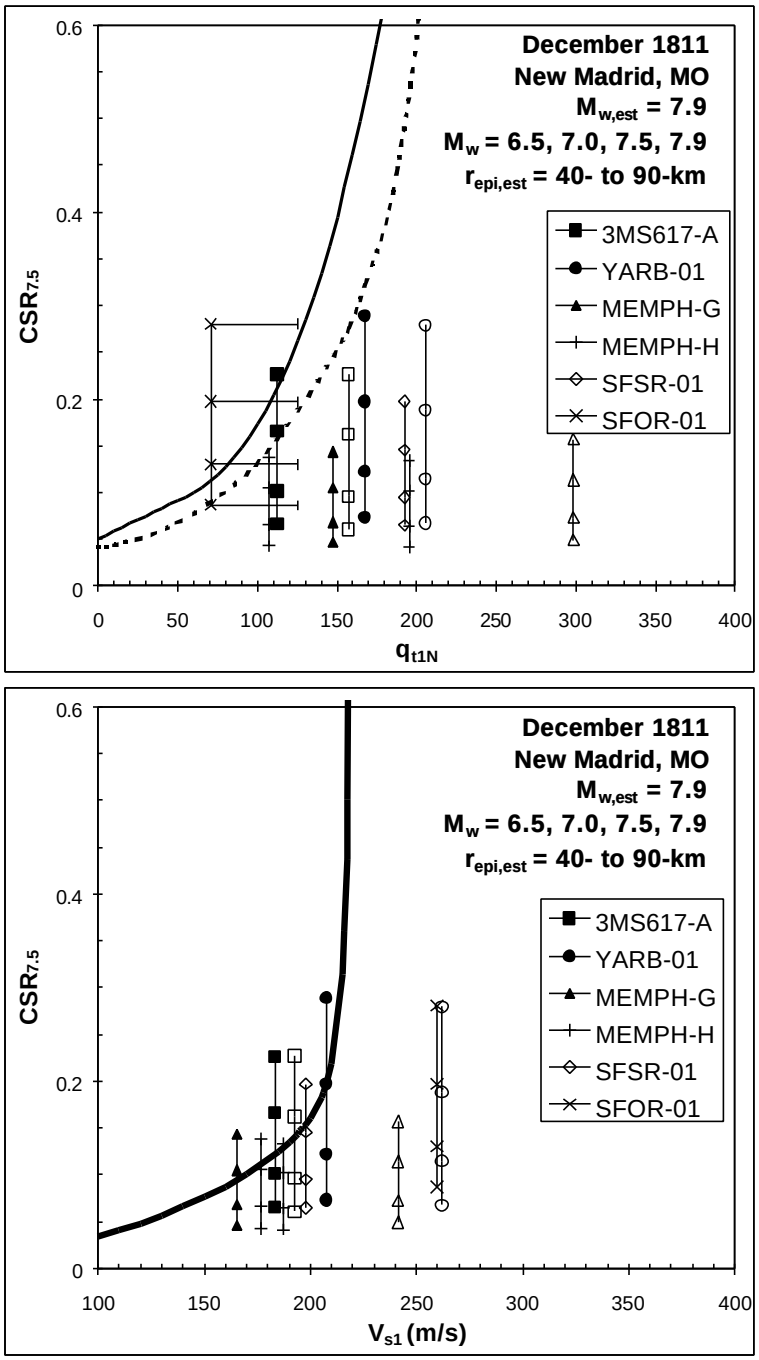


**Figure 6.9 Liquefaction Plots for December 1811 New Madrid Earthquake**

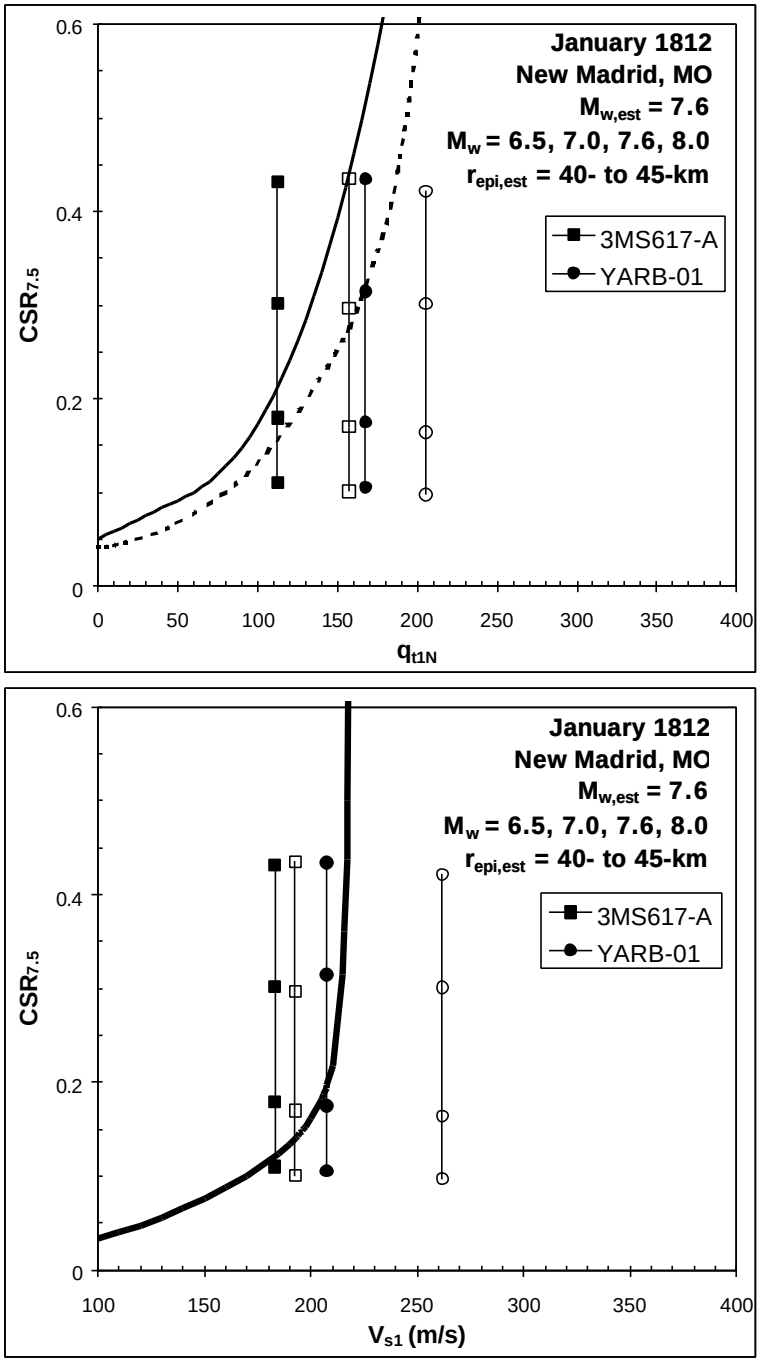


**Figure 6.10 Liquefaction Plots for January 1812 New Madrid Earthquake**

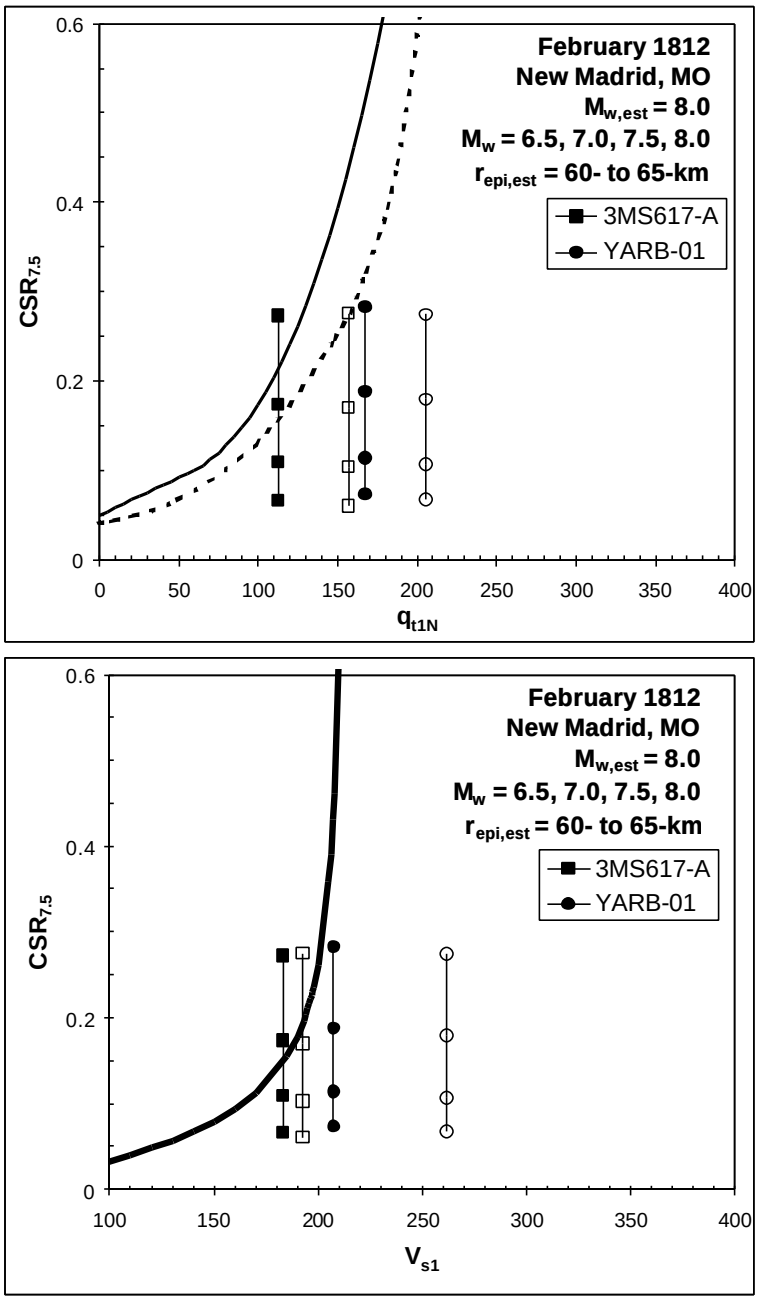


**Figure 6.11 Liquefaction Plots for February 1812 New Madrid Earthquake**

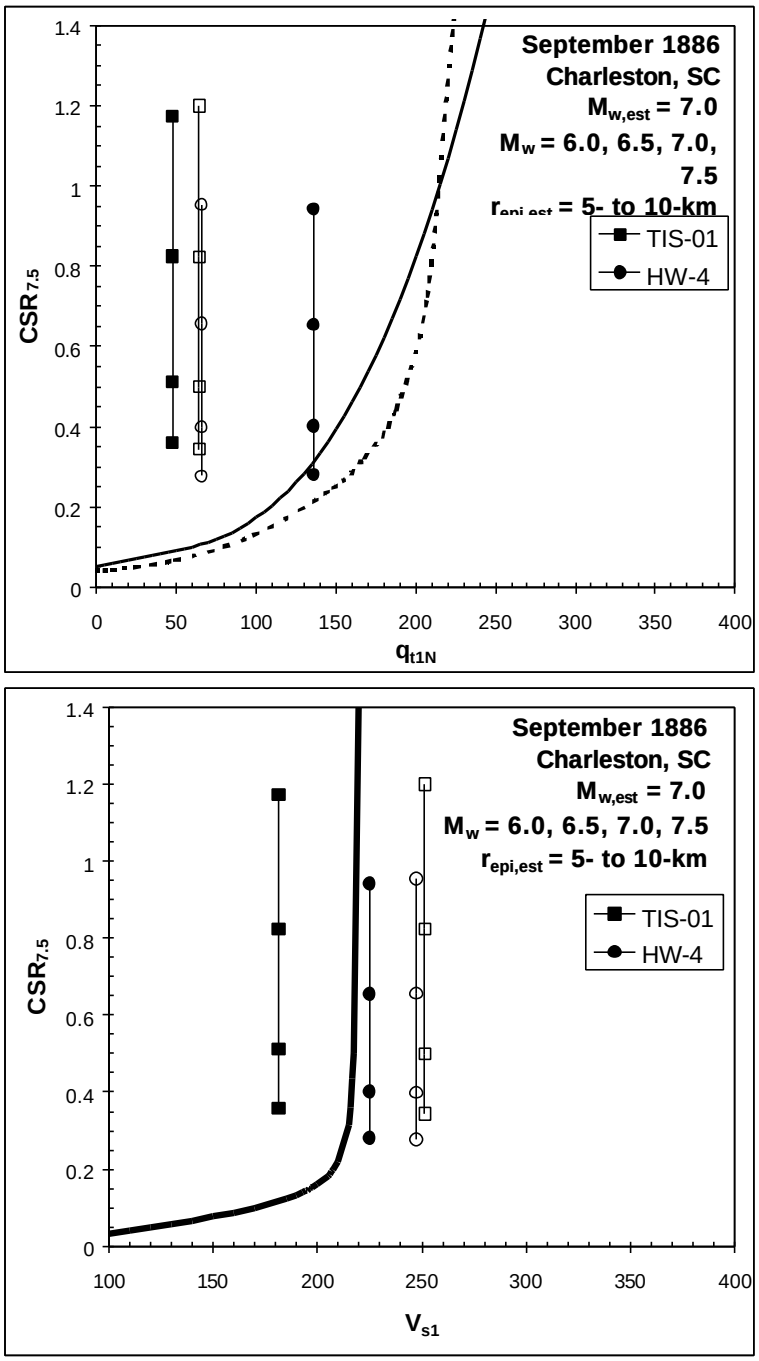


**Figure 6.12 Liquefaction Plots for September1886 Charleston, SC Earthquake**

## 6.4 Arias Intensity based Method

Results of Arias intensity-based analysis for soils in Mid-America will be presented on charts comparing normalized in-situ test parameters to Arias Intensity, $I_{hb}$. Sites and analyzed data will be presented on figures separated into earthquake events. Figure 6.13 shows a sample Arias intensity-based analysis chart from this study, with pertinent information.

Utilizing the methods presented in Figure 6.13, a critical moment magnitude will be selected for each method, each site, and each earthquake. Critical layers are analyzed at constant source to site distance. Utilizing magnitude dependent Arias intensity attenuation relationships, the induced $I_{hb}$ becomes solely a function of earthquake magnitude. An $I_{hb}$ line will be vertically increasing with magnitude for a critical soil layer of constant properties. The critical magnitude represents the intersection of the $I_{hb}$ line with the Arias intensity resistance. For this study, Equation 4.28 will represent the Arias intensity resistance. This critical magnitude represents a factor of safety near unity that would cause borderline liquefaction. Figures 6.14 through 6.19 display the results of Arias intensity-based analyses for six different earthquakes.

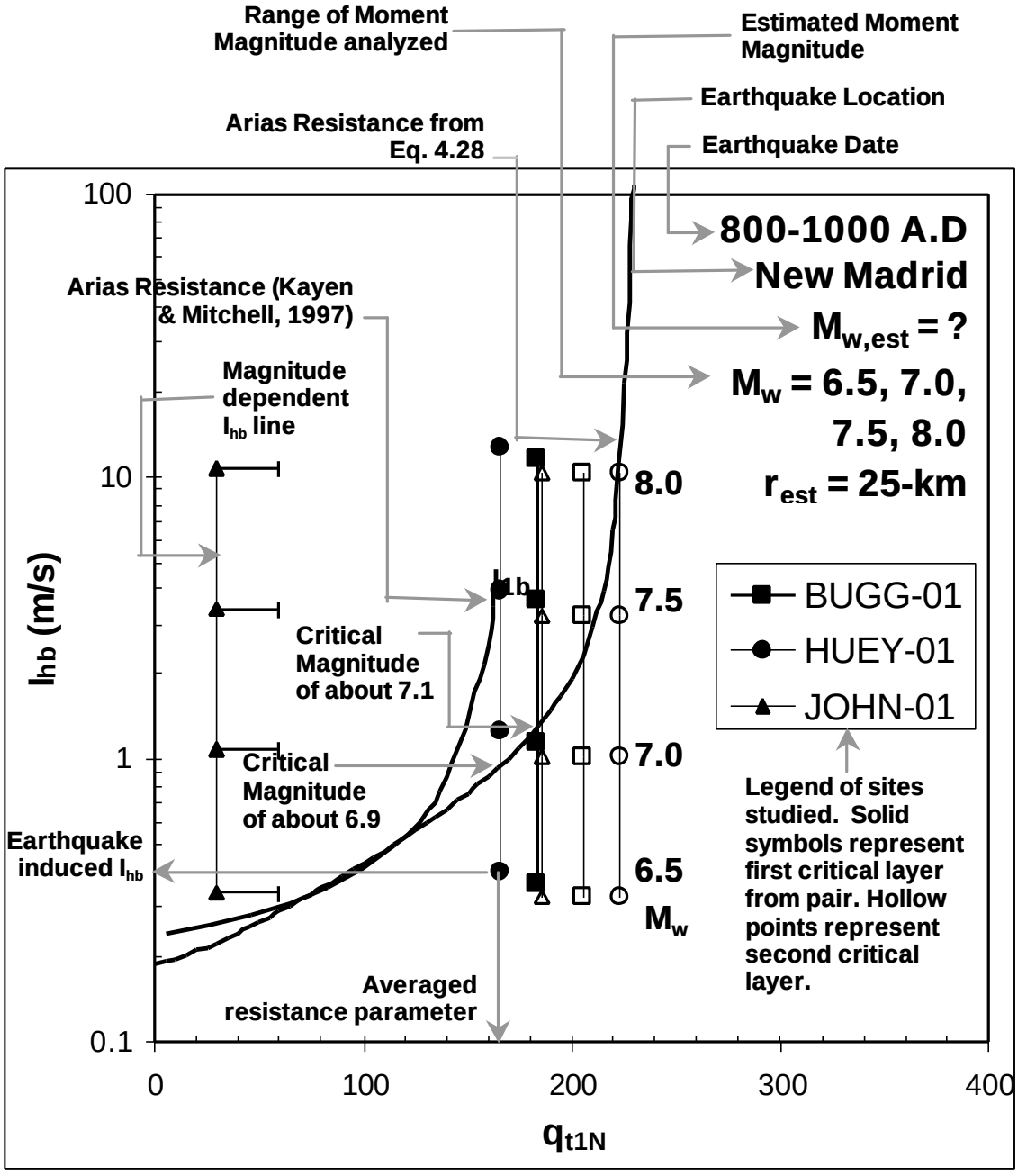


**Figure 6.13. Key Aspects of Arias Intensity-based Analysis Charts for This Study**

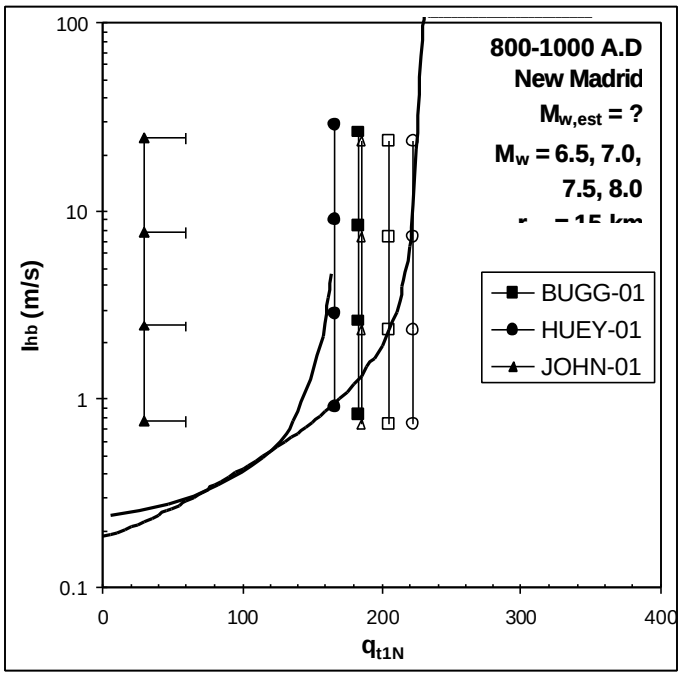


**Figure 6.14 (a) Arias Intensity Liquefaction Plots for 800-1000 New Madrid Earthquake at $r_{epi}$ = 15km**

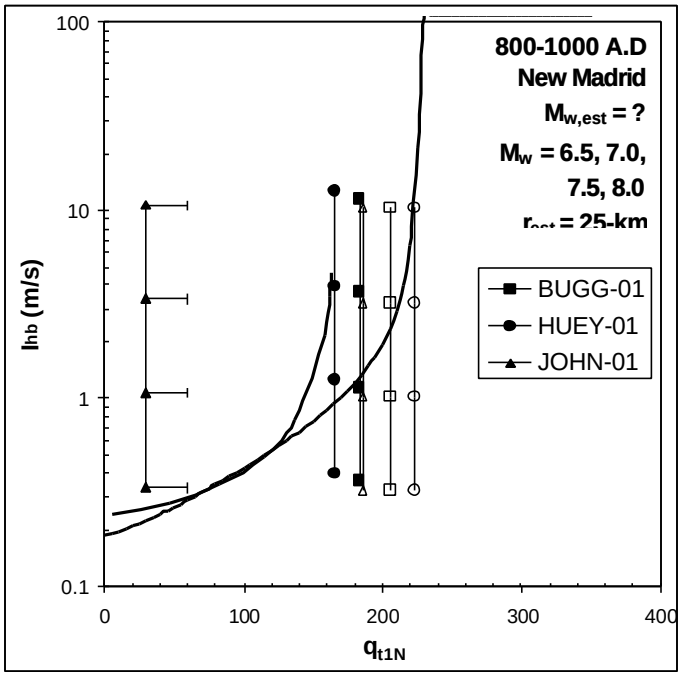


**Figure 6.14 (b) Arias Intensity Liquefaction Plots for 800-1000 New Madrid Earthquake at $r_{epi}$ = 25 km**

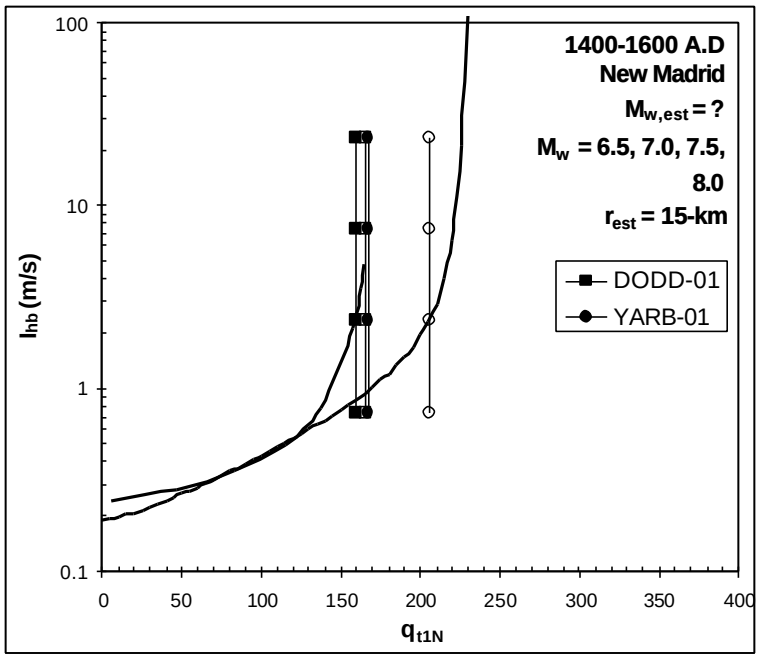


**Figure 6.15 (a) Arias Intensity Liquefaction Plots for 1400-1600 New Madrid Earthquake at $r_{epi}$ = 15km**

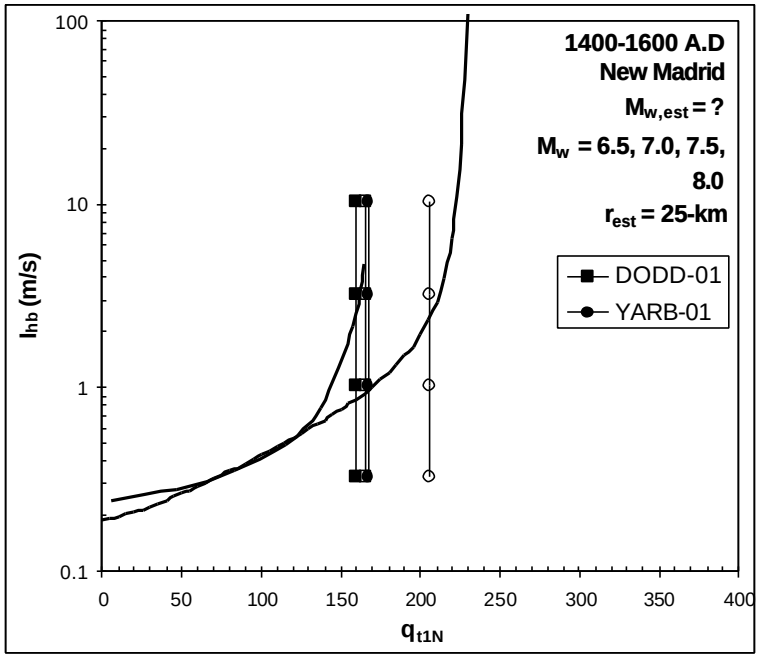


**Figure 6.15 (b) Arias Intensity Liquefaction Plots for 1400-1600 New Madrid Earthquake at $r_{epi}$ = 25 km**

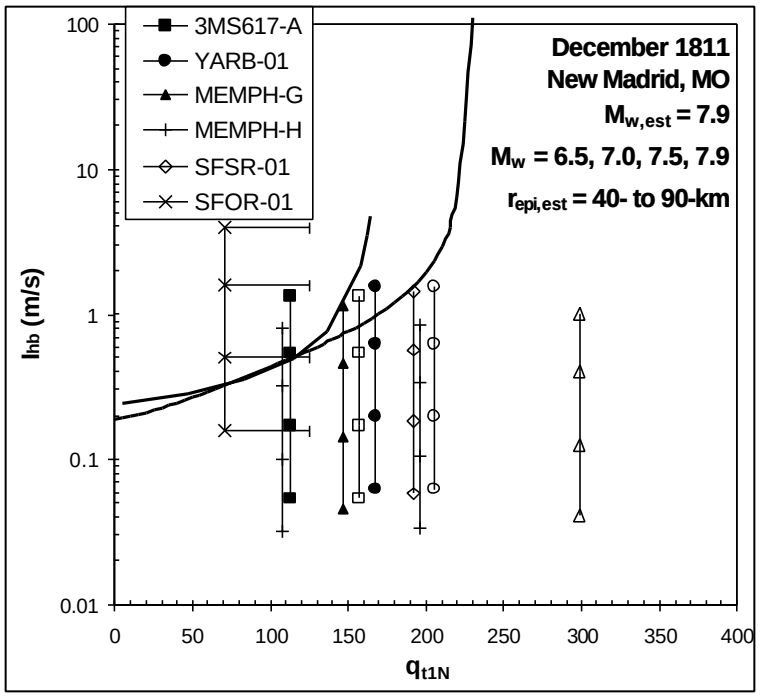


**Figure 6.16 Arias Intensity Liquefaction Plots for December 1811 New Madrid Earthquake**

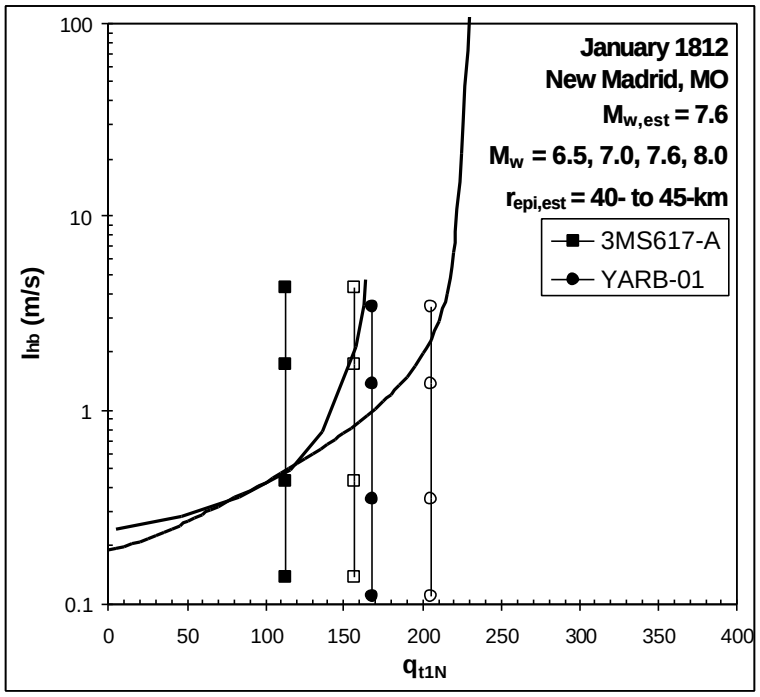


**Figure 6.17 Arias Intensity Liquefaction Plots for January 1812 New Madrid Earthquake**

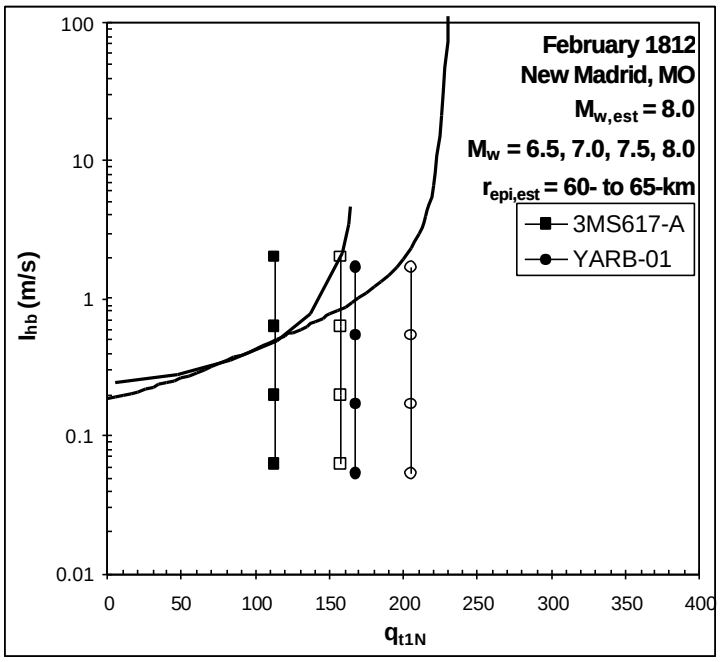


**Figure 6.18 Arias Intensity Liquefaction Plots for February 1812 New Madrid Earthquake**

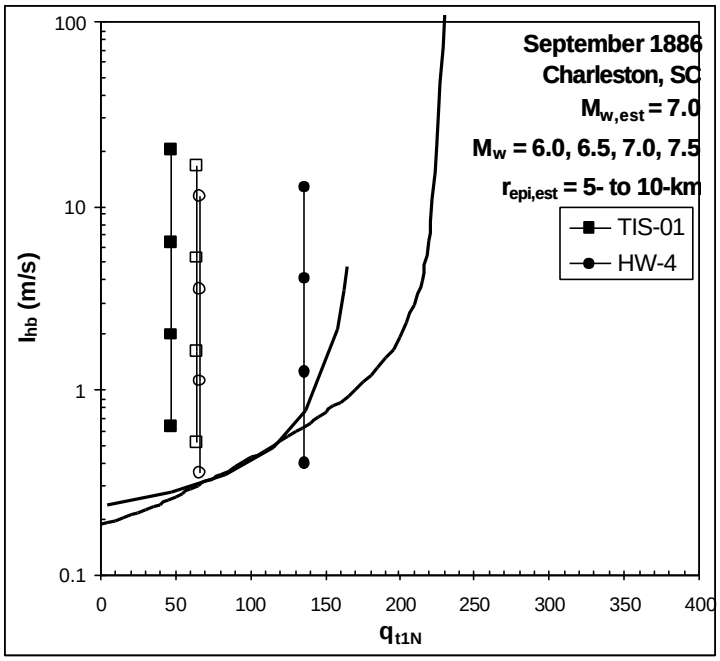


**Figure 6.19 Arias Intensity Liquefaction Plots for Septemeber 1886 Charleston, SC Earthquake**

## 6.5 Cyclic Strain Based Method

Cyclic strain based analysis procedures estimate soil properties from in-situ test parameters and incorporate the results in a rational framework for liquefaction analysis, rather than simplified charts. Cyclic strain methods are presented in detail in Chapter 4, but pertinent aspects will be discussed here. Shear modulus is determined from shear wave velocity (Eq. 2.3 & 2.4), and a modified form of the Seed & Idriss (1971) simplified procedures is utilized to estimate induced shear strain levels (Eq. 4.17). A modified hyperbola (Eq. 2.6) is used for modulus reduction schemes incorporated into the analysis. The critical number of cycles to induce liquefaction, $n_t$, is determined as a function of strain level and $K_o$ (Eq. 4.23). Therefore, this parameter is controlled by cone tip resistance as well as shear wave velocity for the analysis procedures used here. This section will present results from cyclic strain-based analysis on the 22 critical layers presented in the previous section. Soil layer parameters are presented in Table 6.2, and average SCPTu parameters are presented in Table 6.3.

Results of cyclic strain-based analysis will be presented on charts comparing normalized in-situ test parameters to the ratio number of earthquake cycles (n) to the number of cycles to failure ($n_t$). Since this method combines results from both shear wave velocity and cone tip resistance, the two charts are not independent of each other as they are for cyclic stress ratio analyses. Separate charts are presented for direct comparison of stress and strain methods. While this method is capable of predicting pore pressure generation and initial liquefaction, graphical representation of number of cycles compared to critical number of cycles presents similar information in a clearer manner.

At initial liquefaction, $n/n_t$ will be equal to unity just as pore pressure ratio ($r_u$; Fig. 4.9). Sites and analyzed data will be presented on figures separated into earthquake events. Figure 6.20 shows a sample cyclic strain-based analysis chart from this study, with pertinent information.

Utilizing the methods presented in Figure 6.20, a critical moment magnitude will be selected for each site and each earthquake. Critical layers are analyzed at constant source to site distance. Utilizing magnitude dependent acceleration attenuation relationships, the acceleration at the site is solely a function of earthquake magnitude at constant source to site distance. Induces strain levels, and cycles to failure ($n_t$) will be constant for each soil layer, and the equivalent number of cycles (n) will be a function of the earthquake magnitude. Therefore, the graphical representation of data in Figures 6.21 to 6.26 will be a function of earthquake magnitude and layer properties. The $n/n_t$ ratio will be zero if the induced strain levels are below the plastic threshold strain, $\gamma_t^p$. A line will be vertically increasing with magnitude for a critical soil layer of constant properties once $\gamma_t^p$ is exceeded. The critical magnitude represents the intersection of the $n/n_t$ line with the pore pressure ratio at initial liquefaction ($r_u = 1$). This critical magnitude can be associated with a factor of safety near unity that would cause borderline liquefaction. Figures 6.21 through 6.26 display the results of cyclic strain-based analyses for six different earthquakes.

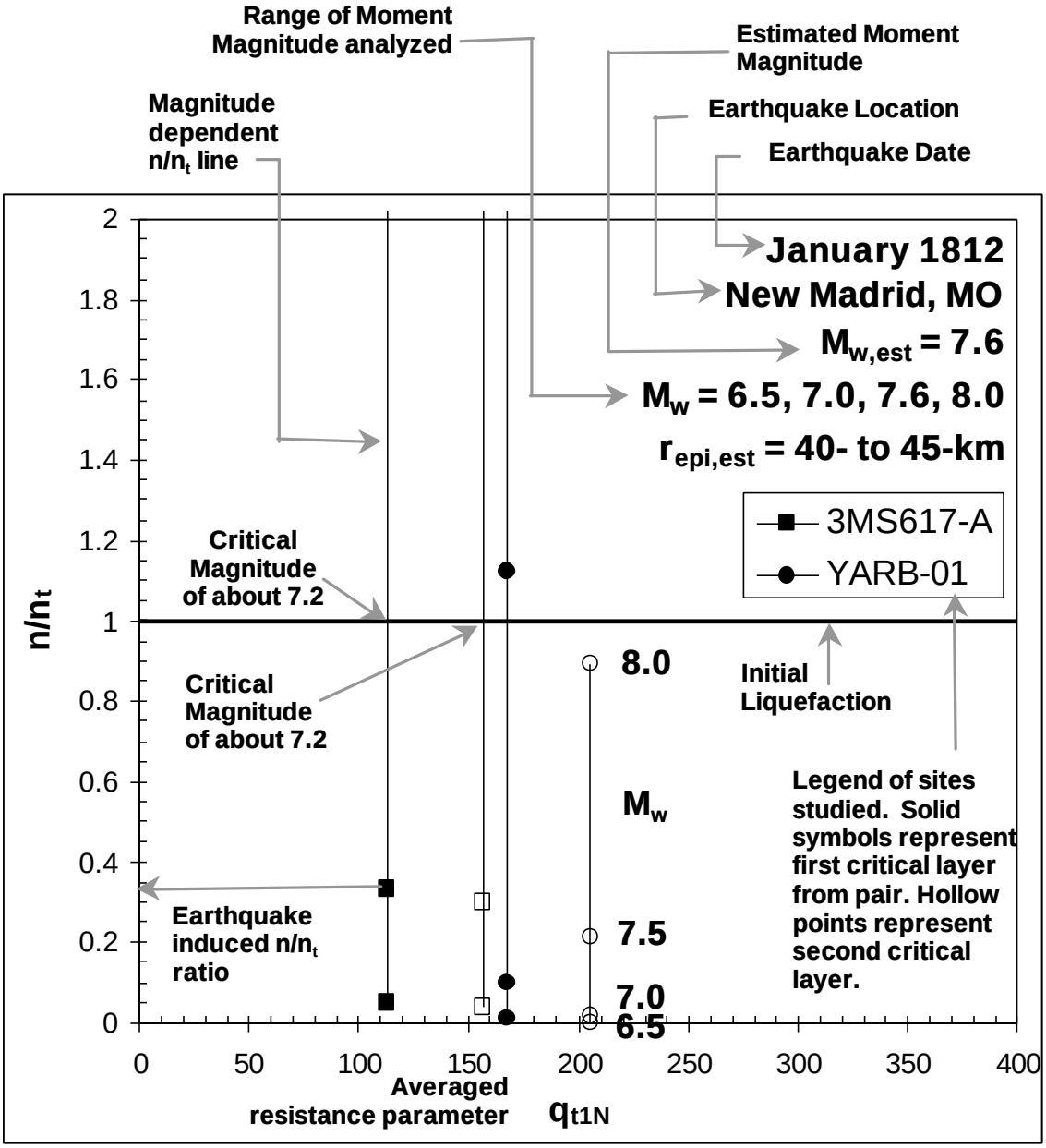


**Figure 6.20. Key Aspects of Cyclic Strain based Analysis Charts for This Study**

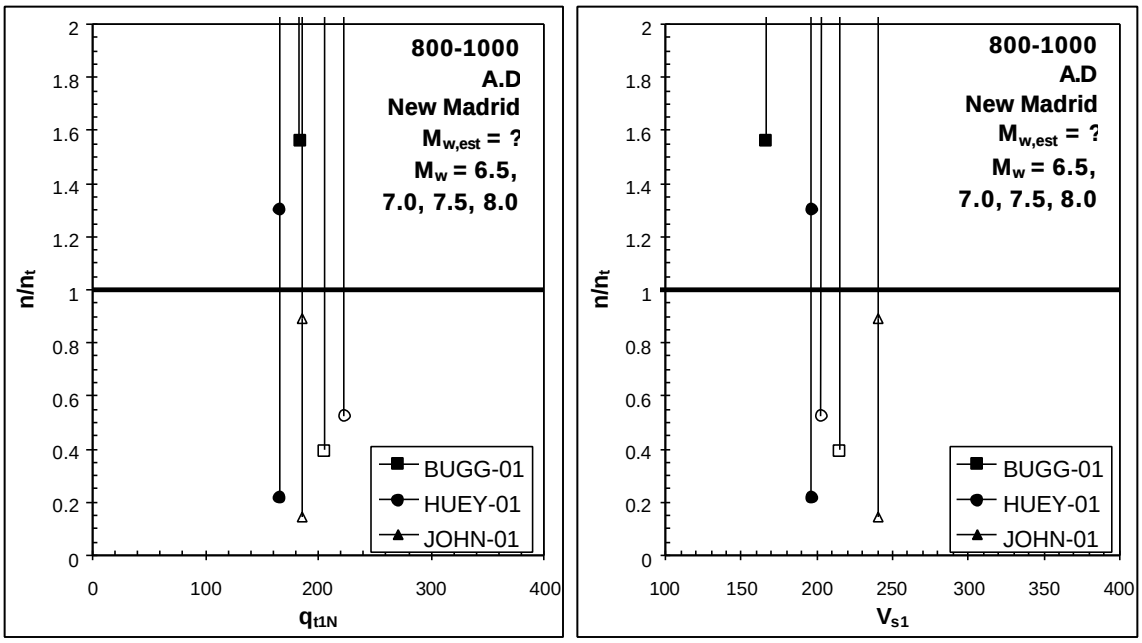


**Figure 6.21 (a) Cyclic Strain Liquefaction Plots for 800-1000 New Madrid Earthquake at $r_{epi}$ = 15km**

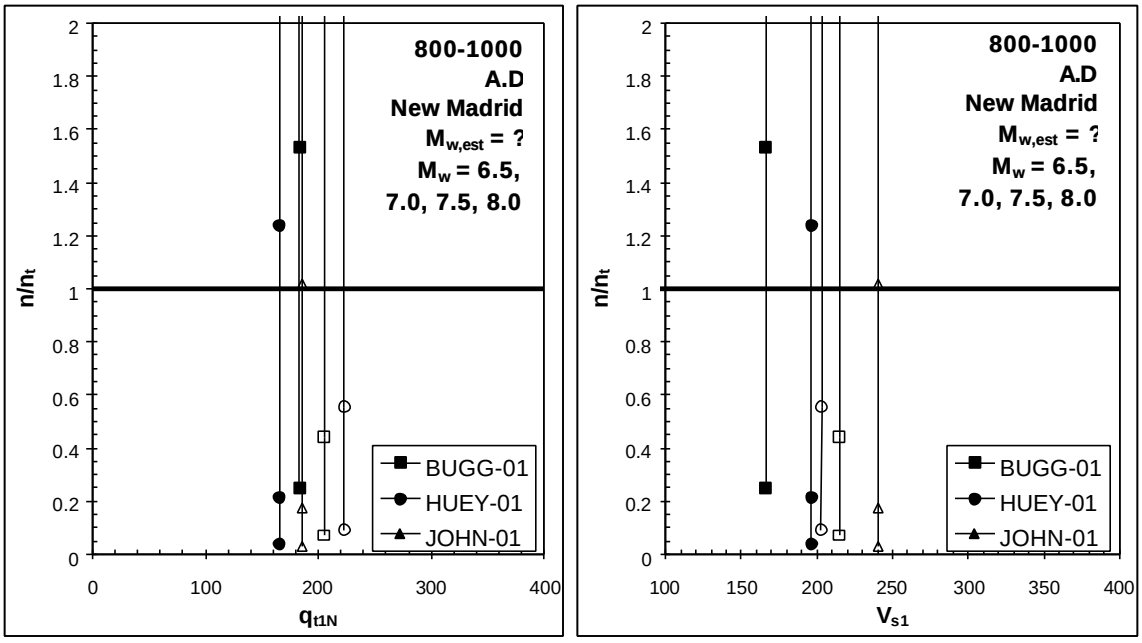


**Figure 6.21 (b) Cyclic Strain Liquefaction Plots for 800-1000 New Madrid Earthquake at $r_{epi}$ = 25 km**

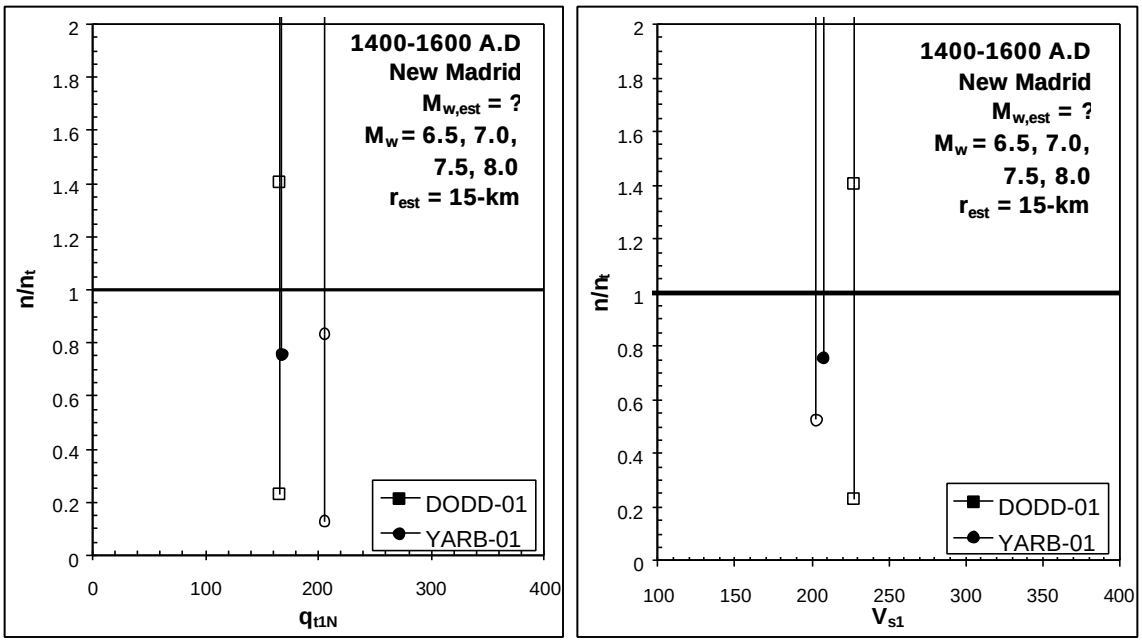


**Figure 6.22 (a) Cyclic Strain Liquefaction Plots for 1400-1600 New Madrid Earthquake at $r_{epi}$ = 15km**

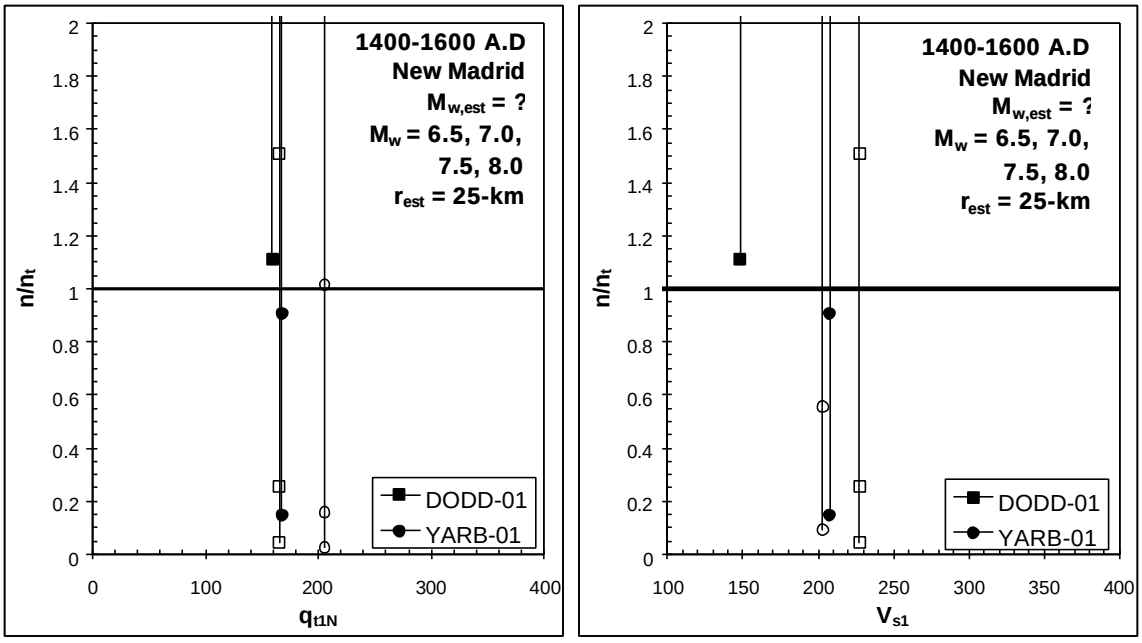


**Figure 6.22 (b) Cyclic Strain Liquefaction Plots for 1400-1600 New Madrid Earthquake at $r_{epi}$ = 25 km**

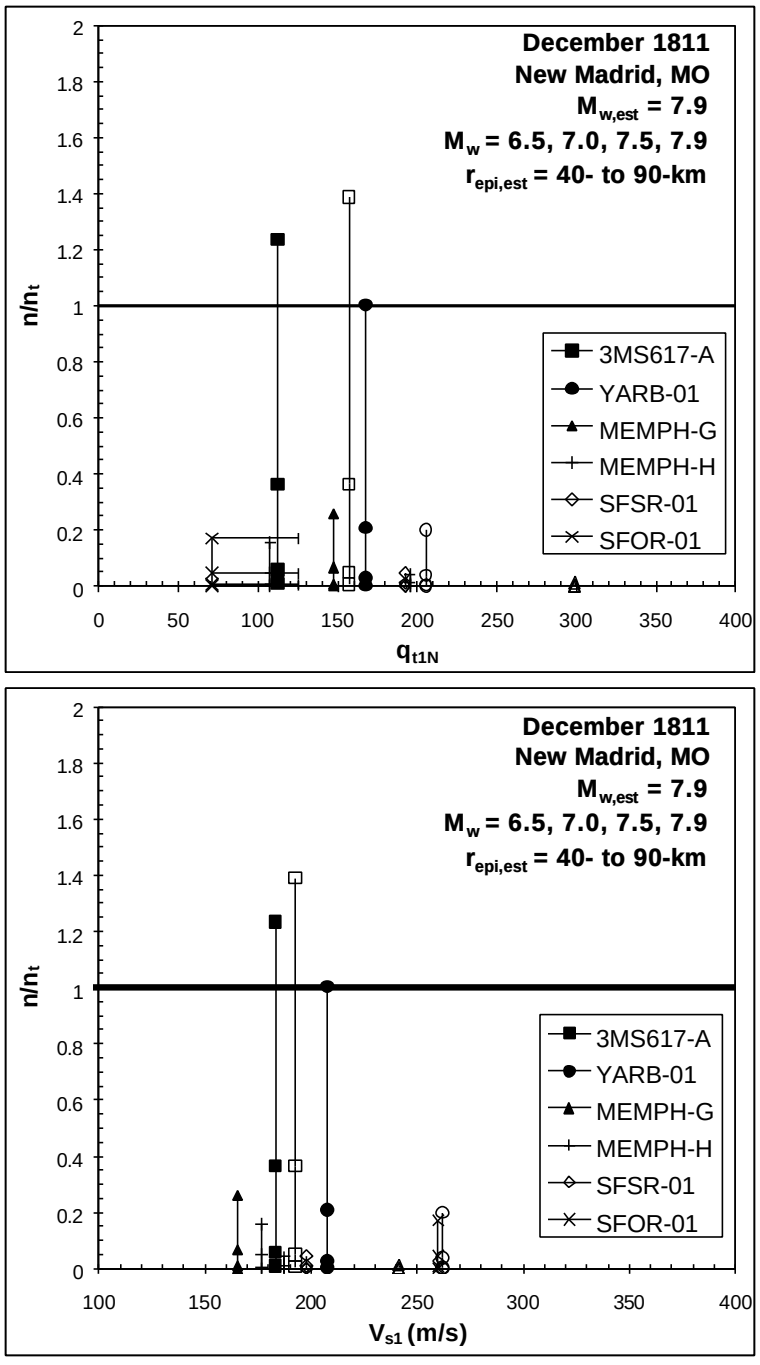


**Figure 6.23. Cyclic Strain Liquefaction Plots for December 1811 New Madrid Earthquake**

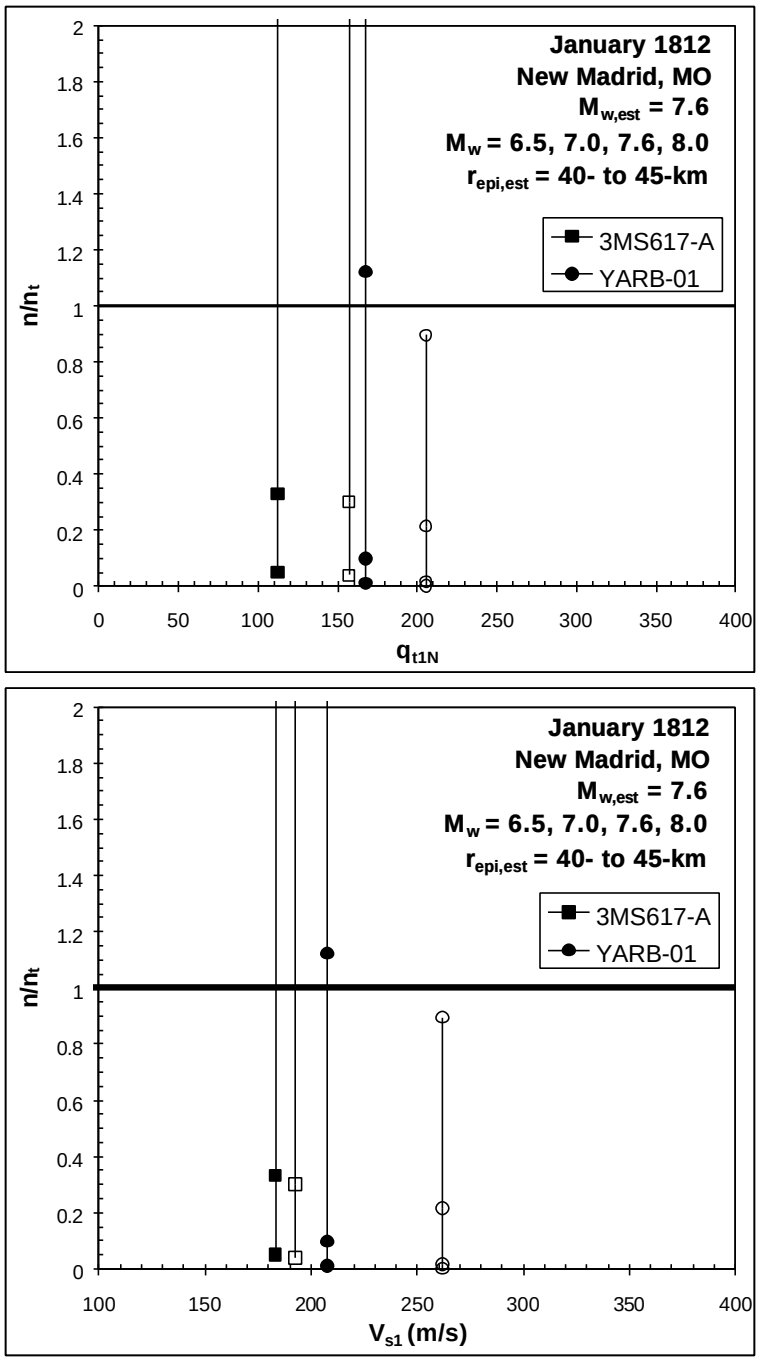


**Figure 6.24 Cyclic Strain Liquefaction Plots for January 1812 New Madrid Earthquake**

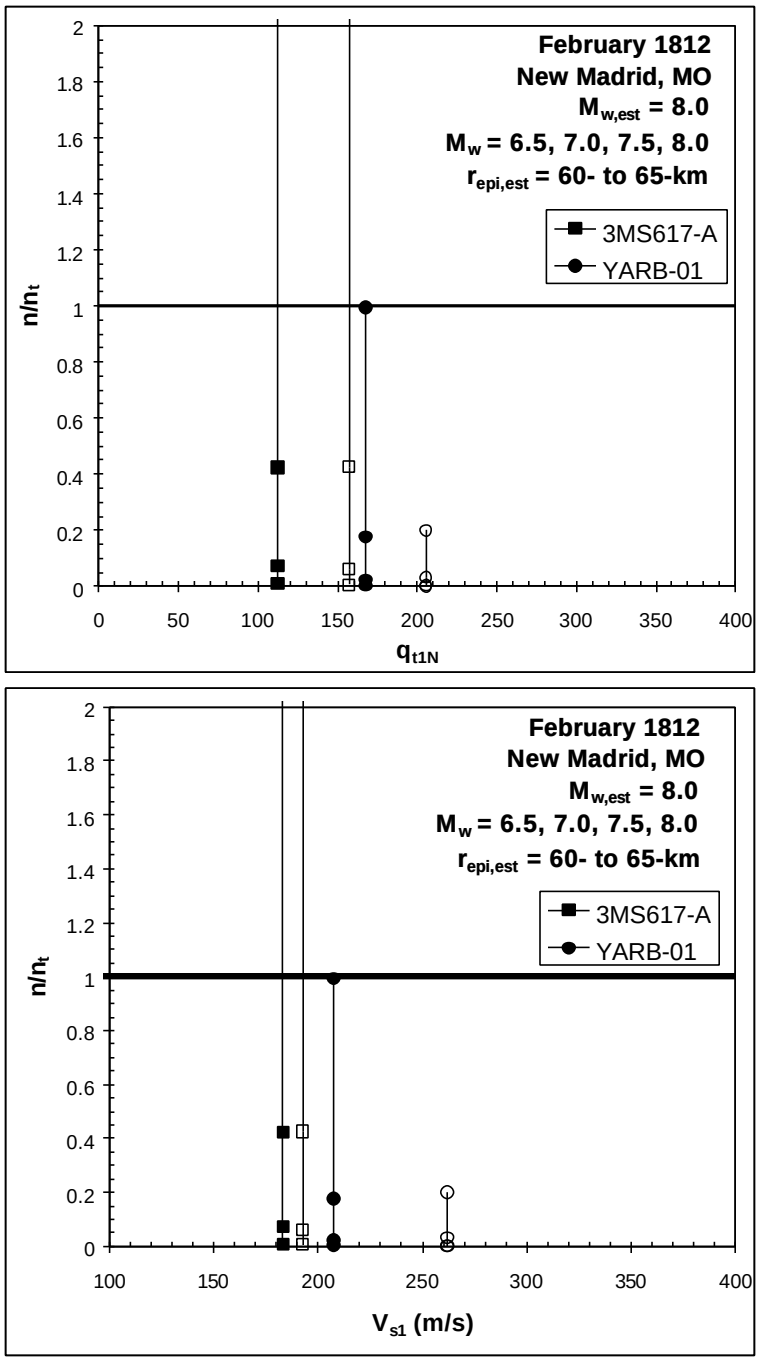


**Figure 6.25 Cyclic Strain Liquefaction Plots for February 1812 New Madrid Earthquake**

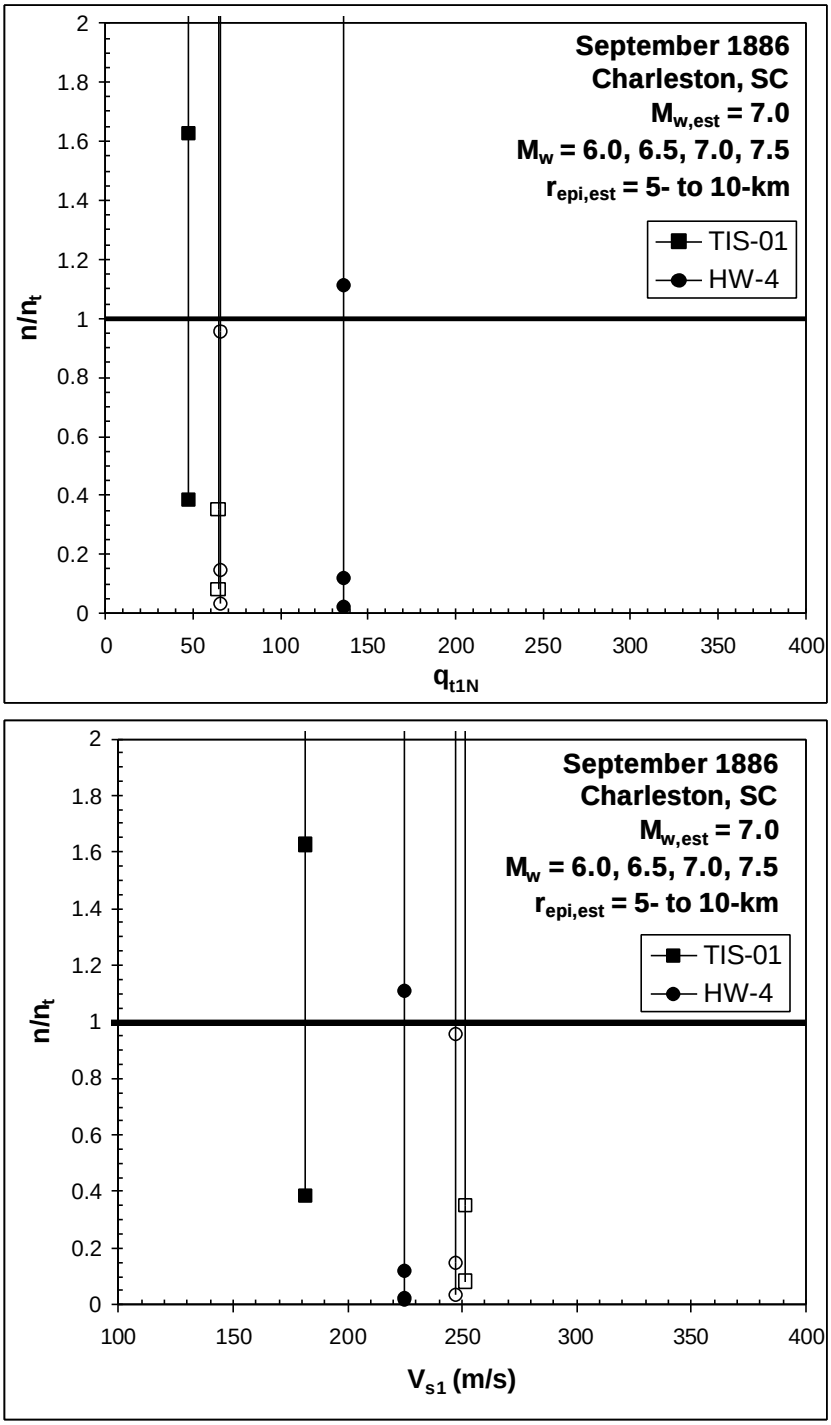


**Figure 6.26 Cyclic Strain Liquefaction Plots for September 1886 Charleston, SC Earthquake**

## 6.6 Comparison of Methods

One objective of this study was to assess the application of current liquefaction analysis methods developed for interplate earthquakes, to the anticipated motions resulting from an intraplate event in Mid-America. Four frameworks for liquefaction assessment have been applied to the field data from 6 earthquakes.

1. Cyclic stress-based method for cone tip resistance;
2. Cyclic stress-based method for shear wave velocity;
3. Arias intensity-based method for cone tip resistance;
4. Cyclic strain-based method utilizing both shear wave velocity and cone tip resistance.

Critical magnitudes determined for each scenario, as discussed in the previous three sections, are presented in Table 6.5. Table 6.6 displays the comparison of each of the analysis methods.

In general, each method compares well with each other, except the cyclic stress method based on shear wave velocity sometimes predicts higher liquefaction resistance and sometimes predicts lower resistance. Discrepancies have been shown when directly comparing the small strain property of shear wave velocity to the large strain phenomena of liquefaction (Roy et al., 1997). Even though the CRR curve for the shear wave velocity method was based on cyclic strain theory (Andrus & Stokoe, 1997), the effects of aging and cementation may significantly increase $V_s$, but are difficult to assess. The cyclic strain based procedures are strongly controlled by the stiffness determined from shear wave velocity methods. The theoretical cyclic strain framework, which

## Table 6.5. Inferred Minimum Magnitude to Cause Liquefaction

| Sounding | $r_{epi,est}$ | Critical Magnitude | | | | | | | |
|---|---|---|---|---|---|---|---|---|---|
| | | Cyclic Stress | | | | Arias Intensity | | Cyclic Strain | |
| | | $q_{c1}$ | | $V_{s1}$ | | $q_{c1}$ | | | |
| New Madrid 800 – 1000 | | | | | | | | | |
| BUGG-01a | 15 / 25 | 7.0 | 7.4 | Y | Y | 6.7 | 7.1 | Y | 6.8 |
| BUGG-01b | 15 / 25 | 7.5 | 7.7 | 7 | 7.5 | 7.0 | 7.4 | 6.6 | 7.1 |
| HUEY-01a | 15 / 25 | 6.7 | 7.2 | Y | 6.5 | 6.5 | 6.7 | 6.8 | 7.4 |
| HUEY-01b | 15 / 25 | 8.0+ | N | Y | 6.5 | 6.5 | 6.7 | 6.8 | 7.4 |
| JOHN-01a | 15 / 25 | Y | Y | Y | Y | Y | Y | Y | Y |
| JOHN-01b | 15 / 25 | 7.0 | 7.5 | N | N | 6.7 | 7.1 | 7.1 | 7.5 |
| New Madrid 1400-1600 | | | | | | | | | |
| YARD-01a | 15 / 25 | 6.5 | 7.0 | Y | 6.5 | 6.6 | 7.0 | 6.6 | 7.1 |
| YARB-01b | 15 / 25 | 7.5 | 7.8 | Y | 6.6 | 7 | 7.4 | 7.1 | 7.5 |
| DODD-01a | 15 / 25 | 6.5 | 7.0 | Y | Y | 6.6 | 6.9 | Y | 6.5 |
| DODD-01b | 15 / 25 | 6.5 | 7.0 | N | N | 6.7 | 7.0 | 6.8 | 7.3 |
| New Madrid December 1811; $M_{w,est}$ = 7.9 | | | | | | | | | |
| MEMPH-G1 | 75 | N | | 7.5 | | 7.7 | | $r_u$ = 0.2 @ 7.9 | |
| MEMPH-G2 | 75 | N | | N | | N | | N | |
| SFSR-01 | 70 | N | | 7.6 | | 7.9+ | | $r_u$ = 0.04 @ 7.9 | |
| MEMPH-H1 | 90 | N | | 7.6 | | 7.7 | | $r_u$ = 0.04 @ 7.9 | |
| MEMPH-H2 | 90 | N | | 7.9 | | N | | $r_u$ = 0.1 @ 7.9 | |
| SFOR-01 | 40 | 7.5 | | N | | 7.1 | | $r_u$ = 0.12 @ 7.9 | |
| YARB-01a | 60 | 8.0+ | | 7.6 | | 7.7 | | $r_u$ = 1.0 @ 7.9 | |
| YARB-01b | 60 | N | | N | | N | | $r_u$ = 0.14 @ 7.9 | |
| 3MS617-A1 | 65 | 7.5 | | 7.1 | | 7.5 | | $r_u$ = 1.0 @ 7.9 | |
| 3MS617-A2 | 65 | N | | 7.4 | | 7.7 | | $r_u$ = 1.0 @ 7.9 | |
| New Madrid January 1812; $M_{w,est}$ = 7.6 | | | | | | | | | |
| YARB-01a | 45 | 7.6 | | 7.0 | | 7.4 | | 7.6 | |
| YARB-01b | 45 | N | | N | | 7.8 | | $r_u$ = 0.6 @ 8.0 | |
| 3MS617-A1 | 40 | 6.8 | | 6.6 | | 7.1 | | 7.2 | |
| 3MS617-A2 | 40 | 7.6 | | 6.8 | | 7.3 | | 7.2 | |
| New Madrid February 1812, $M_{w,est}$ = 8.0 | | | | | | | | | |
| YARB-01a | 65 | N | | 7.7 | | 7.7 | | $r_u$ = 1.0 @ 8.0 | |
| YARB-01b | 65 | N | | N | | N | | $r_u$ = 0.1 @ 8.0 | |
| 3MS617-A1 | 60 | 7.4 | | 7.1 | | 7.4 | | 7.6 | |
| 3MS617-A2 | 60 | 8.0 | | 7.3 | | 7.6 | | 7.6 | |
| Charleston, SC September 1886, $M_{w,est}$ = 7.0 | | | | | | | | | |
| HW-4a | 10 | Y | | N | | 6.2 | | 6.9 | |
| HW-4b | 10 | Y | | N | | Y | | 7.1 | |
| TIS-01a | 5 | Y | | Y | | Y | | 6.2 | |
| TIS-01b | 5 | Y | | N | | Y | | 6.7 | |

Y - critical $M_w$ < 6.0; N - Critical $M_w$ > 8.0

**Table 6.6. Comparison of Simplified Liquefaction Analysis Methods**

| | $q_{c1N}$, CSR | $V_{s1}$, CSR | $q_{c1N}$, Arias | Cyclic Strain |
|---|---|---|---|---|
| **$q_{c1N}$, CSR** | | the $q_c$ method typically predicted higher $M_w$ than the $V_s$ method | agreed well throughout | The methods agreed fairly well, except in Charleston, SC |
| **$V_{s1}$, CSR** | | | the $q_c$ method typically predicted higher $M_w$ than the $V_s$ method | The cyclic strain method predicted a high $M_w$, except in Charleston, SC |
| **$q_{c1N}$, Arias** | | | | agreed well throughout |
| **Cyclic Strain** | | | | |

incorporates modulus reduction with increasing shear strain, appears to account for $V_s$-liquefaction strain level incompatibility.

Considering the analysis methods used input ground motions of a similar original (e.g. Attenuation relationships based on Herrmann & Akinci, 1999 Modified USGS M3 model), the relative critical magnitudes to induce liquefaction should be similar. Ground motion differences may result from magnitude scaling factors and Arias Intensity attenuation relationships. Figure 6.25 compares lower bound critical magnitudes necessary for liquefaction to previous estimations of magnitude in the New Madrid

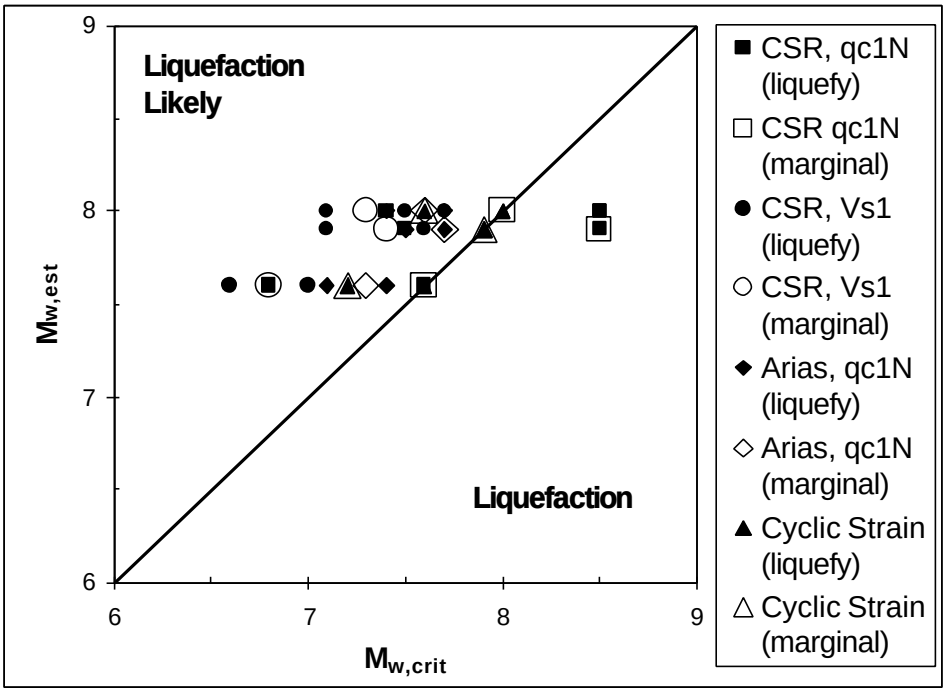


[1] Marginal liquefaction represents denser critical layers from liquefaction sites

**Figure 6.25. Comparison of Lower Bound Magnitude Required for Liquefaction to Previous Estimations of Moment Magnitude (NMSZ)**

seismic zone. Data are presented from critical layers at sites that showed surface evidence of liquefaction. The solid symbols represent the loose critical layers with a high liquefaction potential, while the open symbols represent the denser critical layers with a lower liquefaction potential. Since extensive liquefaction was observed within the NMSZ, it is expected that the earthquake magnitude would be higher than the lower bound critical magnitude. From the data in this figure, marginal, denser layers, appear to be susceptible to liquefaction as well. If it is considered that the loose layer was formed by porewater migrating from the dense layer and becoming trapped under a silty clay cap, it would be expected that the dense layer liquefied during the earthquake event. Considering the uncertainty associated with ground motion parameters used in this study, current liquefaction assessment methods appear to be appropriate for analysis in Mid-America.

# CHAPTER 7

# CONCLUSIONS AND FUTURE WORK

## 7.1. Conclusions

In-situ geotechnical site characterization by the seismic piezocone provides a number of parameters that can be used for liquefaction assessment and site response analysis.

- The frequency of readings (at least every 50 mm) and the four independent measurements ($q_t$, $f_s$, $u_2$, and $V_s$) recorded in a SCPTu sounding provide excellent stratigraphic profiling capabilities necessary to identify "loose" clean sands and silty sands below the groundwater table which are potentially susceptible to liquefaction. Penetration porewater pressure measurements at the $u_2$ position provide a reading of near hydrostatic water pressures in clean sands that can be used to identify the water table depth, which is a necessary facet of any liquefaction investigation.
- Direct liquefaction analysis can be performed using cyclic stress based procedures for normalized cone tip resistance and normalized shear wave velocity. Arias intensity methods, which are independent of the uncertainty associated with arbitrary magnitude scaling factors, are also available for normalized cone tip resistance. These methods generally appeared to accurately assess liquefaction hazards at Mid-America, considering the uncertainty in ground motion parameters. Some inconsistencies were noticed using shear wave velocity methods, which may result

from strain incompatible between shear wave velocity measurements (small-strain) and liquefaction behavior (large strain).

- Rational liquefaction analysis can be performed using cyclic strain based procedures. Small strain stiffness is directly determined from the seismic cone, and in-situ state of the soil can be evaluated from CPT tip resistance. Using empirical- or laboratory-determined shear modulus reduction schemes bridge the gap between small- and large-strain behavior.

While there is redundancy in analysis, there is still little confidence in what can be concluded from these studies. Uncertainty is inherent in the analysis since procedures were developed primarily for interplate earthquakes from China, Japan, and California, and have not been calibrated for large intraplate events in Mid-America. Additional uncertainty exists from the selection of ground motion parameters in Mid-America. A model based on the depth and stiffness of the soil column was used to generate ground motion parameters for this study, but this model does not incorporate the nonlinear soil properties that will affect ground motions for a large event. Potential for amplification or damping of motions by the deep soil column will control critical ground parameters used for analysis. Attenuation of ground motions between epicentral distances of about 5- to 70-km is significant. Therefore accurate evaluation of the source-to-site distance is paramount in liquefaction studies.

It can be inferred from the layering and consistency characteristics of soil deposits at liquefaction sites in the New Madrid seismic zone that liquefaction resulted in loose sands near the surface from excess porewater pressures becoming trapped below low

permeability clay or silt layers. While analyses from this study evaluated two separate layers per sounding, it is likely that liquefaction occurred throughout the depth of the deposit. This would result in the observed profile of a low permeability silty clay cap, over loose shallow sands, over densified deeper sands.

## 7.2 Future Work

The data available from the seismic piezocone penetration test provide the stiffness parameters necessary to perform a site-specific response analysis of ground motions, such as SHAKE (Fig. 7.1). This would eliminate the empirical $r_d$ and $r_b$ stress reduction coefficients used in the simplified procedures. Strain levels for use in cyclic strain based methods can also be generated from a site-specific analysis. Assessment of analysis methods presented in this study utilizing equivalent linear and nonlinear models may additional provide insight into the liquefaction behavior of deposits profiled in this study.

Questions often arise as to the applicability of using post earthquake field performance data to estimate pre-earthquake sand-state. There is likely significant disturbance, whether it is densification of a loose layer through subsidence or loosening of a dense layer from pore pressure migration into that layer. Pre- and post-earthquake studies have been performed at liquefaction sites (e.g., Frost et al., 1993; Chameau et al., 1998) to evaluate potential earthquake effects on deposits. Additional studies in Mid-America may provide additional insight into the effects of liquefaction induced densification on penetration resistance and soil stiffness, especially at sites where re-

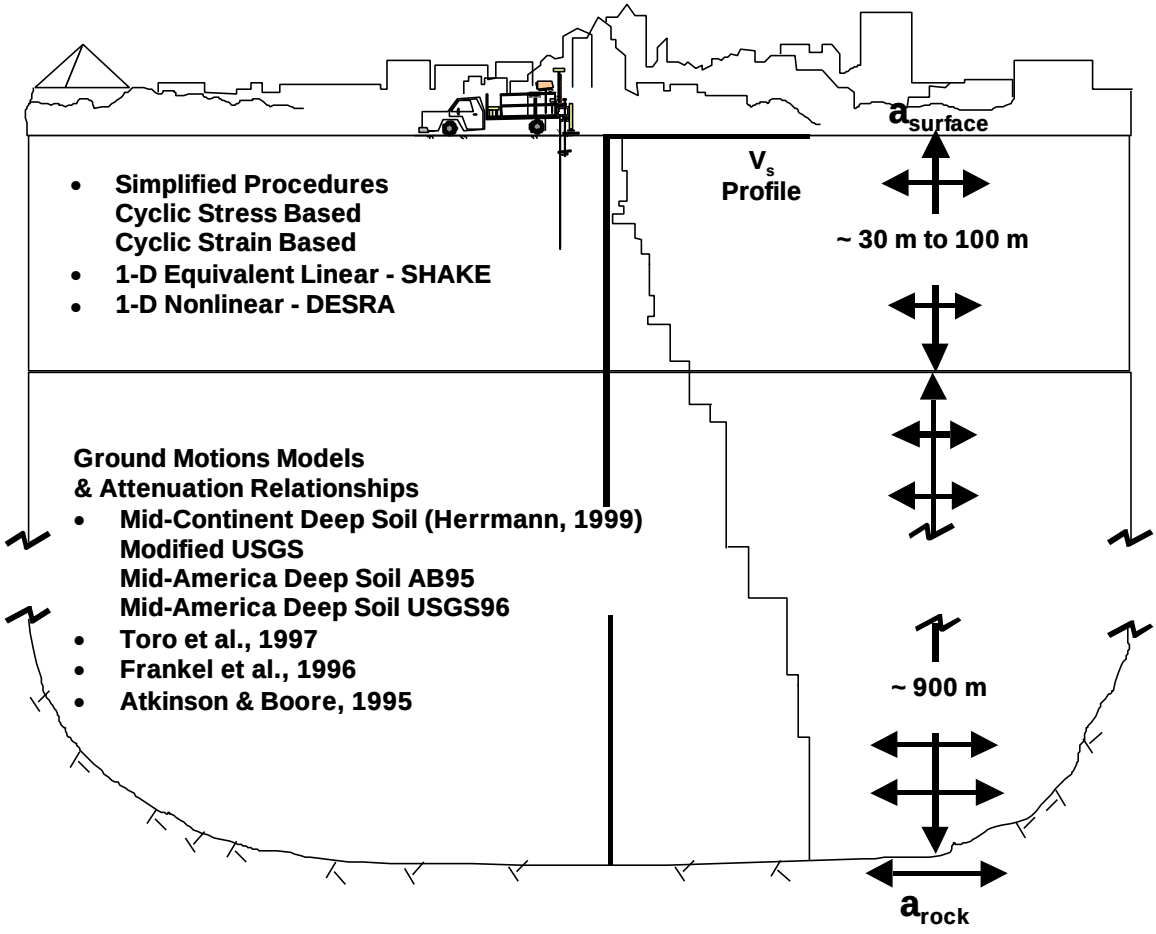


**Figure 7.1. Ground Motions and Seismic Analysis in Mid-America**

liquefaction is evident (e.g. sand dikes venting through existing liquefaction induced sand dikes).

From laboratory and field investigations it appears that sands from selected sites from Mid-America are relatively clean (FC < 5 %). It is desirable to verify these predictions using conventional drilling and sampling techniques. Additionally, laboratory testing of strength, stiffness, and critical state properties of sands throughout Mid-America could be used to supplement the data collected in this study. Cyclic laboratory testing on disturbed as well as frozen specimens would supplement the database of Japanese sites used to generate the limiting value of CPT tip resistance for cyclic resistance curves used in this study.

Difficulties arise when deciding upon the input ground motions for site specific analysis, since no strong ground motion data is available for the Mid-America region. Depth of analysis is another concern for site response studies in the 600- to 1000-m deep soils of the Mississippi River Valley and Atlantic Coastal Plain. It is preferable to use actual time histories rather than synthetic ground motions based on stochastic white noise (Youd, 1997), but actual ground motions are not available for intraplate earthquakes in Mid-America. Continued ground motion studies in Mid-America are of great importance for earthquake engineering.

Since the uncertainty associated with ground motions in the Mid-America region greatly effects the outcome of liquefaction analyses, a direct assessment of liquefaction resistance of a deposit is desirable. The initial development of a vibrocone penetrometer (VCPT) is ongoing through a joint project at Georgia Tech and Virginia Tech (Schneider

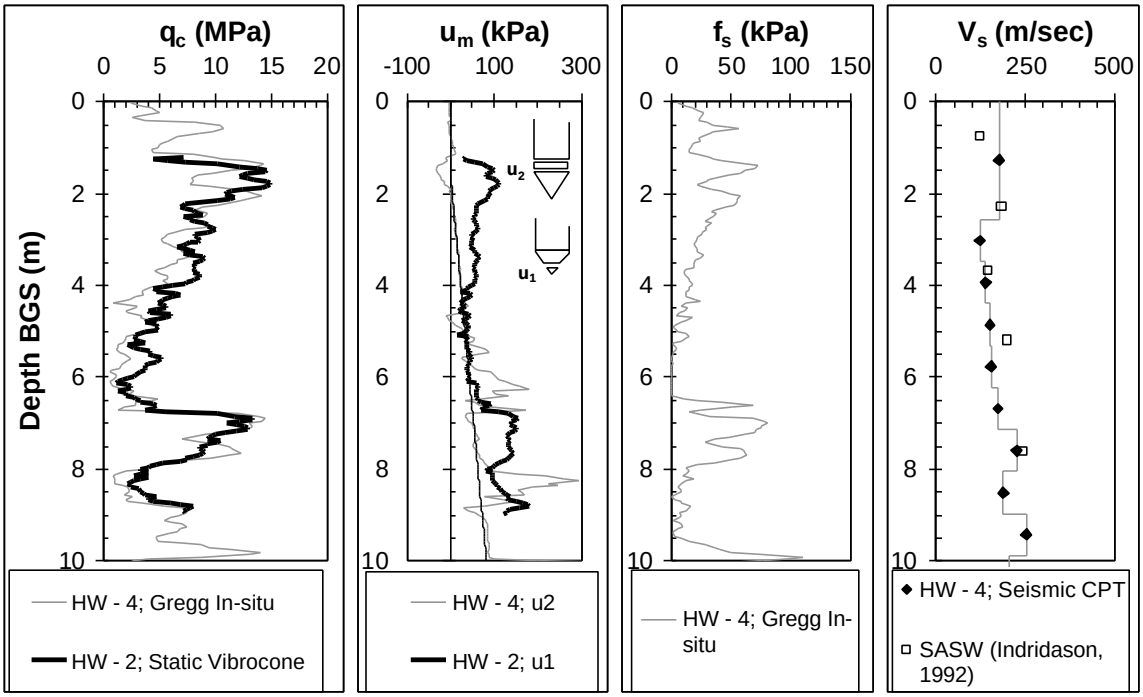


**Figure 7.2. Static piezovibrocone and seismic piezocone soundings at Hollywood Ditch, Charleston, SC**

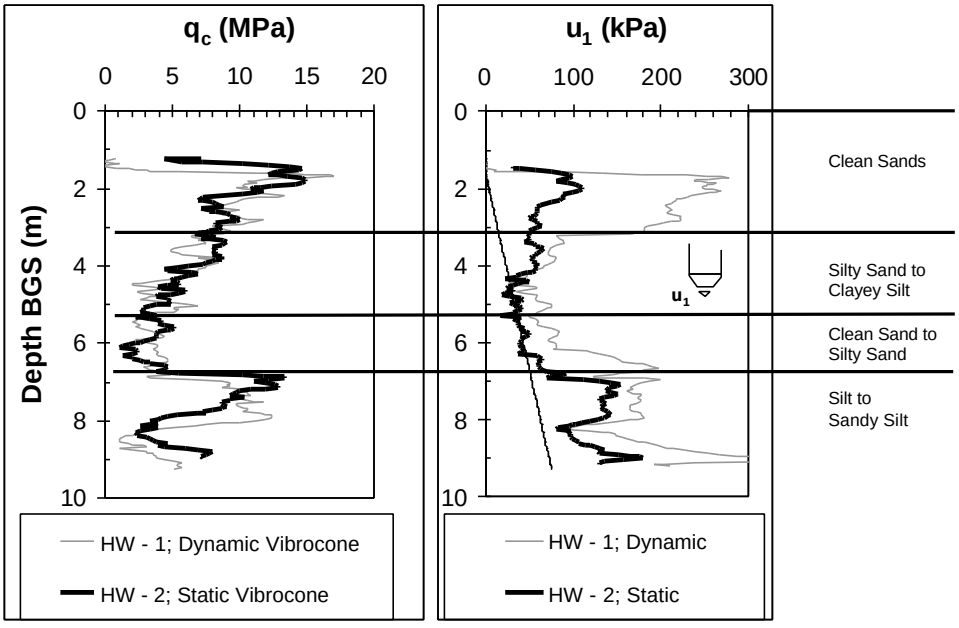


**Figure 7.3. Comparison of static and dynamic piezovibrocone soundings at Hollywood Ditch, Charleston, SC**

et al., 1998). Initial trial field studies have been performed in Charleston, SC and calibration chamber testing is ongoing at Virginia Tech. Preliminary results look promising, with additional porewater pressures generated from vibratory penetration (Fig. 7.2; 7.3). Additional vibrocone testing at liquefaction sites in Mid-America will aid in the understanding of the liquefaction response of soil in Mid-America.

# APPENDIX I.

# SOIL PROPERTIES

## I.1 Overview

An introduction to engineering soil classification, effective stress-state in soils, and engineering definitions of soil properties is presented in a framework related to geotechnical earthquake engineering. Earthquake induced liquefaction is generally associated with contractive granular soils, while site amplification effects are typically seen in soft, high plasticity, clay deposits. From simplified liquefaction resistance charts (i.e. Stark & Olson, 1995), the input parameter of fines content or mean grain diameter is needed. Initial cyclic stress based methods were based on the belief that liquefaction is a function of relative density (Seed & Lee, 1966). Cyclic strain based methods show the initial build up of pore pressures is a function of small-strain shear modulus, $G_{max}$, as well as modulus reduction, $G/G_{max}$. Threshold shear strains and modulus reduction appear to be a function of plasticity, as well as other factors (Vucetic & Dobry, 1991). For the cyclic strain method, the shape of pore pressure generation curves is expected to be a function of current stress state as well as past effective stresses, i.e., $\sigma_{vo}'$, $K_o$, and OCR (Vasquez-Herrera, et al., 1988). Definitions of these properties will be presented in the following sections.

## I.2 Soil Characterization and Basic Properties

An engineering definition of soil type will be required for geotechnical earthquake analyses. The most common methods have been visual and manual classification, simple index tests, and incorporation into the unified soil classification system (USCS). Figure I.1 displays typical laboratory classification procedures and classification schemes. The most common way to display the results of laboratory classification is through a grain size distribution (GSD) curve. Figure I.2 displays the GSD for sand from a liquefaction site in Blytheville, AR, as well as a silty sand - sandy silt from the Piedmont Province in Georgia. From this curve typical gradation properties can be determined, and then used for soil classification.

Sieve analyses are performed following the general procedures outlined in ASTM D422, and GSD curves can be assessed by evaluating:

- Median grain size, $D_{50}$ - where D is particle diameter in millimeters and the subscripted number represents the percentage of particles finer by weight. For this case $D_{50}$ refers to the particle size in millimeters relating to 50 percent finer by weight;
- Effective grain size, $D_{10}$ - the particle size in millimeters relating to 10 percent finer by weight.
- Coefficient of uniformity, $C_u = D_{60}/D_{10}$;
- Coefficient of curvature, $C_c = D_{30}^2 / (D_{10} \cdot D_{60})$.

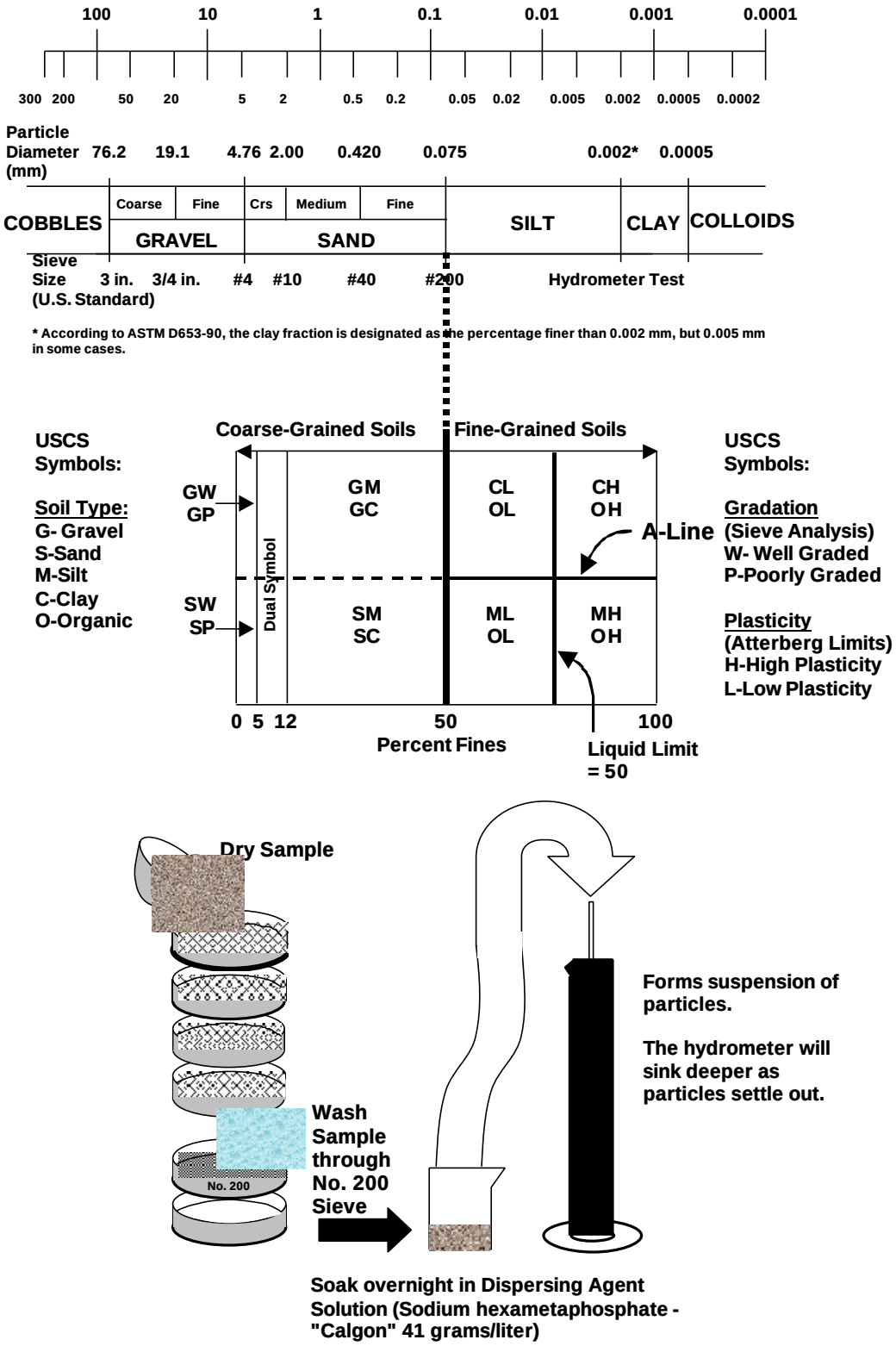


**Figure I.1. Laboratory Soil Classification Methods**

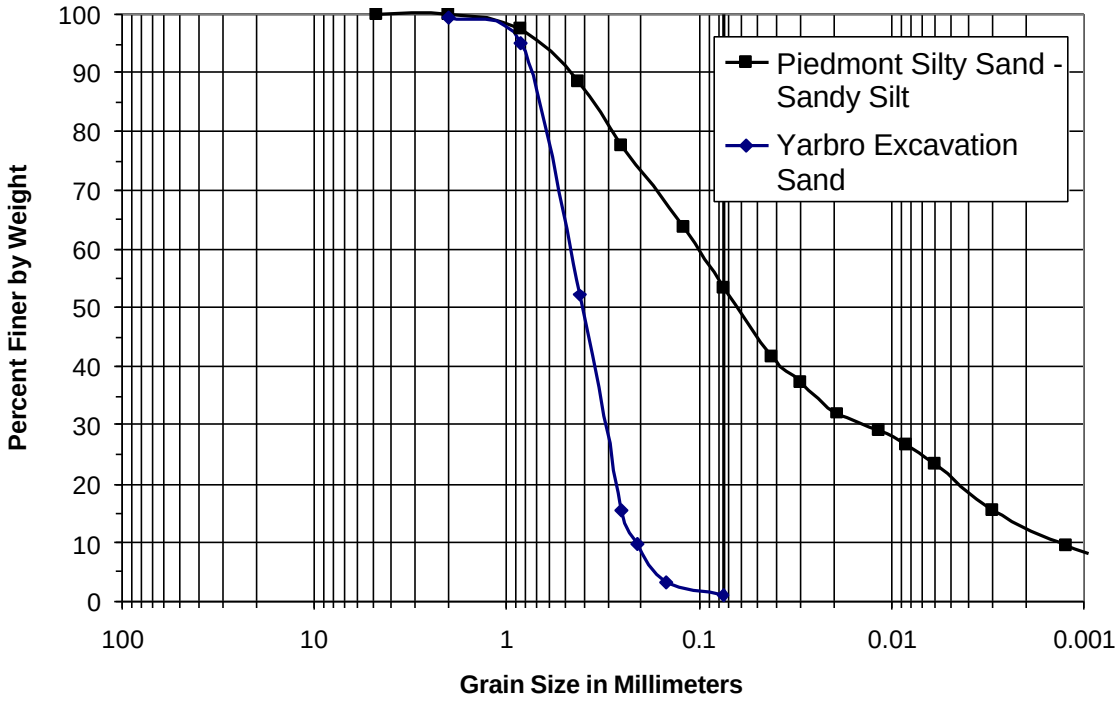


**Figure I.2. Grain Size Distribution Curves for two Sandy Soils**

**Table I.1. Grain Properties of Sandy Soils from Figure I.2**

| Soil | $D_{50}$ | $D_{10}$ | $C_u$ | $C_c$ | Percent Fines | USCS Symbol |
|---|---|---|---|---|---|---|
| Piedmont | 0.065 | 0.0013 | 76.9 | 1.73 | 54 | SM-ML |
| Yarbro | 0.41 | 0.21 | 2.3 | 0.95 | 1 | SP |

The separation between coarse grained soils and fine grained soils will be 0.075 millimeters, which is related to a number 200 sieve. The separation between silt and clay is 0.002 millimeters, and can be estimated from hydrometer analysis (ASTM D-422). For example, the representative grain properties and associated USCS symbol for the sandy soils in Figure I.2 are presented in Table I.1.

For engineering purposes, the particle size of fine grained soils will not as important as plasticity characteristics when estimating the soils response to loading. Therefore the simple index tests of Liquid Limit, LL, and Plastic Limit, PL, were adapted for classification purposes. These tests are described in ASTM D4318 as well as BS 1377.

## 1.3 Consistency of Granular Materials

To assess the consistency of granular soil the property of relative density is typically used. The relative density is a function of void ratio (e), which is defined as:

$$e = \frac{V_v}{V_s} \tag{I.1}$$

where $V_v$ is the volume of voids (fluids) in the soil matrix, and $V_s$ is the volume of solids in the soil matrix. It is considered that void ratio may be maximized in a very loose structure ($e_{max}$) and minimized for a very dense structure ($e_{min}$). These maximum and minimum values are quite variable, but can be estimated using laboratory testing procedures (ASTM D4253; ASTM D4254). The relative density of a soil is then defined as a function of maximum and minimum density, as well as current void ratio:

$$D_r = \frac{e_{\max} - e}{e_{\max} - e_{\min}} \tag{I.2}$$

To estimate the consistency of an in-situ soil deposit, relative density is often used. If maximum and minimum void ratios are known, $D_r$ may be determined by estimates of in-situ void ratio. Table I.2 presents correlations between CPT tip resistance and relative density. Table I.3 presents correlations between SCPTu measurements and in-situ void ratio.

**Table I.2. Correlations between In-Situ $D_r$ to CPT Measurements**

| Relationship | Notes | Reference |
|---|---|---|
| $68\left[\log\left(\frac{q_c}{\sqrt{p_a \cdot s_{vo}'}}\right)-1\right]$ | • $p_a$ is atmospheric pressure<br>• $q_c$ and $\sigma_{vo}'$ are in the same units<br>• based on boundary condition uncorrected calibration chamber data<br>• mainly unaged clean quartz sands<br>• to utilize field data, divide field determined $q_c$ by $K_q$, where: $K_q = 1 + (D_r - 30) / 300$ | Jamiolkowski et al., 1985b |
| $100 \cdot \left[\frac{q_{c1}}{305 \cdot OCR^{0.2}}\right]^{0.5}$ | • $q_{c1} = q_c/(\sigma_{vo}')^{0.5}$, where $q_c$ and $\sigma_{vo}'$ are in the same units<br>• based on boundary condition corrected calibration chamber data<br>• n = 544<br>• unaged sands<br>• to account for aging, divide $q_{c1}$ by $C_A$, where: $C_A = 1.2 + 0.05 \cdot \log\left(\frac{t}{100}\right)$ | Mayne & Kulhawy, 1991<br><br>Kulhawy & Mayne, 1990 |

**Table I.3. Correlations between In-Situ Void Ratio and SCPTu Measurements**

| Relationship | Notes | Reference |
|---|---|---|
| $1.159-0.230 \cdot \log(q_{c1})$ | • $q_{c1} = q_c/(\sigma_{vo}')^{0.5}$, where $q_c$ and $\sigma_{vo}'$ are in the same units<br>• based on calibration chamber test data<br>• applicable to normally consolidated unaged, clean, quartz sands<br>• n = 494; $r^2 = 0.668$ | Mayne, 1995 |
| $1.232-0.245\log(q_{c1})$ | • $q_{c1} = q_c/(\sigma_{vo}')^{0.5}$, where $q_c$ and $\sigma_{vo}'$ are in the same units<br>• based on calibration chamber test data<br>• applicable to overconsolidated (OC) consolidated unaged, clean, quartz sands<br>• n = 149; $r^2 = 0.820$ | Mayne, 1995 |
| $1.152-0.233 \cdot \log(q_{c1}) + 0.043 \cdot \log(OCR)$ | • $q_{c1} = q_c/(\sigma_{vo}')^{0.5}$, where $q_c$ and $\sigma_{vo}'$ are in the same units<br>• based on calibration chamber test data<br>• applicable to unaged, clean, quartz sands<br>• n = 643; $r^2 = 0.691$ | Mayne, 1995 |
| $\frac{381 - V_{S1}}{259}$ | • $V_{s1} = V_s/(\sigma_{vo}')^{0.25}$, where $\sigma_{vo}'$ is in atmospheric units and $V_s$ is in m/s<br>• based on laboratory tests on Ottawa sand | Robertson et al., 1995 |
| $\frac{311 - V_{S1}}{188}$ | • $V_{s1} = V_s/(\sigma_{vo}')^{0.25}$, where $\sigma_{vo}'$ is in atmospheric units and $V_s$ is in m/s<br>• tests on Syncrude sand | Cunning et al., 1995 |

## I.4 Effective Stress State in Soils

Saturated soil response to shearing will be controlled by mechanics of the soil structure as well as stress-state from induced water pressures. The particulate matrix of a

soil will increase in strength with increased confining stress. As depth increases so will the vertical confining stress:

$$s_{vo} = \int g_t \cdot dz \qquad \text{(I.3)}$$

where $s_{vo}$ is the total vertical stress in the soil, $z$ is depth, and $g_t$ is the total unit weight equal to $r_t \cdot g$, where $r_t$ is the total mass density and $g$ is the acceleration due to gravity. Hydrostatic water pressure, $u_o$, will increase with depth below the water table as:

$$u_o = h_w g_w \qquad \text{(I.4)}$$

where $h_w$ is the depth below the water table and $g_w$ is the unit weight of water. The total stress will act to confine the element, and the water pressure will act oppositely in all directions. The pore water pressure during undrained failure will be composed of the hydrostatic pore water pressure as well as shear-induced water pressures, $\Delta u_{shear}$. If the rate of shear is slow enough to allow drainage, $\Delta u_{shear}$ will equal zero. During loading or the process of in-situ testing, octahedral pore pressures, $\Delta u_{oct}$, may be induced. The total composite pore pressure, u, may be expressed as:

$$u = u_o + Du_{shear} + Du_{oct} \qquad \text{(I.5)}$$

The strength of the soil will controlled by the effective stress, $s'_{vo}$:

$$s'_{vo} = s_{vo} - u \qquad \text{(I.6)}$$

The horizontal stress will also be effected by the hydrostatic pore water pressure as:

$$s'_{ho} = s_{ho} - u \qquad \text{(I.7)}$$

The ratio of horizontal to vertical effective stress is known as the coefficient of lateral stress at rest, $K_o$:

$$K_o = \frac{s'_{ho}}{s'_{vo}} \qquad \text{(I.8)}$$

The coefficient of earth pressure at rest, $K_o$, can also be estimated by the relationship presented by Mayne & Kulhawy (1982):

$$K_o = (1-\sin f')OCR^{\sin f'} \qquad \text{(I.9)}$$

where OCR is the overconsolidation ratio and ϕ' is the effective stress friction angle. Each of these properties will be discussed below.

**Table I.4. Correlations between SCPTu parameters and In-Situ Stress State**

| Property | Relationship | Notes | Reference |
|---|---|---|---|
| $\sigma_{ho}'$ | $q_c^{1.6} \cdot 10^{(1.144-0.0186 \cdot Dr)}$ | • $\sigma_{ho}'$ is in kPa, $q_c$ is in MPa, and $D_r$ is in percent<br>• based on calibration chamber test data<br>• applicable to unaged, clean, quartz sands<br>• $\sigma_{ho}' = K_o \cdot \sigma_{vo}'$ | Mayne, 1991 |
| Stress History, OCR, & Stress State, $K_o$ | $K_o = 0.192\left(\frac{q_c}{p_a}\right)^{0.22}\left(\frac{s_{vo}'}{p_a}\right)^{-0.31} OCR^{0.27}$<br><br>$K_o = (1-\sin\phi')OCR^{\sin\phi'}$ | • $p_a$ is atmospheric pressure<br>• based on boundary condition corrected calibration chamber data<br>• estimate friction angle from above procedures, and iterate to solve to equations simultaneously | Mayne, 1995<br><br>Mayne & Kulhawy, 1982 |

Throughout a soil deposits formation and geologic history, it will undergo different stress conditions. Increased effective stresses or apparent effective stresses on an element of soil can result from groundwater fluctuation, aging, cementation, mechanical pre-stressing, as well as desiccation. The preconsolidation stress, $p'_c$ is defined as the maximum past stress the soil element has experienced throughout its history and is commonly represented by the overconsolidation ratio, OCR:

$$OCR = \frac{p'_c}{s'_{vo}} \tag{I.10}$$

From the concepts of critical state soil mechanics (CSSM), an overconsolidated soil (OCR > 1) generally deforms elastically within the yield locus ($\sigma' < p'_c$), while a normally consolidated soil (OCR = 1) acts elasto-plastically with an expanding yield surface (Wood, 1990). Table I.4 display correlations between SCPTu parameters and the in-situ stress state of sands. To utilize the Ko, OCR, f' relationship presented in Mayne & Kulhawy (1982) and Table I.4, knowledge of effective stress friction angle will be required. This is discussed in the following section.

## I.5 Strength Properties of Granular Materials

The drained strength of granular materials is typically expressed using Mohr-Coulomb failure criteria (with effective cohesion intercept c' = 0):

$$\tau_{max} = (\sigma'_{vo})\tan\phi' \qquad (I.11)$$

where $\tau_{max}$ is the maximum shear strength, and $\phi'$ is the effective stress friction angle. Early studies of frictional resistance showed a linear increase with confining stress, but additional consideration of the particulate nature of soils showed that friction angle is controlled by other factors as well. Rowe (1962) showed that effective stress friction angle in soils was a sum of a constant sliding friction, as well as void ratio dependent particle rearrangement and dilatency. Additional studies by Lee and Seed (1967) showed $\phi'$ to be a function of sliding friction, dilatency, crushing, and re-arrangement, which are

all functions of normal stress. Table I.5 displays correlations between CPT tip resistance and effective stress friction angle, $\phi'$.

**Table I.5. Correlations between $q_c$ and $f'$**

| Relationship | Notes | Reference |
|---|---|---|
| $\arctan\left[0.10+0.38\cdot\log\frac{q_c}{s_{vo}'}\right]$ | • where $q_c$ and $\sigma_{vo}'$ are in the same units<br>• based on calibration chamber test data<br>• mainly clean quartz sands<br>• laboratory $\phi'$ from triaxial tests at chamber $\sigma_{ho}'$ | Robertson & Campanella, 1983 |
| $30.8\cdot\left[\log\left(\frac{f_s}{s_{vo}'}\right)+1.26\right]$ | • where $f_s$ and $\sigma_{vo}'$ are in the same units<br>• evaluation of lateral stress from $f_s$ measurements<br>• comparison with field data (SBPMT, DMT, etc.)<br>• Assesses disturbed $K_o$ condition as $K_p$ | Masood & Mitchell, 1993 |
| $17.6^o+11\cdot\log(q_{c1})$ | • $q_{c1} = q_c/(\sigma_{vo}')^{0.5}$, where $q_c$ and $\sigma_{vo}'$ are in the same units<br>• based on calibration chamber test data<br>• mainly unaged clean quartz sands<br>• laboratory $\phi'$ from triaxial compression tests<br>• n = 633, $r^2$ = 0.64 | Kulhawy & Mayne, 1990 |

A soils stress path to failure can be plotted in p'-q space, where $p'=\frac{s'_v+2s'_h}{3}$ and $q=(s'_v-s'_h)$. A failure surface M is defined as a function of $\phi'$, which differs in compression and extension. During shear, the stress state (p' and q) will move towards this failure envelope in a manner dependant upon soil properties and type of loading. In void ratio - stress space, a unique critical state of constant volume and unlimited shear strain has been shown to exist (e.g., Poulos, 1981). During drained shear, a soil specimen

will exhibit volume change while moving towards this line. During undrained shear, a soil element will generate excess pore water pressures to move towards failure. Studies of laboratory tests revealed a potential surface within the failure envelope where rearrangement of grains during shear may lead to an unstable soil structure. A collapse surface is said to exist where loss of contact points between grains leads to structural collapse, rapid increase in pore pressures, and flow to the critical void ratio (Alarcon-Guzman et al., 1988). Depending upon stress conditions and type of loading, flow structure may be more important to evaluate than the critical state line.

When subjected to earthquake shaking, collapsible soils will tend to contract, generating positive pore pressures in the absence of drainage. As the pore water pressure increases, the effective stress will decrease (Eq. I.6), leading to a loss of strength. When the excess pore water pressure ($\Delta u$) equals the original effective stress, the effective stress goes to zero ($u = \sigma_{vo}$) causing initial liquefaction (Seed & Lee, 1966).

## I.6 Critical State Properties of Granular Materials

The importance of volume change characteristics of sands during shear was initially presented in Casagrande (1936). This paper discussed that when sheared, loose and dense soils will change volume and move towards a unique critical void ratio where unlimited deformation is possible with no volume change. Further research showed that the critical void ratio decreases with increasing normal stress. If the soil is saturated and drainage is not permitted during loading, there can be no global volume change in the specimen. Contraction and dilation tendencies will then be accounted for by pore

pressure response. The development of Critical State Soil Mechanics (CSSM; Roscoe, Schofield & Wroth, 1958; Schofield & Wroth, 1968) has experimentally and numerically quantified the presence of a critical state for soils, generally for normally consolidated clays. Experimental validation of these concepts using sands had been limited by lack of soil matrix compression under isotropic conditions (Wood, 1990).

The uniqueness of the critical state line for sands has been the subject of debate. Stress controlled tests presented in Castro (1969) showed the presence two distinct critical failure lines in e-log $\sigma_3$' space, instead of a unique critical state line. An $\bar{e}_F$ line represented a liquefaction induced flow structure, while an $\bar{e}_S$ line represented steady state deformation. The $\bar{e}_F$ line was generated by undrained and drained tests on loose specimens, and the $\bar{e}_S$ line was generated by undrained tests on dense specimens. These lines were further defined (and renamed as the F and S lines) by the work of Alarcon-Guzman et al. (1988). The F line represents the critical state line for sands generated from strain softening behavior, while the S line represents strain hardening behavior. There is an area between these two lines where quasi-steady state and limited strain softening may occur. The difference between the S line and F line can be explained by the development of shear bands within dilative triaxial specimens. As a dilative specimen is sheared, a distinct failure plain will be generated. The stress-strain response of the soil will not be controlled by the global void ratio of the specimen, but by the interface between the two blocks separated by the shear band. This interface will be controlled by the void ratio and confining stress within the shear band. Studies of local void ratio in dense specimens by Desrues et al. (1996) and Frost et al. (1999) showed that

local void ratio within shear bands approaches that of the critical state determined from loose specimens. Considering the critical state line from contractive tests, and the presence of shear banding and subsequent effect of local void ratio in dilative specimens, a unique critical state line regardless of stress path or testing procedure is accepted.

Since the slope of the critical state line has been shown to be controlled by particle shape, and the position of the critical state line has been shown to be controlled by gradation (Poulos et al., 1985), studies as to the effects of particle crushing have been undertaken. Been et al. (1991) concluded that a sharp break in the slope of the critical state line on a semi-log plot, Figure I.3a, is the result of particle crushing. In a discussion to that paper, Verdugo (1992) presented the same data on a linear plot, Figure I.3b, and discussed exaggeration as a result of the semi-log scale. Been (1999) determined that curvature in the critical state line is not an issue of great importance, and there is no theoretical reason for the log-linear relationship. Depending upon the stress range of concern, a linear relationship or bi-linear logarithmic relationship may be desirable for ease in mathematical interpretation. Upward curvature of the critical state line at low stresses on a linear plot and downward curvature at high stresses on a semi-log plot should be taken into consideration during analysis.

During undrained shear (e.g. earthquake loading) the soil element will act under a constant volume condition, with volume change characteristics resulting in pore pressure response. The critical state line will act as a demarcation between contractive, positive pore pressure generation, and dilative, negative pore pressure generation. Therefore if

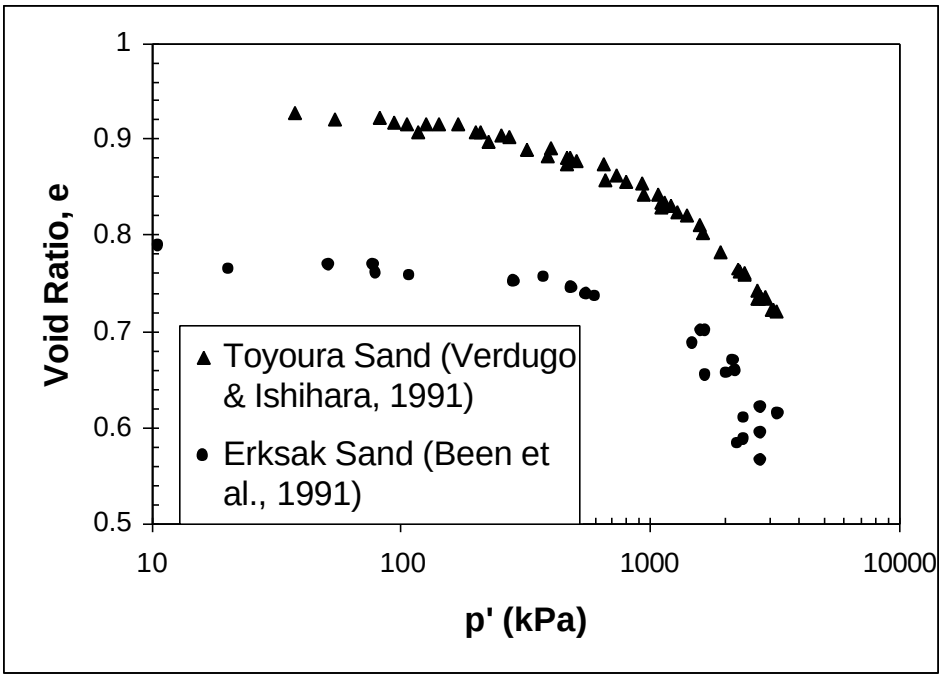


**Figure I.3a. Critical state line for Toyoura and Erksak Sands on semi-log scale**

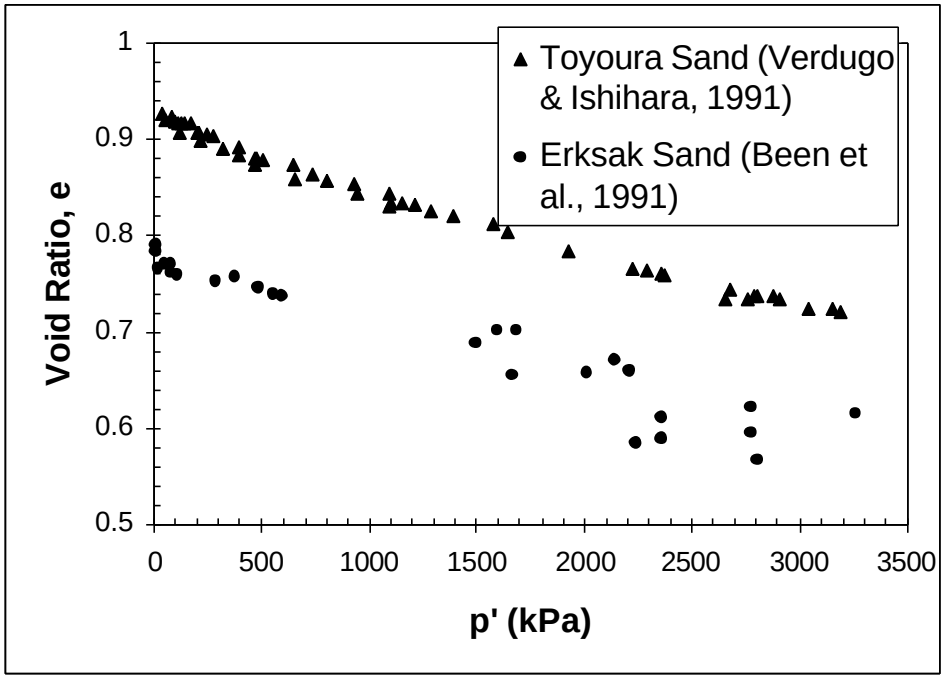


**Figure I.3b. Critical state line for Toyoura and Erksak Sands on linear scale**

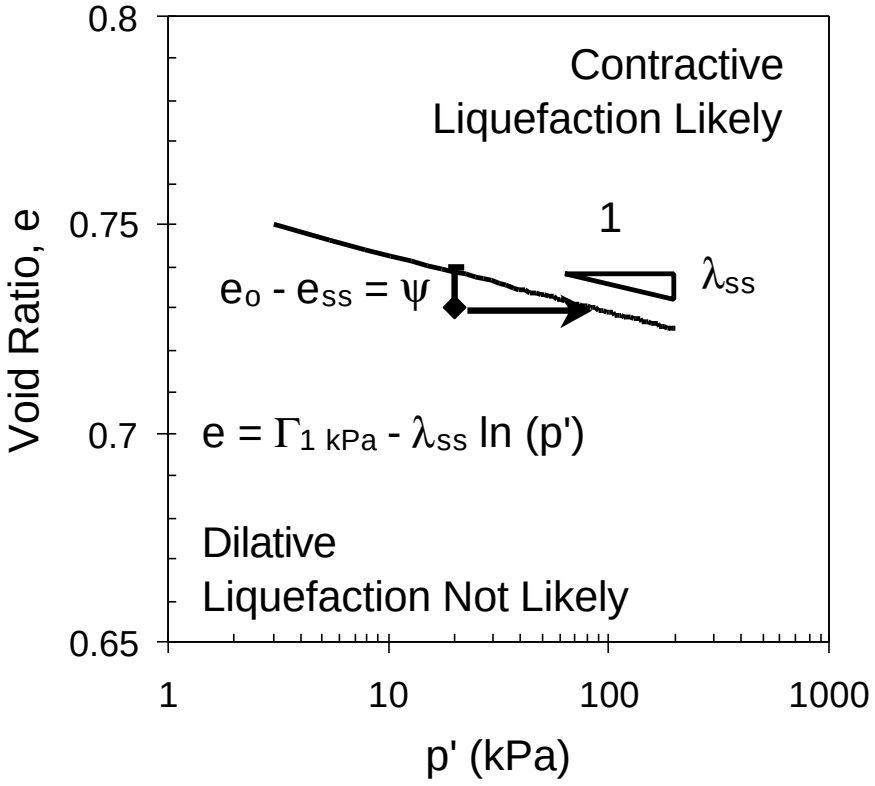


**Figure I.4. State Approach to Liquefaction Assessment**

the in-situ state, e, $\sigma_{vo}'$, and $K_o$, or state parameter, $\psi$, is known, an estimation of liquefaction resistance can be determined. Concern with the utilization of remolded laboratory specimens to soils in the field has been expressed for liquefaction analyses (Vaid & Thomas, 1995). Lack of soil structure and aging are a concern in laboratory specimens, as well as scale effects and natural variability. Estimation of state parameter from in-situ tests is still developing, and is discussed in Jefferies (1999) and Shuttle & Jefferies (1998).

## I.7 Small Strain Properties

Small strain properties of shear wave velocity ($V_s$) and maximum shear modulus ($G_{max}$) were previously discussed in Chapter 2. It is desirable to measure these properties in-situ via methods such as crosshole testing, downhole testing, spectral analysis of surface waves, etc. If preliminary estimates of $V_s$ and $G_{max}$ are desired and penetration test data is available, correlations contained in Table I.6 are available for use.

**Table I.9. Correlations between Cone Tip resistance and Small Strain Properties**

| Property | Relationship | Notes | Reference |
|---|---|---|---|
| Shear Wave Velocity, $V_s$ | $277 \cdot (q_c)^{0.13} (\sigma_{vo}')^{0.27}$ | • $V_s$ in m/s; $q_c$ and $\sigma_{vo}'$ in kPa<br>• based on Italian sands | Baldi et al., 1989 |
| | $V_{s1} = 102 \cdot (q_{c1})^{0.25}$ | • $V_{s1}$ in m/s<br>• $V_{s1} = V_s \cdot (p_a/\sigma_{vo}')^{0.25}$<br>• $q_{c1} = q_c (P_a/\sigma_{vo}')^{0.5}$<br>• sand field data | Robertson et al., 1992b |
| | $V_{s1} = 135 \cdot (q_{c1})^{0.23}$ | • $V_{s1}$ in m/s<br>• site specific field data for Alaska sand | Fear & Robertson, 1995 |

**Table I.9. Continued**

| | | | |
|---|---|---|---|
| Shear Wave Velocity, $V_s$ | $V_{s1} = f(q_{c1}, FR)$ | • based on field data<br>• incorporated into classification chart | Olsen, 1994 |
| | $1.75(q_c)^{0.627}$ | • $V_s$ in m/s; $q_c$ in kPa<br>• based on 31 intact and fissured clays sites<br>• n = 481; $r^2 = 0.736$ | Mayne & Rix, 1995 |
| | $14.02(q_c)^{0.364} \cdot (e_o)^{-0.490}$ | • $V_s$ in m/s; $q_c$ in kPa<br>• based on 31 intact and fissured clays sites<br>• n = 364; $r^2 = 0.846$ | Mayne & Rix, 1995 |
| | $14.13 \cdot q_c^{0.359} \cdot e_o^{-0.473}$ | • $V_s$ in m/s; $q_c$ in kPa<br>• application to clay soils<br>• field data collected from 36 clay sites<br>• n = 406; $r^2 = 0.885$ | Hegazy & Mayne, 1995 |
| Small Strain Stiffness, $G_{max}$ | $(G_{max})_1 = f(q_{c1}, FR)$ | • based on field data<br>• incorporated into classification chart | Olsen, 1988 |
| | $1634 \cdot (q_c)^{0.250}(\sigma_{vo}')^{0.375}$ | • $G_{max}$, $q_c$, and $\sigma_{vo}'$ are in kPa<br>• based on sand field data and calibration chamber test results | Rix & Stokoe, 1991 |
| | $2.78(q_c)^{1.335}$ | • $G_{max}$ and $q_c$ are in kPa<br>• based on field data from 31 clay sites<br>• n = 481; $r^2 = 0.713$ | Mayne & Rix, 1993 |
| | $406(q_c)^{0.695} e_o^{-1.130}$ | • $G_{max}$ and $q_c$ are in kPa<br>• based on field data from 31 clay sites<br>• n = 418; $r^2 = 0.901$ | Mayne & Rix, 1993 |

# APPENDIX II

# GROUND MOTION PARAMETERS

## II.A Ground Motion Parameters

Many parameters exist which can be used to characterize earthquake related ground motions. These include, but are not limited to, moment magnitude ($M_w$), peak ground acceleration (PGA), and Arias intensity. These parameters are discussed in the following sections.

## II.B Moment Magnitude

Without modern seismographs, scales relating earthquake-induced damage to intensity were used (e.g. Modified Mercalli, Japanese Meteorological Agency). To quantify earthquake size measurements of earthquake magnitude were developed from modern instrumentation, but early methods were typically empirical and device dependant (Kramer, 1996). Some early magnitude scales include Richter Local Magnitude, $M_L$, Surface Wave magnitude, $M_S$, Short Period Body Wave Magnitude, $m_b$, Long Period Body Wave, $m_B$, and the Japanese Meteorological Agency magnitude, $M_{JMA}$. Since these methods are a function of measured seismic waves and not fault rupture, they are not directly related and tend to reach a constant maximum value. Figure II.1 displays saturation of various magnitude scales. A brief description of scales is

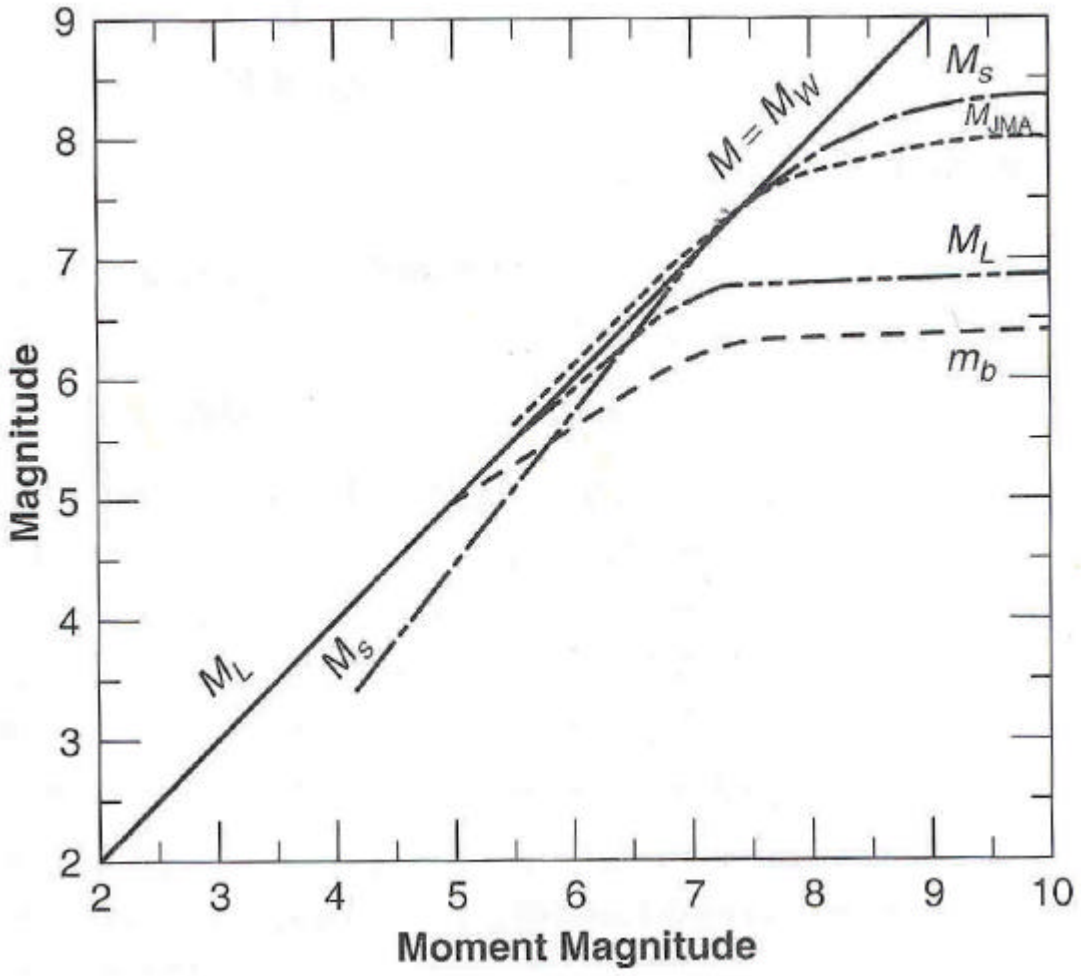


**Figure II.1. Comparison of Empirical Magnitude Scales to Moment Magnitude (Idriss, 1985)**

**Table II.1. Description of Empirical Magnitude Scales (adapted from Stover & Coffman, 1993)**

| Magnitude Scale | Equation | Notes |
|---|---|---|
| Local (Western United States) | $M_L = \log A - \log A_o$ | • $A$=maximum trace amplitude in millimeters written by a Wood-Anderson torsional seismometer<br>• $\log A_o$=a standard value as a function of distance where the distance is $\leq$ 600 km<br>• can calibrate for other seismometers<br>• listed for depths $\leq$ 70 km |
| Local & Regional (Eastern United States) | $M_n = 3.75 + 0.90 \cdot \log(D) + \log(A/T)$ $0.5^o \leq D \leq 4.0^o$<br><br>$Mn = 3.30 + 1.66 \cdot \log(D) + \log(A/T)$ $4.0^o \leq D \leq 30.0^o$ | • for North America east of the Rocky Mountains<br>• $A/T$ in micrometer per second calculated from 1-second $L_g$ waves<br>• $D$=distance in geocentric degrees<br>• may be referred to as $M_{bLg}$ |
| Surface Wave | $M_S = \log(A/T) + 1.66 \cdot \log(D) + 3.3$ | • $A$=maximum vertical surface-wave ground amplitude in micrometers<br>• $T$=period in seconds<br>• $D$=distance in geocentric degrees (station to hypocenter) and $20 \leq D \leq 160^o$<br>• not computed for depths greater than 50 km |
| Short Period Body Wave | $m_b = \log(A/T) + Q(D,h)$ | • $A$=ground amplitude in micrometers<br>• $T$=period in seconds; $0.1 \leq T \leq 3$<br>• $Q$=function of distance and depth as presented in Guterberg & Richter (1956) where $D \geq 5^o$ |
| Felt Area | based on isoseismal maps and magnitude – intensity correlation | • form of body wave magnitude |

contained in Table II.1.

To eliminate saturation effects, a more fundamental magnitude scale based on the seismic moment ( $M_0 = mA\overline{D}$ , where $m$ is the rupture strength of the material along the fault, $A$ is the rupture area, and $\overline{D}$ is the average amount of slip). If seismic moment is expressed in dyne-cm, the moment magnitude, $M_W$, can be expressed as (Kramer, 1996):

$$M_W = \frac{\log M_0}{1.5} - 10.7 \qquad \text{(II.1)}$$

The moment magnitude of an earthquake will also have an influence on a number of

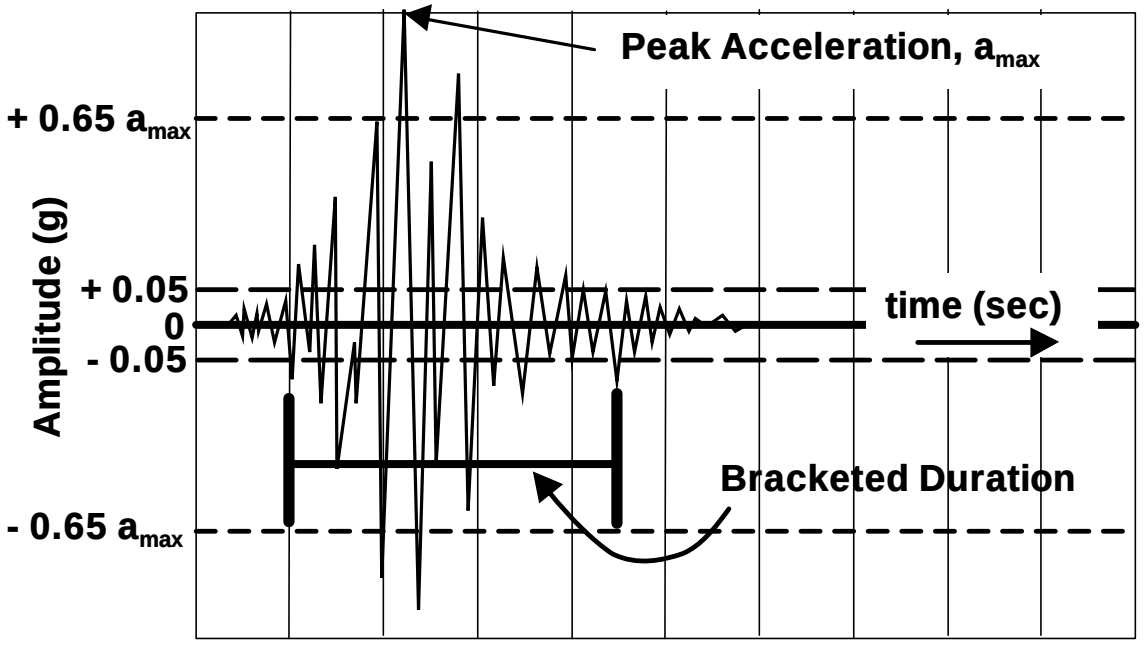


**Figure II.2. Graphical Representation of Ground Motion Parameters**

other ground motion properties, such as duration (e.g., Chang & Krinitzky, 1977), significant stress cycles (e.g., Seed et al., 1985), acceleration (e.g., Toro et al., 1997), and Arias Intensity (e.g. Kayen & Mitchell, 1997). Figure II.2 displays a graphical representation of the ground motion parameters mentioned above.

## II.C Peak Ground Acceleration

For geotechnical analyses, the peak horizontal ground acceleration (PGA or $a_{max}$) is typically used to characterize the amplitude of a particular ground motion. The vertical component of motion is not typically used since it is usually lower than the peak horizontal acceleration (e.g., Newmark & Hall, 1982) and gravity induced static forces provide a substantial factor of safety against vertical motion (Kramer, 1996). If acceleration measurements are recorded in two perpendicular directions, the vector sum can be used to determine the amplitude and direction of motion (Kramer, 1996). Figure II.2 displays the maximum acceleration on an example accelerogram.

The value associated with 65 percent of $a_{max}$ is typically associated with the average amplitude of significant ground motion (Seed & Idriss, 1971). The earthquake duration and number of significant stress cycles is not a function of acceleration, and thus parameters in addition to acceleration (e.g. Magnitude Scaling Factors (MSF); Chapter 3) are needed to characterize ground motions for simplified procedures.

## II.D Arias Intensity

Arias intensity represents the cumulative energy per unit weight in a given direction that is absorbed by a set of single degree of freedom oscillators (Arias, 1970). Considering that the damping of a nonliquified soil deposit will not significantly affect the calculation of Arias intensity, the case where the damping ratio approaches zero will be used (Kayen & Mitchell, 1997). Horizontal Arias intensity can be calculated as the sum of the area under acceleration time histories in the x- and y- directions:

$$I_h = I_{xx} + I_{yy} = \frac{p}{2g}\int_0^{t_o} a_x{}^2(t)dt + \frac{p}{2g}\int_0^{t_o} a_y{}^2(t)dt \qquad \text{(II.2)}$$

Where $I_h$ is the horizontal Arias intensity, $I_{xx}$ is the Arias Intensity in the x direction, $I_{yy}$ is the Arias intensity in the direction perpendicular to $I_{xx}$, and $a_x(t)$ and $a_y(t)$ are the acceleration time histories in the x and y directions respectively. The acceleration time history values are squared for integration purposes to eliminate negative area during integration. The values are subsequently divided by two, which negates the squared component. It is recommended that numerical integration by the trapezoidal method be used to determine Arias intensity (Youd et al., 1997). Since the entire acceleration time history is accounted for, no additional parameters are necessary to characterize earthquake motion.

# APPENDIX III.

## SEISMIC PIEZOCONE DATA COLLECTION SYSTEM AND SHEAR WAVE ANALYSIS PROCEDURES

### III.A. Cone Penetrometers and Field Testing

Three electronic cone penetrometers, each manufactured by Hogentogler, were used during the investigations. The piezocones were vertically advanced at the standard rate of 2 cm/sec (Lunne et al., 1997) using the Georgia Tech GeoStar open chasis cone truck. Readings of tip resistance ($q_c$), sleeve friction ($f_s$), inclination ($i$), and pore pressure ($u_m$) were taken every 5-cm (2.5-sec).

Inside the penetrometer, approximately 25-cm behind the tip, are a velocity geophone and an inclinometer. The inclinometer is used to assess the verticality of the sounding to warm against excessive drift. The geophone detects vertically-propagating, horizontally-polarized shear waves generated at the ground surface at intervals of approximately 1-meter, corresponding to successive rod additions.

The filter elements consisted of high-density polypropylene that was saturated with glycerin in a small vacuum chamber prior to testing. Filter elements were changed to minimize clogging , and the cone was re-saturated between each test to ensure accurate pore pressure data.

The data acquisition system used during testing was a commercial Hogentogler field computer unit interfaced with the GT - GeoStar cone truck. A 10-pin electonic

cable connects the pennetrometer through the rods to the computer. Depth readings were taken using a gear system attached to the hydraulic rams, and a proximity switch to trigger readings every 5-cm.

The GeoStar truck-mounted rig has a set of hydraulic rams attached to the rear of a 6.7 tonne Ford F-350 Super Duty truck chassis. The unit has a reaction mass of approximately 4 tonnes without anchoring and an additional 20 tonne reaction with earth anchoring. The earth anchoring system was required to achieve substantial penetration depth in dense sand of the Mississippi River Valley. Figure III.1 displays a photograph of the Georgia Tech GeoStar cone truck. Figure III.2 displays a drawing of the GT cone truck, and identifies pertinent information involved with a downhole shear wave velocity test.

**Figure III.1. Georgia Tech GeoStar Open Chassis Cone Truck**

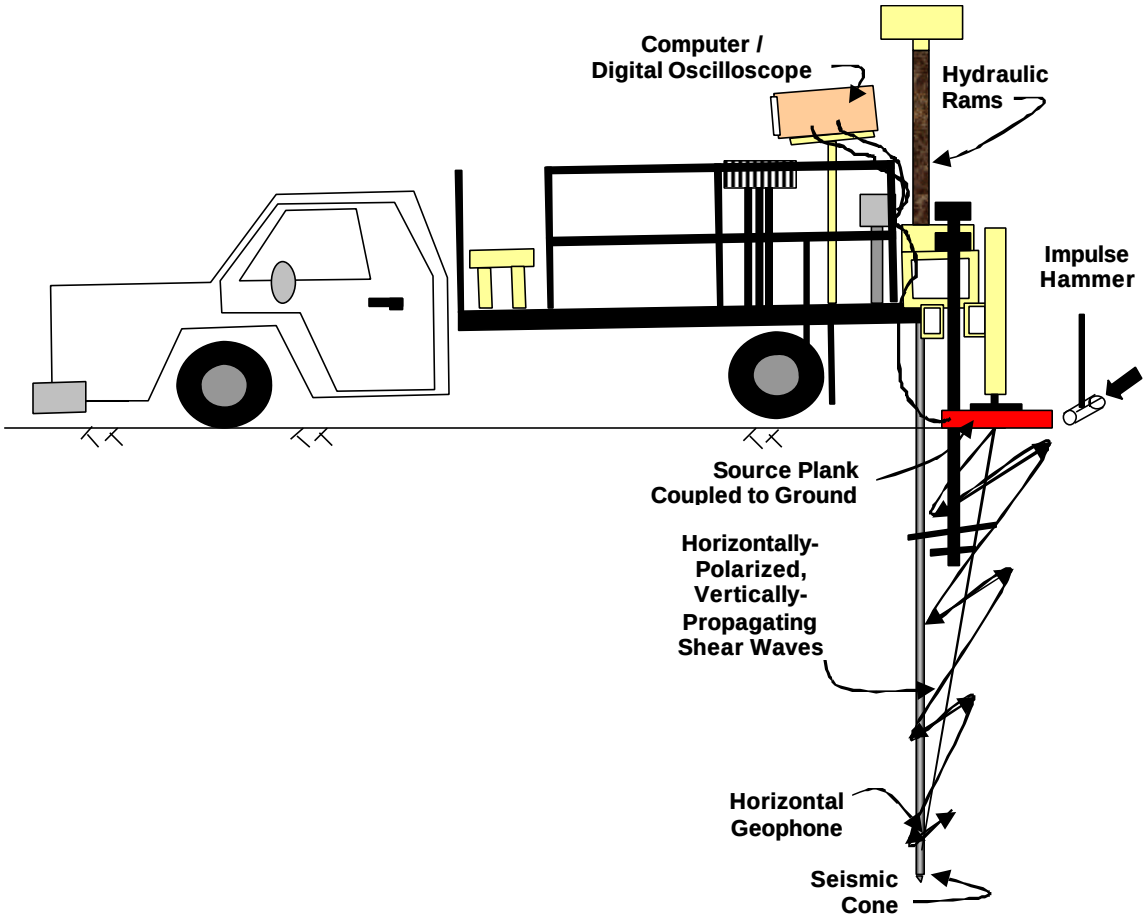


**Figure III.2. Illustration of GeoStar Cone Truck and Downhole Seismic Setup**

## III.B. Seismic Piezocone Testing Procedures

Cone penetration tests (CPT) were performed in general accordance to ASTM D-5778 guidelines using an electronic cone penetrometer and computer data acquisition system. In each of the soundings, shear wave arrivals were measured at regular intervals of approximately 1-meter. A special instrumented hammer was used to trigger a surface source rich in shear waves from a horizontal steel beam. The steel beam was coupled to the ground by the weight of the GeoStar cone truck, under a hydraulic outrigger. A single horizontal velocity geophone located within the penetrometer served as a receiver for the signal, which was displayed on the Hogentogler computer screen.

At least four separate wave records were generated at each depth utilizing left-strike and right-strike polarization. Two waves were taken, compared for repeatability, and then averaged if an acceptable match was recorded. The process was repeated for an addition pair of waves, which were used to determine the first crossover pseudo-interval shear wave velocity ($V_s$). Pseudo-interval $V_s$ is obtained from incremental measurements between successive wave time arrivals and the incremental distance to the geophone (Campanella et al., 1986). For the initial depth interval, shear wave first arrival times were utilized to calculate the shear wave velocity. Thereafter, an iterative process of analyzing the difference between successive peak, trough, and first-crossover points on each shear wave was utilized to provide repeatable velocities. First crossover velocities are presented on the figures and in the data.

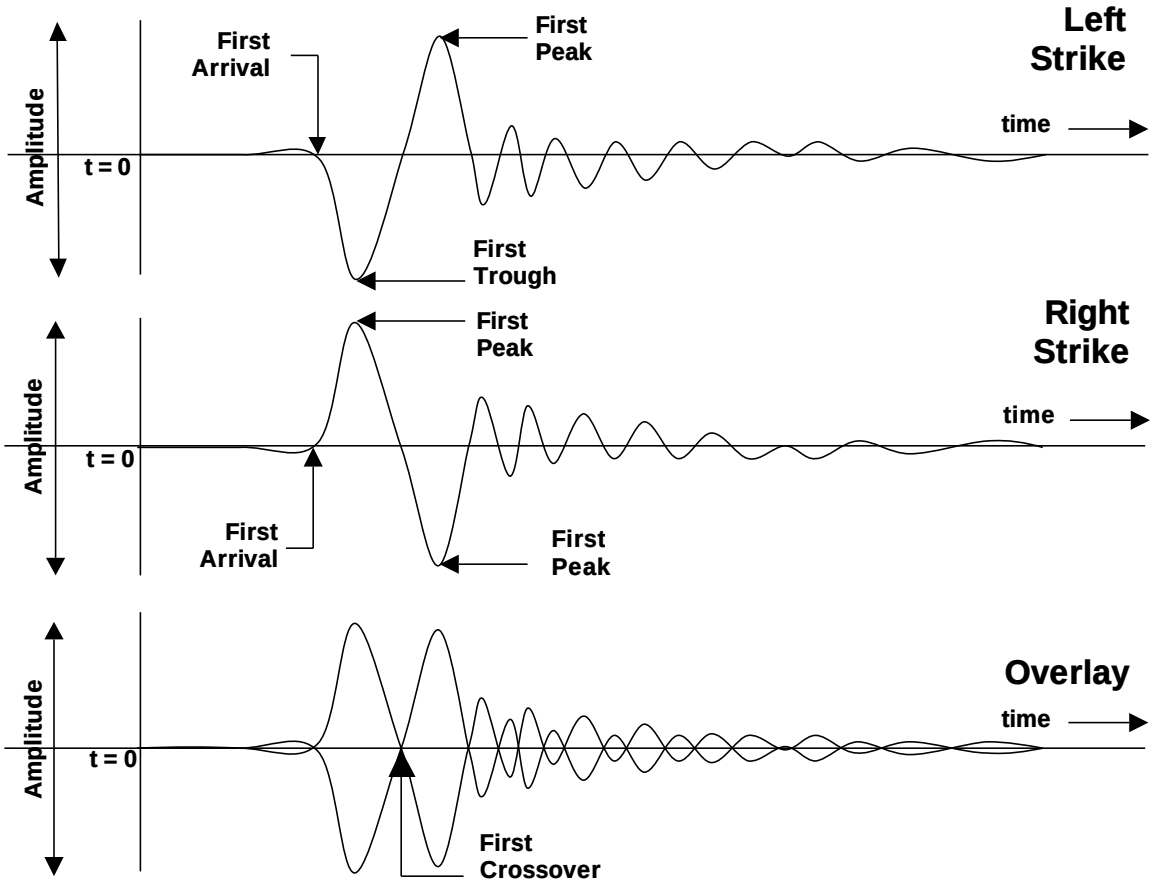


**Figure III.3. Shear wave arrival time analysis procedure**

# APPENDIX IV

# TEST SITES ANDSOUNDING LOCATIONS

## IV.A Areas Studied and Site Selection

Earthquake hazards in Mid-American are generally grouped into the areas surrounding the New Madrid Seismic Zone (NMSZ) and the Charleston, SC earthquake region. Therefore, the field-testing associated with this study concentrate in these areas as well. A majority of the sites selected were in coordination with the work of previous paleoliquefaction studies:

- Charleston, SC (Clough & Martin, 1990; Martin & Clough, 1994)
- NE Arkansas and SE Missouri (Tuttle et al., 1998; Tuttle et al., 1996; Wolf et al., 1998; Collier, 1998; Van Arsdale, 1998; Schweig, 1998;),
- Memphis and Shelby County, TN (VanArsdale, 1998; Gomberg, 1999).

This study is meant to complement the work from these previous studies by evaluating deeper source soils. Table IV.1 displays all in-situ test sounding and surface sand sampling locations that will be discussed in this thesis, along with other pertinent information. Test sites within these zones of study will be discussed individually within each section. It should be noted that unless noted, longitude and latitude measurements were recorded with a Garmin hand-held unit with an accuracy of about $\pm$ 15 m.

**Table IV.1. In-situ testing and Sampling in Mid-America Earthquake Region**

| Location | Test | I.D. | Longitude | Latitude | Max Depth (m) |
|---|---|---|---|---|---|
| ***Memphis, TN Area*** | | | | | |
| Shelby Farms (SF) | 10T SCPTu$_2$ | MEMPH-G | 35.11722 | -89.80555 | 31.40 |
| Shelby Farms (SF) | DMT | SFDMT-01 | 35.11722 | -89.80555 | 8.80 |
| Shelby Farms (SF) | Sand Sample | SF | NA | NA | Surface |
| SF Shooting Range | 10T SCPT | SFSR-01 | 35.12917 | -89.84155 | 30.40 |
| SF Shooting Range | 15T SCPT | SFSR-02 | 35.12905 | -89.84030 | 25.25 |
| Houston Levee | 10T SCPTu$_2$ | MEMPH-H | 35.10833 | -89.73052 | 20.40 |
| Houston Levee | Sand Sample | HL | NA | NA | Surface |
| Wolf River Blvd. | 10T SCPTu$_2$ | MEMPH-I | 35.09927 | -89.80247 | 12.15 |
| N 2$^{nd}$ Street | 10T SCPTu$_2$ | MEMPH-J | 35.19078 | -90.04502 | 14.70 |
| Wolf / Mississippi | Sand Sample | WRMS | NA | NA | Surface |
| Monopole Tower[1] | 10T SCPTu$_2$ | MEMPH-K | 35.15042 | -90.12953 | 31.70 |
| Shelby Forrest | 10T SCPTu$_2$ | SFOR-01 | 35.35780 | -90.01883 | 21.40 |
| Shelby Forrest | 15T SCPT | SFOR-02 | 35.35843 | -90.01982 | 20.95 |
| ***Northeast Arkansas and Southeast Missouri Area*** | | | | | |
| Yarbro Excavation | 10T SCPTu$_2$ | YARB-01 | 35.98233 | -89.93310 | 28.00 |
| Yarbro Excavation | Sand Sample | YE | NA | NA | ~ 2 to 3 |
| Bugg 40 | 10T SCPTu$_2$ | BUGG-01 | 35.97277 | -89.90780 | 38.50 |
| Bugg 40 | 10T SCPTu$_2$ | BUGG-02 | 35.97225 | -89.90792 | 34.20 |
| 3MS617 | 15T SCPTu$_2$ | 3MS617-A | 35.99262 | -89.83557 | 32.50 |
| 3MS617 | 10T CPTu$_2$ | 3MS617-C | 35.99277 | -89.83553 | 31.20 |
| 3MS617 | 5T CPTu$_2$ | 3MS617-D | 35.99267 | -89.83527 | 15.85 |
| Huey House | 15T SCPTu$_2$ | HUEY-01 | 35.98353 | -89.88650 | 26.00 |
| Dodd Farm | 15T SCPTu$_2$ | DODD-01 | 36.09485 | -89.84832 | 30.85 |
| Dodd Farm | 15T SCPTu$_2$ | DODD-02 | 36.09458 | -89.84833 | 25.35 |
| Dodd Farm | 15T CPTu$_2$ | DODD-03 | 36.09423 | -89.84817 | 32.30 |
| Dodd Farm | DMT | DODD-04 | 36.09398 | -89.84833 | 17.00 |
| Dodd Farm | DMT | DODD-05 | 36.09468 | -89.84813 | 10.40 |
| Dodd Farm | DMT | DODD-06 | 36.09462 | -89.84813 | 15.00 |
| Johnson Farm | 15T SCPTu$_2$ | JOHN-01 | 36.11920 | -89.84393 | 25.15 |
| I-155 Bridge[2] | 15T SCPTu$_2$ | I155-01 | 36.11888 | -89.61493 | 25.50 |
| I-155 Bridge[2] | 10T CPTu$_1$ | I155-02 | 36.11888 | -89.61493 | 21.70 |
| I-155 Bridge[2] | 15T SCPTu$_2$ | I155-03 | 36.11888 | -89.61493 | 23.10 |
| I-155 Bridge[2] | 10T CPTu$_1$ | I155-05 | 36.11888 | -89.61493 | 18.00 |
| I-155 Bridge[2] | DMT | I155-06 | 36.11888 | -89.61493 | 15.85 |
| I-155 Bridge[2] | DMT | I155-07 | 36.11888 | -89.61493 | 15.85 |

**Table IV.1. Continued**

| | | | | | |
|---|---|---|---|---|---|
| ***Charleston, SC*** | | | | | |
| Hollywood Ditch | VPCPT | HW-1 | NA | NA | 9.27 |
| Hollywood Ditch | $CPTu_1$ | HW-2 | NA | NA | 9.02 |
| Hollywood Ditch | $SCPTu_2$ | HW-4 | NA | NA | 19.20 |
| Thompson Industrial | $SCPTu_2$ | TIS-01 | NA | NA | 14.4 |
| Thompson Industrial | VPCPT | TIS-02 | NA | NA | 8.92 |
| Thompson Industrial | $CPTu_1$ | TIS-03 | NA | NA | 9.13 |

[1] Longitude and latitude determined from street address using http://www.mapblast.com
[2] Longitude and latitude taken at reference point shown in Figure 4.10

## IV.B Memphis, TN Area

Nine cone penetration tests with downhole seismic measurements and one flat dilatometer sounding were performed at eight test sites located from the eastern suburbs of Memphis, TN to West Memphis, AR. Surface sand samples were also taken at three sites. Figure 4.1 shows the approximate locations of the sites with reference to pertinent landmarks. Single soundings were performed to get a general idea of stratigraphic changes across the Memphis area. Multiple soundings were performed at Shelby Farms Shooting Range and Shelby Forest to evaluate local variation in shear wave velocity and how they may affect the results of various geophysical tests. Each test site will be discussed in more detail in the following sub-sections.

### IV.B.1 Shelby Farms

The Shelby Farms site was located in a power utility easement and Shelby County park area off of Germantown Road, in Germantown, TN. The areas tested were about 20 to 30 meters west of TVA Tower 2533, north of the Wolf River. Figures 4.2 and 4.3

show the test site and layout of the soundings, respectively. This site contained a sand dike mapped previously by researchers from the University of Memphis located along the riverbank approximately 20 m south of the sounding. Dating of the dike has not yet been completed, but it is believed to have originated during the New Madrid earthquakes. A sand specimen was taken from a surface sand bar on the Wolf River adjacent to the site.

**IV.B.2 Shelby Farms Shooting Range**

The Shelby Farms shooting range was a site set up by the USGS to compare shear wave velocity measurements taken by a variety of different methods (personal communication J. Gomberg, 1999). Figures 4.4 and 4.5 show the test site and layout of the soundings respectively.

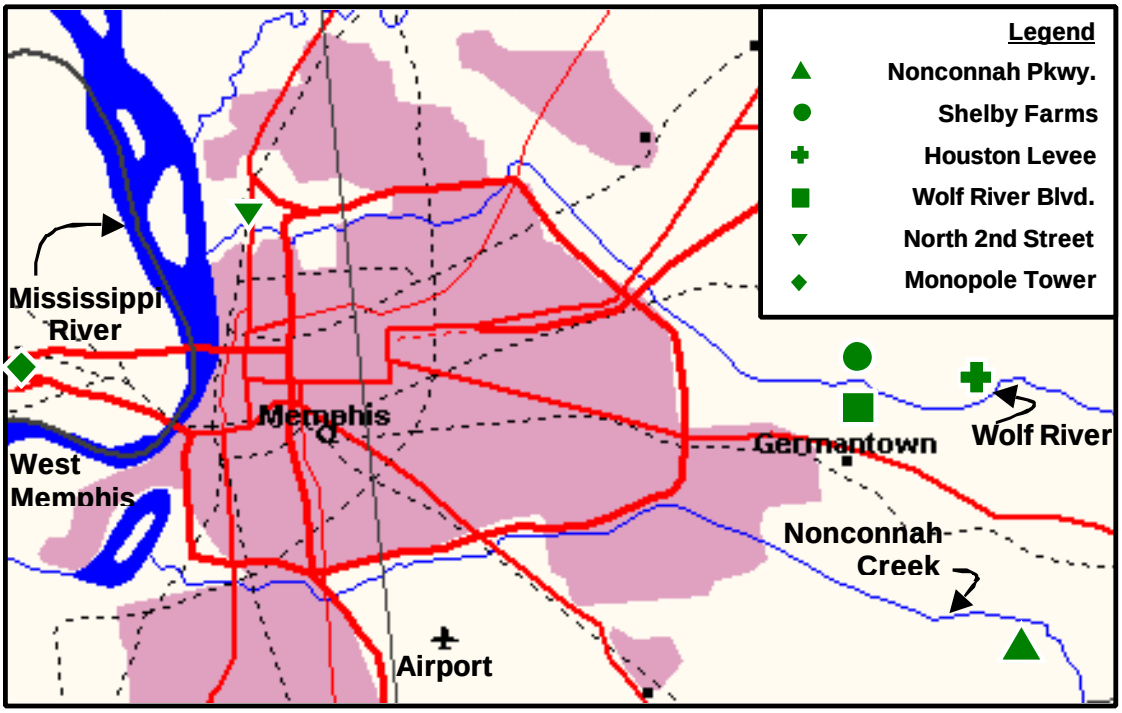


**Figure IV.1. Location of Memphis Test Sites**

**Figure IV.2. Seismic Cone Testing at Shelby Farms**

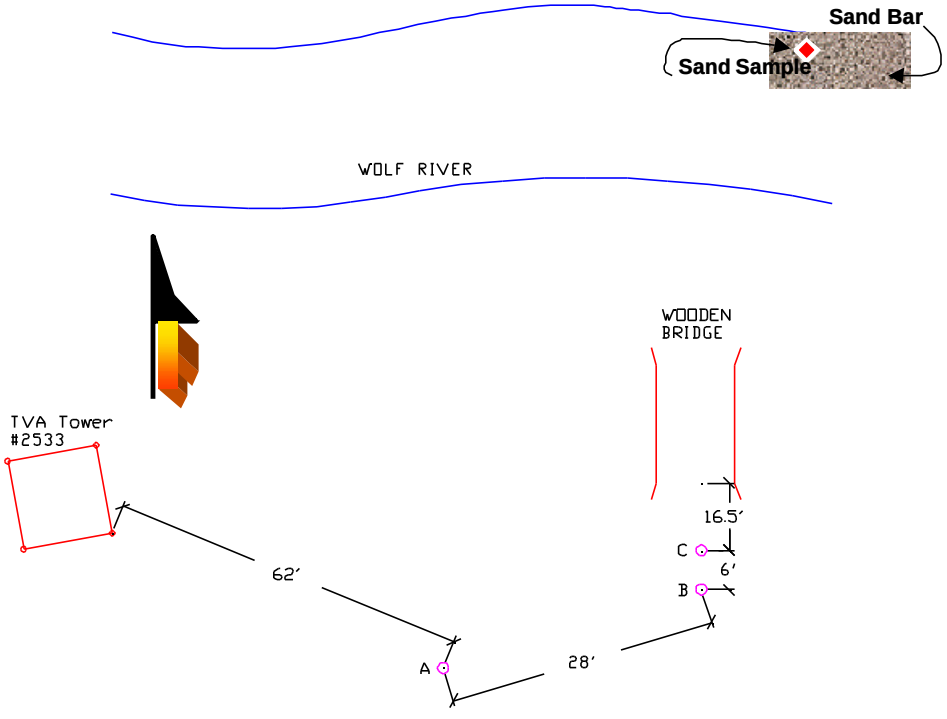


**Figure IV.3. Sounding Layout at Shelby Farms Site, Germantown, TN**

**Figure IV.4. Seismic Cone Testing at Shelby Farms Shooting Range**

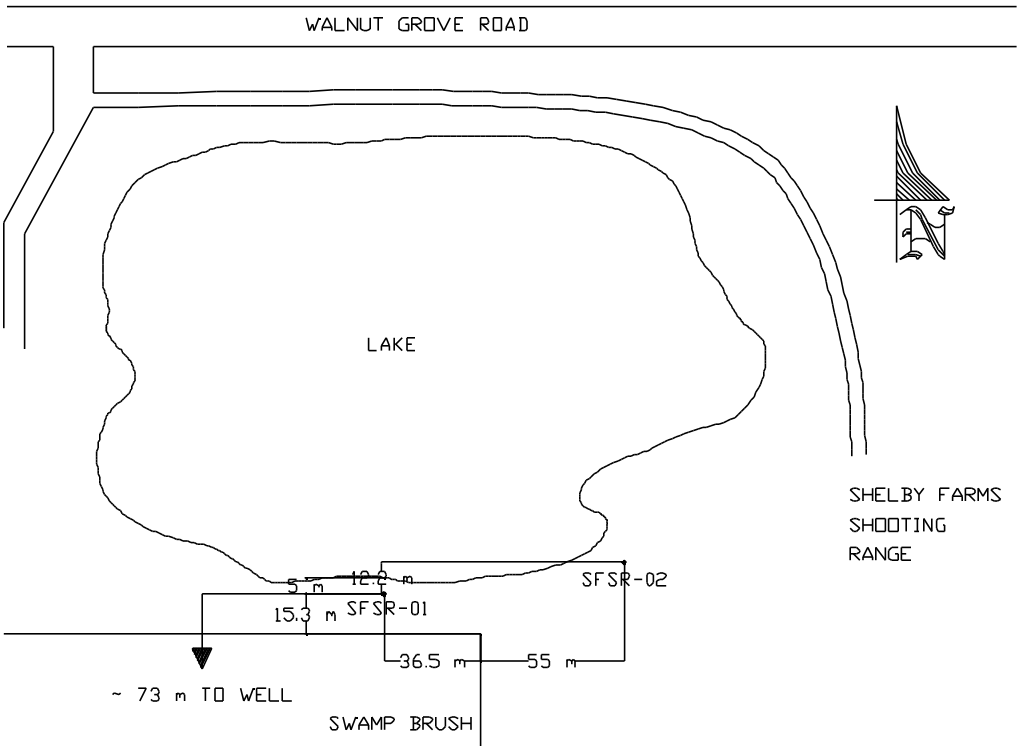


**Figure IV.5. Sounding Layout at SF Shooting Range Site, Germantown, TN**

### IV.B.3 Houston Levee Road

This site was located to the west of Houston Levee Road, on the north side of the Wolf River. Figures 4.6 and 4.7 show the test site and location of the sounding, respectively. The sediments in this area should have been deposited in a similar manner as those at the Shelby Farms site. The existence of relic liquefaction features has not yet been discovered at this site. At the time of our visit, the site was heavily wooded and covered with brush. A sand specimen was taken from a surface sand bar adjacent to the site.

### IV.B.4 Wolf River Boulevard Construction Site

New buildings were being constructed west of the Courtyard Marriott on Wolf River Boulevard. This provided an additional test site in the vicinity of the previously mapped Shelby Farms sand dike. Approximately 5 meters of new fill overlaid the natural soils in the area tested. Figures 4.8 and 4.9 show the test site and location of the sounding respectively.

### IV.B.5 North 2nd Street (Bell Properties)

A high concentration of paleoliquefaction features was found along the Wolf River in the northwestern part of Memphis, TN (personal communication R. VanArsdale, 1998). A large area of land, known as the Bell Property, located north of the Wolf River and east off of North Second Street became available for testing. At the time of the visit, the

**Figure IV.6. Test Location at Houston Levee**

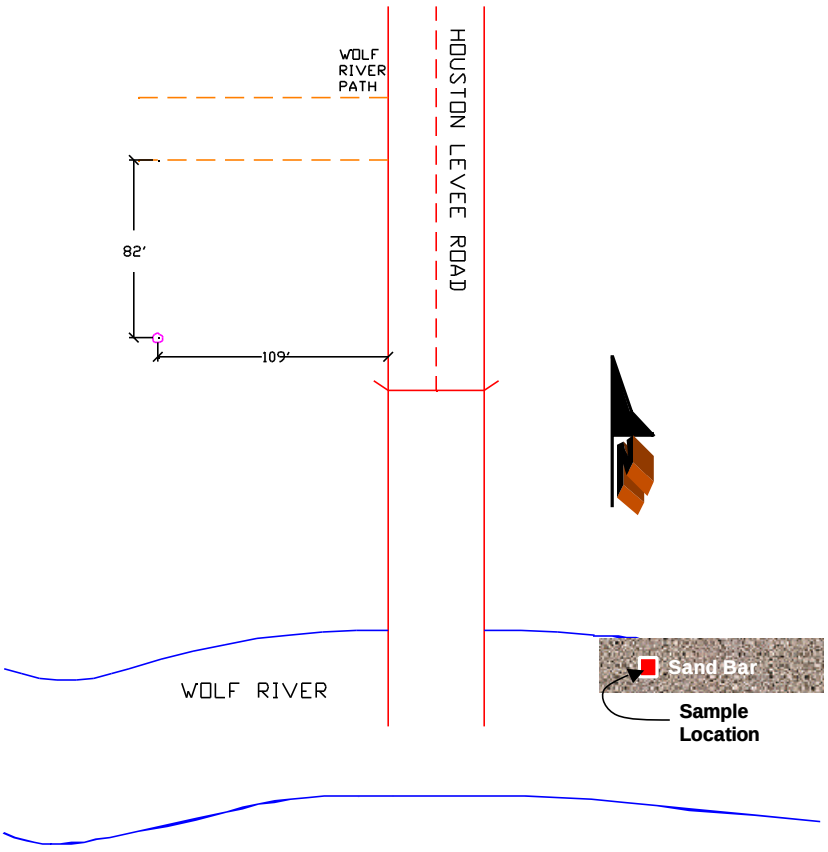


**Figure IV.7. Sounding Location at Houston Levee Site, Germantown, TN**

**Figure IV.8. Test Site at Wolf River Boulevard Construction Site**

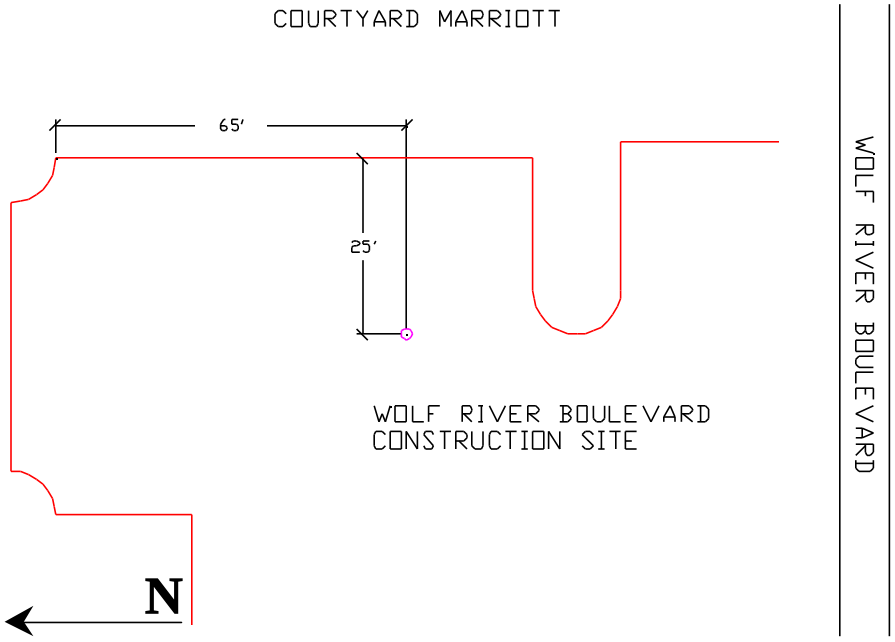


**Figure IV.9. Sounding Location at Wolf River Boulevard Site**

property served as a bean field. Due to the dry weather, the surface crust of silt was desiccated with a noticeable network of fissures. One sounding was performed near where the property sloped down to the banks of the Wolf River.

### IV.B.6 Monopole Tower

A site adjacent to a recently-drilled borehole became available in West Memphis, AR. This provided an interesting opportunity to compare an interpreted CPT profile with soils samples collected at approximately 1.5-meter intervals using SPT drive methods. Also, this sounding was located in the floodplain west of the Mississippi River. This provided an opportunity to compare soundings along the Wolf River to those just west of the Mississippi River. Due to the dry weather, the surface crust of silt was desiccated with a noticeable network of fissures. Figures 4.10 and 4.11 show the site and location of the tests respectively.

### IV.B.7 Shelby Forest

Shelby Forrest was a site set up by the USGS to compare shear wave velocity measurements taken by a variety of different methods (personal communication J. Gomberg, 1999). As opposed the other test sites in the Memphis area, this site was located in the Pleistocene uplands (Bluffs) and near surface soils are not composed of river deposits. This site was located Figures 4.12 and 4.13 show the test site and layout of the soundings respectively.

**Figure IV.10. Testing in West Memphis, AR**

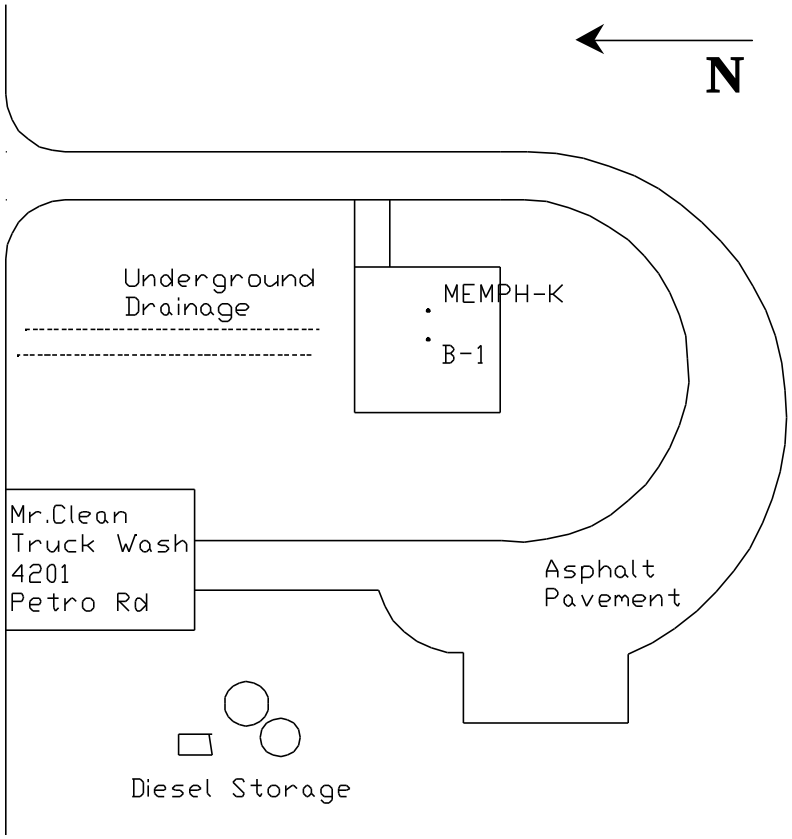


**Figure IV.11. Test Locations at Monopole Tower, West Memphis, AR**

**Figure IV.12. Testing at Shelby Forest**

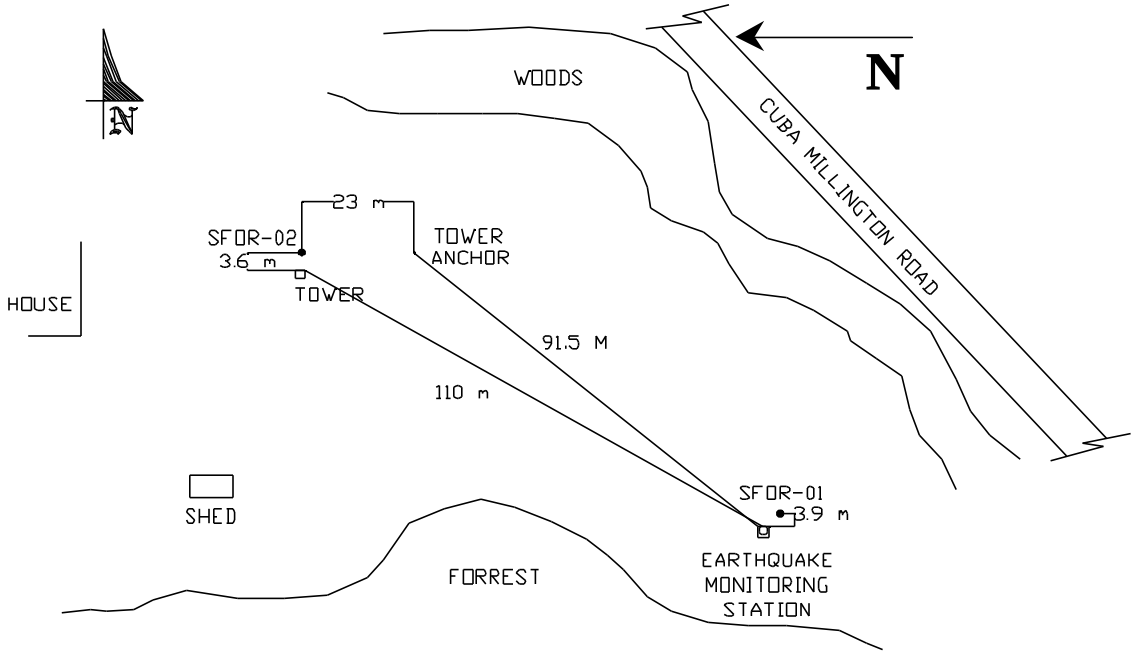


**Figure IV.13. Test Locations at Shelby Forrest,**

## IV.C Northeast Arkansas and Southeast Missouri

Fourteen soundings were performed at six test sites located in Northeast Arkansas and Southeast Missouri, and one sounding was performed in Memphis, TN. Figure 4 shows the approximate locations of the sites in AR and MO with reference to pertinent landmarks. Single soundings were performed at most locations, but multiple soundings were performed to compare results of different penetrometers in similar soils and evaluate soil conditions as distance from liquefaction features increased. Each test site will be discussed in more detail in the following sub-sections.

### IV.C.1 Yarbro Excavation

Yarbro (YARB) excavation is located between the Pemiscot Bayou and Arkansas Route 150, north of Blytheville. Figures IV.15 and IV.16 show the test site and location of the sounding respectively. The site is adjacent to a large sand excavation, which shows evidence of a sand blow in the vicinity of the SCPTu sounding. The site has been previously studied and dated by Tuttle and Schweig (1995) and Tuttle et al. (1996). The liquefaction features appear to date from 1400-1600 and from 1811-1812.

### IV.C.2 Bugg 40 (Haynes -307)

Bugg 40 (BUGG) is located off of Route 61, just south of the 150 Spur Split. Figures IV.17 and IV.18 show the test site and layout of the soundings respectively. Paleoliquefaction studies have been performed at this site, and are discussed in Tuttle et al. (1998). Two soundings were performed. The first (BUGG-01) was adjacent to a mapped liquefaction feature, and the second (BUGG-02) was located in an area of no liquefaction features. These liquefaction features have been dated to occur between 800-

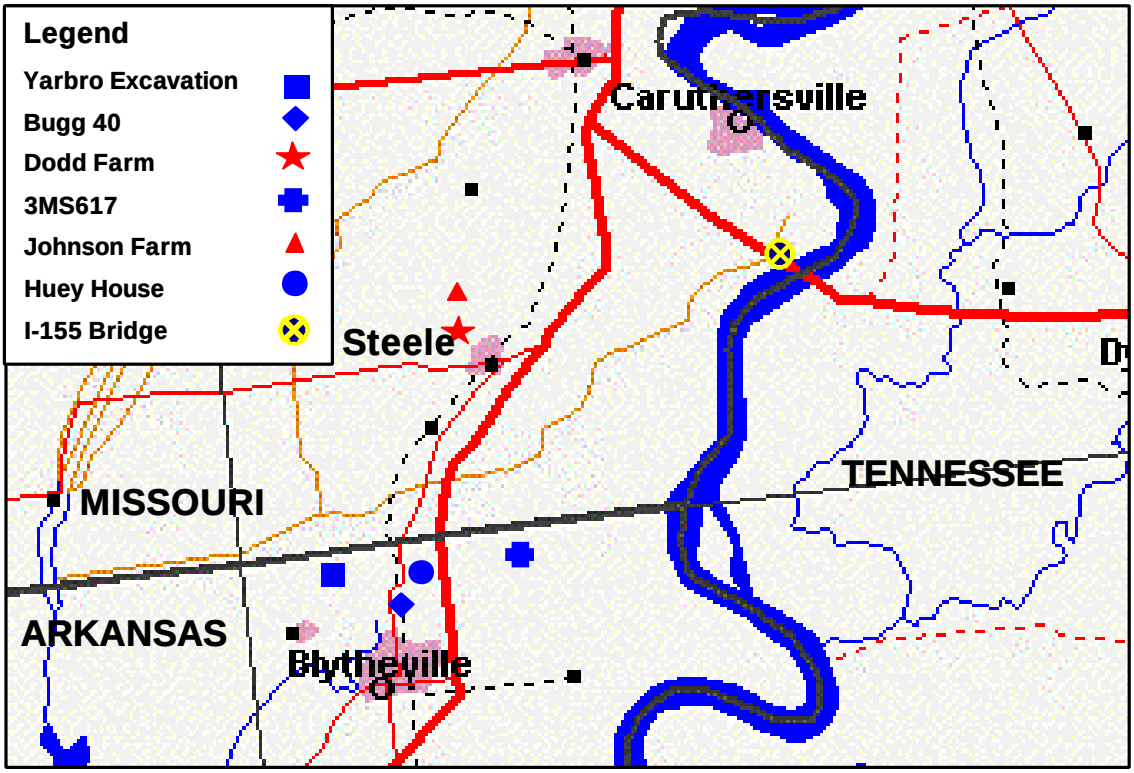


**Figure IV.14. Location of Test Sites in Northeast AR and Southeast MO**

**Figure IV.15. Yarbro excavation test site**

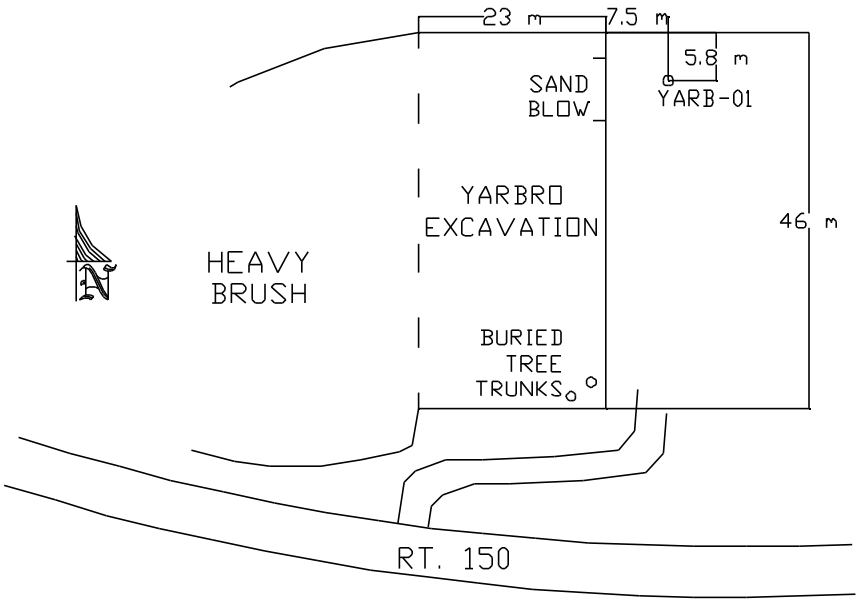


**Figure IV.16. Test layout at Yarbro excavation test site**

**Figure IV.17. Bugg 40 test site**

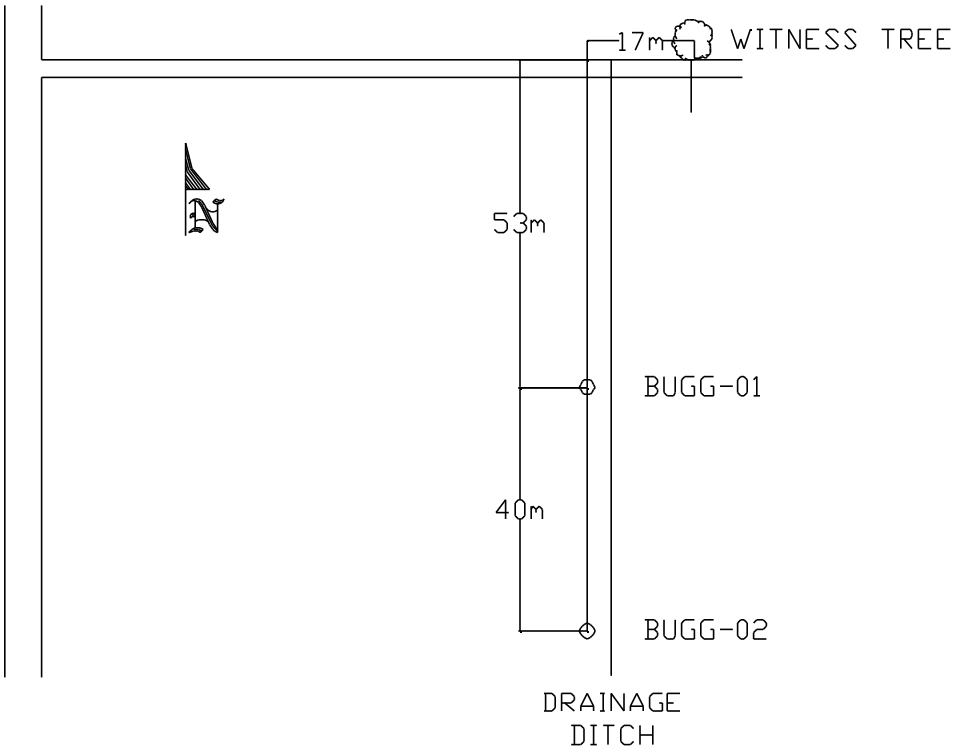


**Figure IV.18. Test layout at Bugg 40 test site**

1000 (Tuttle et al., 1998). Additional geophysical reconnaissance data is available at this site, and has been presented in Wolf et al. (1998) and Collier (1998).

### IV.C.3 3MS617 (Sigmund Site)

At the time of in-situ testing, an archeological dig and paleoliquefaction study were underway. Figures IV.19 and IV.20 show the test site and layout of the soundings respectively. Two trenches were being mapped, and surface artifacts were being collected for dating purposes. Three soundings were performed close to an approximately 1-meter wide sand blow. Dating of the site has not yet been completed, but the liquefaction feature adjacent to the test locations is believed to be an 1811-1812 feature (Schweig, 1998).

### IV.C.4 Huey House

The Huey House (HUEY) site is located on the south side of Route 150, north of Blytheville, AR. Figure IV.21 shows the test layout and the anticipated location of the paleoliquefaction study trench at this site. One sounding was performed at this site in the general area of a mapped sand blow. Previous studies date the liquefaction feature from between 880 and 1000 (Tuttle et al., 1998).

### IV.C.5 Johnson Farm

Johnson farm (JOHN) is located north of Steel Missouri, along the Pemiscot Bayou. Figure IV.22 shows the test layout and the location of 2 trenches from previous paleoliquefaction studies. One sounding was performed at this site in the general area of a mapped sand blow. Previous studies date the liquefaction feature from between 770 and 1200 (Tuttle et al., 1998).

**Figure IV.19. 3MS617 test site**

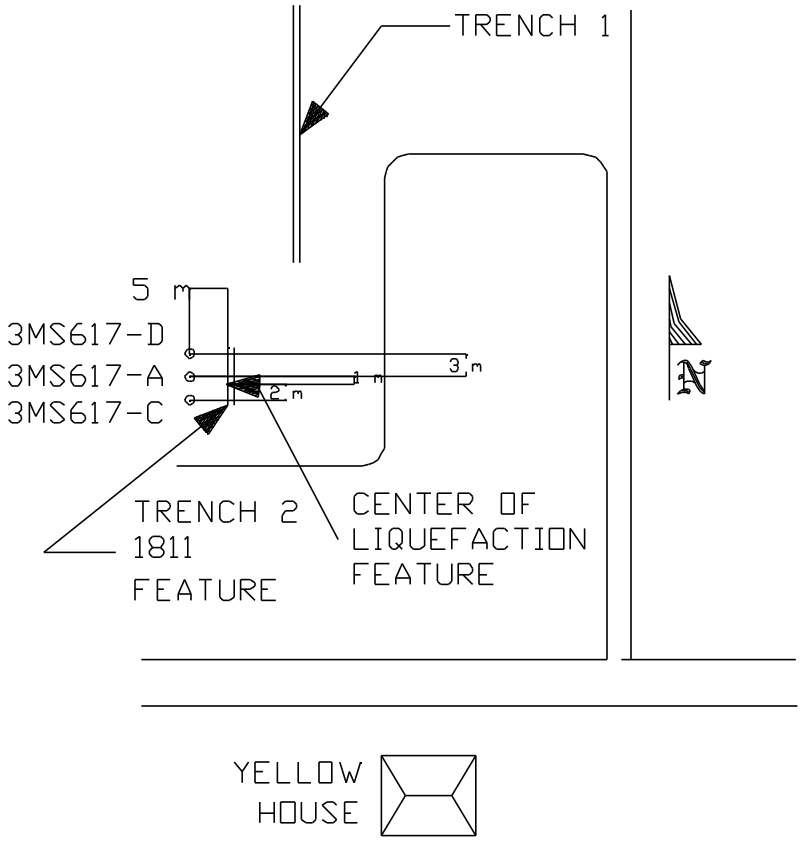


**Figure IV.20. Test layout at 3MS617 site**

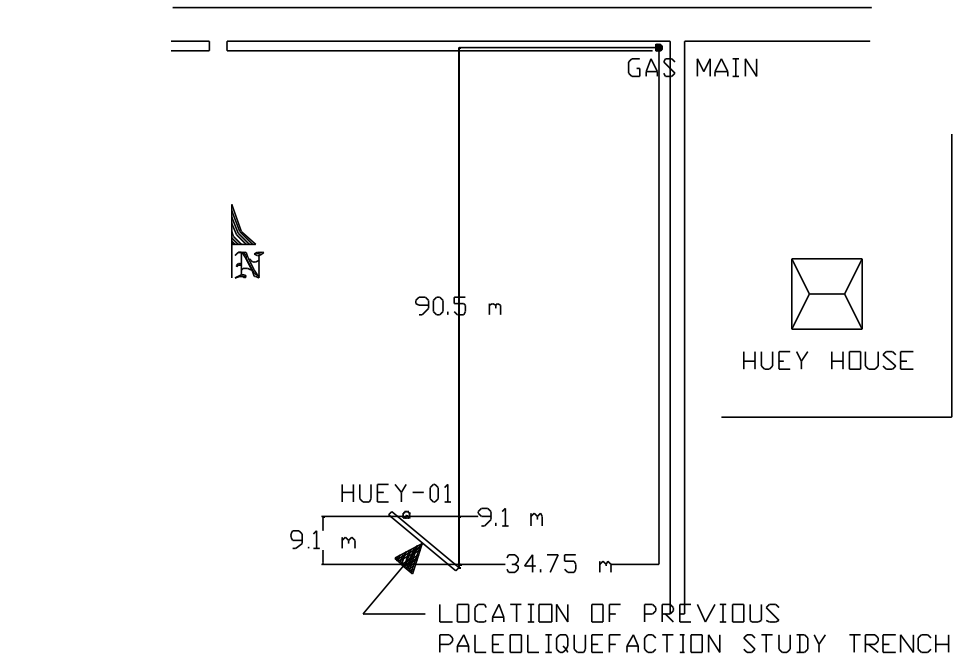


**Figure IV.21. Test layout at Huey House site**

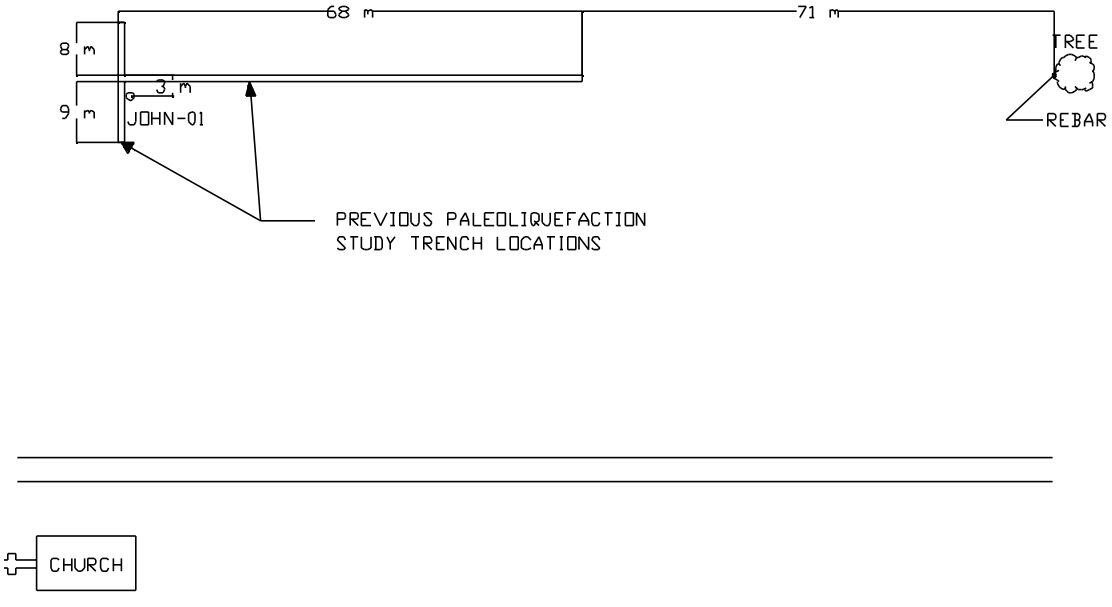


**Figure IV.22. Test layout at Johnson farm site**

## IV.C.6 Dodd Farm

Dodd farm (DODD) is located north of Steel Missouri, and south of the Johnson site. Figure IV.23 and IV.24 show the test site and layout of the soundings respectively. Three CPTu soundings were performed at this site, and 3 DMT soundings were performed adjacent to the CPTs at a later date. One of each test type (SCPTu, DODD-01; DMT, DODD-06) was performed in the general area of a previous paleoliquefaction study trench. A liquefaction feature is believed to have originated between 1400 and 1670 (Tuttle et al., 1998). Additional pairs of soundings were performed to analyze soil conditions at increasing distance from the liquefaction feature. Geophysical surveys have been performed at this site, and are reported in Collier (1998).

## IV.C.7 I-155 Bridge

This bridge is a key lifeline facility. It is the only major bridge crossing the Mississippi River between Memphis & St. Louis. A subsurface investigation and sesimic retrofit were performed on the Tennessee side of the river in 1994 (Woodward Clyde, 1994). This study herein was concerned with soil properties on the Missouri Side of the river. Seismic piezocones tests with pore pressure readings taken midface and behind the tip were performed during this study. Flat dilatometer tests were also performed at this site. Figure IV.25 displays the layout for testing performed at the I-155 bridge. Figure IV.26 displays a close up of tests between the third and fourth column set and Figure IV.27 is a photograph of the cone truck. Figure IV.28 displays a closeup of tests between the fourth and fifth column set, and Figure IV.29 presents a photograph of the dilatometer setup.

**Figure IV.23. Dodd farm test site**

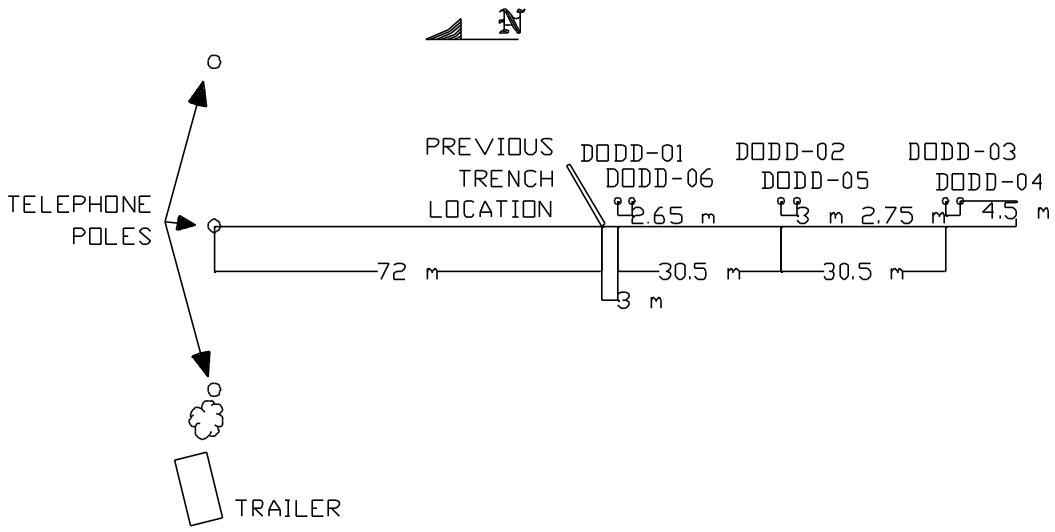


**Figure IV.24. Test layout at Dodd farm**

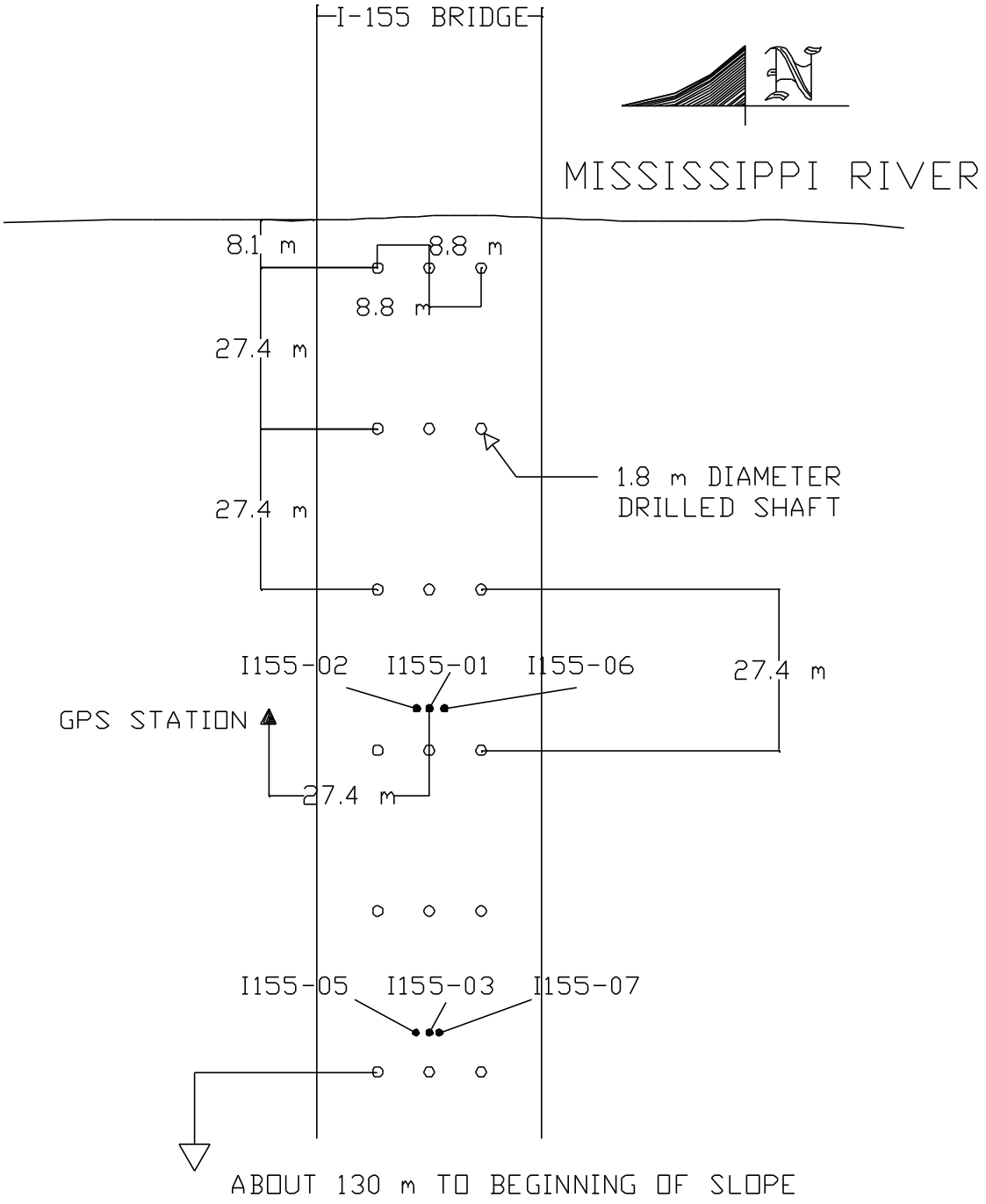


**Figure IV.25. Layout of all tests performed under the I-155 bridge**

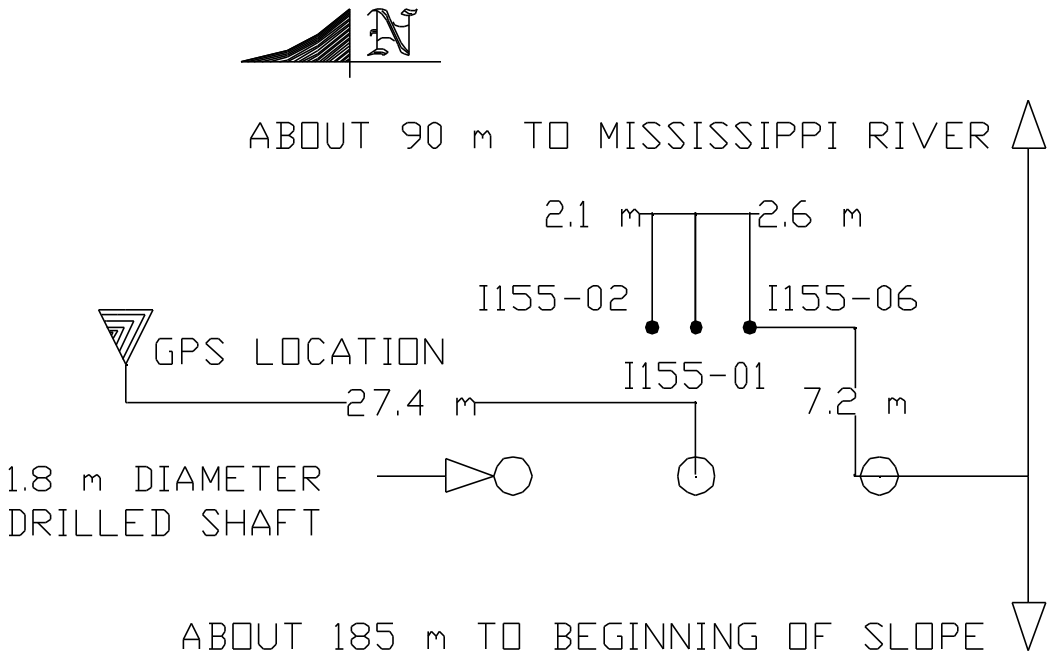


**Figure IV.26. Detailed layout of tests between third and fourth column set**

**Figure IV.27. Photograph of GT GeoStar Truck set up under I-155 Bridge**

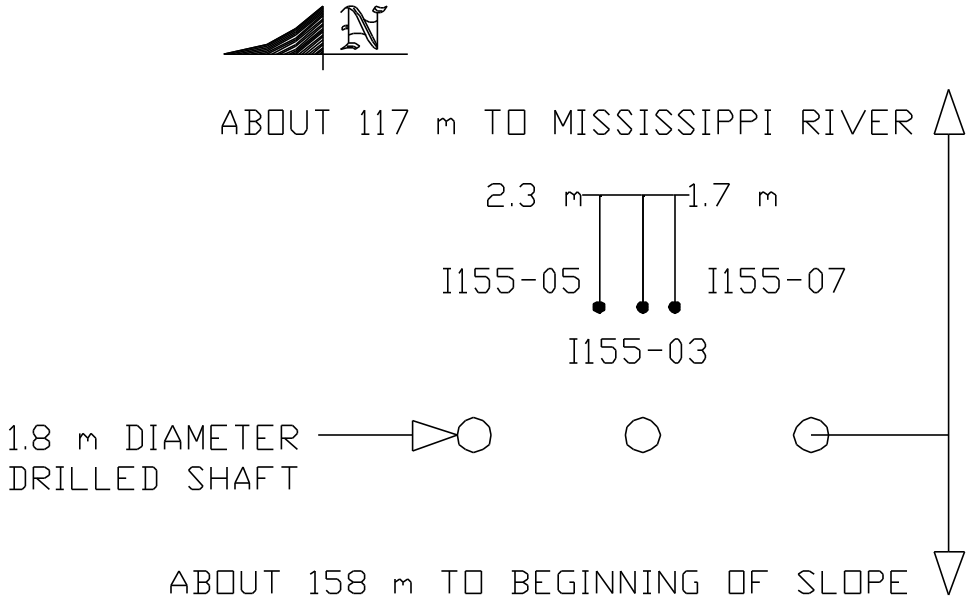


**Figure IV.28. Detailed layout of tests between fourth and fifth column set**

**Figure IV.29. Photograph of setup for Dilatometer Testing at I-155 Bridge**

## IV.D Charleston, S.C.

Soundings in Charleston, SC were performed at previously studied historic liquefaction sites (Clough & Martin, 1990; Martin & Clough, 1994). Liquefaction at these sites was expected to have occurred during the 1886 event, which had an epicenter about 15 miles northwest of Charleston near Sommerville and Middleton Place (Martin, 1990). Two sites were investigated with seismic piezocones performed at each. Figure 4.30 displays approximate site locations with reference to Charleston. In addition, Vibrocone soundings were performed at each site to test the feasibility of the initial pneumatic impulse generator as a tool for liquefaction evaluation (Schneider et al., 1999). Each test site will be described in more detail in the following subsections.

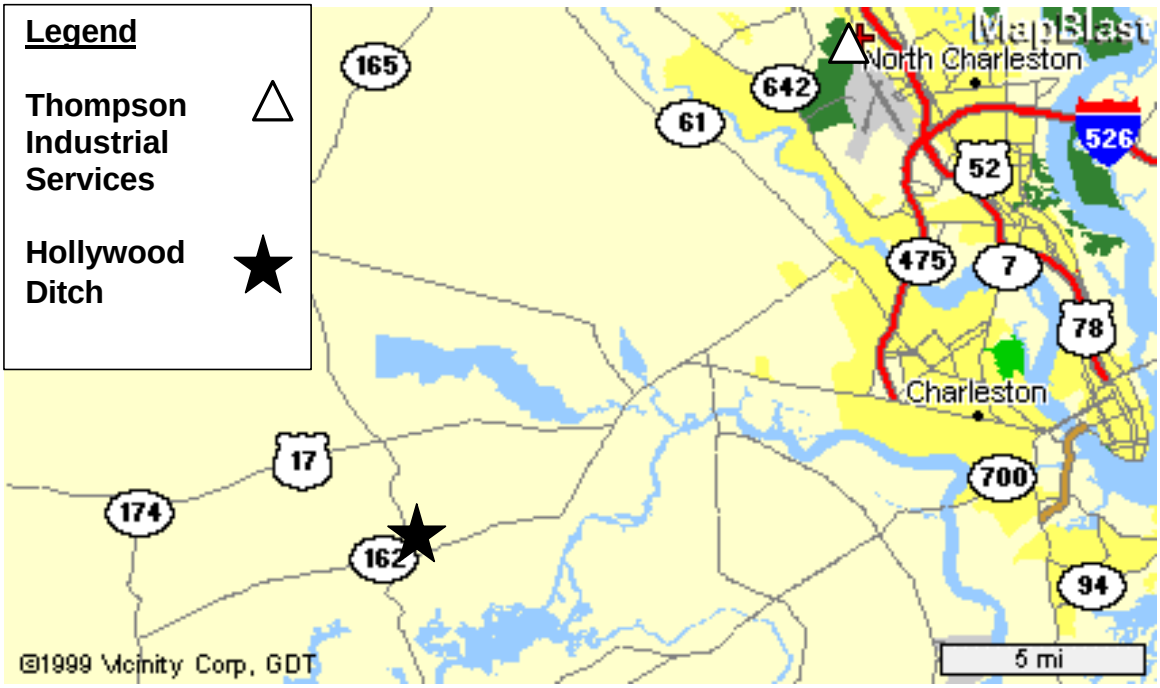


**Figure IV.30. Location of Test Sites in the Charleston, S.C. Area (www.mapblast.com)**

### IV.D.1 Hollywood Ditch

Hollywood Ditch (HW) was located in the town of Hollywood, SC and consisted of a series of drainage ditches running east-west and north-south (Martin, 1990). The section tested in this study was along an east-west trench, about 30 m east of State Rout 165. A soil boring (W-100) was located about 225 m west of S. R. 165, and a CPT sounding (CPT 0+515) was located about 250 m east along the drainage ditch (Martin, 1990). Extensive liquefaction was observed along the sides of the drainage ditches in this area as reported by Obermeir et al. (1986).

### IV.D.2 Thompson Industrial Services

Thompson Industrial Services (TIS) is a site located between the prior studied sites of Ten Mile Hill and Eleven Mile Post (Clough & Martin, 1990). The site consists of an open field which was wooded until recently. Figure IV.33 displays a photograph of the site, and Figure IV.34 presents a sounding layout map. While no surface evidence of liquefaction was noticed at this site, no studies were performed at this location. The site classifies as a non liquefy site, but it is located between two of the most severe areas of liquefaction from the Charleston, SC 1886 event (Martin, 1990). For analysis purposes, it is considered that liquefaction may have occurred in these soils.

**Figure IV.31. Hollywood Ditch Site**

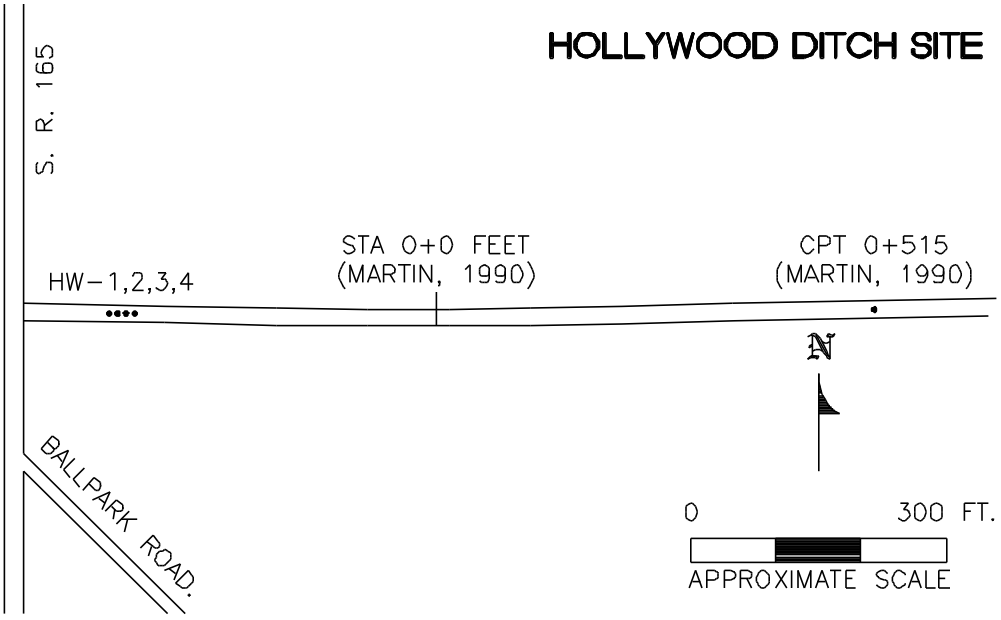


**Figure IV.32. Test layout at Hollywood Ditch test site**

**Figure IV.33. Thompson Industrial Services (TIS) Site**

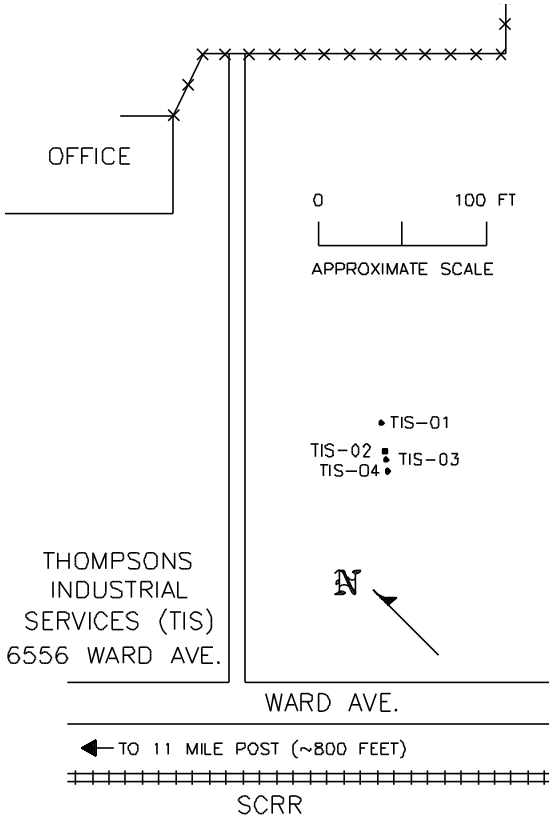


**Figure IV.34. Test layout at TIS site**

## REFERENCES


Alarcon-Guzman, A., Leonards, G.A., and Chameau, J.L. (1988). Undrained monotonic and cyclic strength of sands, *Journal of Geotechnical Engineering,* 114 (10), ASCE, pp. 1089-1108.

Ambraseys, N.N. (1988). Engineering seismology, *Earthquake Engineering and Structural Dynamics*, 17, pp. 1-105.

Andrus, R.D., and Stokoe, K.H. (1997). Liquefaction resistance based on shear wave velocity, *Proceedings*, Workshop on Evaluation of Liquefaction Resistance, NCEER-97-0022, Multidisciplinary Center for Earthquake Engineering Research, Buffalo, NY, pp. 89-128.

Andrus, R.D., Stokoe, K.H., and Chung, R.M. (1999). Draft guidelines for evaluating liquefaction resistance using shear wave velocity measurements and simplified procedures, *NISTIR 6277*, National Institute of Standards and Technology, Gaithersburg, MD, 121 pp.

Arango, I. (1996). Magnitude scaling factors for soil liquefaction evaluation, *Journal of Geotechnical Engineering*, 122 (11), ASCE, pp. 929-936.

Arango, I. (1997). Historical and continued role of the Standard Penetration Test method in geotechnical earthquake engineering, *Proceedings, 3rd Seismic Short Course on Evaluation and Mitigation of Earthquake Induced Liquefaction Hazards*, San Francisco, March 14.

Arias, A. (1970). A measure of earthquake intensity, *Seismic Design for Nuclear Power Plants*, MIT Press, Cambridge, MA.

Atkinson, G.M., and Boore, D.B. (1995). Ground-motion relations for eastern North America, *Bulletin of the Seismological Society of America*, 85, pp. 17-30.

Atkinson, G.M., and Boore, D.B. (1997). Some comparisons between recent ground-motions relations, *Seismological Research Letters*, 68 (1), pp. 24-40.

ASTM D422-63 (1999). *Standard Test Method for Particle-Size Analysis of Soils*, ASTM Section 4, Vol. 4.09 Soil and rock (1) D420-D4914.

ASTM D854-92 (1999). *Standard Test Method for Specific Gravity of Soils*, ASTM Section 4, Vol. 4.09 Soil and rock (1) D420-D4914.

ASTM D1586-98 (1999). *Standard Test Method for Penetration Testing and Spilt-Barrel Sampling of Soils*, ASTM Section 4, Vol. 4.09 Soil and rock (1) D420-D4914.

ASTM D4253-93 (1999). *Standard Test Methods for Maximum Index Density and Unit Weight of Soils Using a Vibratory Table*, ASTM Section 4, Vol. 4.09 Soil and rock (1) D420-D4914.

ASTM D4254-91 (1999). *Standard Test Method for Minimum Index and Unit Weight of Soils and Calculation of Relative Density*, ASTM Section 4, Vol. 4.09 Soil and rock (1) D420-D4914.

ASTM D4318-93 (1999). *Standard Test Method for Liquid Limit, Plastic Limit, and Plasticity Index of Soils*, ASTM Section 4, Vol. 4.09 Soil and rock (1) D420-D4914.

ASTM D4633-85 (1999). *Standard Method for Determination of Stress Wave Energy of Dynamic Penetrometer Systems*, ASTM Section 4, Vol. 4.09 Soil and rock (1) D420-D4914.

ASTM D5778-95 (1997). *Standard Test Method for Performing Electronic Friction Cone and Piezocone Penetration testing of Soils*, ASTM Section 4, Vol. 4.09 Soil and Rock (II).

ASTM D6066-96 (1996). *Standard Practice for Determining Normalized Penetration Resistance of Sands for Liquefaction Resistance Evaluation,* ASTM Section 4, Vol. 4.09 Soil and Rock (II).

Baldi, G., Bellotti, R., Ghionna, V.N., Jamiolkowski, M., and LoPresti, D.C.F. (1989). Modulus of sands from CPTs and DMTs, *Proceedings of the Twelfth International Conference on Soil Mechanics and Foundation Engineering*, Vol. 1, Rio de Janeiro, pp. 165-170.

Baldwin, K.C., deAlba, P.A., and Jones, A.N. (1990). Relationship between acoustic and mechanical properties of two marine clays, *Proceedings of the Conference on Shear Waves in Marine Sediments*, Kluwer Academic Publishers, Dordrecht . pp. 95.

Bates, C.R. (1989). Dynamic soil property measurements during triaxial testing, *Geotechnique*, 39(4), pp. 721-726.

Bauer, B. (1999). Shear wave velocity of geologic formations of the Mississippi River Valley, personal communication to Bob Herrmann, Illinois Geologic Society.

Been, K. (1999). The critical state line and its application to soil liquefaction, *Physics and Mechanics of Soil Liquefaction*, Balkema, Rotterdam, pp. 195-204.

Been, K., Crooks, J.H.A., Becker, D.E., and Jefferies, M.G. (1986). The cone penetration test in sands; part I, state parameter interpretations, *Geotechnique*, 36, pp. 239-249.

Been, K., and Jefferies, M.G. (1985). A state parameter for sands, *Geotechnique*, 35 (2), pp. 99-112.

Been, K., Jefferies, M.G., Crooks, J.H.A., and Rothenburg, L. (1987). The cone penetration test in sands: part II, general inference of state, *Geotechnique*, 37, pp. 285-299.

Been, K., Jefferies, M.G., and Hachey, J. (1991). The critical state of sands, *Geotechnique*, 41 (3), pp. 365-381.

Berry, K.M., Olson, S.M., and Lamie, M. (1998). Cone penetration testing in the Mid-Mississippi River Valley, *Geotechnical Site Characterization*, Vol. 2, Balkema, Rotterdam, pp. 983-987.

Bollinger, G.A. (1983). Speculation on the nature of seismicity at Charleston, South Carolina, *Studies Related to the Charleston, South Carolina, Earthquake of 1886 - Tectonics and Seismicity*, U.S. Geologic Survey Professional Paper 1313, pp. T1-T11.

Bollinger, G.A. (1977). Reinterpretation of the intensity data for the 1886 Charleston, South Carolina earthquake, *Studies Related to the Charleston, South Carolina, Earthquake of 1886, A Preliminary Report*, U.S. Geologic Survey Professional Paper 1028, pp. 17-32.

Boore, D.B. (1996). SMSIM - Fortran program for simulating ground motions from earthquakes: version 1.0, *USGS Open File Report 96-80-A.*

Boore, D.B., and Joyner, W.B. (1991). Estimation of ground motion at deep soil sites in eastern North America, *Bulletin of the Seismological Society of America*, 81(6), pp. 2167-2185.

Boulanger, R.W., Mejia, L.H., and Idriss, I.M. (1997). Liquefaction at Moss Landing during the Loma Prieta earthquake, *Journal of Geotechnical and Geoenvironmental Engineering*, 123 (5), ASCE, pp. 453-467.

Broms, B.B., and Flodin, N. (1988). History of soil penetration testing, *Penetration Testing 1988*, ISOPT-1, Balkema, Rotterdam, pp. 157-220.

BS 1377 (1990)., Standard test method for Fall Cone method, *British Standards*, Part 1 & 2.

Campanella, R.G. (1994). Field methods for dynamic geotechnical testing: an overview of capabilities and needs, *Dynamic Geotechnical Testing II*, ASTM STP 1213, Philadelphia, pp. 3-23.

Campanella, R.G., Gillespie, D., and Robertson, P.K. (1982). Pore pressures during cone penetration, *Proceedings 2nd European Symposium on Penetration Testing*, Vol. 2, Amsterdam, pp. 507-512.

Campanella, R.G., and Robertson, P.K. (1988). Current status of the piezocone test, *Penetration Testing 1988*, Balkema, Rotterdam, pp. 93-116.

Campanella, R.G., Robertson, P.K., and Gillespie, D. (1986). Seismic cones penetration tests, *Use of In-Situ Tests in Geotechnical Engineering*, ASCE GSP 6, pp. 116-130.

Casagrande, A. (1936). Characteristics of cohesionless soils affecting the stability of slopes and earth fills, *Contributions to Soil Mechanics*, Boston Society of Civil Engineers, 1940, pp. 257 - 276.

Castro, G. (1969). Liquefaction of sands, *Harvard Soil Mechanics Series 87*, Harvard University, Cambridge, Massachusetts.

Chang, F.K., and Krinitzsky, E.L. (1977). Duration, spectral content, and predominant period of strong motion earthquake records from western United States, *Miscellaneous Paper 5-73-1*, U.S. Army Corps of Engineers Waterways Experiment Station, Vicksburg.

Chen, B.S., and Mayne, P.W. (1994). Profiling the overconsolidation ratio of clays by piezocone tests, *Report No. GIT-CEEGEO-94-1*, School of Civil and Environmental Engineering, Georgia Institute of Technology, Atlanta, GA, 279 pp.

Chameau, J.-L., A., Clough, G.W., Frost, J.D., and Reyna, F.A.M. (1998). Liquefaction characteristics of the San Francisco bayshore fills, *The Loma Prieta Earthquake of October17, 1989 – Liquefaction*, United States Geologic Survey Professional Paper 1551-B, pp. 9-24.

Clough, G.W., and Martin, J.R., II. (1990). Geotechnical setting for liquefaction events in the Charleston, South Carolina Vicinity, *Proceedings H.B. Seed Memorial Symposium*, Vol. 2, BiTech Publishers, Vancouver, B.C.

Collier, J.W. (1998). *Geophysical Investigations of Liquefaction Features in the New Madrid Seismic Zone: Northeastern Arkansas and Southeastern Missouri*, M.S. Thesis, Auburn University, Auburn, AL, 163 pp.

Cunning, J.C., Robertson, P.K., and Sego, D.C. (1995). Shear wave velocity to evaluate in-situ state of cohesionless soils, *Canadian Geotechnical Journal*, 32, pp. 848-858.

Darendeli, M.B., (1997). Dynamic properties of soils subjected to 1994 Northridge earthquake, *MS Thesis*, School of Civil Engineering, The University of Texas at Austin, Austin, TX, 605 pp.

Decourt, L., Muromachi, T., Nixon, I.K., Schmertmann, J.H., Thorburn, S., and Zolkov, E. (1988). Standard penetration test (SPT): International reference test procedure, *Penetration Testing 1988, ISOPT-1*, Vol. 1, Balkema, Rotterdam, pp. 3-26.

Desrues, J., Chambon, R., Mokni, M., and Mazerolle, F. (1996). Void ratio evolution inside shear bands in triaxial sand specimens studied by computed tomography, *Geotechnique*, 46 (3), pp. 123-132.

Dobry, R., Elgamal, A.-W., and Bazair, M. (1989). Pore pressure and acceleration response of Wildlife site during the 1987 Earthquake, *Proceedings from the Second U.S.-Japan Workshop on Liquefaction, Large Ground Deformation and their Effects on Lifelines*, NCEER-89-0032, Multidisciplinary Center for Earthquake Engineering Research, Buffalo, NY, pp. 145-160.

Dobry, R., Ladd, R.S., Yokel, F.Y., Chung, R.M., and Powell, D. (1982). Prediction of pore water pressure buildup and liquefaction of sands during earthquakes by the cyclic strain method, *NBS Building Science Series 138*, National Bureau of Standards, Gaithersburg, MD, 150 pp.

Douglas, B.J., and Olsen, R.S. (1981). Soil classification using electric cone penetrometers, *Cone Penetration Testing and Experience*, ASCE, pp. 209-227.

Dutton, C.E. (1889). The Charleston earthquake of August 31, 1886, *U.S. Geologic Survey Annual Report, 1887-1888*, pp. 203-528.

Elgamal, A.-W., Zeghal, M., Parra, E., Gunturi, R., Tang, H.Y., and Stepp, J.C. (1996). Identification and modeling of earthquake ground response - I. Site amplification, *Soil Dynamics and Earthquake Engineering*, 15, pp. 499-522.

Fam, M., and Santamarina, J.C. (1997). A study of consolidation using mechanical and electromagnetic waves, *Geotechnique*, 47 (2), pp. 203 - 219.

Farrar, J.A. (1998). Summary of Standard Penetration Test (SPT) energy measurement experience, *Geotechnical Site Characterization*, Vol. 2, Balkema, Rotterdam, pp. 919-926.

Fear, C.E., and Robertson, P.K. (1995). Estimation of the undrained shear strength of sand: a theoretical framework, *Canadian Geotechnical Journal*, 32, pp. 859-870.

Finn, W.D.L., Lee, K.W., and Martin, G.R. (1977). An effective stress based model for liquefaction, *Journal of Geotechnical Engineering Division*, ASCE, 103 (GT6), pp. 517-533.

Frankel, A., Mueller, C., Barnhard, T., Perkins, D., Leyendecker, E.V., Dickman, N., Hanson, S., and Hopper, M. (1996). National Seismic-Hazard Maps: Documentation June 1996, *USGS Open-File report 96-532.*

Frost, J.D., Chameau, J.-L.A., Reyna, F.A.M., and Karanikolas, P. (1993). Performance of fill soils during the Loma Prieta earthquake, *Proceedings*, Third International Conference on Case Histories in Geotechnical Engineering, Vol. 3, St. Louis, pp. 541-546.

Frost, J.D., Chen, C.-C., Park, J.-Y., and Jang, D.-J. (1999). Quantitative characterization of microstructure evolution, *Physics and Mechanics of Soil Liquefaction*, Balkema, Rotterdam, pp. 169 - 177.

Garcia, S. R. (1991). *Interrelationship Between the Initial Liftoff and Extended Pressure Readings of the Marchetti Flat Blade Dilatometer in Soils*, M.S. Thesis, Georgia Institute of Technology, Atlanta, GA, 119 pp.

Gohn, G.S., Houser, B.B., and Schneider, R.R. (1983). Geology of the lower mesozoic sedimentary rocks in Clubhouse Crossroads test hole #3, near Charleston, South Carolina, *Studies Related to the Charleston, South Carolina, Earthquake of 1886 - Tectonics and Seismicity*, U.S. Geologic Survey Professional Paper 1313, pp. D1-D17.

Green, R.K., Cooling, T.L., Mejia, L.H., and Abrahamson, N.A. (1995). Earthquake motions and seismic evaluation of Cape Girardeau bridge, *Lifeline Earthquake Engineering,* ASCE, pp. 517-524.

Gutenberg, B., and Richter, C.F. (1956). Magnitude and energy of earthquakes, *Annali di Geofisica*, 9 (1), pp. 2825-2852.

Hardin, B.O., and Drnevich, V.P. (1972). Shear modulus and damping in soils: design equations and curves, *Journal of the Soil Mechnaics and Foundation Division*, 94(2), ASCE, pp. 353-368.

Hegazy, Y.A., and Mayne, P.W. (1995). Statistical correlations between shear wave velocity and cone penetration data for different soil types, *Proceedings, International Symposium on Cone Penetration Testing (CPT '95)*, Vol. 2, Swedish Geotechnical Society Report No. 3:95, Linkoping, pp. 173-178.

Herrmann, R.B. (1999). Personal Communication, April (Department of Earth and Atmospheric Sciences, St. Louis University, St. Louis, MO).

Herrmann, R.B., and Akinci, A. (1999). Mid-America Ground Motion Models, http://www.eas.slu.edu/People/RBHerrmann/MAEC/maecgnd.html, Department of Earth and Atmospheric Sciences, Saint Louis University, St. Louis, MO, 63103, 8 pp.

Herrmann, R.B., Ortega, R., and Akinci, A. (1999). Mid-America probabilistic hazard maps, http://www.eas.slu.edu/People/RBHerrmann/HAZMAP/hazmap.html , Department of Earth and Atmospheric Sciences, Saint Louis University, St. Louis, MO, 63103, 5 pp.

Holzer, T.L., Youd, T.L., and Hanks, T.C. (1989). Dynamics of liquefaction during the 1987 Superstition Hills, California, earthquake, *Science*, 244, pp. 56-59.

Hoyos, L.R. Jr., Sheppard, B., Shao, Y., and Macari, E.J. (1999). Results of resonant column testing program performed on sands from Memphis, TN, and West Memphis, AR, *Interim Report, MAEC Project No. GT-1, Dynamic Properties of Mid-American Soils*, April, pp. 17.

Hryciw, R.D., and Thomann, T.G. (1993). Stress-history-based model for $G^e$ of cohesionless soils, *Journal of Geotechnical Engineering*, 119 (7), ASCE, pp. 1073-1093.

Idriss, I.M. (1985). Evaluating seismic risk in engineering practice, , *11th International Conference on Soil Mechanics and Foundation Engineering*, Vol. 1, Balkema, Rotterdam, pp. 255-320.

Idriss, I.M. (1991). Response of soft sites during earthquake, *H. Bolton Seed Memorial Symposium*, Vol. 2, BiTech Publishers, Ltd., Vancouver, pp. 273-289.

Idriss, I.M. (1999). An update of the Seed-Idriss simplified procedure for evaluating liquefaction potential, *Presentation Notes*, Transportation Research Board '99 Workshop on New Approaches to Liquefaction Analysis, Washington D.C., January 10, 21 pp.

Idriss, I.M., Lysmer, J., Hwang, R., and Seed, H.B. (1973). QUAD4 – A computer program for evaluating the seismic response of soil structures by variable damping finite element procedures, *Report No. EERC 73-16*, Earthquake Engineering Research Center, University of California, Berkeley, CA, 67 pp.

Idriss, I.M., and Sun, J.I. (1992). *User's manual for SHAKE91, A computer program for conducting equivalent linear seismic response analysis of horizontally layered soil deposits*, Center for Geotechnical Modeling, Department of Civil & Environmental Engineering, University of California, Davis, August.

Indridason, J.K. (1992). Strain based evaluation of liquefaction during the 1886 Charleston earthquake, *Research Project*, School of Civil and Environmental Engineering, Georgia Institute of technology, Atlanta, GA, 158 pp.

Ishibashi, I. (1992). Discussion to, Effect of soil plasticity on cyclic response, *Journal of Geotechnical Engineering*, 118 (5), ASCE, pp. 830-832.

Ishihara, K. (1985). Stability of natural deposits during earthquakes, *Proceedings, 11th International Conference on Soil Mechanics and Foundation Engineering*, Vol. 1, Balkema, Rotterdam, pp. 321-376.

Ishihara, K. (1993). Liquefaction and flow failures during earthquakes, *Geotechnique*, 43 (3), pp. 351-415.

Ishihara, K., Anazawa, Y., and Kuwano, J. (1987). Pore water pressures and ground motions monitored during the 1985 Chiba-Ibaragi earthquake, *Soils and Foundations*, 27 (3), pp. 13-30.

Ishihara, K., Shimizu, K., and Yamada, Y. (1981). Pore water pressures measured in sand deposits during an earthquake, *Soils and Foundations*, 21 (4), pp. 85-100.

Jamiolkowski, M., Baldi, G., Bellotti, R., Ghionna, V., and Pasqualini, E. (1985a). Penetration resistance and liquefaction of sands, *Proceedings Eleventh International Conference on Soil Mechanics and Foundation Engineering*, Vol. 4, Balkema, Rotterdam, pp. 1891-1896.

Jamiolkowski, M., Ladd, C.C., Germaine J.T., and Lancellotta, R. (1985b). New developments in field and laboratory testing of soils, *Proceedings Eleventh International Conference on Soil Mechanics and Foundation Engineering*, Vol. 1, Balkema, Rotterdam, pp. 57-153.

Jefferies, M.G. (1999). A critical view of liquefaction, *Physics and Mechanics of Soil Liquefaction*, Balkema, Rotterdam, pp. 221-235.

Johnston, A.C., and Schweig, E.S. (1996). The enigma of the New Madrid earthquakes of 1811-1812, *Annual Review of Earth and Planetary Sciences*, 24, pp. 339-384.

Jones, G., and Rust, E. (1982). Piezometer penetration testing, *Proceedings 2nd European Symposium on Penetration Testing*, Vol. 2, Amsterdam, pp. 607-613.

Kavazanjian, E. (1999). Personal Communication, January (GeoSyntec, Hunnington Beach, CA).

Kayen, R.E., and Mitchell, J.K. (1997). Assessment of liquefaction potential during earthquakes by Arias intensity, *Journal of Geotechnical and Geoenvironmental Engineering*, ASCE, 123 (12), pp. 1162-1174.

Kayen, R.E., Mitchell, J.K., Seed, R.B., Lodge, A., Nishio, S., and Coutinho, R. (1992). Evaluation of SPT, CPT, and shear wave velocity based methods for liquefaction potential assessment using Loma Prieta data, *Proceedings 4th Japan-U.S. Workshop on Earthquake Resistance Design of Lifeline Facilities and Countermeasures for Soil Liquefaction*, NCEER-92-0019, Buffalo, NY, pp. 177-192.

Keane, C.M., and Prevost, J.H. (1989). An analysis of earthquake data observed at the Wildlife liquefaction array site, Imperial County, California, *Proceedings from the Second U.S.-Japan Workshop on Liquefaction, Large Ground Deformation and their Effects on Lifelines*, NCEER-89-0032, Multidisciplinary Center for Earthquake Engineering Research, Buffalo, NY, pp. 176-192.

Konrad, J.M. (1988). Interpretation of Flat Plate Dilatometer Tests in Sands in Terms of the State Parameter, *Geotechnique*, 38 (2), pp. 263-277.

Kramer, S.L. (1996). *Geotechnical Earthquake Engineering*, Prentice Hall, Upper Saddle River, NJ, 653 pp.

Kulhawy, F.H., and Mayne, P.W. (1990). Manual on estimating soil properties for foundation design, *Report EL-6800*, Electric Power Research Institute, Palo Alta, CA, August, 306 pp.

Kuo, C.-Y., and Frost, J.D. (1997). Initial fabric and uniformity of a sand specimen - an image analysis approach, *Mechanics of Deformations and Flow of Particulate Materials*, ASME-ASCE-SUS Joint Summer Meeting, pp. 214-227.

Ladd, R.S., Dobry, R., Dutko, P., Yokel, F.Y., and Chung, R.M. (1989). Pore-water pressure buildup in clean sands because of cyclic straining, *Geotechnical Testing Journal*, 12 (1), ASTM, pp. 77-86.

Lambe, T.W., and Whitman, R.V. (1969). *Soil Mechanics*, John Wiley & Sons, New York, 553 pp.

Lee, K.L., and Seed, H.B. (1967). Drained strength characteristics of sands, *Journal of the Soil Mechanics and Foundation Division*, 93 (SM6)., ASCE, pp. 117-141.

Lee, M.K.W., and Finn, W.D.L. (1978). DESRA-2: Dynamic effective stress response analysis of soil deposits with energy transmitting boundary including assessment of liquefaction potential, *Soil Mechanics Series No. 38*, Department of Civil Engineering, University of British Columbia, Vancouver, June, 57 pp.

Liao, S.S.C., and Whitman, R.V. (1986). Overburden correction factors for SPT in sand, *Journal of Geotechnical Engineering*, 112 (3), ASCE, pp. 373-377.

Liu, H.-P., Hu, Y., Dorman, J., Chang, T.-S., and Chiu, J.-M. (1997). Upper Mississippi embayment shallow seismic velocities measured in situ, *Engineering Geology*, 46, pp. 313-330.

Lunne, T., Eidsmoen, T., Gillespie, D., and Howland, J.D. (1986). Laboratory and field evaluation of cone penetrometers, *Use of In-Situ Tests in Geotechnical Engineering*, ASCE GSP 6, pp. 714-729.

Lunne, T., Robertson, P.K., Powell, J.J.M. (1997). *Cone Penetration Testing in Geotechnical Practice*, Blackie Academic & Professional, New York, 312 pp.

Marchetti, S. (1980). In-Situ Tests by Flat Dilatometer, *Journal of Geotechnical Engineering*, 106 (GT3), pp. 299-321.

Martin, J.R. (1990). Implications from a geotechnical investigation of liquefaction phenomena associated with seismic events in the Charleston, SC area, *Ph.D. Thesis*, School of Civil Engineering, Virginia Polytechnic and State University, Blacksburg, VA, 414 pp.

Martin, J.R. II., and Clough, G.W. (1994). Seismic parameters from liquefaction evidence, *Journal of Geotechnical Engineering*, 120 (8), ASCE, pp. 1345-1361.

Masood, T., and Mitchell, J.K. (1993). Estimation of in-situ lateral stresses in soil by cone penetration tests, *Journal of Geotechnical Engineering*, 119 (10), ASCE, pp. 1624-1639.

Mayne, P.W. (1991). Tentative method for estimating $\sigma_{ho}$' from $q_c$ data in sands, *Calibration Chamber Testing*, ISSOCT-1, Elsevier, New York, pp. 249-256.

Mayne, P.W. (1995). CPT determination of overconsolidation ratio and lateral stresses in clean quartz sands, *Proceedings, International Symposium on Cone Penetration Testing (CPT '95)*, Vol. 2, Swedish Geotechnical Society Report No. 3:95, Linkoping, pp. 215-220.

Mayne, P.W., and Kulhawy, F.H. (1982). $K_o$ - OCR relationships in soil, *Journal of Geotechnical Engineering Division*, 108 (GT6), pp. 851-872.

Mayne, P.W., and Kulhawy, F.H. (1991). Calibration chamber database and boundary effects correction for CPT data, *Calibration Chamber Testing*, Elsevier, New York, pp. 257-264.

Mayne, P.W., Kulhawy, F.H., and Kay, J.N. (1990). Observations on the development of pore-water stresses during piezocone penetration in clays, *Canadian Geotechnical Journal*, 27 (4), pp. 418-428.

Mayne, P.W., Mitchell, J.K., Auxt, J.A., and Yilmaz, R. (1995). U.S. National Report on CPT, *Proceedings, International Symposium on Cone Penetration Testing (CPT '95)*, Vol. 1, Swedish Geotechnical Society Report No. 3:95, Linkoping, pp. 263-276.

Mayne, P.W., and Rix, G.J. (1993). $G_{max}$ - $q_c$ relationships for clays, *Geotechnical Testing Journal*, 16 (1), ASTM, pp. 54-60.

Mayne, P.W., and Rix, G.J. (1995). Correlations between shear wave velocity and cone tip resistance in natural clays, *Soils and Foundations*, 35 (2), pp. 107-110.

Mayne, P.W., Schneider, J.A., and Martin, G.K. (1999). Small- and large-strain soils properties from seismic flat dilatometer tests, *Proceeding*, Pre-failure deformation characteristics of geomaterials, Torino '99, Balkema, Rotterdam, 8 pp.

Mitchell, J.K., and Brandon, T.L. (1998). Analysis and use of CPT in earthquake and environmental engineering, *Geotechnical Site Characterization*, Vol. 1, Balkema, Rotterdam, pp. 69-97.

NCEER (1997). Summary report, *Proceedings*, Workshop on Evaluation of Liquefaction Resistance, NCEER-97-0022, Multidisciplinary Center for Earthquake Engineering Research, Buffalo, NY, pp. 1-40.

Newmark, N.M., and Hall, W.J. (1982). Earthquake spectra and design, *EERI Monograph*, Earthquake Engineering Research Institute, Berkeley, CA, 103 pp.

Norton, W.E. (1983). In-situ determination of liquefaction potential using the PQS probe, *Technical Report GL-83-1*, U.S. Army Corps of Engineers, Waterways Experiment Station, Vicksburg, MS, 101 pp.

Nuttli, O.W., and Brill, K.G. Jr. (1981). 1981, Catalog of central United States earthquakes since 1800 of $m_b \geq 3.0$, Part II and Appendix B-2: in Barstow, N.L., K.G. Brill Jr., O.W. Nuttli and P.W. Pomeroy, *An Approach to Seismic Zonation for Siting Nuclear Electric Power Generating Facilities in the Eastern United States*, NUREG/CR-1577, U.S. Nuclear Regulatory Commission, Washington, D.C., p. 97-143, B2-1-B2-31, 4 plates (#411).

Nuttli, O.W., and Herrmann, R.B. (1984). Ground motion of Mississippi Valley earthquakes, *Journal of Technical Topics in Civil Engineering*, 110 (1), ASCE, pp. 54-69.

Obermeier, S.F., Jacobson, R.B., Powars, D.S., Weems, R.E., Hallbick, D.C., Gohn, G.S., and Markewich, H.W. (1986). Holocene and late Pleistocene earthquake-induced sand blows in coastal South Carolina, *Proceedings*, 3rd U.S. National Earthquake Engineering Conference, Charleston, S.C, pp. 197-208.

Olsen, R.S. (1984). Liquefaction analyses using the cone penetration test, *Proceedings of the 8th World Conference of Earthquake Engineering*, Vol. 3, pp. 247-254.

Olsen, R.S. (1988). Using the CPT for dynamic site response characterization, *Earthquake Engineering and Soil Dynamics II*, ASCE GSP 21, pp. 374-388.

Olsen, R.S. (1994). *Normalization and prediction of geotechnical properties using the cone penetration test (CPT)*, Technical Report GL-94-29, U.S. Army Corps of Engineers, Vicksburg, August, 292 pp.

Olsen, R.S. (1997). Cyclic liquefaction based on the cone penetrometer test, *Proceedings*, Workshop on Evaluation of Liquefaction Resistance, NCEER-97-0022, Multidisciplinary Center for Earthquake Engineering Research, Buffalo, NY, pp. 225-276.

Olsen, R.S., and Mitchell, J.K. (1995). CPT stress normalization and prediction of soil classification, *Proceedings, International Symposium on Cone Penetration Testing (CPT '95)*, Vol. 2, Swedish Geotechnical Society Report No. 3:95, Linkoping, pp.

Olson, S.M. (1997). Liquefaction shear strength of granular soils, *Preliminary Proceedings of the Workshop: Post-Liquefaction Shear Strength of Granular Soils*, NSF CMS-95-31678, Urbana, Illinois, pp. 123-146.

Olson, S.M., and Stark, T.D. (1998). CPT based liquefaction resistance of sandy soils, *Geotechnical Earthquake Engineering and Soil Dynamics III*, ASCE GSP 75, pp. 325-336.

Pond, E. C. (1996). Seismic parameters for the central United States based on paleoliquefaction evidence in the Wabash Valley, *Ph.D. Thesis*, School of Civil and Environmental Engineering, Virginia Polytechnic and State University.

Poulos, S.J. (1981). The steady state of deformations, *Journal of the Geotechnical Engineering Division*, 107 (GT5), ASCE, pp. 553-562.

Poulos, S.J., Castro, G., and France, J.W., (1985). Liquefaction evaluation procedure, *Journal of Geotechnical Engineering*, 111 (6), ASCE, pp. 772-792.

Reyna, F., and Chameau, J.L. (1991). Dilatometer based liquefaction potential of sites in the Imperial Valley, *Proceedings*, Second International Conference on Recent Advances

in Geotechnical Earthquake Engineering and Soil Dynamics, Vol. 1, St. Louis, pp. 385-392.

Risk Engineering (1994). Seismic hazard evaluation and multiple-support artificial ground motions for the A-1700 bridge, Pemiscot County, Missouri, Dyer County, Tennessee, *Report*, prepared for Sverdrup Civil Inc., Maryland Heights, Missouri, 63043, 146 pp.

Rix, G.J., and Stokoe, K.H. (1991). Correlation of initial tangent modulus and cone penetration resistance, *Calibration Chamber Testing*, ISSOCT-1, Elsevier, New York, pp. 351-362.

Robertson, P.K. (1990). Soil classification using the cone penetration test, *Canadian Geotechnical Journal*, 27 (1), pp. 151-158.

Robertson, P.K., and Campanella, R.G. (1983). Interpretation of cone penetrometer test: Part I: Sand, *Canadian Geotechnical Journal*, 20 (4), pp. 718-733.

Robertson, P.K., and Campanella, R.G. (1983). Interpretation of cone penetrometer test: Part II: Clay, *Canadian Geotechnical Journal*, 20 (4), pp. 734-745.

Robertson, P.K., and Campanella, R.G. (1985). Liquefaction potential of sands using the CPT, *Journal of Geotechnical Engineering*, 111 (3), ASCE, pp. 384-403.

Robertson, P.K., Campanella, R.G., Gillespie, D., and Greig, J. (1986). Use of piezomenter cone data, *Use of In-Situ Tests in Geotechnical Engineering*, ASCE GSP 6, pp. 1263-1280.

Robertson, P.K., Sasitharan, S., Cunning, J.C., and Sego, D.C. (1995). Shear-wave velocity to evaluate in-situ state of Ottawa sand, *Journal of Geotechnical Engineering*, 121 (3), ASCE, pp. 262-273.

Robertson, P.K., Woeller, D.J., and Finn, W.D.L. (1992a). Seismic cone penetration test for evaluating liquefaction potential under cyclic loading, *Canadian Geotechnical Journal*, 29, pp. 686-695.

Robertson, P.K., Woeller, D.J., Kokan, M., Hunter, J., and Luternaur, J. (1992b). Seismic techniques to evaluate liquefaction potential, *45th Canadian Geotechnical Conference*, Toronto, Ontario, October 26-28, pp. 5:1-5:9.

Robertson, P.K., and Wride (Fear), C.E. (1997). Cyclic liquefaction and its evaluation based on the SPT and CPT, *Proceedings*, Workshop on Evaluation of Liquefaction Resistance, NCEER-97-0022, Multidisciplinary Center for Earthquake Engineering Research, Buffalo, NY, pp. 41-88.

Robertson, P.K., and Wride, C.E. (1998). Evaluating cyclic liquefaction potential using the cone penetration test, *Canadian Geotechnical Journal*, 35 (3), pp. 442-459.

Rowe, P.W. (1964). The stress dilatency relations for static equilibrium of an assembly of particles in contact, *Proceedings*, Royal Society, London, Series A, Vol. 269, pp. 500-527.

Roy, D., Campanella, R.G., Byrne, P.M., and Hughes, J.M.O. (1997). Strain level and uncertainty of liquefaction related index tests, *Uncertainty in the Geologic Environment: From Theory to Practice*, Vol. 2, GSP 58, ASCE, New York, pp. 1149-1162.

Samiezade-Yazd, M., Herrmann, R.B., Malagnini, L., and Liu, W. (1999). A regional comparison of vertical ground motion in North America, http://www.eas.slu.edu/People/RBHerrmann/GroundMotion/ , Department of Earth and Atmospheric Sciences, Saint Louis University, St. Louis, MO, 63103, 37 pp.

Santamarina, J.C., Fam, M.A., and Klein, K. (1999). *Particulate Materials: Characterization with Elastic and Electromagnetic Waves*, John Wiley & Sons, under contract.

Sata, K., Kokusho, T., Matsumoto, M., and Yamada, E. (1996). Nonlinear seismic response and soil property during strong motion, *Soils and Foundations Special Issue on the 1995 Hyogoken-Nambu Earthquake*, January, pp. 41-52

Saucier, R.T. (1994). *Geomorphology and Quaternary Geologic History of the Lower Mississippi Valley*, U.S. Army Corps of Engineers Waterways Experiment Station, Vicksburg.

Schofield, A.N., and Wroth, C.P. (1968). *Critical State Soil Mechanics*, McGraw-Hill, London.

Schmertmann, J.H. (1986). Suggested Method for Performing the Flat Dilatometer Test, *ASTM Geotechnical Testing Journal*, 9 (2), pp. 93-101.

Schneider, J.A., and Mayne, P.W. (1998a). "Results of Seismic Piezocone Penetration Tests Performed in Memphis, TN and West Memphis, AR," *Interim Report, MAEC Project No. GT-3*, November, pp. 67.

Schneider, J.A., and Mayne, P.W. (1998b). "Results of Seismic Piezocone and Flat Dilatometer Tests Performed in Blytheville, AR, Steele, MO, and Shelby County, TN *Interim Report, MAEC Project No. GT-3*, December, pp. 125.

Schneider, J.A., Mayne, P.W., Hendren, T.L., and Wise, C.M. (1999). Initial development of an impulse piezovibrocone for liquefaction evaluation, *Physics and Mechanics of Soil Liquefaction*, Balkema, Rotterdam, pp. 341-354.

Schweig, E.S. (1998). Personal Communication, October, (CERI - Memphis).

Schweig, E.S., and VanArsdale, R.B. (1996). Neotectonics of the upper Mississippi embayment, *Engineering Geology*, 45, pp. 185-203.

Schnabel, P.B., Lysmer, J., and Seed, H.B. (1972). SHAKE: a computer program for earthquake response analysis of horizontally layered sites, *Report EERC 72-12*, Earthquake Engineering Research Center, University of California, Berkeley.

Seed, H.B. (1979). Soil liquefaction and cyclic mobility evaluation for level ground during earthquakes, *Journal of the Geotechnical Engineering Division*, 105 (GT2), ASCE, pp. 201-255.

Seed, H.B., and DeAlba, P. (1986). Use of SPT and CPT tests for evaluation of the liquefaction resistance of soils, *Use of In-Situ Tests in Geotechnical Engineering*, ASCE GSP 6, pp. 281-302.

Seed, H.B., and Idriss, I.M. (1970). Soil moduli and damping factors for dynamic response analysis, *Report No. EERC 70-10*, Earthquake Engineering Research Center, University of California, Berkeley, reprinted in *H. Bolton Seed Selected Papers*, Vol. 1, BiTech Publishers, Ltd., Vancouver, pp. 277-308.

Seed, H.B., and Idriss, I.M. (1971). Simplified procedure for evaluating soil liquefaction potential, *Journal of Soil Mechanics and Foundation Division*, ASCE, 97 (SM9), pp. 1249-1273.

Seed, H.B., Idriss, I.M., and Arango, I. (1983). Evaluation of liquefaction potential from field performance data, *Journal of Geotechnical Engineering*, ASCE, 109 (3), pp. 458-482.

Seed, H.B., Idriss, I.M., Makdisi, F., and Banerjee, N. (1975). Representation of irregular stress time histories by equivalent uniform stress series in liquefaction analysis, *EERC 75-29*, Earthquake Engineering Research Center, University of California, Berkeley.

Seed, H.B., and Lee, K.L. (1966). Liquefaction of saturated sands during cyclic loading, *Journal of Soil Mechanics and Foundation Division*, ASCE, 92 (SM6), pp. 105-134.

Seed, H.B., Tokimatsu, K., Harder, L.F., and Chung, R.M. (1985). Influence of SPT procedures in soil liquefaction resistance evaluations, *Journal of Geotechnical Engineering*, ASCE, 111 (12), pp. 1425-1445.

Seed, R.B., and Harder, L.F. (1990). SPT-based analysis of cyclic pore pressure generation and undrained residual strength, *H. Bolton Seed Memorial Symposium,* Vol. 2, BiTech Publishers, Vancouver, pp. 351-376.

Sego, D.C., Hofmann, B.A., Robertson, P.K., and Wride, C.E. (1999). Undisturbed sampling of loose sand using in-situ ground freezing, *Physics and Mechanics of Soil Liquefaction,* Balkema, Rotterdam, pp. 179-191.

Senneset, K., and Janbu, N. (1985). Shear strength parameters obtained from static CPT, *Strength Testing of Marine Sediments,* ASTM STP 883, Philadelphia, pp. 41-54.

Senneset, K., Janbu, N., and Svano, G. (1982). Strength and deformation parameters from cone penetration tests, *Proceedings 2nd European Symposium on Penetration Testing,* Vol. 2, Amsterdam, pp. 863-870.

Shen, C.K., Wang, Z., and Li, X.S. (1991). Pore pressure response during 1986 Lotung earthquakes, *Proceedings, Second International Conference on Recent Advances in Geotechnical Earthquake Engineering and Soil Dynamics,* March 11-15, 1991, St. Louis, Missouri, pp. 557-563.

Shibata, T., Oka, F., and Ozawa, Y. (1996). Characteristics of ground deformations due to liquefaction, *Soils and Foundations Special Issue on the 1995 Hyogoken-Nambu Earthquake,* January, pp. 65-79.

Shibata, T., and Teparaksa, W. (1988). Evaluation of liquefaction potential of soils using cone penetration tests, *Soils and Foundations,* 28 (2), pp. 49-60.

Shibuya, S., Nakajima, M., Hosona, T. (1994). Pseudo elastic shear modulus of a Holocene clay deposit, *Proceedings of the International Symposium on Pre-Failure Deformation Characteristics of Geomaterials,* Vol. 1, pp. 293.

Shuttle, D., and Jeffereis, M. (1998). Dimensionless and unbiased CPT interpretation in sand, *International Journal for Numerical and Analytical Methods in Geomechanics*, 22, pp. 351-391.

Skempton, A.W. (1986). Standard penetration test procedures and the effects of overburden pressure, relative density, particle size, ageing, and overconsolidation, *Geotechnique*, 36 (3), pp. 425-447.

Sladen, J.A. (1989). Problems with interpretation of sand state from cone penetration tests, *Geotechnique,* 39, pp. 323-332.

Stark, T.D., and Mesri, G. (1992). Undrained shear strength of liquefied sands for stability analysis, *Journal of Geotechnical Engineering*, 118 (11), ASCE, pp. 1727-1747.

Stark, T.D., and Olson, S.M. (1995). Liquefaction resistance using CPT and field case histories, *Journal of Geotechnical Engineering*, 121 (12), pp. 859-869.

Stokoe, K.H.,II, Darendeli, M.B., and Menq, F.-Y. (1999). Rosrine Project: Phases I and II, Summary of RC/TS laboratory test results, *Lecture notes from*, Symposium on Site Response Issues, MIT, Boston, March 19, 125 pp.

Stover, and Coffman (1993). *Seismicity of the United States 1568 - 1989 (Revised)*, U.S. Geological Survey Professional Paper 1527.

Street, R. (1999). Shear wave velocity of Paleozoic rocks in Mid-America, personal communication to Bob Herrmann, University of Kentucky.

Suzuki, Y., Tokimatsu, K., Koyamada, K., Taya, Y., and Kubota, Y. (1995b). Field correlation of soil liquefaction based on CPT data, *Proceedings, International Symposium on Cone Penetration Testing (CPT '95)*, Vol. 2, Swedish Geotechnical Society Report No. 3:95, Linkoping, pp. 583-588.

Suzuki, Y., Tokimatsu, K., Taye, Y., and Kubota, Y. (1995b). Correlation between CPT data and dynamic properties of in-situ frozen samples, *Proceedings, 3rd International Conference on Recent Advances in Geotechnical Earthquake Engineering and Soil Dynamics*, St. Louis, Vol. I, pp. 249-252.

Talwani, P. (1982). Internally consistent pattern of seismicity near Charleston, South Carolina, *Geology*, 10, pp. 654-658.

Tanaka, H. (1995). National report - the current state of CPT in Japan, *Proceedings, International Symposium on Cone Penetration Testing (CPT '95)*, Vol. 1, Swedish Geotechnical Society Report No. 3:95, Linkoping, pp. 115-124.

Thevanayagam, S., Wang, C.C., and Ravishankar, K. (1996). Determination of post-liquefaction strength: steady state vs. residual strength, *Uncertainty in the Geologic Environment*, ASCE GSP 58, pp. 1210-1224.

Tokimatsu, K., Kuwayama, S., and Tamura, S. (1991). Liquefaction potential evaluation based on Rayleigh wave investigation and its comparison field behavior, *Proceedings Second International Conference on Recent Advances in Geotechnical Earthquake Engineering and Soil Dynamics*, March 11-15, 1991, St. Louis, Missouri, pp. 357-364.

Toro, G.R., Abrahamson, N.A., and Schneider, J.F. (1997). Model of string ground motions from earthquakes in central and eastern North America: Best estimates and uncertainties, *Seismological Research Letters*, 68 (1), pp. 41-57.

Tuttle, M.P., Lafferty, R.H., Guccione, M.J., Schweig, E.S., Lopinot, N., Cande, R.F., Dyer-Williams, K., and Haynes, M. (1996). Use of Archeology to Date Liquefaction Features and Seismic Events in the New Madrid Seismic Zone, Central United States, *Geoarchaeology: An International Journal*, 11 (6), pp. 451-480.

Tuttle, M.P., Lafferty, R.H., and Schweig, E.S. (1998). Dating of Liquefaction Features in the New Madrid Seismic Zone and Implications for Earthquake Hazard, NUREG/GR-0017, U.S. Nuclear Regulatory Commission (in press).

Tuttle, M.P., and Schweig, E.S. (1995). Archeological and Pedological Evidence for Large Prehistoric Earthquakes in the New Madrid Seismic Zone, Central United States, *Geology*, 23, pp. 253-256.

Tuttle, M.P., and Schweig, E.S. (1996). Recognizing and Dating Prehistoric Liquefaction Features: Lessons Learned in the New Madrid Seismic Zone, Central United States, *Journal of Geophysical Research*, 101 (B3), pp. 6171-6178.

USGS (1996). Peak Acceleration (%g) with 2 % Probability of Exceedence in 50 Years (site: NEHRP B-C boundary), http://geohazards.cr.usgs.gov/eq/hazmaps/250pga.gif.

USGS (1999). USGS Earthquake Hazards Web Site, http://www.usgs.gov/eq/.

Vaid, Y.P., and Thomas, J. (1995). Liquefaction and postliquefaction behaviour of sand, *Journal of Geotechnical and Geoenvironmental Engineering*, 121 (2), pp. 163-173.

Van Arsdale, R. (1998a). Personal Communication, September, (University of Memphis).

Van Arsdale, R. (1998b). *Seismic Hazards of the Upper Mississippi Embayment*, Contract Report GL-98-1, U.S. Army Corps of Engineers Waterways Experiment Station, 132 pp.

Vasquez-Hererra, A., Dobry, R., and Ng, T.-T. (1988). Pore pressure buildup and liquefaction failure of anisotropically consolidated sand due to cyclic straining, *Hydraulic Fill Structures*, ASCE GSP 21, pp. 346-366.

Verdugo, R. (1992). The critical state of sands: Discussion, *Geotechnique*, 42 (2), pp. 655-663.

Vreugdenhil, R., Davis, R., and Berrill, J. (1994). Interpretation of cone penetration results in multilayered soils, *International Journal for Numerical and Analytical Methods in Geomechanics,* 18, pp. 585-599.

Vucetic, M.L., and Dobry, R. (1991). The effects of soils plasticity on cyclic response, *Journal of Geotechnical Engineering*, 117 (1), ASCE, pp. 898-907.

Whittenberg, P.L. et al. (1977). *Natural and Physical Characteristics of Memphis and Shelby County*, Office of Planning and Development, Memphis and Shelby County, November.

Wolf, L.W., Collier, J.W., Tuttle, M.P., and Bodin, P. (1998). Geophysical Reconnaissance of Earthquake-Induced Liquefaction Features in the New Madrid Seismic Zone, *Journal of Applied Geophysics*, 39, pp. 121-129.

Wood, D.M. (1990). *Soil Behaviour and Critical State Soil Mechanics,* Cambridge University Press, Cambridge, 462 pp.

Woods, R.D. (1994). Laboratory measurement of dynamic soil properties, *Dynamic Geotechnical Testing II*, ASTM STP 1213, Philadelphia, pp. 165-190.

Wroth, C.P. (1984). The interpretation of in-situ soil tests, *Geotechnique*, 34 (4), pp. 449-489.

Wroth, C.P. (1988). Penetration testing - A more rigorous approach to interpretation, *Penetration Testing 1988*, Balkema, Rotterdam, pp. 303-311.

Yantis, B.R., Costain, J.K., and Ackermann, H.D. (1983). A reflection seismic study near Charleston, South Carolina, *Studies Related to the Charleston, South Carolina, Earthquake of 1886 - Tectonics and Seismicity*, U.S. Geologic Survey Professional Paper 1313, pp. G1-G20.

Yasuda, S., and Tohno, I. (1988). Sites of re-liquefaction caused by the 1983 Nihonkai-Chuba earthquake, *Soils and Foundations*, 28 (2), pp. 61-72.

Youd, T.L. (1984). Recurrence of liquefaction at the same site, *Proceedings of the Eighth World Conference on Earthquake Engineering*, Volume III, San Francisco, CA, July 21-28, pp. 231-238.

Youd, T.L. (1997). Seismic factors for use in evaluating earthquake resistance, *Proceedings*, Workshop on Evaluation of Liquefaction Resistance, NCEER-97-0022, Multidisciplinary Center for Earthquake Engineering Research, Buffalo, NY, pp. 191-200.

Youd, T.L. (1999). Physics and mechanics of liquefaction from field records and experience, *Physics and Mechanics of Soil Liquefaction*, Balkema, Rotterdam, pp. 325-334.

Youd, T.L., and Holzer, T.L. (1994). Piezometer performance at Wildlife liquefaction site, California, *Journal of Geotechnical Engineering*, 120 (6), pp. 975.-995

Youd, T.L., Kayen, R.E., and Mitchell, J.K. (1997). Liquefaction criteria based on energy content of seismograms, *Proceedings*, Workshop on Evaluation of Liquefaction Resistance, NCEER-97-0022, Multidisciplinary Center for Earthquake Engineering Research, Buffalo, NY, pp. 217-224.

Youd, T.L., and Noble, S.K. (1997). Magnitude scaling factors, Workshop on Evaluation of Liquefaction Resistance, NCEER-97-0022, Multidisciplinary Center for Earthquake Engineering Research, Buffalo, NY, pp. 149-165.

Zeghal, M., and Elgamal, A.-W. (1994). Analysis of site liquefaction using earthquake records, *Journal of geotechnical Engineering*, 120 (6), ASCE, pp. 996-1017.

Zeghal, M., Elgamal, A.-W., and Parra, E. (1996). Identification and modeling of earthquake ground response - II. Site liquefaction, *Soil Dynamics and Earthquake Engineering*, 15, pp. 523-547.